JRC Scientific and Technical Reports

NEMEA-4
Neutron Measurements, Evaluations and Applications

Nuclear data needs for Generation-IV and accelerator driven systems
Proceedings of the CANDIDE workshop
16-18 October 2007

Edited by Arjan Plompen

EUR 23235 EN - 2008

JRC
EUROPEAN COMMISSION

irmm
Institute for Reference Materials and Measurements

The mission of the IRMM is to promote a common and reliable European measurement system in support of EU policies.

European Commission
Joint Research Centre
Institute for Reference Materials and Measurements

Contact information
Address: A.J.M. Plompen, European Commission, Joint Research Centre, Institute for Reference Materials and Measurements, Retiesweg 111, 2440 Geel, Belgium
E-mail: Arjan.Plompen@ec.europa.eu
Tel.: +32 (0) 14 571 381
Fax: +32 (0) 14 584 273

http://irmm.jrc.ec.europa.eu/
http://www.jrc.ec.europa.eu/

JRC 42917

EUR 23235 EN
ISBN 978-92-79-08274-0
ISSN 1018-5593
DOI 10.2787/13092

Luxembourg: Office for Official Publications of the European Communities

Printed in Belgium

NEMEA-4
Neutron Measurements, Evaluations and Applications

Nuclear data needs for Generation-IV and accelerator driven systems
Proceedings of the CANDIDE workshop
16-18 October 2007
Prague, Czech Republic

Edited by Arjan Plompen

Foreword

October 16-18, 2007, the workshop NEMEA-4 was held at the Kaiserstein Palace in Prague, Czech Republic. The fourth edition of this workshop on Neutron Measurements, Evaluations and Applications was organised on behalf of the European coordination action CANDIDE by the Institute for Reference Materials of the Joint Research Centre with support of the Nuclear Physics Institute of the Academy of Sciences of the Czech Republic (ASCR). CANDIDE is the Coordination Action for Nuclear Data for Industrial Development in Europe that focusses at establishing nuclear data needs from an industry point of view for the near and midterm future. It has a strong networking component to mobilise researchers to address those needs. As such, the workshops NEMEA-4 and its planned sequel NEMEA-5 are important vehicles of CANDIDE networking activities. In particular, NEMEA-4 addressed the topic of data needs, while NEMEA-5 will consider the state-of-the-art in nuclear data production methods.

NEMEA-4 carried as a subtitle "Nuclear data needs for Generation-IV and accelerator driven system". In this context an important contribution to the workshop was made by Subgroup 26 of the Nuclear Energy Agency of the Organisation for Economic Cooperation and Development. This subgroup, which addresses sensitivity studies to establish nuclear data requirements for design and performance studies of advanced reactors, completed its activities with a set of presentations at the workshop and a subsequent progress meeting. This valuable contribution to NEMEA -4 and the CANDIDE project was made possible by the efforts of the subgroup coordinator M. Salvatores who also participated in the program advisory committee. A short session on other applications pointed to interests in nuclear data of the fusion and the medical communities. A large number of researchers from the nuclear data producing community took note of the data needs emerging from these sensitivity studies and presented their efforts and commitments in the domains of nuclear data measurement, evaluation and validation.

The NEMEA series of workshops were initiated as an enlargement initiative of the Joint Research Centre. They have been organised in Candidate Countries and New Member States of the European Union and facilitated attendance of scientists from these new parts of the EU. Also on this occasion the enlargement aspect was important, as witnessed by the venue of and attendance to the workshop and by the excellent overview of activities presented by the Czech colleagues from Rez. This time the main support for this aspect, duly acknowledged, is from CANDIDE and the ensuing sponsorship of the Research Directorate General of the European Commission.

I would hereby like to express my gratitude to the local organisers of the Nuclear Physics Institute of the ASCR. The team of P. Bem and J. Dobes provided us with excellent provisions that made the workshop a pleasant and successful event. I furthermore acknowledge the support of the program advisory committee, H. Aït Abderrahim of SCK-CEN, Belgium, J. Blomgren of the University of Uppsala, Sweden, R. Jacqmin of CEA, France, A. Koning of NRG, The Netherlands, D.N. Carpentier of EDF, France, R.W. Mills of Nexia Solutions, UK, M. Salvatores of CEA, France, FZK, Germany and ANL, USA, and J. Dobes of NPI ASCR, Czech Republic and the organisational support of C. Cabanillas Platero, I. Celen, E. Kubrychtová and S. Lehto.

Arjan Plompen
January 2008

The Kaiserstein palace

The nearby Charles' Bridge

Group photo of the participants

Contents

Opening session

Non-fission applications of nuclear data

Nuclear data evaluation

Nuclear data experiments

Benchmark experiments

Advanced reactor systems

Poster presentations

CANDIDE - Coordination Action on Nuclear Data for Industrial Development in Europe

J. Blomgren[1)], E. Bauge[2)], D. Cano Ott[9)], S. Csifrus[5)], K. Dahlbacka[6)], I. Gonçalves[13)], E. González[9)], H. Henriksson[15)], R. Jacqmin[2)], A. Koning[4)], D. Lecarpentier[12)], E. Malambu[8)], A. Mengoni[14)], R. Mills[11)], A. Plompen[3)], G. Rimpault[2)], V. Starý[7)], C. Trakas[10)], P. Vaz[13)], C. Zimmerman[11)]

1) Department of Neutron Research, Uppsala University, Box 525, S-751 20 Uppsala, Sweden
2) Commissariat à l'Energie Atomique, France
3) Joint Research Centre - Institute for Reference Materials and Measurements, EU
4) Nuclear Research and consultancy Group, the Netherlands
5) Budapest University of Technology and Economics, Hungary
6) Teollisuuden Voima Oy, Finland
7) Nuclear Research Institute Řež, Czech Republic
8) Studiecentrum voor Kernenergie · Centre d'étude de l'Energie Nucléaire, Belgium
9) Centro de Investigaciones Energéticas, Medioambientales y Tecnológicas, Spain
10) AREVA, France
11) Nexia Solutions, United Kingdom
12) Electricité de France, France
13) Instituto Tecnológico e Nuclear, Portugal
14) International Atomic Energy Agency, UN
15) Nuclear Energy Agency, OECD

Jan.Blomgren@tsl.uu.se

Abstract: A Co-ordinated Action has been launched with the ambition to establish a durable network on nuclear data efforts that are important in the context of minimising the high-level waste stream of nuclear energy. This implies optimal incineration of all actinides that nowadays constitute spent nuclear fuel, in critical and sub-critical reactors. As a consequence, the scope of the project encompasses transmutation in fast critical reactors as well as sub-critical accelerator-driven systems (ADS). The purpose is to identify the needs for improved nuclear data, assess the present status of knowledge, and to estimate what accuracy can be reached with state-of-the-art techniques.

Introduction

The EC-supported Coordination Action (CA) CANDIDE, Coordination Action on Nuclear Data for Industry Development in Europe, addresses the following two objectives:

- Establishment of better links between academia, research centres and industry end users of nuclear data. This is reflected in the project name.
- Assessment of nuclear data needs for advanced nuclear reactors. The emphasis is on the radioactive waste issue, i.e., either waste transmutation in critical or sub-critical devices or minimizing the production of nuclear waste in future nuclear reactors, as envisaged in some fast critical systems.

For a long time activities concerning all aspects of nuclear data for commercial nuclear power reactors, i.e., nuclear data production, theory, evaluation, validation and industrial use, have been part of a well-organized international community, monitored by large international organizations, like OECD. Recently, a new nuclear data community has been formed around the production of nuclear data for accelerator-driven systems, while the other ingredients of traditional nuclear data work (e.g. evaluation and validation) have to a large degree been missing up to now. The present project aims at establishing links for this new community to the existing structure of coordinated nuclear data activities in general, and to provide links to industry in particular.

Another recent development in Europe has been the enlargement of the EU, which opens new possibilities in the realm of nuclear data. Integration - both of different research communities and between new and previous member states - is an important objective of the CANDIDE project. Moreover, improved training and integration are essential parts of the CA, exemplified by the development of a European course on nuclear data to be part of the project.
In the public literature, the concept of transmutation is quite often used in a restricted sense, synonymous to accelerator-driven systems for incineration of spent nuclear fuel. CANDIDE has been designed with the intention to consider transmutation in a broader, more general sense, i.e., incineration of spent nuclear fuel by changing the nature of the elements through nuclear reactions. As a consequence, the scope of the proposed CA will encompass transmutation in fast critical reactors as well as sub-critical systems (ADS).
The purpose of CANDIDE is not to produce new experimental data or evaluations, but to review the current modes of nuclear data production, assess the present status of our knowledge, estimate what accuracy can be reached with state-of-the-art numerical simulation techniques, identify the needs for improved nuclear data, and suggest appropriate actions to be taken to meet those needs. A large fraction of the existing data were obtained far back in time, and it might be beneficial to identify cases where new experiments on already measured reactions could exploit technology improvements. Key input is expected from industrial partners, since they are closely involved in application of nuclear data libraries and their performance.
The final result of the CA will be a report describing the state-of-the-art and giving recommendations to EC outlining how nuclear data research should be organized in FP7 and beyond. Moreover, the organisation of workshops and a training course will lead to broader European involvement in the subject.

Nuclear data for transmutation of spent nuclear fuel

In the public debate of today, the concept of *transmutation* has often become synonymous with accelerator-driven systems (ADS) for incineration of nuclear waste. This is not surprising, because ADS represents a very innovative option, while the use of critical reactors represent a more conventional alternative. In CANDIDE, however, we will consider transmutation in a very broad sense, not restricted to a particular system or scenario.
Presently, nuclear waste transmutation options are investigated as part of reactor and fuel cycle studies for existing reactor types (PWR, BWR, CANDU), i.e., GEN-III, for evolutionary designs of existing reactors, GEN-III+ (EPR, AP600, etc), for GEN-IV reactors (SFR, GFR, LFR, MSR, SCWR, VHTR) or for dedicated transmuters (such as ADS). All these activities generate a significant amount of nuclear data needs either for the feasibility phase of these studies or for the performance phase.
Up to now, there has been a very large research volume spent on data on neutron-induced nuclear reactions up to 20 MeV. This was carried out from around 1950 until today, and was motivated by the needs in the development of civil nuclear power, as well as weapons applications and fusion technology. During the last decade, nuclear data at higher energies have been in the limelight due to the discussions about ADS.
The approaches in these two disciplines differ significantly. This is neither a surprise nor a bad choice, because the underlying physics differs significantly, resulting in different research strategies. Below 20 MeV, a single cross section can be of paramount importance to the entire application. An example is the neutron capture resonance at 6.7 eV in ^{238}U that provides the Doppler effect so important for the stability of critical reactors. Moreover, some cross sections are fundamentally inaccessible to theory, in particular in the resonance region. As a result, at low energies more or less complete data coverage for major elements is required. Above 20 MeV, the situation is fundamentally different. The cross sections are slowly varying in energy, and the behaviour of the system is always dictated by the sum of a large number of reactions, none of which strongly dominates the performance. Therefore, getting a grip on the overall picture has been a more natural ambition in an initial stage, rather than providing precision data on a single reaction.
Thanks to the nuclear data campaigns for ADS in FP5 and FP6, we have now reached a stage where such an overall picture, although fairly rough in many respects, is appearing. As a consequence, the uncertainty in modelling of various ADS concepts due to nuclear data uncertainties have decreased significantly during the last few years. There is, however, still

plenty of room for improvement of ADS-relevant nuclear data, only part of which will be fulfilled by IP-EUROTRANS [1].
Up to now, nuclear data at the energies of critical reactors (less than 10 MeV) and accelerator-driven systems (up to 1 GeV) have not been systematically treated on an equal basis. The importance of this aspect was recently highlighted at the International Workshop on Nuclear Data Needs for Generation IV Nuclear Energy Systems [2], after which a WPEC subgroup was established to investigate the nuclear data needs for advanced reactor systems [3]. We find it important for the further development of nuclear data activities for transmutation, and even for the entire research on transmutation, that the nuclear data from these very different regimes can be compared and used in a consistent manner. This is a major underlying theme of CANDIDE.
In general, the safe, economical, and reliable operation of a nuclear reactor depends on the use of nuclear data to predict several important characteristics of plant operation. In the case of transmutation in general, the major benefit of accurate nuclear data relates specifically to avoiding unnecessary conservatism in design and operation such as shielding requirements, power coefficients for a core loaded with minor actinides, and the related power requirements of the proton accelerator for ADS systems.
Another important difference between a dedicated transmutation system - critical or sub-critical - and a conventional critical power reactor is that for the latter, deficiencies in detailed nuclear data can partly be overcome through normalizing calculations to existing reactor measurements or experience from the operation of prototypes and test rigs. The desire to pursue new designs (Gen-IV as well as ADS concepts) without performing extensive reactor experiments dictates using nuclear data that will support reactor calculations that give dependable results even without experimental re-normalization.
On a (very) broad level, the nuclear data requirements for transmutation of waste fall into two classes: (1) resonance and fast neutron reactions for materials that are specific to transmutation: unconventional structural materials, coolants and (in the case of ADS) targets, and minor actinides, whose abundance in the core is much larger than in a conventional reactor, (2) energy regimes that extend beyond the fast neutron region (up to hundreds of MeV) for the above materials and conventional materials. The first class applies to any transmutation method, i.e., including critical reactors, whereas the second class exclusively applies to ADS. In this project, we will consider both classes.
Although the motivation for the present project arises from waste minimization using novel reactor types, conventional power reactors can still benefit from the outcome of the CA. Indeed, nuclear data needs that apply to a critical power system, in general also apply to transmutation systems, critical as well as sub-critical. For example, the important interplay between ^{238}U fission, capture and inelastic scattering, is crucial for a precise determination of criticality. Minimizing the uncertainties in these data is also important for transmutation systems. One interest of the CA is to identify needs that are common to various applications.

Training and networking

CANDIDE is not limited to involvement of existing activities, but will also promote growth for the future. Therefore, an important part of the project is the development of a dedicated training course on nuclear data for young professionals, the European course on Experiment, Theory and Evaluation of Nuclear Data (EXTEND) to be held in Budapest in September 2008. The target group of this course are young professionals, primarily recently employed staff in industry and at research centres, as well as PhD students in the field.
Summer schools in nuclear engineering (e.g., the Eugene Wigner School on Reactor Physics [4] within the ENEN [5] association or the Frédéric Joliot - Otto Hahn summer school [6]) are regularly organized, and there are relatively frequent summer schools on fundamental nuclear physics. Up to now, however, there have been few initiatives to bridge these two communities. EXTEND has been designed to fill this gap.
Besides the development of EXTEND, other activities on training and mobility of young industry professionals and researches, as well as European integration are also foreseen. The most visible example is the extension of the NEMEA workshops series, organized by IRMM, which are included in the CA. The previous NEMEA workshops have been targeting nuclear data research in Eastern Europe, but have now been enlarged to be open to all Europe. Our intention is to make these workshops meeting places for all European scientists in the field, including the nuclear industry, which has previously not been the case. The

outcomes of two previous such workshops have been beneficial for the present proposal, in so far that they have promoted valuable links between old and new member states in general, and scientists from these in particular.

Project strategy

As has been described above, we have identified possibilities to enlarge the nuclear data activities in Europe by integrating the new research communities (ADS research, new member and candidate states) into the already existing structures for nuclear data work, and CANDIDE will address these issues by organizing open workshops intended for bridging gaps between these communities. Moreover, the project itself has been designed to make industry a more visible player in the research-related activities via the top-down approach of CANDIDE. Last but not least, the development of a new course for young professionals is in line with these goals, but it is also intended to foster closer links between nuclear physics and reactor physics.

The project involves a wide range of industry partners. Three reactor construction or manufacturing organizations are represented. AREVA (France) is a leading manufacturer of nuclear reactors in Western Europe, having received widespread attention recently with the two EPRs under construction in Finland and France. The BNFL group (UK) has a wide range of reactors on its repertoire, gas-cooled reactors in the UK as well as light-water reactors (LWR) manufactured by Westinghouse. The Skoda corporation in the Czech Republic is constructing heavy structural parts to nuclear reactors, like reactor vessels, and are represented in the present CA via their technical support organization, NRI Řež.

Two power utilities, TVO (Finland) and EdF (France), participate in the project, representing light water reactor technology. Fuel manufacturing is represented by Nexia/BNFL and AREVA, while reprocessing is represented by Nexia/BNFL.

Design of future ADS-related facilities is represented by SCK•CEN (Belgium) and CIEMAT (Spain).

The validation (CEA Cadarache, NRG Petten) and evaluation (CEA Cadarache, CEA Bruyères-le-Châtel, NRG Petten) teams of the proposed CA represent leading European competence in the field. ITN (Portugal) contributes expertise in nuclear data related to spallation targets. The current-day computer power enables sophisticated nuclear reaction modelling and validation against integral experiments with both deterministic and Monte Carlo software.

On the experimental side, IRMM Geel is the dedicated EU lab for reactor-relevant nuclear data (0-20 MeV), while TSL Uppsala is the primary European facility for neutrons above 20 MeV (up to 200 MeV), which will cover important input for ADS neutronics.

With these partners, we cover the entire chain from industry to experiments, with a top-down approach. The industry partners define the needs from the end-users' perspective, and their participation guarantees that the work is application-oriented. The role of the non-industry partners is to assess the possibilities to provide data of sufficient quality to meet the application needs. As a consequence, the issue of which data is required or need to be improved is primarily an industry concern, while the question of how to reach those goals is mostly dealt with by the non-industry partners. Efficient dissemination is guaranteed by the involvement of the IAEA and OECD/NEA Data Banks.

Improved training, as well as integration of new member states, are important issues for the CA. Improvement of training on nuclear data is undertaken in close collaboration with European Nuclear Education Network (ENEN) [5], and it brings educational resources in old and new member states together. Additional integration is provided by the strong involvement of industry throughout Europe. Close contacts with the EFNUDAT [7] integrated infrastructure initiative have been established.

Project scientific content

As outlined above, the project concerns the integration of nuclear data efforts for all types of transmutation-relevant nuclear systems, i.e., critical thermal and fast reactors, as well as accelerator-driven systems. Up to now, various nuclear-data projects have concentrated on different sub-sets of the global issue. In the present CA, we attempt to unify important aspects of these activities, with the ambition to provide a consistent basis for comparisons of various waste transmutation options.

A general approach to nuclear data for waste management would imply a very large project. To keep the task limited to a reasonable size, but still with the potential to provide results of relevance to the assessment of various transmutation strategies, the work has to be concentrated to a few issues that are of key importance to both fast critical reactors and ADS.
Up to now, the nuclear data research at classical reactor energies, up to 20 MeV, and the ADS-motivated research above 20 MeV have been conducted with very different approaches. This has made sense, because the pre-conditions have been very different. With the recent development in nuclear data for ADS, resulting from FP5 and FP6 projects, we believe it is now possible to conduct research on what is common to critical reactors and ADS.
A major unifying aspect is the role of neutrons. In both concepts, the major incineration is due to neutron-induced fission. Moreover, other neutron-induced reactions, like capture and scattering, play significant roles in all these techniques. Another common aspect is that the core will contain large amounts of minor actinides, although the composition differs among various systems. Furthermore, the design studies around GEN-IV type systems encompass not only the core but also the full fuel cycle. One important GEN-IV criterion is the reduction of radioactive waste that is competing against other criteria such as sustainability (full use of Uranium or Thorium ores), economics, safety and reliability, proliferation resistance and physical protection.
As a natural consequence of this, a study that could cover only the transmutation aspect of a core would not be complete. We therefore envisage the project to cover all nuclear data that have some relation to the reactors and their associated fuel cycles, whether they are dedicated specifically to transmutation (just like ADS) or if transmutation is only one of their key features.
In the present CA, we intend to assess the data situation for all neutron energies, from thermal and up to the highest available (200 MeV), both experimentally and theoretically. In the first instance, the focus of the CA should be on cores of fast reactors and ADS. Nuclear data are of great relevance also for irradiation effects on materials, radiation protection and a number of other issues. A possible list of data to be studied is given below:

- General purpose files that include (1) cross-sections induced by neutrons, protons and gammas, (2) secondary particle energy distributions, and (3) fission spectra and energy release.
- Gamma production induced by different reaction types.
- Fuel cycle data (fission yields, spallation yields, decay heat).
- Activation files.

Participants from nuclear industry should give guidance on the proper parameters to be investigated and optimised. These needs should be translated into data evaluation and measurement requests, to be carried out in FP7 and beyond. Part of the effort in this CA consists of a critical assessment of major and minor actinide data in the latest nuclear data libraries and an assessment of the corresponding uncertainties. This should in a natural way lead to well-focused measurement requests.
As has been emphasized, the industrial needs will drive the assessment within the CA. It is worthwhile to point at the close connection of the present collaboration with the OECD-NEA High Priority Request List for nuclear data, where such well-defined requests are collected and reviewed to mobilise the community for their resolution. CANDIDE will serve to identify and propagate the EU interests in this domain and to provide the focus for future EU research on nuclear data. Also in the area of follow up on the formulated requests, CANDIDE is well connected to running EC projects, especially the JEFF project, as mentioned previously.

Acknowledgements
This work was financially supported by the European Union, contract 036397.

References

[1] EUROTRANS - European Research Programme for the Transmutation of High-Level Nuclear Waste in an Accelerator-Driven System.http://nuklear-server.ka.fzk.de/eurotrans/.
[2] Proceedings of the International Workshop on Nuclear Data Needs for Generation IV Nuclear Energy Systems, ed. P. Rullhusen (Antwerpen, Belgium, 5-7 April 2005). http://www.jrc.cec.eu.int/gen4-workshop/main.html.
[3] M. Salvatores et al., in these proceedings. See also the Proceedings of International Conference on Nuclear Data for Science and Technology, Nice, France, April 22-27, 2007.
[4] The Eugene Wigner School on Reactor Physics. http://www.reak.bme.hu.

[5] The European Nuclear Education Network. http://www.sckcen.be/ENEN.
[6] The Frédéric Joliot & Otto Hahn Summer School on Nuclear Reactors. http://www-cadarache.cea.fr/fr/cadarache/ecoles/fjohss2007.htm
[7] G. Barreau on behalf of the EFNUDAT consortium, Proceedings of International Conference on Nuclear Data for Science and Technology, Nice, France, April 22-27, 2007. www.efnudat.eu.

Research Activities at Nuclear Physics Institute ASCR Rez

J. Dobeš, P. Bém

Nuclear Physics Institute Řež, CS-25068 Řež, Czech Republic
dobes@ujf.cas.cz

Abstract: Nuclear Physics Institute (NPI) is a major Czech institution in the field of nuclear physics. Both the basic research in nuclear physics and the applications of nuclear physics and its methods in the interdisciplinary and oriented areas form the NPI mission.
The basic nuclear physics research concerns studies of bulk strongly interacting matter in heavy ion collisions, investigation of nuclei far from the stability line, nuclear astrophysics experiments involvement in effort to determine neutrino mass by means of low energy electron spectroscopy, and theoretical and mathematical physics studies.
In the interdisciplinary and applied fields, the research activities are aimed at implementation of nuclear analytical methods using neutrons as well as charged particles beams, condensed matter and material research by means of neutron scattering and diffraction, studies of physical processes and nuclear data important for the prospective energetic technologies, development of ionising-radiation dosimetry and studies of the radiation biological effects, research and development of the radiopharmaceuticals, and development of cyclotron technique.
The studies employing fast neutron generators at NPI cyclotron are discussed in more details. Characterization of neutron fields provided by generators is given. The use in a program relevant to fusion and ADS technologies is presented.

Introduction

Nuclear Physics Institute ASCR (NPI) is a major Czech institution in the field of nuclear physics. Its mission consists in pursuing basis research in nuclear physics and related disciplines and in using the nuclear physics methods and procedures in interdisciplinary fields of science and research. There is about 220 employees in the NPI, 90 of them are scientists.

Basic research

Nuclear physics provides fundamental insights to the understanding the structure of the world. It has also important consequences for other natural sciences. Most principal projects of nuclear physics are so evolved that they are realisable only within wide international collaboration. NPI activities in the basic research are therefore oriented mostly to the participation at topical international experiments. At the same time, the use of local facilities and equipment is also often important.

Heavy nuclei collisions

Activities are oriented first of all to the international projects HADES at GSI Darmstadt, STAR at BNL and ALICE at CERN which are large top international projects studying the behavior and changes in nuclear matter at the extreme conditions appearing during the high-energy heavy nuclei collisions.

Nuclei far from the stability line

The research is based on the collaboration with JINR Dubna, GANIL Caen and ISOLDE CERN. The properties of nuclei with extreme isospin value are studied, where profound changes and completely new effects in nuclear structure appear.

Nuclear astrophysics

The field is treated in collaboration mainly with Texas A&M University and LNS/INFN Catania. The experiments run in Texas and Catania and also at the NPI cyclotron. Indirect techniques proved to be very useful in obtaining information on low - cross section astrophysical rates. Particularly, the method of Asymptotic Normalization Coefficients (ANC) has been developed providing proton capture rates from proton transfer reactions.

Neutrino mass determination from electron spectroscopy
The physicists from NPI participated at the foundation of the international project KATRIN in 2001. The project aims at the construction of unique electron spectrometer and subsequent measurement of the tritium beta spectrum achieving ten times higher sensitivity to the neutrino mass than provided by the present experiments.

Theoretical physics
Activities are concentrated mainly in the studies of non-nucleonic aspects of hadronic systems, meson exchange currents in few-nucleon systems, hypernuclear physics, and interactions of hadrons with nuclei. There are many international collaborations of NPI in theoretical physics including experiment proposals for the advanced foreign facilities.

Mathematical physics
The research is oriented mainly to the quantum mechanical systems in geometrically non-trivial regions, e.g. of the quantum waveguides shape. Further on, the studies of the PT-symmetric theories with non-hermitean Hamiltonians are pursued.

Interdisciplinary and applied research

Nuclear physics and related fields have important interdisciplinary and applied aspects, especially for the energetic and material research, in the industry and environmental applications, and in the life-science. They essentially contribute to the improvements of the quality of life and to the development of modern society economy. There are high requests on the research and development in the applied nuclear sciences and they have long-time perspectives.

Nuclear analytical methods
By the broadness and quality of the implemented nuclear analytical techniques, NPI is a unique centre even on the international scale. The groups working here are oriented at the material, environmental and medical research and they have extended local and international collaborations. Neutron activation analysis is used as well as charged beams of the new tandem accelerator Tandetron 3 MV installed in 2006 and an old Van de Graaff accelerator.

Neutron diffraction
The LVR-15 research reactor of the Nuclear Research Institute Řež is in use for these studies. The activity is aimed at the material research, at the development of neutron-optics elements and neutron-diffraction techniques and also at the development of software packages for the European neutron-diffraction community.

Radiation dosimetry
Research in the field is directed to micro-dosimetry and radiation biophysics. The subject is highly interdisciplinary and studied in collaboration with domestic institutions, JINR Dubna, and also within the European programs. Research in the fields of radiotherapy and environmental studies, having the strong social requirements, is also performed.

Radiopharmaceuticals
Activities in the field at NPI started in nineties. They are oriented especially to the research, development and production of short-lived radioisotopes for diagnostic and therapeutic processes.

Cyclotron
The research and development at the cyclotron are devoted mainly to generation, acceleration and formation of the charged particles beams that are used for basic research experiments as well as for applications, mostly for radiopharmaceuticals production. NPI runs also an electron accelerator microtron.

The NPI cyclotron-based fast neutron facility

Neutronics of the fusion-relevant technologies
The concept of International Fusion Material Irradiation Facility (IFMIF) consists in high-power deuteron accelerator (40 MeV) and lithium (liquid jet) target. The neutron source reaction d(40 MeV)+Li produces a white spectrum with mean energy of 14 MeV and a energy range up to 35 MeV (weak tail up to 55 MeV). The calculations of neutronic responses in the components

of IFMIF Test Cell need the activation-cross-sections (ACS) database, which is validated against experiments at relevant (IFMIF-like) energy range.
For integral benchmark experiments, the white-spectrum neutron source was developed at NPI using the variable-energy cyclotron U-120M. To simulate the neutron spectrum in the energy range relevant to IFMIF, the new source reaction p(37MeV)+D_2O(thick target) has been investigated and high-power heavy-water-flow target was then developed. To determine the neutron spectral flux in the position of irradiated samples, the activation foil method was used.
In the review on a status of nuclear data files [1], a number of elements relevant to IFMIF were identified for which neutron activation data are inadequate and new ACS measurements above 20 MeV are needed. Therefore, in parallel to white-spectrum p/d-Be and p-D_2O sources, the quasi-monoenergetic p-^{7}Li source with neutron energies between 20 to 37 MeV has been build up.
In frame of the EFDA Collaboration on the IFMIF project, the research program concerns mainly the validation of EASY-2007 on Eurofer-97 components (Cr, Vn, Ti) and on a large set of dosimetry-foil nuclides employing both the integral and differential cross section measurements. Further large-scale program is devoted to the experimental tests of spectral flux monitors for IFMIF and SPIRAL-2 facilities. A radiation-hardness investigation of the ATLAS- Hadronic Endcap Calorimeter Electronics is under way (CERN collaboration).

High-power D_2O target station
The D_2O target station was build up on the beam line of the cyclotron operated in the negative-ion mode of acceleration. In this mode, high proton beam power (600W for 37 MeV) and good beam-current stability present suitable basis for neutron activation experiments. To control the heat dissipation of proton beam, the flowing target medium with intensive external cooling has been selected and relevant assembly for flowing-medium target operation was developed.
To avoid presence of bubbles in the target volume caused by electro-dissociation and micro-evaporation effects, the drift velocity together with inlet/outlet pressure on the cell were empirically adjusted. Parameters are controlled by pressure-compensator system (Argon gas) equipped by break bleeding valves and glass-level gauge remotely monitored by TV circuit.

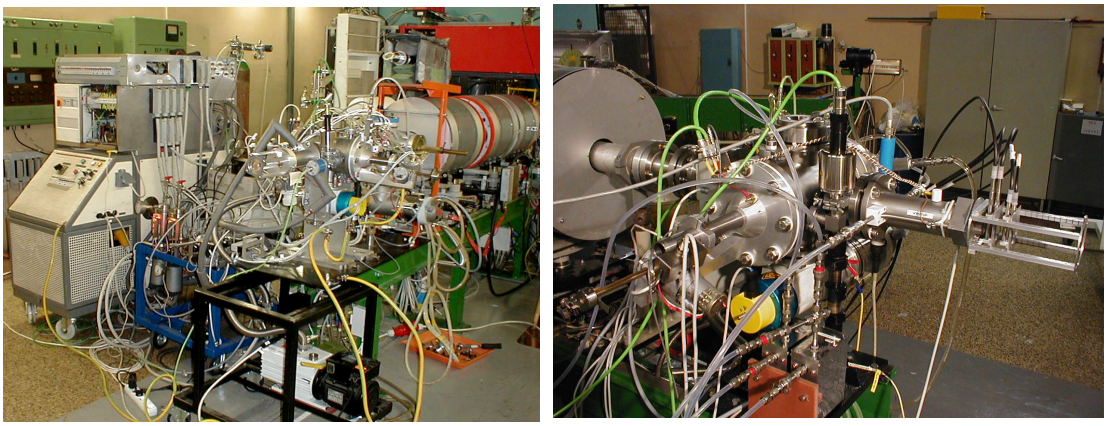

Figure 1. *The assembly for an investigation and operation of the flowing D_2O target of NPI cyclotron-based fast neutron generator.*

The target cell together with the driving and cooling systems is insulated from the earth in such a way that proton current on the target can be accurately measured. The current of proton beam together with the drift, temperature and pressure of flowing water in topic parts of the system are measured, digitized and registered by PC. In Figure 1, a photograph of the D_2O-target station is given.

Determination of spectral flux at sample positions
Because of intensity reason, the irradiated samples are inserted very close to the source target. Due to the averaging of cross-section observables over sample- and target dimension, the spectral yield measured at large distance of the detector from target of source reaction

("point-like-geometry" arrangement of experiment) is not sufficient to determine the spectral flux at sample position.
As the most appropriate method, the multi-foil activation technique was utilized to determine the spectral neutron flux across the irradiated samples and to investigate the integration effects in details. A set of dosimetry foils (Al, Ti, Fe, Co, Ni, Y, Nb, Lu and Au) was irradiated by neutrons from the p-D_2O source at various distances from the target. Standard gamma-spectrometry technique was employed for determination of induced γ-ray activities of reaction products. The reaction rates, specific- and saturated activities were calculated from measured data.
The full set of foils was irradiated at 3 and 156 mm distances. Up to 29 activation reactions were employed for the neutron spectra adjustment [2]. In the unfolding procedure, a modified form of SAND-II code was used (the nuclear data from EAF-2005 library for neutron energies to 55 MeV were added). For the unfolding iterative procedure the initial guess neutron spectrum measured by scintillation unfolding technique (at proton energy of 37 MeV) was used.

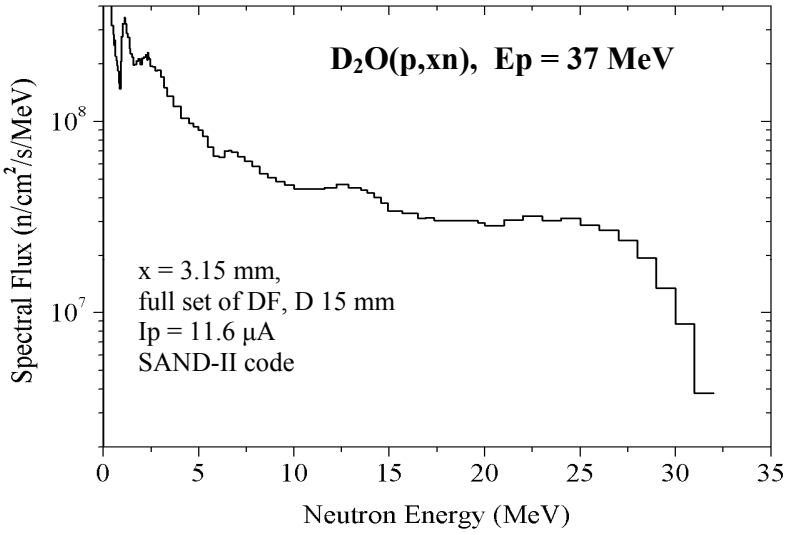

Figure 2. *Neutron spectral flux of the D_2O(p,xn) source reaction at 3 mm distance from the backing surface of D_2O target as obtained from the γ-activities of dosimetry foils by the SAND-II code [N2].*

In the energy range 10 to 25 MeV, the uncertainties of adjusted spectrum amount 3%. Above this range the uncertainty is estimated at the level of 20-30% [2]. To achieve better knowledge of the spectrum below 10 and above 25 MeV, the measurements of (n,n') reactions on ^{93}Nb, ^{103}Rh and ^{115}In and high threshold reactions ^{209}Bi(n,xn) are in progress. Above 7 MeV neutron energy, the flux Y, amounts 5.4^{10} n/cm^2/s for the nearest distance from the target bottom and for 15 μA proton beam current.

ADS experiment
The consortium of major nuclear research institutions of the Czech Republic has been established in 1998 to solve the issues of spent nuclear fuel using ADS and Fluoride-molten-salt reactor systems.
Subcritical assembly "BLAŽKA" (multiplication factor k_{eff} = 0.56) has been designed at the CTU Prague. The blanket contains 232 fuel elements EK-10 (UO_2 + Mg alloy, 10% of ^{235}U, 1856 g of ^{235}U in total), surrounded by the NaF salt blocks (with polyethylene covers) and the graphite blocks assembled in regular square lattice clustered around by the reflector. Central graphite block of the blanket can be replaced by another materials and/or equipments (external neutron source). Another channels in the blanket serve for an installation of various detector assemblies.

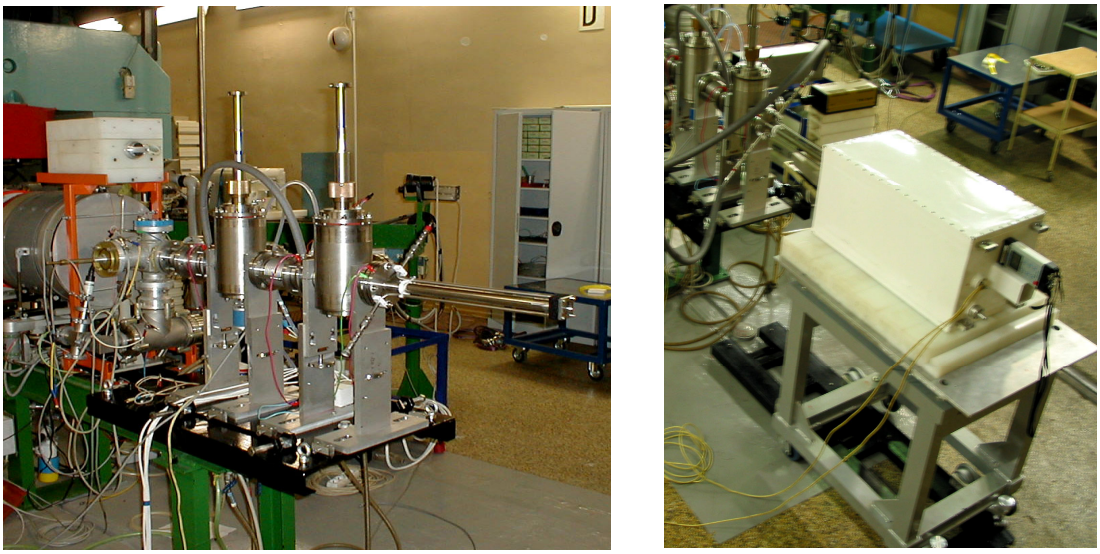

Figure 3. *The set-up of Be-target station (left) and the subcritical assembly (right)*

Design of external neutron source has been developed at NPI Řež. The fast neutron facility comprises high–power target station for liquid and solid targets. The collimator-free beam-guide ensure transport of accelerated ions from negative-ion extractor (of the NPI cyclotron U-120M) to the neutron source target. The neutron sources operate in the pulse mode. Outer dimensions of target station allow inserting into the centre of the subcritical assembly.
The d(18MeV)+Be(thick target) neutron source reaction was used in the first experiments focused mainly on the assembly responses to the neutron source power and to the position of external source in the blanket. An investigation of delayed neutrons was carried out as well. Three boron corona detectors were used for the “on-line” neutron detection. Preliminary results are compared with Monte Carlo (MCNP and MCNPX) simulations.

References

[1] R. A. Forrest, J. Kopecky, M. Pillon, K. Seidel, S. P. Simakov, P. Bém, M. Honusek and E. Simeckova, Validation of EASY-2005 using integral measurements, Monography, 5534 pp, UKAEA FUS 526, January 2006 Culham Science centre, Abingdon, Oxfordshire, OX14 3DB, UK.

[2] S.P. Simakov, P. Bém, V. Burjan, M. Götz, M. Honusek, U. Fischer, V. Kroha, J. Novák and E. Šimečková, Development of activation foils method for the IFMIF neutron flux characterization. 24-rd Symposium on Fusion Technology (SOFT-24), Warsaw, 18.-23. 09. 2006 Fus. Eng. and Design, to be published.

Research program of the SPHINX project in the framework of the Molten Salt Reactor development in the Generation IV International Forum activity

M. Hron, M. Mikisek

Nuclear Research Institute Rez plc, Husinec – Rez 130, 250 68 Rez, Czech Republic
hron@nri.cz

Abstract: Nuclear power is expected to become a source of energy being able to cover a significant part of the world energetic demand in the future. But its big disadvantage, the risk of the spent nuclear fuel, has to be solved. The Molten Salt Reactor (MSR) - SPHINX (SPent Hot fuel Incinerator by Neutron fluX) concept solves this principal problem of spent fuel treatment by means of so-called nuclear incineration.
It means burning of fissionable part of its inventory and transmutation of other problematic radionuclides by use of nuclear reactions with neutrons in a MSR - SPHINX system. This reactor system is an actinide burner and a radionuclide transmuter.
The R&D program of MSR - SPHINX concept contains reactor physical, chemical (partitioning) and structural material parts. In the frame of physical part, there are besides computational analyses also experimental activities involved in the program, which serves for a validation of computer codes and, finally, for a verification of design inputs for designing of a demonstration unit of the MSR-type. The molten fluoride salt demonstration unit is required to show the operation and design performance for closing the nuclear spent fuel cycle for PWR or VVER reactors operated in the once-through cycle mode.
The experimental program has been focused, in its first stage, on a short-term irradiation of small size samples of molten-salt systems as well as structural materials proposed for the MSR blanket in the field of high neutron flux of research reactors.
The proposed next stage of the program is focused on a large-scale experimental verification of design inputs by use of MSR-type inserting zones into the existing light water moderated experimental reactor LR-0, which may allow to modify it to experimental zero power salt reactor SR-0.
These realized experiments help us also to verify computational codes used, and to recognize some anomalies related to fluorides utilization.

Introduction

New transmutation technologies should make it possible to return a fuel component contained in nuclear fuel burned up in conventional nuclear reactors back to nuclear fuel cycle and to turn a significant part of long-lived nuclear waste (heavy metals from the transuranium region) to useful energy without rests and by an irreversible way.
Molten-Salt Reactor (MSR) represents one of the promising high temperature nuclear reactor types for future generation of electricity and of heat for hydrogen production. It also could be used as transmuter to burn plutonium and other transuranium elements occurring in the spent nuclear fuel of nowadays-existing nuclear reactor types. Molten-Salt Reactor is usually characterized, as a non-classical nuclear reactor type due to a specific character of its fuel, which is liquid – constituted by a molten fluoride salt mixture circulating between a reactor core and a heat exchanger. The fission material (uranium and/or transuranium elements) is dissolved in carrier molten salt, which is also a heat-transferring agent.
The other, very promising mode of Molten-Salt Reactor operation is based on the use of Th – U fuel cycle with minimized production of long-lived nuclear waste in comparison to the U – Pu fuel cycle currently used in present reactor types. In this mode, the MSR works as a reactor-breeder producing own fissile material ^{233}U from fertile ^{232}Th. Essentially the main advantages of MSR comes out from the prerequisite, that this reactor type should be directly connected with the “on-line” reprocessing of circulating liquid (molten-salt) fuel. This fuel salt clean up is necessary within a long run to keep the reactor in operation. As a matter of principle, it permits to clear away typical reactor poisons like xenon, krypton, lanthanides etc. and also the products of burned plutonium and transmuted minor actinides.

Renaissance of MSR technology in the frame of Generation IV international forum

About 25 years of interruption of any significant activities in the area of MSR technology development has caused rather difficult conditions for present day effort in the research and development of MSR technology in the frame of Generation IV International Forum. In September 2002, the Generation IV International Forum selected six nuclear reactor system concepts for further development as the fourth generation of nuclear power reactors. Among this six selected systems also appeared MSR. The MSR has been the only one concept with a significant innovation – liquid fuel circulating in the primary circuit and allowing an at least qausi-continuous recycling of fuel in a closed fuel cycle. The closed fuel cycle may be tailored to an efficient burn up of plutonium and minor actinides or to an efficient breeding ^{233}U and shifting the whole fuel cycle towards thorium – uranium cycle nearly avoiding generation of transuranium elements. For a coordination and leading of the R&D effort of the countries interested in individual systems, there have been the Steering Committees formed for each reactor concept including MSR. During the year 2005, there have been organized two meetings of the MSR SC. They decided beside others a principal division of the interest and responsibility of individual members for different priorities in the MSR R&D program:

1. Demonstration of feasibility and evaluation of performance of MSR as a ^{232}Th - ^{233}U breeder according to Generation IV criteria (France),
2. Evaluation of the performance of MSR for the amount and hazard of nuclear waste namely the LWR spent fuel (Euratom),
3. Exploration of the potential of molten salts as an efficient coolant for solid fuel reactors, as an alternative to gasses or liquid metals (USA)

The R&D program of MSR - SPHINX concept

One of the main feature of the SPHINX project is the developed concept of the transmuter and namely its blanket (core). This concept is based on the idea of utilization of an efficient burning of transuranium nuclei in a large size fuel channel in the epithermal energy range where the majority of their isotopes have resonances in their neutron cross-sections. The system might be critical system with the reactivity as well as power controlled by specific for the flowing liquid fuel control systems (based upon a control of liquid fuel composition or its flow characteristics) or a subcritical system (with the subcriticality margin of the order of several betas) which reactivity (keeping the prescribed level of subcriticality) is controlled in the same manner as in the above described case of a critical system and the system is kept in a steady state as well as its power is controlled (driven) by an external neutron source or by a driving zone (a part of a conventional reactor core).
The elementary module (Fig. 1) can be designed as a definitely subcritical hexagonal fuel channel being surrounded by six hexagonal graphite blocks, which being equipped by coaxial tubes (in which molten fluorides of long-lived radionuclides may flow) allowing an efficient transmutation of the long-lived radionuclides by an intensive flux of well thermalized neutrons. These elementary modules, which can be closely packed (joint) into a critical system or arranged in a complex of autonomous subcritical elementary modules driven by a set of external neutron sources or by a driving zone (a reactor core of another type, e.g. PWR, surrounding the subcritical elementary modules) represent in any case an intensive source of energy as well as of epithermal neutron flux which might be slowed down in graphite blocks and allow to incinerate very efficiently at least some of long lived fission products in a well-thermalized neutrons escaping the transmuter core.
These two purposes of the proposed blanket system utilization make it possible to use it as an efficient nuclear incinerator and actinide burner and, simultaneously, as an efficient energy source. Let us note that once such system is developed and proved it might serve as a new clean source of energy just by switching - over from uranium-plutonium to thorium-uranium fuel cycle and thus practically excluding generation of actinides. Before we are able to design a device we have to perform a broad experimental verification of design inputs for credible designing of a demonstration transmuter.
The feasibility of the main features of the SPHINX concept, its individual processes and the corresponding technological and operational units should be verified by an operation of a demonstration complex with power output of about 10 MWt. However, design of such a demonstration transmuter should be preceded by an extensive experimental verification of the

inputs. The process of experimental verifications has begun in 2002; the obtained results and the experimental programs and projects have been described in details in a series of publications [4].
One of the most impressive examples of experimental program is the utilization of the zero power experimental reactor LR-0 (Light-water Reactor) being operated in the Nuclear Research Institute Řež, Czech republic. This full scale physical model of the PWR cores was preliminary modified to zero power experimental reactor SR-0 (Salt Reactor) allowing to measure all the neutronic characteristics of the MSR burner and or breeder blanket at first by room temperature and in future stage by conditions close to operational. So far, there have been some preparatory modifications and experimental programs performed in the frame of the national project EROS (Experimental zeRO power Salt reactor SR-0) being supported by Ministry of Industry and Trade of the Czech Republic and partly by the Radioactive Waste Repository Authority and Czech Power Generating Board with the continuous information of the Euratom community as well as the MSR SC of GIF.

The current status of the EROS project experimental program

The first (more or less geometrical) testing of a prototype SR-0 hexagonal shaped block manufactured from nuclear aluminum and inserted into the LR-0 driving core was performed at the end of the year 2005. During the first half of the year 2006, the internal structures of the prototype blocks have been manufactured and tested allowing to perform the first series of critical experiments with 3 different variants (contents) of the SR-0 prototype block (Fig. 2) Since July 2006, the prototype blocks have been completed and inserted individually (Fig. 3) into the LR-0 driving core (Fig.4) and during September and October 2006 the first critical experiments with the individual prototype blocks inserted into the corresponding LR-0 driving cores have been performed. Second series of critical experiments with inserting zones modeling elementary modules of the SR-0 blanket have been performed in the first half of 2007. Results of calculations (Fig. 5) will be verified by experimental measurements. The primary results of measurements performed so far (critical levels of light water moderator, reaction rates of reactions concerning activation detectors, gamma-scanning in various position of inserted zone) are being evaluated.

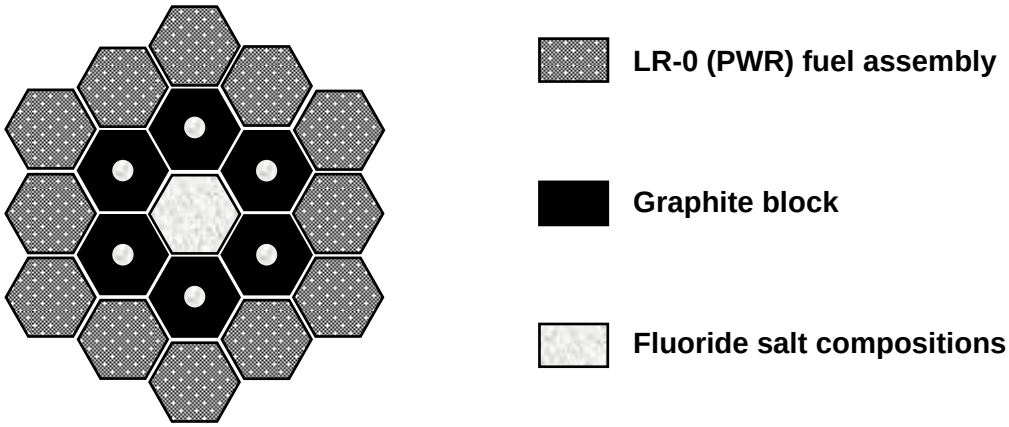

***Figure 1**. Modeling of the elementary module of the SR-0 blanket by MSR-type inserted zones*

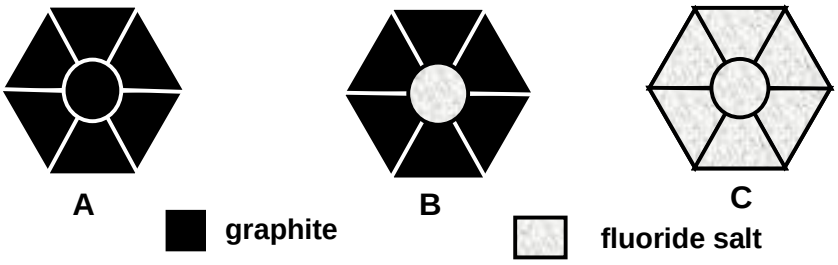

***Figure 2**. Modeling of the three types of prototype blocks of the SR-0 blanket*

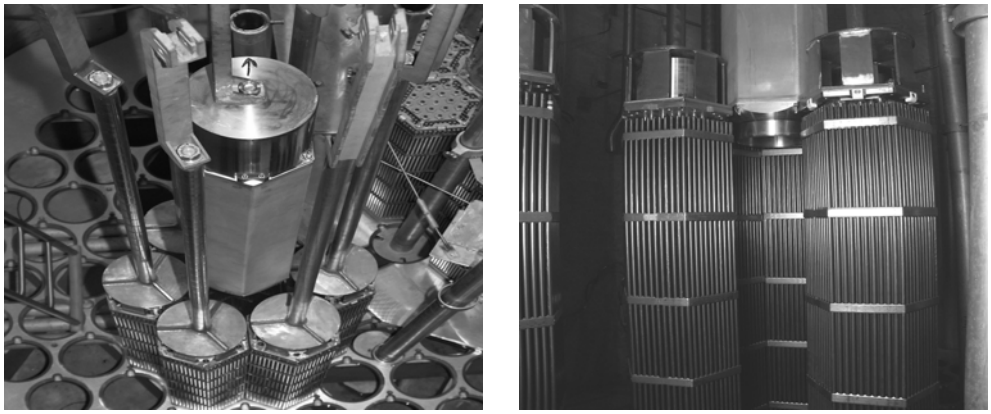

Figure 3. *The prototype blocks, while inserted into the LR-0 driving core*

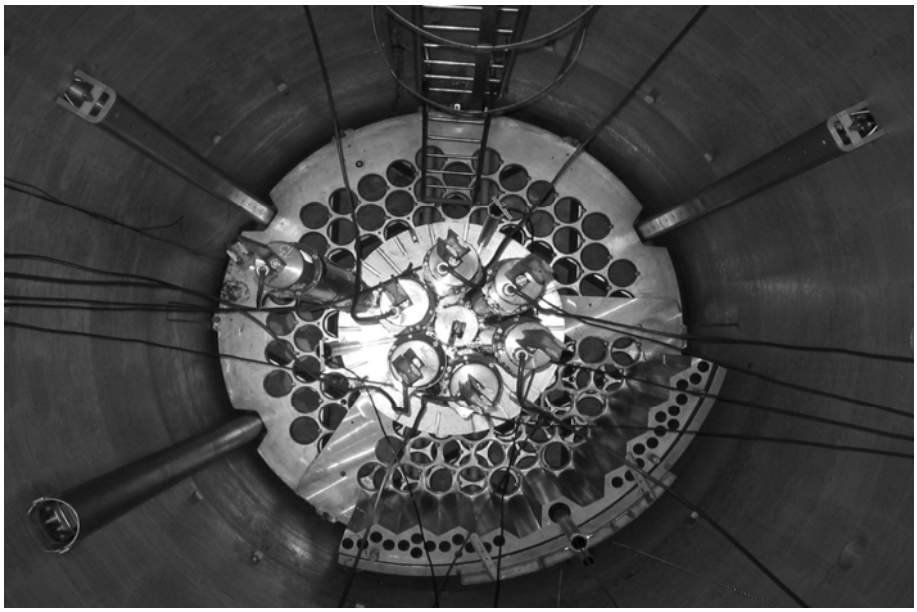

Figure 4*. The view into the LR-0 driving core*

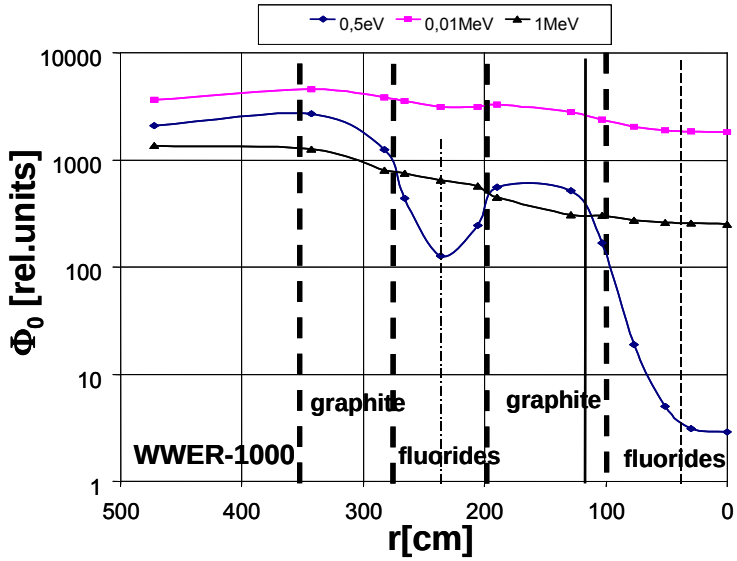

Figure 5. *Calculated radial distribution of neutron flux in the SPHINX elementary module*

In the second half of the year 2007, one of the elementary modules has been arranged and adopted (Fig. 6) for an irradiation by hard spectrum of neutrons generated by neutron generator which was installed at the cyclotron accelerator in the Institute of Nuclear Physics of the Czech Academy of Sciences located in Rez near Prague (Fig. 7).

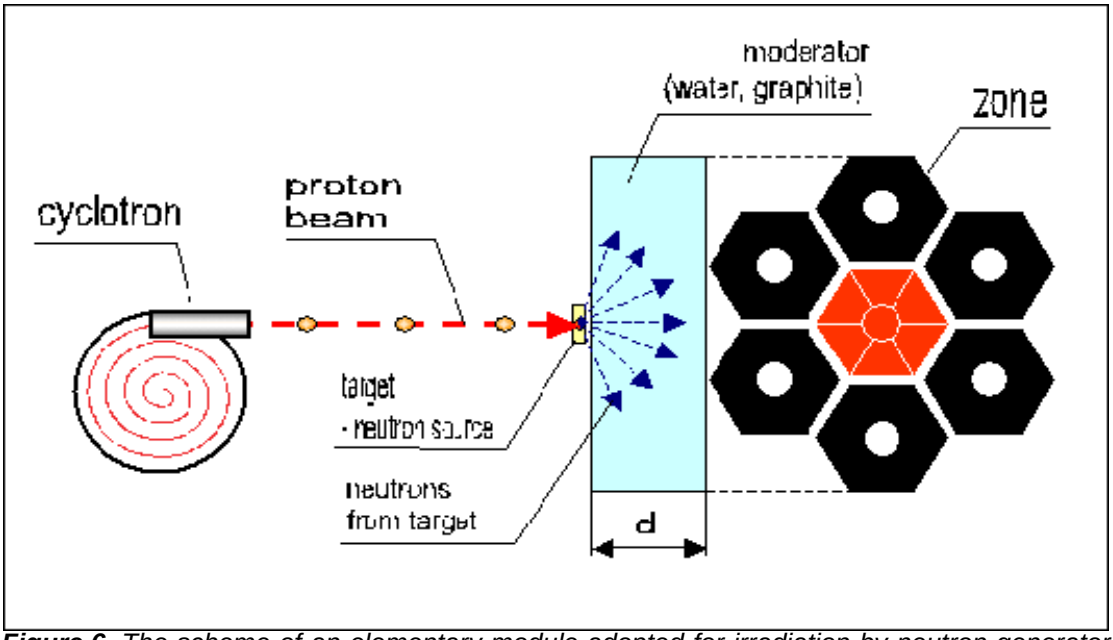

Figure 6. *The scheme of an elementary module adopted for irradiation by neutron generator being installed at the cyclotron accelerator*

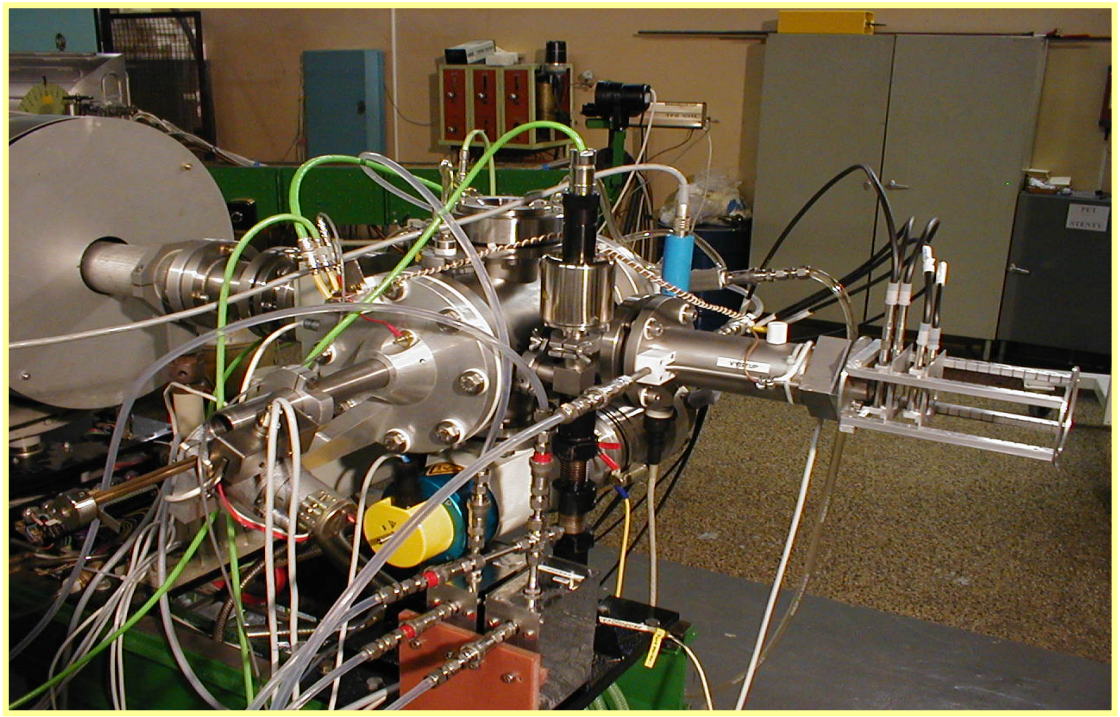

Figure 7. *The NG 2 neutron generator at the experimental hall of the cyclotron laboratory in the Institute of Nuclear Physics in Rez*

Summary and Conclusions

The Molten Salt Reactor (MSR) - SPHINX (SPent Hot fuel Incinerator by Neutron fluX) concept has been under development in the Czech Republic and incorporated into the European framework program and recently into a proposed R&D program of MSR

development in GEN IV as an actinide burner in resonance neutron spectrum and a radionuclide transmuter in a well-thermalized neutron spectrum.
In the frame of its reactor physical part, there have been experimental activities involved in the program, recently, which serves for a verification of design inputs for designing of a demonstration unit of the MSR-type. The experimental program, which has been focused, in its first stage, on a short-term irradiation of small size samples of molten-salt systems as well as structural materials proposed for the MSR blanket in the field of high neutron flux of research reactors, will be in the proposed next stage of the program focused on a large-scale experimental verification of design inputs by use of MSR-type inserted zones into the existing light water moderated experimental reactor LR-0, which may allow to modify it to experimental zero power salt reactor SR-0. There has been a preparatory stage of the project called EROS started in the year 2006 and a brief description of the so far prepared and performed experiments was introduced. New experiments with MSR-type zones irradiated by cyclotron based neutron source are planned at the end of 2007 and should go on in the year 2008. The whole SPHINX project research program and namely its experimental part EROS is open for a broader multinational collaboration.

Acknowledgement
The SPHINX project as well as its part, the project EROS being focused on a preparation of an experimental zero power salt reactor SR-0 have been supported by the Ministry of Industry and Trade of the Czech Republic and partly by the Radioactive Waste Repository Authority and Czech Power Generating Board. The authors would like to express a deep gratitude for that long-term financial and technical support.

References

[1] M. Hron, “Project SPHINX - Spent Hot Fuel Incinerator By Neutron Flux (The Development of a New Reactor Concept with Liquid Fuel Based on Molten Fluorides)”, 1st International Symposium on Innovative Nuclear Energy Systems for Sustainable Development of the World, Tokyo, Japan, (31 October-4 November, 2004).
[2] T. Nakajima, H. Groult, “Fluorinated materials for energy conversion”, Chapter 24, Elsevier Science& Technology, 2005.
[3] J.-C. Garnier et al., "The MOST Project: Key – Points and Challenges for the Feasibility of Molten Salt Reactors“, International Congress on Advances in Nuclear Power Plants (ICAPP’05), May 15-19, 2005, Seoul, Korea.
[4] M. Hron, “Project E R O S (Experimental zeRO power reactor SR-0 with Salt fuel) Development of a New Reactor Concept with Liquid Fuel Based on Molten Fluorides for Reducing the Amount and Hazard of Nuclear Waste“, International Conference GLOBAL’05, Tsukuba, Japan, October 9-13, 2005.
[5] M. Hron and M. Mikisek: “Experimental Verification of Design Input of the SPHINX Concept of MSR (Project EROS – Experimental Zero Power Reactor SR-0 with Salt fuel)” 2nd International Symposium on Innovative Nuclear Energy Systems for Sustainable Development of the World, Yokohama, Japan, (26 - 30 November, 2006).

Nuclear research at IRMM and the JRC

A.J.M. Plompen

European Commission, Joint Research Centre, Institute for Reference Materials and Measurements, Retieseweg 111, 2440 Geel, Belgium
arjan.plompen@ec.europa.eu

Abstract: The Joint Research Centre (JRC) is a Directorate General of the European Commission (EC) that was founded as a result of the Treaty of Rome. It consists of seven institutes on five sites in Europe that have developed from an emphasis on nuclear research, to research in a wide range of fields of interest to European citizens. Here some aspects about nuclear research will be highlighted in the JRC and in the Institute for Reference Materials and Measurements (IRMM). Some examples will be given of recent nuclear data measurements.

The Joint Research Centre

The JRC was founded as a result of the Treaty of Rome, signed in 1957, which states that the EC shall establish a joint nuclear research centre that may involve separate establishments. Currently, the JRC consists of seven institutes that are located in five different sites, the IRMM in Geel, Belgium, the Institute for Energy (IE) in Petten, The Netherlands, the Institute for Transuranium elements (ITU) in Karlsruhe, Germany, the Institute for Prospective Technological Studies (IPTS) in Sevilla, Spain, the Institute for Health and Consumer Protection (IHCP), the Institute for Environment and Sustainability (IES) and the Institute for Protection and Security of the Citizen (IPSC) in Ispra, Italy. The names of these institutes clearly reflect the diversified nature of the activities of the JRC that has developed over the years from an initial nuclear character. The multi-annual work program for Framework Program 7 (FP7) has five themes, "Prosperity in a knowledge intensive society", "Solidarity and the responsible management of resources", "Security and freedom", "Europe as a world partner" and "Euratom". Research should support legislation and, in general, serve society. As a directorate general, the JRC is the responsibility of the Commissioner for Science and Research, Janez Potoçnik [1].

JRC Euratom

The nuclear activities of the JRC are part of Euratom, the European Atomic Energy Community. Activities concern nuclear fusion and fission energy and involve the two DGs under the responsibility of the Commissioner for Science and Research, the Research DG (RTD) and the JRC. RTD is responsible for the so-called indirect actions of EURATOM which are implemented through competitive calls, while the JRC is responsible for the direct actions. The JRC's direct actions are limited to the domain of nuclear fission energy. Under the umbrella of nuclear safety and security about 45% of the activities are in the domain of waste management, environmental impact and basic knowledge, 25% concerns nuclear safety and 30% is nuclear security. The JRC owns the High Flux Reactor which is operated by the Nuclear Reactor consultancy Group (NRG) in Petten and the JRC is involved in decommissioning and waste management of its sites. Projects of JRC Euratom are carried out at IRMM, IE (nuclear safety and nuclear waste), ITU (nuclear waste, safeguards and basis science) and IPSC (safeguards) [2]. JRC coordinates the European Community's contribution to the Generation-IV International Forum (GIF).

The Institute for Reference Materials and Measurements

IRMM was founded as the Central Bureau for Nuclear Measurements in 1960. Its Van de Graaff accelerator laboratory started in 1962 and the Geel linear electron accelerator laboratory GELINA started in 1965. In 1993 the institute was renamed to IRMM to reflect the process of diversification and the ensuing change of emphasis that had evolved over the years. IRMM's mission is to promote a common and reliable European measurement system in support of EU policies. Current application areas are food safety and quality, biotechnology, health, environment, agriculture and nuclear security [2, 3].

Euratom at IRMM
IRMM Euratom consists of four projects. Two of these involve neutron measurements, "ND-STDS Basic research in nuclear physics and nuclear data standards" and "ND-MINWASTE Nuclear data for radioactive waste management and safety of new reactor developments", one concerns nuclear safeguards "METRO Providing metrological tools to support nuclear safeguards activities" and one concerns radionuclide metrology "RADMET Radionuclide metrology for primary standardisation and policy support" [2,3]. IRMM's nuclear measurements support studies to improve safety of existing nuclear power plants, to develop a new generation of nuclear power plants, to reduce nuclear waste by transmutation and to improve the knowledge of nuclear processes.

IRMM neutron measurements and international collaboration
The Neutron Physics unit that runs actions ND-MINWASTE and ND-STDS is extensively involved in international collaborations that involve many users of its neutron measurement facilities. Currently, it is engaged in six indirect actions of the European Commission, EUROTRANS (the integrated project on European transmutation), NUDAME (a transnational access facility), Ancient Charm[1] (Analysis by Neutron resonant Capture Imaging and other Emerging Neutron Techniques: new Cultural Heritage and Archeological Research Methods), EFNUDAT (an integrated infrastructure initiative European Facilities for Nuclear Data Measurements), CANDIDE (Coordination Action on Nuclear Data for Industrial Development in Europe), and EUFRAT (European facility for innovative reactor and transmutation neutron data, transnational access, starting 2008). Several collaboration agreements with European partners are active, e.g. with the Commissariat à l'Énergie Atomique (CEA, France), the National Institute for Physics and Nuclear Energy (NIPNE, Romania), the Institute for Nuclear Research and Nuclear Energy (INRNE, Bulgaria) and the Istituto Nazionale di Fisica Nucleare (Italy). The unit takes part in the collaboration between EURATOM and the US Department of Energy. The involvement concerns fission measurements with Los Alamos National Laboratory, and capture, transmission and elastic scattering measurements as well as detector characterisation with Oak Ridge National Laboratory. IRMM also participates in a collaboration between Euratom and Atomic Energy of Canada Ltd on elastic scattering of deuterium in the interest of operational safety of CANDU reactors.
The unit participates and defines part of its projects through collaborations organised by the OECD Nuclear Energy Agency (the Joint Evaluated Fusion and Fission file project - JEFF, the Working Party on Evaluation Cooperation WPEC and the Nuclear Science Committee - NSC), as well as by the IAEA Nuclear Data Section (NDS). The NDS organises so-called Coordinated Research Projects (CRPs) and examples of IRMM involvement are the Th/U CRP, the standards CRP, a CRP on standards for Neutron Activation Analysis (NAA), the Reference Input Parameter Library-3 CRP and the Minor Actinide Nuclear Reaction Data CRP. IRMM participates as observer for the EC in the International Nuclear Data Committee which advises on the program of work of the NDS.

Neutron measurements

Here several examples will be given of ongoing work. More information about recent work may be obtained from the proceedings of the ND2007 conference, 22-27 April 2007, Nice, France (to be publ.) and from the proceedings of the AccApp07 conference 30 July - 3 August 2007, Pocatello, Idaho, USA (to be publ.). Neutron measurements are carried out at two accelerator based neutron sources, GELINA the Geel Linear Electron LINear Accelerator laboratory that hosts a pulsed white neutron source for high resolution neutron time-of-flight measurements with neutrons of energies between 10 meV and 20 MeV [4-6], and the Van de Graaff laboratory that is specialised in quasi mono-energetic neutron fields with energies from 0.1 to 21 MeV [7].
Measurements of inelastic scattering cross sections and cross sections for (n, 2n) reactions constituted a highlight in recent years. The isotopes that were studied were ^{52}Cr [8], ^{58}Ni, ^{206,207,208}Pb, ^{209}Bi [9] and most recently ^{56}Fe [10]. The methodology and the use of digitizers are described in references [11, 12]. For ^{56}Fe a measurement campaign was conducted in

[1] Funded through NEST (New and Emerging Science and Technology) as a STREP (Specific Targeted Research Project)

2007 and the preliminary results are shown in another contribution to these proceedings [10]. Here an accuracy of better than 5% is claimed for the first 4 MeV of excitation energy. Data for ^{56}Fe were taken with the recently installed GAINS setup (Germanium array for inelastic neutron scattering) that will evolve from eight to ultimately twelve detectors. GAINS was first operated in 2007 and will be completed in 2008. It is open to proposals from external users. An agreement with the National Institute for Physics and Nuclear Engineering in Bucharest, Romania was established to support neutron measurement collaborations, including GAINS.

Earlier measurements on lead and bismuth were contributed to the EUROTRANS integrated project. These have recently been used in new evaluations for these isotopes by the EUROTRANS collaboration and these new evaluations will be part of the next version of the JEFF library (JEFF-3.2). The new evaluations for lead and bismuth also benefitted from recent capture measurements at GELINA on lead (^{206}Pb [13]) and ^{209}Bi (ND2007 proceedings). For the latter the isomer ratio for the ^{209}Bi(n,γ)^{210m,g}Bi was determined by measuring characteristic gamma-rays identified with germanium detectors. This work is part of EUROTRANS and is carried out in collaboration with CEA.

Another important collaboration with CEA addresses cross section measurements on ^{241}Am. Samples of $^{241}AmO_2$ were prepared at ITU using impregnation techniques developed in the innovative fuels program of that JRC institute. The raw, high purity $^{241}AmO_2$ material was contributed by CEA. Measurements benefitted from the NUDAME transnational access scheme. So far, five data points were obtained for the ^{241}Am(n,2n)^{240}Am reaction by means of the activation technique using quasi mono-energetic neutrons at the Van de Graaff laboratory. In addition, low energy transmission measurements were carried out for neutron energies from 0.1 to 5 eV. These data are currently under analysis and several additional measurement campaigns are scheduled to optimise the measurement conditions needed to obtain improved transmission data.

A very successful example of the participation in CRPs organised by IAEA-NDS concerns the capture data that were obtained at GELINA for ^{232}Th. Measurements were performed in the resolved and unresolved resonance region and the latter were shown to be state-of-the-art in terms of final accuracy (<2%) [14, 15]. The data were contributed to a joint evaluation by the CRP and excellent consistency was obtained with measurements from the n_TOF collaboration and other authors. The evaluated file for ^{232}Th was adopted in the most recent release of the Evaluated Nuclear Data File of the USA (ENDF/B-VII) and will be adopted for JEFF-3.2.

With Oak Ridge National Laboratory (ORNL) capture and transmission measurements are being performed for important fission products such as Rh and Cs. Transmission and capture results are being determined at the GELINA facility and the resonance analysis is carried out with assistance of ORNL. For the interpretation of the unresolved resonance region IAEA-NDS and INRNE are involved.

In the domain of neutron-induced fission measurements there are several interesting activities. First there is the search for a fission isomer in ^{235}U. Using quasi mono-energetic neutrons of 0.95 and 1.27 MeV incident on a sample of ^{234}U of high purity cyclic activation of a fission isomer attempted. An isomer was identified with a half life of 3.6(1.8) ms that shows delayed fission [16]. Second, measurements are being carried out to study the prompt fission neutron spectrum for incident neutrons of 0.5 MeV on ^{235}U. Finally, in a collaboration with the University of Gent the fission of ^{236}U was studied in the range from 1 eV to 10 keV. For accurate measurement a high purity sample is required with a minimum amount of ^{235}U. For the residual impurity of this isotope the contribution was subtracted on the basis of a back-to-back fission yield measurement with on the one side the high purity ^{236}U and on the other side ^{235}U. Results show that there are many fewer resonances with a sizeable fission width than was established in the literature and the resonance integral is about two orders of magnitude reduced compared to current evaluations.

A study of the ^{16}O(n,α) reaction was undertaken at the Van de Graaff laboratory. This work was started as a result of a high priority request from a subgroup of the Working Party on Evaluation Cooperation [17]. Measurements were conducted in the energy range up to 6 MeV over a period of two years and a final accuracy of 6.5% was achieved, meeting the required accuracy. Modifications for evaluated files have been proposed and the results will be released following a final publication.

Very interesting was the development of Neutron Resonance Capture Analysis (NRCA) that allows to determine sample composition by non-destructive analysis. Here, the GELINA neutron time-of-flight facility is used in combination with a capture setup based on C6D6

detectors to identify and quantify elements by characteristic resonances of their isotopes. NRCA has been applied to artefacts of archeological interest such as pottery and bronze works [18]. The success of NRCA was the starting point for the Ancient Charm project which investigates related techniques and the possibilities to perform imaging of elemental distributions in artefacts. NRCA may also be used to identify and quantify impurities of samples used in cross section measurements [19].

References

[1] For information about the JRC, see ec.europa.eu/dgs/jrc, for the Commissioner for Science and Research, ec.europa.eu/Commission_Barroso/Potocnik.
[2] JRC project definitions may be found at projects-2007.jrc.ec.europa.eu for 2007 and similarly for other years.
[3] For information about the IRMM consult irmm.jrc.ec.europa.eu.
[4] D. Tronc et al., Nucl. Instr. Meth., A 228, 217 (1985); and references therein.
[5] M. Flaska et al., Nucl. Instr. Meth., A 531, 392 (2004).
[6] D. Ene et al., submitted for publication.
[7] A. Plompen, Proc. Enlargement workshop NEMEA-3, 25-28 October 2006, Borovets, Bulgaria, EUR 22974 EN, ISBN 978-92-79-06158-5, bookshop.europa.eu (2007).
[8] L.C. Mihailescu et al., Nucl. Phys. A 786, 1 (2007).
[9] L.C. Mihailescu et al., Nucl. Phys. A (2008).
[10] A. Negret et al., these proceedings.
[11] L. C. Mihailescu et al., Nucl. Instr. Meth. A 531, 375 (2004).
[12] L. C. Mihailescu et al., Nucl. Instr. Meth. A 578, 298 (2007).
[13] A. Borella et al., Phys. Rev. C 76, 014605 (2007).
[14] A. Borella et al., Nucl. Sci. Eng. 152, 1 (2006).
[15] I. Sirakov et al., Ann. Nucl. Energy, in print.
[16] A. Oberstedt et al., Phys. Rev. Lett. 99, 042502 (2007).
[17] The NEA Nuclear Data High Priority Request List - HPRL, www.nea.fr/html/dbdata/hprl.
[18] H. Postma and P. Schillebeeckx, J. of Radioanal. Nucl. Chem., 265, 297 (2005)
[19] A. Borella et al., these proceedings and references therein.

Nuclear data needs and developments for fusion

R. A. Forrest

Euratom/UKAEA Fusion Association, Culham Science Centre, Abingdon, Oxon, OX14 3DB, UK
robin.forrest@ukaea.org.uk

Abstract: Fusion research has as its aim to achieve as soon as possible the commercial generation of electricity. ITER and IFMIF, which are being built or are under development, are crucial for the design of fusion power plants. ITER is of similar dimensions to a power plant, and will be constructed at Cadarache, France. IFMIF is a materials test facility, based on accelerating deuterons into lithium that will generate intense fluxes of neutrons that will be used to investigate the damage to materials needed in the prototype power plant.
Designs for such devices require neutron and photon transport calculations to generate the spectra required to provide the nuclear responses. Such calculations require cross section data for all the elements present, typically at energies (14 MeV) larger than those required for fission. The design of IFMIF means that neutrons with energies up to 55 MeV are of importance, so increasing further the amount of nuclear data required. Emphasis is given to the development of activation libraries which include many targets, including radioactive ones. The method of importance diagrams has been employed for energies above 20 MeV (relevant to IFMIF) and a large number of new important reactions are identified. Many of these reactions have no experimental data and the needs for accurate calculated cross sections and new measurements are discussed.

Introduction

Fusion research worldwide is focused on developing the ability to generate electricity. The main areas of work are in support of the ITER and IFMIF projects; ITER is a large experimental device that will be constructed at Cadarache in France while IFMIF is a materials testing facility. Following the successful outcome of these projects it will be possible to design and build DEMO which will generate electricity and act as a prototype for future commercial designs. A full description of the roadmap for fusion research and nuclear data needs for ITER and IFMIF were presented at the NEMEA-3 workshop [1] so only a summary is presented here. Nuclear data for fusion can be broadly split into three parts: cross sections for neutronics, cross sections for activation and decay data. The present paper will concentrate on the development of nuclear data for activation, especially on the methods that are available to validate and test the data as well as how the most important reactions can be identified. Only once these are known can a realistic programme of improvement by experiments and theory be undertaken.
ITER is designed [2] to generate 500 MW of fusion power, up to ten times more than the energy supplied. It will be able to demonstrate all the technologies required for DEMO except one; the relatively low fluences mean that the materials will not experience the levels of damage envisaged in DEMO. It is planned that this high fluence testing will be carried out in IFMIF [3], which is being investigated as part of the European/Japanese Broader Approach agreement.
The design and licensing of devices such as ITER and IFMIF rely to a large extent on data provided by neutronics design calculations. These require qualified computational tools and validated nuclear data for the modelling of neutron transport and the calculation of relevant nuclear responses.

Nuclear data for fusion

According to the fusion technology strategy the areas of most importance for nuclear data work are the Test Blanket Modules (TBM) in ITER and in the design of IFMIF [4]. TBMs will provide the capability to test the various blanket concepts. These are very complex components with issues of thermal hydraulics and diagnostics as well as tritium breeding. IFMIF will use beams of high energy deuterons and therefore the interaction of these with materials emphasises other areas of nuclear data. In addition to nuclear data it is necessary

to develop and qualify computational tools, especially in the area of sensitivity analysis and uncertainty and to carry out integral experiments to test the nuclear data and tools.
The range of the nuclear data required for fusion has increased dramatically because of IFMIF. Whereas for ITER only data for neutron and photon transport calculations were needed, for IFMIF the upper energy limit has increased from 20 to 60 MeV and the incident particles now include protons and deuterons as well as neutrons.
Activation calculations require cross sections for a larger number of target nuclides than transport since both stable and radioactive target must be considered. The reason is that in high neutron fluxes long-lived radioactive nuclides are present long enough to react, leading to multi-step pathway production of activity. However, although about twice as many targets and many more reaction types are needed than in a transport file, only cross sections as a function of energy data need to be included. Another type of nuclear data that must be considered, especially for activation calculations, are decay data including half-lives, energy releases and decay modes.

The role of nuclear data

The role of nuclear data for the two projects discussed above; ITER and IFMIF are rather different as is the emphasis that needs to be placed on the two main types of nuclear data, transport and activation. Transport data are required for the main elements in the device under study; they must be comprehensive and should include covariance information. By contrast, for activation impurities, whilst unimportant for transport, often dominate the response in terms of activity or gamma dose rate. This means that once data libraries have been assembled it is necessary to determine which radionuclides are important and the reactions that are responsible for their production.
Deficiencies need to be addressed by new measurements and it is especially important that these cover as wide an energy range as possible. However, many of the reactions identified are unlikely to be measured in the near future because either the target nuclide is radioactive or the daughter nuclide is stable or very long-lived. In such cases it is necessary to rely on model calculations and this area has had major advances recently, not as regards new physical models but rather in the ease of use of the existing models, and the combination of them so that complete nuclear data files can be produced relatively quickly. This enables starter files to be generated that can be supplemented by well measured quantities or even to act as a final file where none existed before. These model codes are starting to address the area of covariances and uncertainty and promise the ability to produce data which are currently missing and much needed.
The current data library for activation used extensively in European studies is EAF-2007 [5]. This contains decay data for 2,231 nuclides, neutron-induced cross section data for 65,565 reactions, deuteron-induced cross section data for 66,864 reactions and proton-induced cross section data for 67,925 reactions. Not all of these data are of equal weight for fusion applications, and it crucial that they are ranked so that scarce resources can be concentrated on the most important. The main tool for this is importance diagrams [6], and these have been recently extended so that the higher energies in EAF-2007 can be treated. As an example of the determination of the important radionuclides and reactions consider one of the importance diagrams for vanadium.
Figure 1 shows the diagram for γ dose. The diagram is generated following a series of inventory calculations carried out with mono-energetic neutrons, and the nuclides that dominate, i.e. produce more than 50% of the dose at various decay times are identified. These results are then shown in the diagram by regions labelled by the nuclide. Thus at decay times greater than ~ 1 10^7 s at energies < 5 eV and ~ 100 eV there are two regions where ^{60}Co dominates. Below 20 MeV this diagram is similar to that shown in the 'Activation Handbook' [7] a large compilation containing importance diagrams covering the energy range up to 20 MeV for all the elements, calculated with EASY-2003. Minor differences are due to changes in the cross sections between the two libraries. Of more interest is the new region above 20 MeV where three new nuclides are shown: ^{48}V, ^{44}Sc and ^{40}K. The fact that new radionuclides appear is somewhat surprising, it was expected that broadly the same set of nuclides would remain dominant even > 20 MeV. So far the study of importance diagrams calculated with EASY-2007 only covers the elements H – Xe so the conclusions are not complete. There are, so far 15 new nuclides seen in the diagrams (Primary nuclides contributing > 50 %), while 109 new Secondary nuclides (contributing > 1 and < 50%) are

found. The new Primary nuclides are ^{7}Be, ^{11}C, ^{48}Ca, ^{50}Cr, ^{66}Ga, ^{72}As, ^{76}Br, ^{82m}Rb, ^{86}Y, ^{108}Cd, ^{114}Cd, ^{109}Sn, ^{124}Sn, ^{124}I and ^{124}Xe. Below 20 MeV the reactions responsible for producing the Primary nuclides are much the same as found previously but above 20 MeV a wide range of more 'exotic' reactions are revealed. Previously only six reactions on ^{14}N were involved in producing the Primary nuclides while for EAF-2007 fifteen now need to be considered. As an example ^{14}N(n,pα)^{10}Be is now involved in the pathways for the production of ^{3}H, ^{8}Li and ^{10}Be.
The analysis for EAF-2007 is not yet complete, but the summary of the EAF-2003 library is given: while 1,917 nuclides are present, 754 are sufficient to describe the activation properties of all elements for irradiations below 20 MeV and decay times up to 10^{6} years. Similarly 1,341 reactions out of the total of 12,617 present suffice to produce all the dominant nuclides. This is a very significant reduction and means that effort can be focussed on improving reactions that are most important for applications such as ITER. This focussing is developed further in references [8] and [9] which discuss the data needs for both decay data and cross sections.

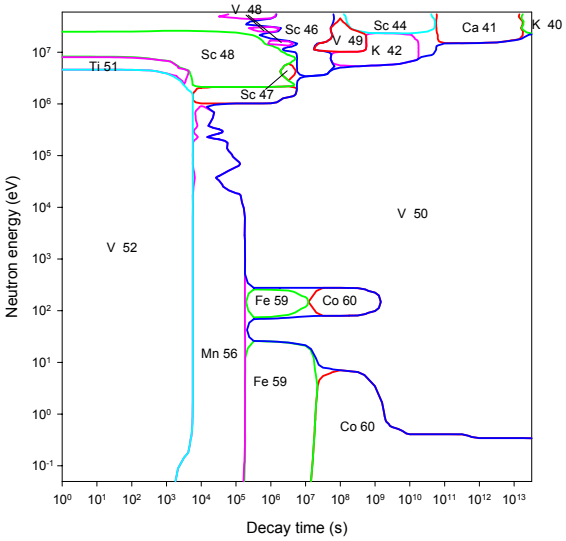

Figure 1. *Dose importance diagram for V.*

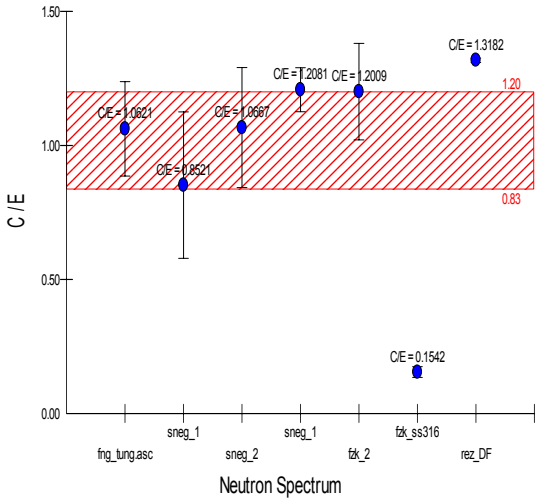

Figure 2. *Integral data for ^{182}W(n,p)^{182}Ta.*

Validation of activation libraries

The validation of the EAF libraries has been done by comparing measurements of the activity of a range of materials in fusion relevant neutron spectra (integral data) and comparing these with calculations with EASY. An approach which associates C/E not with the radionuclide but with the reaction producing it has several advantages. EAF-2007 is being validated at present, in the validation report for EAF-2005 [10], 453 reactions were considered and the report shows C/E plots for each as well as graphs of the differential data. Figure 2 shows results for ^{182}W(n,p)^{182}Ta, in this case there is overlap between the band representing the EAF-2007 library uncertainty and most of the error bars of the individual measurements and so the reaction is judged to be validated. This example shows results for several neutron spectra, unfortunately for most of the reactions there are only one or two C/E values indicating the need for more measurements. When the reactions that have either differential or integral data are counted it is found that there are only about 1,700. This raises the question as to how the majority of reactions in a library such as EAF-2007 can be checked.
A statistical approach has been developed [11] which involves plotting various quantities such as the maximum cross section (σ_{max}) of a reaction as a function of *A* or *s* (asymmetry). Such a plot is shown in Figure 3 for (n,α) reactions and it can be seen that there is a clear trend which makes it easy to identify reactions that are very discrepant. This has been found to be a very efficient method of spotting reactions with gross errors and was used extensively in the production of EAF-2007.

Development needs

For the present 60 MeV activation libraries only the n-induced one has been extensively validated and compared with differential data, much work remains to be done on general improvements of the charged particle libraries. The n-induced library contains uncertainty data for each reaction, but only in a simplified form. There is a need to extend these to more energy groups using existing evaluations, experimental data and model calculations.

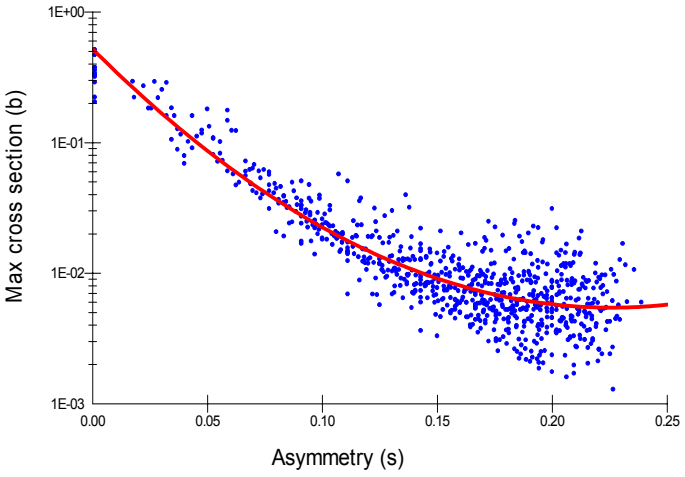

Figure 3. *σ_{max} for (n,α) data in EAF-2007 plotted as a function of asymmetry.*

Uncertainty data are required for both of the charged particle libraries. As noted above only a very small part of the EAF cross section library is supported by experimental data. This needs to be expanded. Especially valuable are data around or above 20 MeV since they can be very important in deciding between different model calculations. Integral data especially with neutron spectra that extend above 20 MeV are also very important in validating data libraries.

Conclusions

Neutron-induced activation files have reached a high standard, and it is known which reactions are of high priority for improvement. The need for new differential data, particularly around 20 MeV are crucial in supporting model calculations. IFMIF is responsible for a major extension of data needs, as all data files need to be extended at least up to 60 MeV. The range of materials is similar to that required for ITER. For activation it has been necessary to consider reactions of both deuterons and protons with materials, and unlike the neutron-induced library the experimental support is limited – there are no integral measurements and even the most important reactions are not yet identified. Uncertainty data (not yet covariances) need extending for the n library and including for the d and p ones. The development work on new tools and the benchmarking and validation of new files is essential, and will expand as the data needs become focussed on the higher accuracies that will become essential to support the final design and operation of the ITER and IFMIF devices.

Acknowledgements

This work, supported by the European Communities under the contract of Association between EURATOM/UKAEA, was carried out within the framework of EFDA. The views and opinions expressed herein do not necessarily reflect those of the European Commission.

References

[1] NEMEA-3, 25-28 October 2006, Borovets, Bulgaria, Proceedings, Editor A.J.M. Plompen, EUR22794 EN, 2007.
[2] N. Holtkamp, An Overview of the ITER Project, 24th Symposium on Fusion Technology, Sept. 2006, Warsaw, Poland. To be published in Fus. Eng. Design.
[3] IFMIF International Team, IFMIF Comprehensive Design Report, 2004.
[4] P. Batistoni, U. Fischer and R.A. Forrest, Requirements for nuclear data development and neutronic analysis efforts in the EU Fusion Technology Program 2007-2013 (FP7), EFF-DOC 959 (2006).
[5] R. A. Forrest, J. Kopecky and J-Ch. Sublet, The European Activation File: EAF-2007 neutron-induced cross section library, UKAEA FUS 535 (2007).
[6] R.A. Forrest, Importance diagrams – a novel presentation of the response of a material to neutron irradiation, Fus. Eng. Design, 43, 209-235 (1998).
[7] M.R. Gilbert and R.A. Forrest, Comprehensive handbook of activation data calculated using EASY-2003, Fus. Eng. Design, 81, 1511-1516 (2006).
[8] R.A. Forrest, Data requirements for neutron activation Part I: Cross sections, Fus. Eng. Design, 81, 2143-2156 (2006).
[9] R.A. Forrest, Data requirements for neutron activation Part II: Decay data, Fus. Eng. Design, 81, 2157-2174 (2006).
[10] R.A Forrest et al., Validation of EASY-2005 using integral measurements, UKAEA FUS 526 (2006).
[11] R.A. Forrest and J. Kopecky, Statistical analysis of cross sections – A new tool for data validation, Fus. Eng. Design, 82, 73-90 (2007).

The use of Neutron Resonance Analysis for the characterization of reference materials used for cross section measurements

A. Borella[1)], H. Postma[2)], M. Moxon[4)], A. Plompen[1)], C. Sage[1,3)] and P. Schillebeeckx[1)]

1) EC-JRC-IRMM, Retieseweg 111, B-2440 Geel
2) IRI, TU-Delft, Mekelweg 15, 2629 JB Delft, the Netherlands
3) CEA SPRC/LEPH, F-13108 Saint Paul lez Durance, France
4) Hyde Copse 3, Marcham, United Kingdom
alessandroborella@yahoo.it

Abstract: The probability that neutrons interact with materials reveals sharp peaks, so-called “resonances”. Since these resonances occur at neutron energies particular for each nucleus, they are very suitable for analyzing the elemental and isotopic composition of materials. They are the basis of two analytical methods “Neutron-Resonance-Capture-Analysis” (NRCA) and "Neutron Resonance Transmission Analysis (NRT)".
In this contribution we review NRCA and present an improved analytical procedure, which is based on a more methodological approach. We also discuss the applicability of NRCA and NRTA to identify and quantify impurities in reference materials used for cross section measurements. We will discuss the characterisation of reference materials for the determination of total and capture cross section in ^{209}Bi and ^{241}Am.

Introduction

The resonances occur at neutron energies typical for each nucleus. They are the basis of an analytical method, “Neutron-Resonance-Capture-Analysis” (NRCA), which has been developed in a joint project of IRI (Delft, NL) and IRMM (Geel, B) [1]. NRCA is a non-destructive method that is applicable to almost all stable isotopes, determines the bulk elemental composition, does not require any sample taking or surface cleaning, and results in a negligible residual radioactivity. The method was validated by comparison with INAA [2] and PGAA [3]. NRCA has been proven useful for the non-destructive quantitative elemental analysis of bronze archaeological artifacts and similar valuable objects [1-4]. In this paper we concentrate on the use of NRCA and NRT for the characterization of samples used in neutron cross section measurements.

Experimental Setup

NRCA and NRT measurements can be carried out at a neutron Time-of-Flight (TOF) facility such as GELINA of the Institute for Reference Materials and Measurements (IRMM) in Geel, Belgium. This facility has been designed and built especially for high-resolution neutron cross section measurements in the resonance region. More details about GELINA can be found in Ref. [5].
In an NRCA measurement, the shape of the neutron spectrum is usually measured with a double Frisch-gridded ionization chamber placed before the sample. The gamma rays, originating from the neutron capture reaction, are detected by a set of C_6D_6-based liquid scintillators (NE230) of 10 cm diameter and 7.5 cm length. Each scintillator is coupled to an EMI9823-KQB photomultiplier through a quartz window, reducing the neutron sensitivity of the detectors as much as possible. C_6D_6 detectors have an excellent time resolution and a very low sensitivity to neutrons. Therefore, these detectors are optimum detectors for neutron TOF-measurements.
NRT measurements are performed using lithium glass scintillators (NE213) as neutron detectors. The Li-glass is mounted inside an Al-can and viewed by two EMI 9823 KQB photomultipliers, which were placed outside the neutron beam. Two BF3 proportional counters are used to monitor the neutron flux of the accelerator and to normalize the spectra.
The resonance structure can be observed by the time-of-flight (TOF) technique for both NRT and NRCA measurement. The TOF of a neutron is determined by the time between the start

signal, given at each electron burst, and the stop signal from the detectors. These pulses are sent to a Fast Time Coder with a 0.5 ns time resolution, designed at the IRMM [6].

Data Analysis

In a transmission measurement one determines the fraction of the neutron beam which traverses without any interaction within the sample. The experiment involves the determination of the ratio of the count rates in a neutron detector from a "sample-in" (C_{in}) and a "sample-out" (C_{out}) measurement. This ratio is defined as the transmission T and is related to the total cross-section σ_t by:

$$T(E) = \frac{C_{in}}{C_{out}} \cong e^{-n\sigma_t} \qquad (1),$$

with n the thickness of the target. In Equation 1, the incoming fluence rate and the detector efficiency cancel out, so there is no calibration uncertainty. Although fundamentally straightforward, there are several difficulties associated with measurements of the total neutron cross-section. The measured transmission, as a function of neutron energy E_n, is broadened due to the finite resolving power of the neutron spectrometer and the Doppler broadening. Due to the presence of the potential scattering NRT shows a lower sensitivity when compared to NRCA.

In an NRCA measurement, for a regular object the response of the capture system $C_{c,k}$ in the region of a well isolated resonance of a nuclide k can be expressed as a function of the capture yield $Y_{c,k}$, the incoming neutron flux φ and the efficiency to detect the capture event $\varepsilon_{c,k}$:

$$C_{c,k}(E_n) = \varepsilon_{c,k}(E_n)\, Y_{c,k}(E_n)\, \varphi(E_n) \qquad (2)$$

The capture yield, i.e. the fraction of the neutron beam that undergoes a (n,γ) reaction in the sample, is a function of the total and capture cross section of nuclide k, expressed as $\sigma_{t,K}$ and $\sigma_{\gamma,k}$, respectively:

$$Y_{c,k}(E_n) \cong (1 - e^{-\sum_j n_j \sigma_{t,j}(E_n)}) \frac{n_k \sigma_{\gamma,k}(E_n)}{\sum_j n_j \sigma_{t,j}(E_n)} + \mu_k \qquad (3)$$

where n_k is the effective thickness for the nucleus k expressed in atoms/barn. The term in brackets accounts for the self-shielding effect and μ_k for the multiple scattering correction.

For a correct treatment of the self-shielding the total, Doppler-broadened cross-section must be used. The observed line shape is a convolution of Eq.3 with the time resolution of the spectrometer.

In order to extract the isotopic abundances and therefore the sample composition, one can perform an analysis based on a methodological approach by identifying the main metrological parameters of the measurement process and applying a so-called Resonance Shape Analysis. Such an analysis can be carried out with the RSA code REFIT developed by M.C. Moxon [8]. This code accounts for the experimental resolution and Doppler broadening, and the self-shielding and multiple scattering in the object.

To perform such an RSA the capture response C_c needs to be transferred into an experimental observed capture yield. Therefore, the response of the capture detector needs to be corrected for the energy dependence of the neutron flux and the detection efficiency for a capture event in a given isotope. These corrections are analogous to the ones that are applied when performing high resolution capture cross section measurements [9, 10]. To correct for the shape of the neutron spectrum we use the response of the ^{10}B ionization chamber. To account for the efficiency to detect a capture event we apply the total energy detection principle in combination with the Pulse Height Weighting Technique (PHWT) [11].

Using the PHWT, the detection efficiency for a capture event σ_c is directly proportional to the total energy released in the capture event E_x (the sum of the neutron binding and neutron kinetic energy in the center of mass system) and independent of the actual cascade path.

Finally, the experimentally observed capture yield $Y_{c,exp}$ is derived from the ratio of the weighted response of the capture detection system and the response of the ^{10}B ionization chamber, both corrected for their relative efficiencies:

$$Y_{c,exp} = K \frac{C_{wc}}{C_n} \frac{\sigma_\alpha}{E_x} \quad (4)$$

where K is an energy independent normalization factor and σ_α is the $^{10}B(n,\alpha)$ cross-section, C_n the count rate from the ^{10}B-ionization chamber, and C_{wc} the weighted count rate of the C_6D_6 detection system, corrected for dead-time losses and background. To derive the capture yield from the raw TOF spectra we used the data processing package AGS (Analysis of Geel Spectra) developed at the IRMM by Bastian [12].

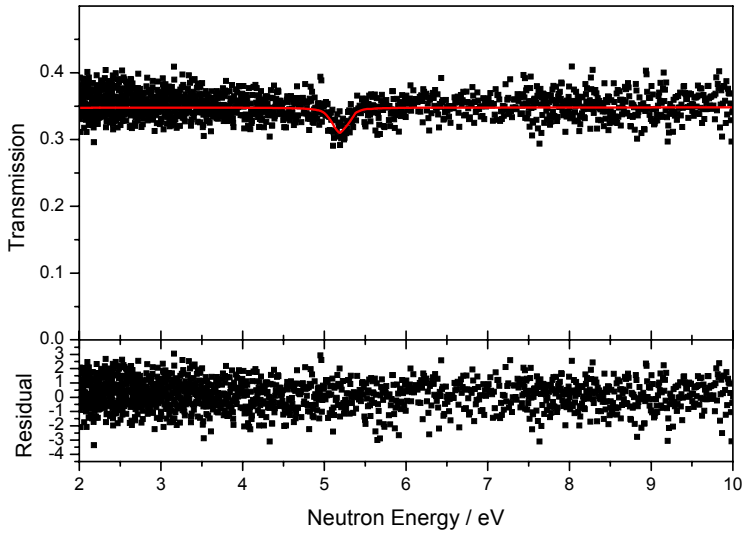

Figure 1. *NRT spectrum for a Bi sample with Ag impurity*

Determination of impurities in reference materials

In this section we demonstrate the exploitation of Neutron Resonant Analysis to quantify impurities in reference materials. To determine the nuclide composition of the objects we performed a resonance shape analysis using the REFIT code. The experimental observables were fitted by a least square procedure by adjusting the relative amount of the observed nuclides and considering all other variables, such as the resonance parameters, as fixed parameters.

Ag impurities in Bi samples

Transmission measurements were recently carried out at the IRMM by S. Kopecky. During the data analysis Ag impurities were found in the sample used. In Fig. 1 a dip around the strong 5.2 eV of ^{109}Ag can be observed. The transmission was fitted using REFIT and the resulting relative abundance of ^{109}Ag was 45±6 ppm. Due to the high thermal cross section of Ag isotopes, we estimated that such an amount of Ag would affect by 15% the results of neutron capture cross section measurements at thermal energies for ^{209}Bi when using such sample.

Impurities in Y_2O_3 matrices

Neutron cross section measurements are being carried out at IRMM on ^{241}Am. In order to obtain uniform samples for the transmission measurements, $^{241}AmO_2$ is dissolved in Y_2O_3 matrices. NRCA measurements on Y_2O_3 matrices were carried out at the IRMM in order to identify impurities which might affect neutron cross section measurements when such matrices are used.

From a preliminary analysis we identified Mo, Mn and Fe impurities, as shown in Fig. 2.

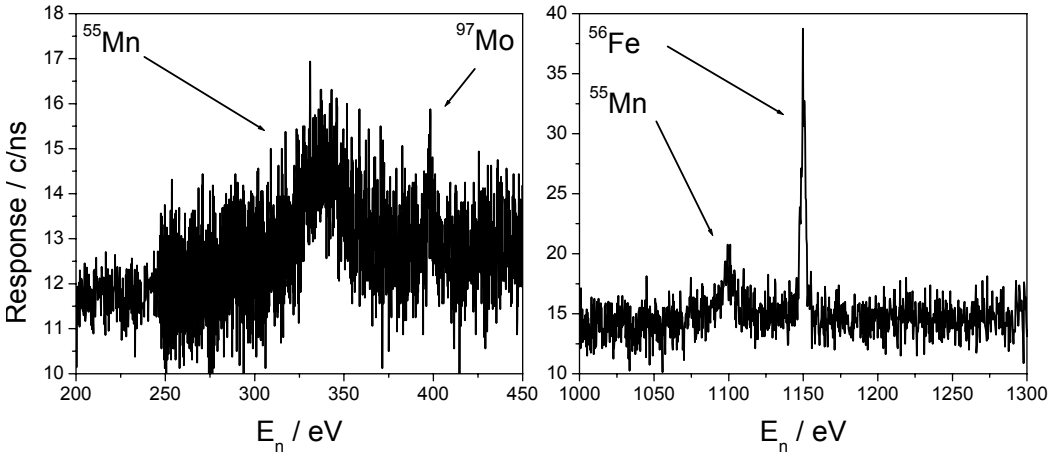

Figure 2. *NRCA spectra for a Y_2O_3 sample with Mo, Mn and Fe impurities*

Conclusions

We showed that NRA can be applied for the characterization of reference materials used for cross section measurements.

Acknowledgements
This work was supported by the European Commission's 6th Framework Programme in the frame of ANCIENT CHARM Work performed with financial support by the European Community "New and Emerging Science and Technology" Contract No 15311

References

[1] H. Postma, M. Blaauw, P. Bode, P. Mutti, F. Corvi., P. Siegler, "Neutron-resonance capture analysis of materials", J. of Radioanal. Nucl. Chem., 248 (2001) 115.
[2] M. Blaauw, H. Postma and P. Mutti, "Quantitative Neutron Resonance Capture Resonance Analysis Verified with Instrumental Neutron Activation Analysis", Nucl. Instr. Meth. A505 (2003) 508.
[3] H. Postma and P. Schillebeeckx, "Non–destructive analysis of objects using neutron resonance capture", accepted for publication in J. for Radioanal. Nucl. Chem. 2005.
[4] H. Postma, P. Schillebeeckx and R.B. Halbertsma, "Neutron-Resonance-Capture-Analysis of some genuine and fake Eutruscan copper-alloy statuettes", Archaeometry 46 (2004) 365.
[5] K.H. Böckhoff, A.D Carlson., O.A. Wasson, J.A. Harvey, and D.C. Larson, "Electron linear accelerators for fast neutron data measurements in support of fusion energy applications", Nucl. Sci. & Eng., 106 (1990) 192.
[6] S. de Jonge, Internal Rep. GE/DE/R/24/87, IRMM, Geel.
[7] J. González, C. Bastian, S. de Jonge, K. Hofmans, Internal Rep. GE/R/INF/06/97, IRMM, Geel.
[8] M.C. Moxon and J.B. Brisland, "GEEL REFIT, A least squares fitting program for resonance analysis of neturon transmission and capture data computer code", AEA-InTec-0630, AEA Technology, October 1991.
[9] P. Schillebeeckx, et al., "High Resolution Cross-section Measurements at the TOF-facility GELINA", XV International School on Nuclear Physics, Neutron Physics and Nuclear Energy September 9 - 13, 2003 Varna, Bulgaria.
[10] A. Borella, K. Volev, A. Brusegan, P. Schillebeeckx, F. Corvi, N. Koyumdjieva, N. Janeva and A. Lukyanov, "Determination of the ^{232}Th(n,γ) Cross Section from 4 to 140 keV at GELINA", Nuclear Science and Engineering, Vol. 152 (2006) 1–14.
[11] A. Borella, G. Aerts, F. Gunsing, M. Moxon, P. Schillebeeckx and R. Wynants, "The use of C6D6 detectors for neutron induced capture cross-section measurements in the resonance region", Nucl. Inst. And Meth. A (2007), doi:10.1016/j.nima.2007.03.034.
[12] C. Bastian, "AGS, a set of UNIX commands for neutron data reduction", Proc. Int. Conf. On Neutron Research and Industry, Crete, Greece, 1996, Ed. G. Vourvopoulos, SPIE – The International Society for Optical Engineering, Vol. 2867, 611, 1997.

Thermal neutron capture cross section measurements using a cold neutron beam

T. Belgya[1)], P. Schillebeeckx[2)] and A. Plompen[2)]

1) Institute of Isotopes Hungarian Academy of Sciences, H-1525, POB 77, Budapest, Hungary
2) European Commission, Joint Research Centre, Institute for Reference Materials and Measurements, Retieseweg 111, 2440 Geel, Belgium

belgya@iki.kfki.hu

Abstract: In this article the methodology of radiative-capture cross section determinations using our cold neutron beam at Budapest will be presented. The methodology will be illustrated with our latest results on ^{14}N (intensity standard), ^{27}Al, ^{129}I, ^{204,206,207}Pb. Some of these illustrative examples were done in cooperation with people from EU JRC IRMM, Geel, Belgium.

Introduction

Thermal-neutron radiative-capture cross sections are important in many fields of applications, including nuclear waste transmutation, reactor design, dosimetry, nuclear medicine and nuclear astrophysics. In the past few years at the PGAA-NIPS facilities of the Institute of Isotopes[1] a complex methodology of determination of thermal-neutron cross sections was worked out[2-4]. In the methodology the most important factor is the precise determination of partial gamma-ray-production cross section[5], which depends strongly on the precision of the intensity standards. We found substantial deviations in the intensities of the high energy capture standards and the high-energy gamma sources of ^{56}Co and ^{66}Ga. We invested a lot of efforts to improve them[6, 7]. The determination of the intensities of the primary high-energy neutron capture source of ^{14}N(n,γ) is our latest improvement, where we have also found deviation from the earlier data[8]. It has an impact on many cross sections determined from gamma-ray experiments and on decay-heat calculations for example[9]. Our intent in this article is to summarize the main features of our methodology of determining cross sections and to illustrate them with some of our recent results including the impact of the new intensity values of the nitrogen standard.

Methodology

Experimental facility

Our PGAA-NIPS facilities at the Budapest Research Reactor have been described many occasions. Here we give only a brief summary. The neutron source is the 10-MW Budapest Research Reactor. The neutrons are cooled in a cold source and guided to the experimental area with a super mirror guide. Just before neutrons reach the experimental area they are divided into two beams using collimators. The upper one serves the PGAA facility, while the lower beam goes further and is used in the NIPS facility. The purpose of the NIPS facility is to accommodate various setups. The PGAA facility is used most often for cross section experiments because it is equipped with a well shielded Compton-suppressed spectrometer, which is well characterized and calibrated. It is also equipped with a neutron-beam chopper, which enables us to perform cyclic activation on samples. A recent detailed description for these facilities can be found in Refs. [1, 10].

Determinations of capture cross sections

The basic quantity we can measure well is the partial gamma-ray-production cross section, which is denoted as σ_γ. The quantity σ_γ is a combination of nuclear constants $\sigma_\gamma = \theta \cdot P_\gamma \cdot \sigma_0$, where θ is the isotopic abundance, P_γ is the absolute gamma-transition probability and σ_0 is the capture cross section. This can be measured using the comparator technique with high precision[11]. Any unknown partial cross section $\sigma_{\gamma X}$ can be obtained relative to a comparator $\sigma_{\gamma C}$ from the following equation

$$\sigma_{\gamma X} = \sigma_{\gamma C} \frac{A_{\gamma X}}{A_{\gamma C}} \frac{n_C \varepsilon(E_{\gamma C}) f(E_{\gamma C})}{n_X \varepsilon(E_{\gamma X}) f(E_{\gamma X})} \quad (1)$$

where n is the number of atoms in the sample, *A* is the peak area, ε is the detector efficiency and *f* is the self absorption of the sample. The capture cross section can be obtained a number of ways from the partial cross sections, which is summarized in Table 1.

Table 1. *Ways of determining thermal capture cross sections*

Method	Equation	Notes
1	$\sigma_{th} = \frac{\sigma_\gamma}{\theta P_\gamma}$	P_γ must be known, for example from beta decay if the captured nucleus is unstable.
2	$\sigma_{th} = \sum_{f=1}^{n-1} \sigma_{\gamma\, C\to f}(1+\alpha_f)(1+PCC_f)$	The sum of all primary transitions from the capture state can be used for nuclei with relatively simple decay scheme.
3	$\sigma_{th} = \sum_{i=2}^{n} \sigma_{\gamma\, i\to g.s.}(1+\alpha_i)(1+PCC_i)$	The sum of all ground state transitions can be used for nuclei with relatively simple decay scheme. Conversion coefficients α must be known.
4	$\sigma_{th} = \sum_i E_i \sigma_{\gamma i}(1+\alpha_i)(1+PCC_i)/B_n$	The energy weighted sum can be used for any nuclei with resolved gamma-transitions. E_i is the energy of the transition, B_n is the binding energy and *PCC* is the pair conversion.

Influence of the new nitrogen intensities on capture cross sections

It is clear from Eq. (1) that the precisions of the cross sections depend on the relative detector efficiency, which can be obtained from experiments with calibration sources. It is therefore ultimate to use well established calibration sources. In a recent article of Belgya[8], it was shown that the accepted intensities of the primary high-energy prompt-gamma source ^{14}N(n,γ) deviate from the values obtained from basic principle. The new values tend to be larger than the accepted values (see Fig. 1).

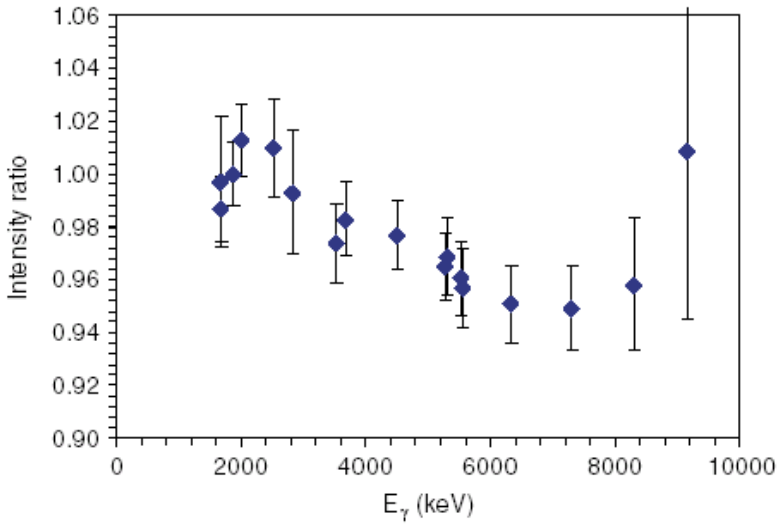

Figure 1. *Ratios of intensities for the strongest ^{14}N capture γ rays. Intensities of Jurney et al.[12] were divided by intensities of Belgya[8].*

This leads a general increase of partial cross sections in the 2.5-8 MeV range, which of course indicate a need for re-evaluation of cross sections based on partial gamma-ray cross sections. A cross check of the validity of the new nitrogen intensities has been calculated for the ^{27}Al(n,γ) reactions[13]. The aluminium capture is a special case where both method 1

and 4 of Table 1 can be determined. The ratio of method 4 and method 1 was calculated. Method 4 was treated as cumulative sum of as a function of gamma-ray energies. Calculating the efficiency with the new nitrogen intensities result in a better description of the thermal cross section than using the old intensities. The result is shown in Figure 2.

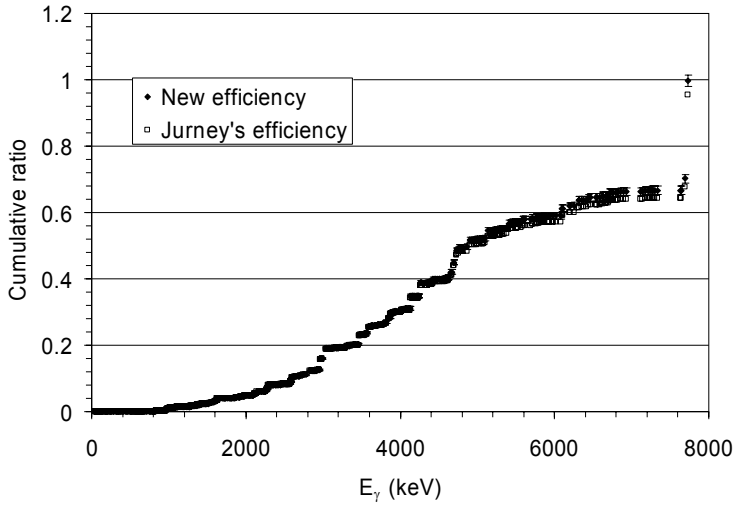

Figure 2. *Cumulative sum of energy weighted partial γ-ray cross sections for Al relative to the partial γ-ray cross section of the 1778 keV decay line.*

Measurement of cross sections of the lead isotopes

Partial gamma-ray production cross sections were determined for a well characterized natural lead-nitrate target for ^{204,206,207}Pb isotopes in collaboration with IRMM. The isotopic composition of the lead-nitrate target was measured with ICP-MS at IRMM. This was then applied to determine cross sections of ^{204,206}Pb using enriched targets (also provided by IRMM). The radiative capture on enriched ^{207}Pb target was measured earlier by Belgya[14]. The new results are summarized and compared to the recent evaluation of Mughabghab[15] in Table 2.

Table 2. *Comparison of cross sections of lead isotopes with the recent evaluation of Mughabghab[15].*

Isotope	This work	Mughabghab	Comment
	(mb)	(mb)	
^{204}Pb	482(20)	661(70)	preliminary
^{206}Pb	28.7(7)	26.6(12)	Increase is due to the N source
^{207}Pb	649(14)	625(30)	increase is due to the N source

Measurement of the cross section of ^{129}I

The ^{129}I is one of the most important LLFP. To measure its thermal radiative-capture cross section is of primary interest in the nuclear data community. The experiments were performed in collaboration with IRMM and the target was also supplied by them. The most recent value of the cross section was determined in a novel chopper method developed at Budapest by Szentmiklósi *et al.*[16]. Method 1, modified to cyclic activation, from Table 1 was used to determine the cross section[17]. The obtained cross section is 30.6(11) b, which agrees well with the recent experiment of Nakamura et al.[18].

Acknowledgements
The support of NAP VENEUS05 No. OMFB 00184/2006, the GVOP-3.2.1.-2004-04-0268/3 and the EU FP6 NMI3 No. RIII-CT-2003-505925 projects are acknowledged.

References

[1] Z. Révay, T. Belgya, Z. Kasztovszky, J. L. Weil and G. L. Molnár, "Cold neutron PGAA facility at Budapest", Nucl. Instr. & Methods B, 213, 385-388 (2004).

[2] T. Belgya, J. Weil, G. L. Molnár and H. F. Wirth, "Thermal neutron capture cross section measurements of 99Tc at the Budapest PGAA-NIPS facility", workshop on Neutron Measurements and Evaluations for Applications 5-8 November 2003, Budapest, Hungary, EUR Report 21100 EN, Luxembourg: Office for Official Publications of the European Communities, ISBN 92-894-6041-5, 159-163 (2004).

[3] T. Belgya, G. L. Molnár, Z. Révay and J. Weil, "Determination of thermal neutron capture cross sections using cold neutron beams", 10th International Conference on Nuclear Data for Science and Technology, September 26 - October 1, 2004, Santa Fe, New Mexico, AIP, 769, 744-747 (2005).

[4] T. Belgya, Z. Revay and L. Szentmiklosi, "Determination of Thermal Neutron Capture Cross Sections Using Cold Neutron Beams at the Budapest PGAA and NIPS Facilities", 12th International Symposium on Capture Gamma-Ray Spectroscopy and Related Topics, September 4-9, 2005 University of Notre Dame, Indiana, USA, AIP Melville, New York, 819, 300-306 (2006).

[5] Z. Révay, R. B. Firestone, T. Belgya and G. L. Molnár, "Prompt Gamma-Ray Spectrum Catalog", Handbook of Prompt Gamma Activation Analysis with Neutron Beams, 173-366 (2004).

[6] G. L. Molnár, Z. Révay and T. Belgya, "Precise determination of gamma-ray intensities for high-energy calibration standards", Summary report of the third research co-ordination meeting on Update of X- and gamma-ray decay data standards foe detector calibration and other applications, IAEA, INDC(NDS)-437, 23-36 (2002).

[7] T. Belgya and G. L. Molnár, "Accurate relative gamma-ray intensities from neutron capture on natural chromium", Nucl. Instr. & Methods B, 213, 29-31 (2004).

[8] T. Belgya, "Improved accuracy of gamma-ray intensities from basic principles for the calibration reaction 14N(n,g)15N", Physical Review C, 74, 024603-1-8 (2006).

[9] T. Belgya, "New method for the determination of accurate gamma-ray intensities for the 14N(n,g)15N high energy standard", 12th international Conference on Capture Gamma-Ray Spectroscopy and Related Topics, September 4-9, 2005 University of Notre Dame, Indiana, USA, AIP, 819, 300-306 (2005).

[10] G. L. Molnár, "Handbook of Prompt Gamma Activation Analysis with Neutron Beams" 1-423 (2004).

[11] Z. Révay and G. L. Molnár, "Standardisation of the prompt gamma activation analysis method", Radiochim. Acta, 91, 361-369 (2003).

[12] E. T. Jurney, J. W. Starner, J. E. Lynn and S. Raman, "Thermal neutron capture by 14N", Physical Review - Section C, 56, 118-134 (1997).

[13] T. Belgya, "New gamma-ray intensities for the 14N(n,g)15N high energy standard and its influence on PGAA and on nuclear quantities", Seventh Int. Conf Methods and Applications of Radioanalytical Chemistry, 3-7, April, 2006, Kaliua-Kona, Hawai'i, USA, Poster (2006). (J. Radio. Nucl. Chem. 2008 in print)

[14] T. Belgya, B. Fazekas, Z. Kasztovszky, Z. Révay, G. Molnár, M. Yeh, P. E. Garrett and S. W. Yates, "Levels of Pb-208 from the Pb-207(n,gamma) reaction with a guided neutron beam", Physical Review C, 57, 2740-2743 (1998).

[15] S. F. Mughabghab, "Thermal neutron capture cross sections resonance integrals and g-factors", Vienna, IAEA, (2003).

[16] L. Szentmiklósi, Z. Révay and T. Belgya, "Measurement of partial gamma-ray production cross-sections and k0 factors for radionuclides with chopped-beam PGAA", Nucl. Instr. and Methods A, 564, 655-661 (2006).

[17] T. Belgya, O. Bouland, G. Noguere, A. Plompen, P. Schillebeeckx and L. Szentmiklósi, "The thermal neutron capture cross section of 129I", International Conference on Nuclear Data for Science and Technology, Nice, France, 22-27 April, 2007, AIP Conference series, in print (2007).

[18] S. Nakamura, H. Harada, T. Katoh and Y. Ogata, "Measurement of thermal neutron capture cross section and resonance integral of the 129I(n,g)130I reaction", J. Nucl. Sci. and Techn., 33, 283-289 (1996).

Activation experiment on Cr in the NPI p-D_2O white-spectrum neutron field

E. Šimečková[1], P. Bém[1], V. Burjan[1], U. Fischer[2], M. Götz[1], M. Honusek[1], V. Kroha[1],J. Novák[1] and S.P. Simakov[2]

1) Nuclear Physics Institute, CZ-250 68 Řež, Czech Republic
2) Forschungszentrum Karlsruhe, D-76021 Karlsruhe, Germany
simeckova@ujf.cas.cz

Abstract: The activation experiment at the NPI cyclotron based fast fast neutron facility with the p(37MeV)+D_2O source reaction has been carried out on chromium in a white neutron spectrum extending up to 35 MeV. The objective of investigation was the check and validation of activation cross-section data in the energy range relevant to fusion (IFMIF) and ADS technologies.
The foils of CrNi alloy (69.9 % Cr, 29.2 % Ni and defined admixture of Co, Fe, Mn, V, Ti and Sc) were activated at mean neutron flux density up to 10^{11} n/cm^2/s at different irradiation times and different distances of sample from the D_2O target (test of measured data consistency). The CrNi samples were stacked in packets containing the monitoring dosimetry foils (Al and Au). The irradiation history was derived from the proton beam current recorded as a function of time during the irradiations. The neutron spectrum at the position of irradiated samples was determined employing the dosimetry-foil technique. The induced gamma-activities of samples were investigated repeatedly after different cooling time intervals by gamma spectrometry technique (two calibrated HPGe detectors of 23 and 50 % efficiency). In summary, the radioactive nuclides ^{51}Ti, ^{48}V, ^{52}V, ^{53}V, ^{46}Sc, ^{48}Sc, ^{48}Cr, ^{49}Cr and ^{51}Cr were identified and specific activities were determined from the n + ^{nat}Cr reactions.
Activation calculations have been performed with FISPACT/EAF-2005. The comparison of calculated and measured activities has revealed a reasonable agreement for half of resulting reaction products and large discrepancies for the other. Pathway analyses shoved that the relevant EAF-2005 chromium activation cross-sections had no experimental verification so far in the latter case. The need to update the EAF-2005 data is clearly indicated in this case.

Introduction

The reduced-activation ferritic-martensitic steel Eurofer-97 is a potential structural material for fusion power plants, the MONICR alloy for fission application, as well. The objective of the Eurofer activation experiment is to provide the experimental data base for validating activation cross-section data in the energy range relevant for the International Fusion Material Irradiation Facility (IFMIF). The element of Cr belongs to a substantial constituent of both materials (Eurofer - 9.21 %; MoNiCr – 6.3 %). Continuing the investigation of Eurofer-97 [1], the elements of W and Ta [2] (constituents of Eu-97, see Tab. 1), samples of CrNi were activated in the neutron field of NPI p-D_2O source.

Table 1. *Composition of Eurofer-97 sample (main constituents).*

Main constituens	Fe	Cr	W	Mn	V	Ta
Weight %	88.5	9.21	1.148	0.502	0.204	0.145
+/-		0.12	0.028	0.012		0.005

Experimental procedure

The samples were irradiated in the neutron spectrum running up to 33 MeV (mean energy of 14 MeV) produced by the neutron source from bombarding the flowing heavy water target by 37 MeV proton beam. The neutron spectrum (in Fig. 1) was measured in the point-like geometry (PLG) by scintilation detector technique, the spectral flux at the position of irradiated samples was determined by multi-foil-activation (MFA). The neutron flux density at the position of irradiated samples was of about 3.6x10^{10} n/cm^2/s^1/9 μA for neutron energies above 7 MeV [3].

The time profile of the neutron source was monitored by proton beam current, recorded by calibrated current-to-frequency converter and collected on PC. The investigated samples were surrounded by aluminum and gold foils for a supplementary monitoring of the neutron flux.

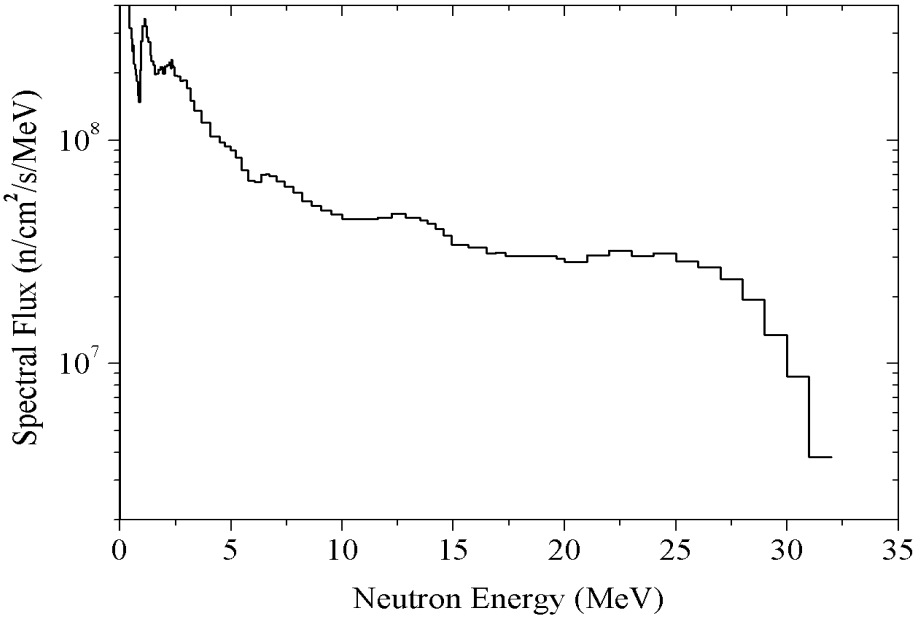

Figure 1. *Neutron spectra from the $D_2O(p,xn)$ source* reaction *for E_p= 37 MeV, I_p = 11.6 μA at the target-sample distance 3.15 mm.*

Sample disks of 15 mm diameter were fabricated from CrNi alloy (69.9 % Cr, 29.2 % Ni and defined admixture of Co-0.010 %, Fe-0.31 %, Mn-0.0016 %, V<0.004 %, Ti< 0.004 % and Sc<0.0001 %) sheet of 0.75 mm thickness.
The CrNi samples were activated at two runs with different irradiation times (11.2 m – short, 89.2 – middle). To test the internal consistency of the experiment, the irradiation was performed at different source-to-target distance (3.1 mm and 156.5 mm).
The activated samples were investigated by two calibrated HpGe detectors of 23 and 50% efficiency and of FWHM 1.8 keV at 1.3 MeV. Gamma spectra were measured repeatedly, after different cooling time intervals. Evaluation of spectra was performed utilizing the NPI code DEIMOS.

Experimental results and analysis

Activated isotopes were identified on the basis of $T_{1/2}$, γ-ray energies and intensity balance. Natural element Cr has 4 stable isotopes – ^{50}Cr (4.35 %), ^{52}Cr (83.79 %), ^{53}Cr (9.50 %) and ^{54}Cr (2.36 %). In some cases a strong gamma-line belongs to decays of couple isotopes with different decay half-times (for example: β^- decay of ^{51}Ti and $\varepsilon(\beta^{+})$ decay of ^{51}Cr – 320 keV line). To obtain resulting specific activities to the end of irradiation of separate parent nuclei in this case we minimized the sum of two decay curves to measured specific activities at various cooling times using the code MINUIT.
By analyzing the spectra, the 9 resulting specific activities A_{sp} in Becquerels per kilogram to the end of irradiation were determined from the reactions n + ^{nat}Cr investigated at short and middle irradiation times. The uncertainty includes statistical errors and the uncertainty of the detector-efficiency calibration (including the geometry factor).
The activation calculations have been performed with European Activation system EASY-2005 (FISPACT/EAF-2005) [4,5]. In Tab. 2 and Fig. 2 the comparison of calculated and measured activities (in term of C/E ratios) for the 9 radio-isotopes detected in the irradiated Cr sample is shown.

Table 2. *Results of C/E analysis. Chromium irradiation in the white p-D_2O spectrum: radioactive inventories, half lives, pathways and C/E ratios with EAF-2005 library.*

Nuclide	$T_{½}$	Reaction Pathway	C(EAF-2005)/E 11.3 min irr.	C(EAF-2005)/E 89.2 min irr.
46 Sc	83.790 d	^{50}Cr(n,pα+)		0.65 +/- 0.03
48 Sc	43.670 h	^{52}Cr(n,pα+)+ ^{50}Cr(n,3p) – 100%	0.92 +/- 0.18	0.75 +/- 0.08
51 Ti	5.800 m	^{52}Cr(n,2p)+ ^{54}Cr(n,α+) – 100%	1.51 +/- 0.05	
48 V	15.974 d	^{50}Cr(n,t) – 100%		4.00 +/- 0.20
52 V	3.745 m	^{52}Cr(n,p) – 88%; ^{53}Cr(n,d+) – 12%	1.33 +/- 0.19	
53 V	1.620 m	^{53}Cr(n,p) – 82%; ^{54}Cr(n,d+) – 18%	2.86 +/- 1.52	
48 Cr	21.561 h	^{50}Cr(n,3n) – 100%	2.01 +/- 1.01	2.48 +/- 0.20
49 Cr	41.900 m	^{50}Cr(n,2n) – 100%	0.88 +/- 0.05	0.72 +/- 0.05
51 Cr	27.706 d	^{52}Cr(n,2n)–98%; ^{54}Cr(n,3n)–1.4%	1.18 +/- 0.02	1.03 +/- 0.04

The comparison of activation calculation for pure Cr and CrNi alloy has shown no interference of activation reactions from allying elements.

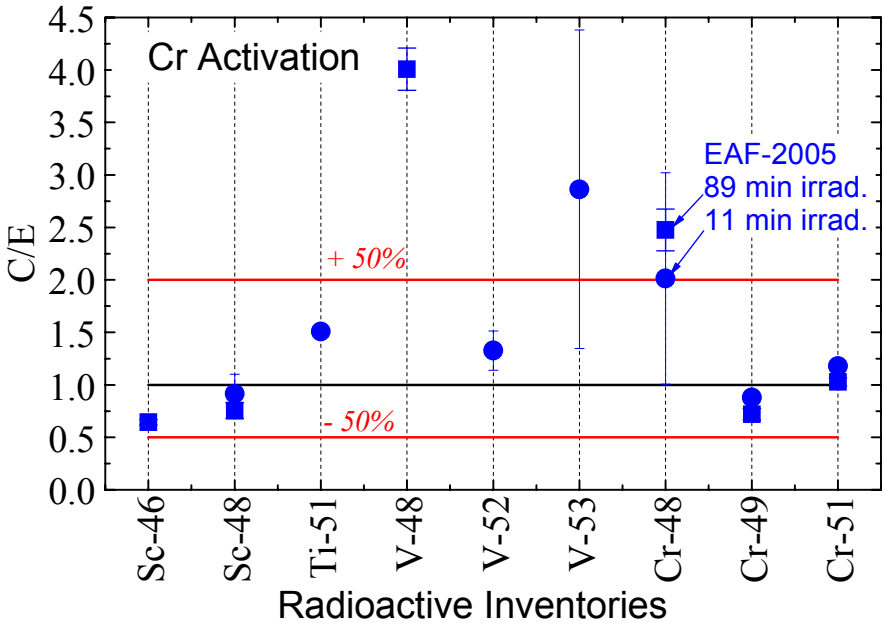

Figure 2. *C/E ration for radioactive isotopes production yields in Chromium, calculated with FISPACT/EAF-2005.*

It is seen that EAF-2005 activation libraries satisfactory predict (practically within experimental and calculation uncertainties) the yields of ^{48}Sc, ^{52}V, ^{49}Cr and ^{51}Cr, but fails to reproduce the other radioactive inventories. Pathway analyses for the production of the specific radio-nuclides have been performed to identify the dominant reactions and the reasons of the observed discrepancies. The results are displayed in Tab. 2 showing that the generation of the radio-activity products is mostly dominated by one single reaction. Such example is shown in Fig. 3. Fig. 3 shows EAF-2005 cross-sections for ^{51}Cr production reactions (left side), which well fit the numerous mono-energetic cross-section measurements below 22 MeV (not shown in Figure 3). Present benchmark gives C/E = 1.10 +/- 0.10 confirming in such a way these differential data and EAF-2005 tendency above 22 MeV. There is only one experimental point for the ^{nat}Cr(n,pα+3p)^{48}Sc reaction (indeed it is the cross-section averaged in the d-Be neutron spectrum extending up to 30 MeV – not in the picture). The EAF-2005 seems to overestimate this experimental point (Fig. 3, right side). This trend is confirmed also by present analysis in which ratio C/E = 2.25 +/- 0.23 is obtained. For production of scandium isotopes with mass numbers 46 and 48 in chromium there were no measurements so far. Therefore the C/E ratios received in the present work are the first verification of the relevant cross-sections in EAF-2005 library and its close to unity indicates confirmation of evaluation.

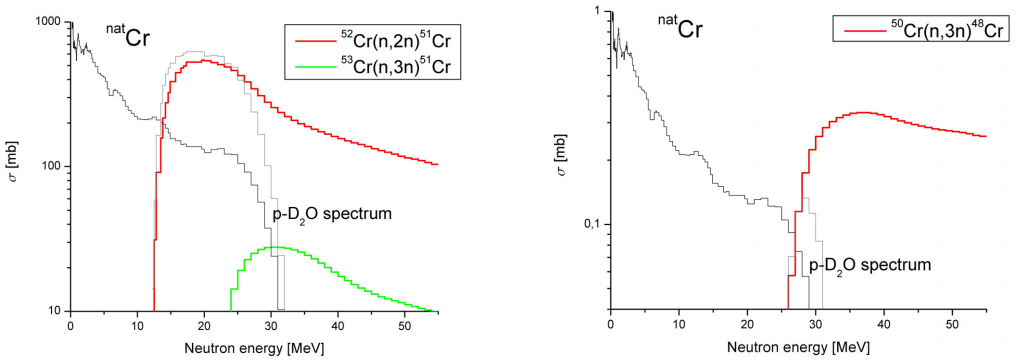

Figure 3. *The reaction cross-section as evaluated in EAF-2005 (reaction $^{nat}Cr(n,2n+3n)^{51}Cr$ on the left side, reaction $^{nat}Cr(n,p\alpha+3p)^{48}Sc$ on the right side). The p-D_2O spectrum is shown for illustration.*

Conclusion

The CrNi alloy foils were irradiated at IFMIF-like neutron field. In the experiment, 9 activation products have been determined from $^{nat}Cr(n,x)$ reactions. The activation calculations have been performed with FISPACT/EAF-2005 and comparison of calculated and measured activities (in term of C/E ratios) has been performed. It was found that EAF-2005 activation library satisfactory predicts (within experimental and calculation uncertainties) the yields of ^{48}Sc, ^{52}V, ^{49}Cr and ^{51}Cr, but fails to reproduce the other radioactive inventories. In addition, to investigate possible presence of weakly activated product and to obtain more reliable data for long-lived isotopes, the measurements with long irradiation time (above 12 hours) will be carried out.

Acknowledgements

This work was performed with partial support of EFDA Technology Program, the Ministry of Education and the Ministry of Trade and Industry of CR.

References

[1] P. Bém, V. Burjan, U. Fischer, M. Götz, M. Honusek, V. Kroha, U. von Möllendorff, J. Novák, S.P. Simakov and and E. Šimečková, “Activation of Eurofer in an IFMIF-like neutron field”, Fusion Eng. and Des., v. 75-79 (2005) p. 1169.

[2] E. Šimečková, P. Bém, V. Burjan, U. Fischer, M. Götz, M. Honusek, V. Kroha, J. Novák, S.P. Simakov, “Activation experiment on Ta and W constituents of the Eurofer-97 steel in the NPI p-D_2O neutron field”, Proc. Enlargement Workshop on Neutron Measurements Evaluations and Applications – NEMEA-3, 25-28 October, Borovets, Bulgaria, 169(2007).

[3] P. Bém, V. Burjan, U. Fischer, M. Götz, M. Honusek, V. Kroha, J. Novák, S.P. Simakov and E. Šimečková, “The NPI cyklotron-based Fast Neutron Facility”, Proc. ND 2007, 22-27 April, 2007, Nice, France, to be publish.

[4] R.A. Forrest, “The European Activation System: EASY-2005 Overview”, Report UKAEA FUS 513 (January 2005).

[5] R.A. Forrest, J. Kopecky and J.-Ch. Sublet, “The European Activation File: EAF-2005 cross section library”, report UKAEA FUS 515 (January 2005).

Benchmark test of activation cross-sections for Cr and Ni using the quasi-monoenergetic neutrons below 35 MeV

M. Honusek[1)], P. Bém[1)], V. Burjan[1)], U. Fischer[2)], M. Götz[1)], V. Kroha[1)], J. Novák[1)], S. P. Simakov[2)], E. Šimečková[1)]

1) Nuclear Physics Institute Řež, CS-25068 Řež, Czech Republic
2) Forschungszentrum Karlsruhe, D-76021 Karlsruhe, Germany
honusek@ujf.cas.cz

Abstract: Continuing the experimental tests of neutron activation cross-section data the activation of Chromium and Nickel was investigated using fast quasi-monoenergetic neutrons from the NPI cyclotron-based neutron source. These nuclides present an important component of the MoNiCr-alloy (the variant of Hasteloy steel for Fluoride-Molten-Salt-Reactor systems); Cr stems also the constituent of a low-activation Eurofer-97 steel (fusion technology).
Sample foils (Cr-Ni alloy) were irradiated by neutrons with spectrum peaked at 19.0, 24.3, 26.6 and 35.6 MeV. They were generated in the source reaction p-^{7}Li by protons at energies of 22.0 27.2, 29.5 and 37.5 MeV, respectively. After irradiation of samples, the induced gamma activities were measured at various cooling times employing the gamma spectrometry method based on the HPGe detector technique.
The analysis of resulting specific activities was carried out in terms of C/E ratio (E - measured reaction rate, C - the predicted value calculated for the neutron spectrum and the corresponding cross section from EAF-2007 library). The neutron flux and spectra at sample positions were calculated using double-differential cross-section data of the source reaction ^{7}Li(p,xn) measured by other authors.
Resulting C/E data of observed isotopes are compared with results of integral benchmark experiment carried out at similar energy range using white-spectrum neutrons from the NPI p-D_2O neutron source.

Introduction

The neutron cross-section data of reactions at incident energies E_n > 20 MeV are needed to improve the accuracy of neutronic calculations incorporated with various fission and fusion technologies like Fluoride-Molten-Salt-Reactor systems, IFMIF (International Fusion Material Irradiation Facility) and for the tests of nuclear reaction models as well.
The neutron activation of Nickel and Chromium - constituents of MoNiCr-alloy and low-activation Eurofer steel - is of importance. There are almost no experimental cross-sections data on Ni and Cr for neutron energies > 20 MeV and only limited data on experimental cross-sections exist for neutron energies < 20 MeV [1].
In the following sections we briefly describe the quasi-monoenergetic p-^{7}Li neutron source, the activation experiment on Cr and Ni foils and the method of data evaluation. The resulting radioactive isotopes were studied by means of gamma spectroscopy methods. The preliminary analysis in terms of C/E results was carried out using the cross-section data from EAF 2007 library and neutron spectra from Ref. [2]. The results were compared with ones measured using D2O neutron source.

Experimental equipment and neutron spectrum

The target station of quasi-monoenergetic neutron source based on ^{7}Li(p,n) reaction was presented in previous works [3,4]. The proton beam from isochronous cyclotron U120M strikes the Li foil at variable energies from 11 to 38 MeV. The carbon backing serves as a beam stopper. The irradiated foils could be placed at and above distance of 48 mm from the Li foil.
To evaluate the neutron spectral flux at sample positions the spectral yield of source reaction p+^{7}Li(C backing) were taken from the Ref. [2]. The spectra consist of quasi-monoenergetic part corresponding to the reactions to g.s. and 0.429 MeV states in ^{7}Be, and of the low-energy tail generated a) by reactions on ^{7}Li leading to further excited states in ^{7}Be and b) by reactions of protons on carbon stopper.

The neutron spectra [2] were measured at different set of energies compared to ones. Therefore, we decided to shift the spectra [2] according to our incident proton energies. An example of this procedure is given in the fig.1 (left). The spectrum taken for the next analysis is the mean of both shifted spectra.
The spectra corresponding to our proton beam energies are shown in the fig. 1 (right).

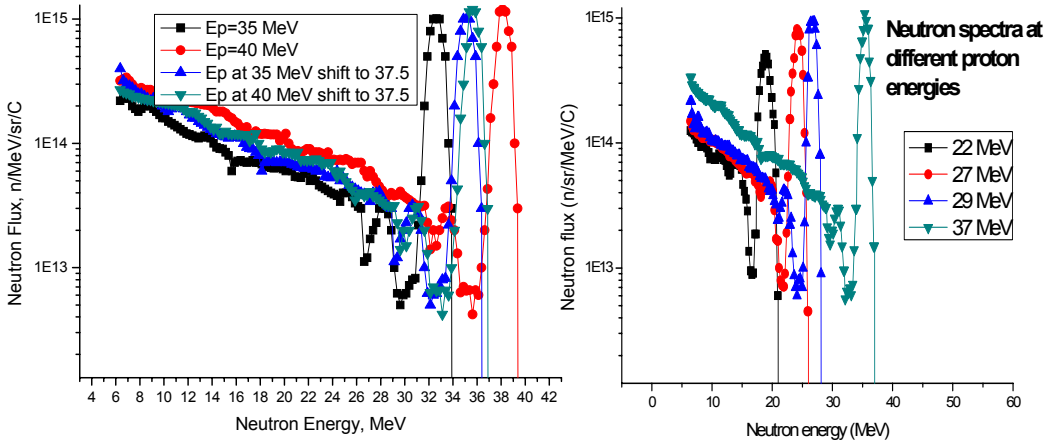

Figure 1. *The neutron spectra measured [2] at the proton energies of 35 and 40 MeV. The corresponding spectra shifted to 37.5 proton energy are shown as well. (left). Spectra used for the next analysis (right).*

Experimental procedure and results

The stack of irradiated foils (NiCr + Au) was activated simultaneously at two distances (48 and 88 mm) from the Li foil to test the effect of the flux-density gradient in the vicinity of neutron source. The Au foil was used as a "reference monitor" [2]. The weights of foils (14 and 15 mm in diameter) were of 0.14 g and 0.7 g for Au and NiCr, respectively. The NiCr alloy (29.2 % Ni and 69.9 % Cr) was used instead of pure Cr material because of better mechanical property. The time profile of the neutron source strength during the irradiation was monitored by the proton beam current on the neutron-source target, recorded by a calibrated current-to-frequency converter on PC. The typical proton beam current was about 3 μA. Irradiated samples were investigated by means of gamma-spectroscopy method. Two calibrated HPGe detectors of 23 and 50 % efficiency and FWHM of 1.8 keV at 1.3 MeV were used. Activated isotopes were identified on the basis of $T_{1/2}$, γ-ray energies and intensities. Cooling times of gamma measurement ranged from minutes to approx. 100 day. (Each foil was measured at approx. 5 cooling times).

Table 1. *Isotopes observed from irradiations of Cr foil.*

Isotope	T1/2	reaction	Threshold (MeV) (Contribution of reaction (for Ep MeV))
Cr48	21.56 h	Cr50(n,3n)	24.058
Cr49	42.3 m	Cr50(n,2n)	13.264
V48	15.974 d	Cr50(n,t+)	12.914
Sc46	83.79 d	Cr50(n,pα+)	10.343
Sc47	3.3492 d	Cr52(n,dα+)	18.931
Sc48	43.67 h	Cr52(n,pα+) Ct53(n,dα+)	12.807 96.6 % (37) 18.626 3.4 % (37)

Resulting isotope activities related to unitary proton beam current were obtained. The lists of observed reactions on Cr and Ni and are shown in Table 1 and Table 2.

Table 2. *Isotopes observed from irradiations of Ni foil.*

Isotope	T1/2	reaction	Threshold (MeV) (Contribution of reaction (for Ep MeV))
Ni56	6.077 d	Ni58(n,3n)	22.857
Ni57	35.60 h	Ni58(n,2n)	12.432
Co55	17.53 h	Ni58(n,nt+)	21.517
Co56	77.27 d	Ni58(n,t+)	11.259
Co57	271.97 d	Ni58(n,d+)	6.051
Co58	70.86 d	Ni58(n,p) Ni60(n,t+)	0 97.5 % (27), 92.7 % (29), 84.1 % (37) 11.699 2.5 % (27), 7.3 % (29), 15.9 % (37)
Co58m	9.04 h	Ni58(n,p) Ni60(n,t+)	0 97.6 % (27), 93.2 % (29), 86.4 % (37) 11.674 2.4 % (27),6.8 % (29), 13.6 % (37)
Co61	1.650 h	Ni61(n,p) Ni62(n,d+)	0.548 29.3 % (22), 13.3 % (27) 9.057 70.7 % (22), 86.7 % (27)
Fe59	44.503 d	Ni60(n,2p) Ni62(n, α+)	10.490 25.2 % (22), 71.0 % (27), 73.9 % (29), 52.0 % (37) 0.450 74.8 % (22), 28.7 % (27), 25.1 % (29), 38.0 % (37)
Mn54	312.3 d	Ni58(n, pα+)	6.424

Comparison of experimental results and calculated values

The comparison is based on the usual C/E ratio, where C and E correspond to the calculated and experimental activity, respectively. In the calculations, the cross section data were taken

Table 3. *C/E values of Isotopes observed from irradiations of Cr.*

Isotope	C/E 48 mm (err.%) C/E 88 mm (err.%)				
	Ep=22 MeV	Ep=27 MeV	Ep=29 MeV	Ep=37 MeV	D2O S/L a)
Cr48			2.118 (8 %) 2.320 (8 %)	1.199 (4%) 1.122 (3 %)	2.01 (50 %) 2.48 (8 %)
Cr49	0.771 (4 %) 0.824 (4 %)	0.746 (4 %) 0.742 (3 %)	0.702(5 %) 0.652 (3 %)	0.566 (4 %) 0.589 (3 %)	0.88 (6 %) 0.72 (7 %)
V48		2.428 (12 %) 2.171 (6 %)	1.125 (4 %) 0.981 (6 %)	1.311 (3 %) 1.108 (3 %)	4.00 (5 %)
Sc46		0.385 (10 %) 0.331 (13 %) *0.630 (10 %)*	0.316 (8 %) 0.257 (8 %) *0.547 (8 %)*	0.279 (4 %) 0.232 (4 %) *0.452 (4 %)*	0.65 (5 %) b)
Sc47				3.376 (4 %) 3.064 (4 %)	
Sc48		1.057 (6 %) 0.767 (6 %)	0.563 (6 %) 0.440 (6 %)	0.522 (12 %) 0.465 (3 %)	0.92 (20 %) 0.75 (11 %)

a) The C/E values obtained for D2O spectrum, Short and Long irradiation [5]
b) The values at 48 mm calculated using EAF 2005

from EAF-2007, the neutron spectra were taken from Ref. [2] (shifted according procedure described above).
The C/E values for Au (cross-sections are more or less known) are close to 1 (ref.[3, 4]), therefore we can come to the conclusion that our approach is correct.

Table 4. *C/E values of Isotopes observed from irradiations of Ni.*

Isotope	C/E 48 mm (err.%)			
	Ep=22 MeV	Ep=27 MeV	Ep=29 MeV	Ep=37 MeV
Ni56			0.856 (5 %)	1.137 (4 %)
Ni57	1.340 (3 %)	1.084 (3 %)	1.056 (3 %)	1.096 (3 %)
Co55				5.115 (6 %)
Co56	1.009 (20 %)	1.778 (4 %)	0.973 (3 %)	1.025 (3 %)
Co57	1.126 (4 %)	0.990 (4 %)	0.943 (5 %)	0.916 (5 %)
Co58+ Co58m	0.819 (3 %)	0.703 (3 %)	0.732 (4 %)	0.535 (4 %)
Co58m	0.844 (8 %)	0.845 (8 %)	0.924 (8 %)	0.564 (8 %)
Co61	1.165 (3 %)	0.989 (3 %)		
Fe59	1.572 (10 %)	1.533 (10 %)	1.142 (8 %)	0.805 (7 %)
Mn54	1.503 (10 %)	1.985 (6 %)	1.553 (8 %)	1.339 (5 %)

Table 3 involved C/E ratios calculated for both distances source-foil, Table 4 involved this ratios for 48 mm distance only. The last column in Table 3 shows the C/E ratios obtained for short and long irradiations at D2O neutron source [5].
The C/E values are calculated using EAF 2007 cross-section except values for D2O source. There is no effect to the overall comparison except values for Sc46; in this case the C/E values based on EAF 2005 are added in Table 3.
In present calculation, the possible difference between spectral yield (measured in the point-like-geometry, Ref. [2] and the form of spectra in the sample position (due to the integration over space and energy) was not taken into account.
C/E ratios lie between 0.2 – 3.5 for reactions on Cr.. For reactions on Ni the C/E ~ 1 or are in the interval 0.5 – 2 except Co55. The further tests of EAF-2007 activation cross-section library are needed.

Conclusions

The isotope activities produced in Cr and Ni foils by neutrons with energies below 35 MeV MeV were measured using the quasi-monoenergetic p-7Li neutron source. The spectral yield data for ^{7}Li(p,n) from Ref. [2] and cross-sections from EAF-2007 were used to the analysis of measured data.
The C/E ratios measured with p-7Li neutron source could be compared with C/E values measured with D2O heavy water neutron source [5], see Table 3. However, the neutron spectra are different, but in both cases high-energy parts exist. The tendency of C/E values is the same in both cases.

Acknowledgements
This work was performed with partial support of EFDA Technology Program, the Ministry of Education and the Ministry of Trade and Industry of CR.

References
[1] R. A. Forrest, J. Kopecky, M. Pillon, K. Seidel, S. P. Simakov, P. Bém, M. Honusek and E. Šimečková, UKAEA Report, UKAEA FUS 526, 2005.
[2] Y. Uwamino et al., NIM A389 (1997) 463.
[3] M. Honusek, P. Bém, V. Burjan, U. Fischer, M. Götz, V. Kroha, J. Novák, S. P. Simakov, E. Šimečková, NEMEA 3, Borovets 2006.
[4] P. Bém, V. Burjan, U. Fischer, M. Götz, M. Honusek, V. Kroha, J. Novák, S .P. Simakov, E. Šimečková, Nuclear Data, Nice 2007.
[5] E. Šimečková, P. Bém, V. Burjan, U. Fischer, M. Götz, M. Honusek, V. Kroha, J. Novák, S. P. Simakov, NEMEA 4, Prague 2007.

What the experience of the CEA-DAM simulation program can bring to the Generation IV project nuclear data

E. Bauge

CEA DAM Ile-de-France, Service de Phyisque Nucléaire, Bruyères-le-Châtel, 91297 Arpajon CEDEX, France.
eric.bauge@cea.fr

Abstract: With the stopping of nuclear testing in 1996, France's CEA-DAM had to start an ambitious program in order to continue fulfilling its missions of designing and demonstrating the safety and reliability of France's strategic deterrence. That demonstration, which relied on full scale testing prior to 1995, now has to be performed with computers and in the laboratory. That simulation program consists in building a “simulator" which is a computer code running on one of the fastest computer in Europe. That computer code implements all the physics and the attached physical constants that completely describe the functioning of a nuclear charge. Of course, the performance of that “simulator" must be assessed by comparing with laboratory experiments as well as with the results of previous nuclear testing. While in the past, some error compensation might have been acceptable thanks to the full scale experimental validation, these compensations must now be avoided at all costs, forcing the description of each of the individual physical process involved to be faithfully modelled and individually validated. In particular, the effect of spatial and temporal discretization must be carefully controlled. Among all the physics which had to be improved for the simulation program, evaluated nuclear data plays a important role in the improvement of the “simulator". Such a challenge is not unlike that faced with the design of Generation IV reactors, for which, given the wide range of options being considered today, financial constraints will severely limit the possibility of full scale testing for all these options. A response to that challenge would be to start an initiative inspired by the return of experience of CEA DAM simulation project.

Why the simulation program ?

After a last test on January 27th 1996, France has stopped nuclear testing, and promptly signed (September 24th 1996) and ratified (April 6th 1998) the Comprehensive Test Ban Treaty (CTBT). That treaty which prohibits nuclear testing and more generally nuclear explosions has been signed by 177 states and ratified by 138. Yet the mission of CEA DAM remains unchanged : design, build, maintain, and dismantle the French nuclear warheads while guaranteeing their safety and reliability during their whole lifetime. That mission must now be fulfilled while adhering to the terms of the CTBT : without nuclear testing. This new constraint led to the start of the simulation program : design and guaranty the French nuclear devices using only numerical simulation and laboratory experiments, without nuclear test.

Physics of nuclear devices

The functioning of a nuclear device can be seen as an energy amplification chain where the energy of the detonator is amplified by chemical explosives to an energy of the order of 1 MJ. That energy is transferred the nuclear fission stage of the devices where it is amplified to energies in the vicinity of 10^6 MJ. That fission energy is subsequently transferred to the fusion stage and amplified to about 10^8 MJ. Along this chain, lots of different bits of physics are involved : kinetic chemistry of explosives, shockwave propagation in materials, equation of state of materials under extreme conditions, fluid dynamics and turbulence, kinetic neutronics, physics of transfer from the fission to the fusion stage, and of course nuclear data. All these physics must not only mastered individually, but their coupling must also be controlled. Moreover, the energy from each stage must be released in carefully controlled conditions, in order to set the “good” initial condition for the following stage. At this point, one should note that nuclear data plays a central role in these physics since it drives the release of energy for the fission and fusion stages, and is also instrumental to interpreting the measurements of past nuclear tests which remain a valuable asset.

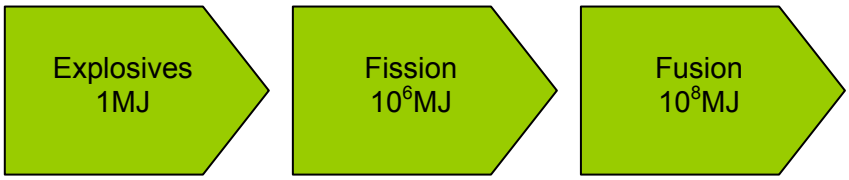

Figure 1. *Schematic view of the functioning of a nuclear device.*

Before 1996

In the era of nuclear testing, the demonstration of the proper functioning of French nuclear devices relied on the empirical proof of nuclear testing. Although, numerical models and laboratory experiments were also an important at this time, the possibility to "calibrate" the parameters of numerical models in order to improve test restitution, emphasises the importance of tests. This approach to design is closely related to the reliance on complex, full scale integral experiments to fine tune model constants, that is presently being used for reactor design. Of course such an approach is no longer sustainable when such integral experiments cannot take place.

The simulation program

A solution to that problem was implemented in CEA DAM in the shape of the simulation program. The simulation program revolves around the construction of a complete numerical model of the functioning of a nuclear device : the simulator. That simulator must implement all the models needed for describing the physics of nuclear devices, including their coupling, without introducing numerical biases (temporal, spatial, angular discretizations). Moreover, the individual models, their constants, as well as their numerical implementations must be validated independently by comparison with carefully designed laboratory experiments. That independent validation of the individual models at a more elementary level is extremely important since it rules out the possibility of error compensation between the different models.
Instead of relying on full scale integral experiments (tests) to calibrate numerical model constants, those constants (including nuclear data) are obtained by precise physical modelling and/or carefully designed laboratory experiments. The data acquired during past nuclear tests is still used, but only to validate the overall output of the simulator. Even this data is subject to re-interpretation since the simulator simulates not only the functioning of the nuclear device but also its interaction with the detectors/diagnostics measuring this data.
Compared to the situation of pre-1996 era, the focus of the simulations program has shifted from numerical models calibrated by nuclear testing to numerical models that are validated by elementary laboratory experiments.
Once the simulator is validated vs. both elementary lab. experiments and past tests data, it is handed down to the users (the designers) who can use it with full confidence within the validated perimeter.

Return of experience

Since the beginning of the simulation program in 1996, several versions of the simulator have been produced, each improving upon the previous one. The progression between early versions of the simulator and the current one is striking. Figure 2 illustrates the improvement of the restitution of a sample of past nuclear tests between an early version of the simulator and the current one. That figure shows that the improving knowledge of elementary physical processes and their implementation in the simulator translates into a real significant improvement of the restitution, to levels that are acceptable for designers. One should note that neither the early nor he current simulator versions are "calibrated" using the tests data. The calculations performed with the early version of the simulator exhibited a general trend towards overprediction of the measurements, which is gone in the current version. The good agreement (most C/E within 1 σ) exhibited by the current version calculation shows that it is possible to improve the models without relying on calibration vs. tests, but relying only on improved physical models and elementary laboratory experiments. It should also be stressed that this exercise is not a theoretical one with no link to applications, already one new device has been designed and guarantied using the simulator and this device has recently entered

the manufacturing stage. The simulator is thus already being used for applied industrial purposes !

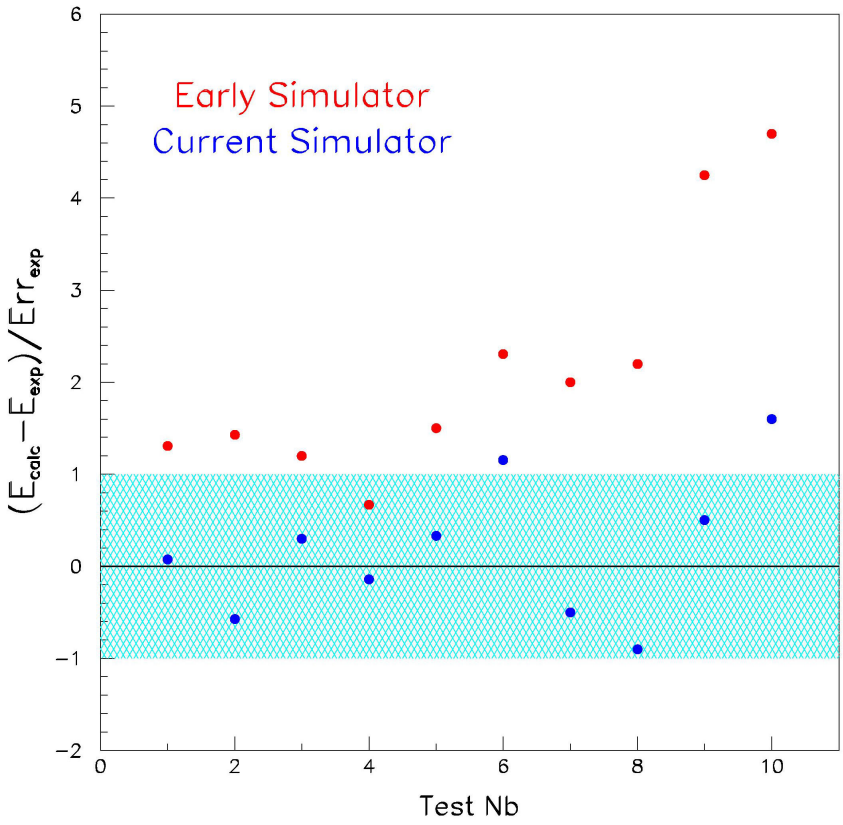

Figure 2. *Comparison between the restitution of a sample of past nuclear tests using early and current versions of the simulator*

.

Necessary conditions

An effort like starting a project of the importance of the simulation program is not a light one. First, initial results might be disappointing : the restitution of past test with early simulator versions were not very satisfactory (as can be seen in Figure 2), and it took a deep and long investment in physical modelling and experimental measurements to achieve the performance of the current simulator. Implementing such complex physical model without numerical bias also necessitated a large increase of the computing capacity of CEA DAM, up to 50 teraflops today. The building of large experimental facilities dedicated to the validation of entire parts of the functioning of devices is also needed for success. The AIRIX flash radiography facility and LMJ laser facility for inertial fusion are two key facilities for the simulation program. Overall, the budget for the simulation program has been estimated to be in the vicinity of 5 billion euros: a large investment, but one that is starting to pay off.

Relevance to the Gen IV project

Before discussing how the experience of the simulation program could be applied to the Gen IV project, let us review peculiarities of the Gen IV project. The Gen IV project encompasses a very wide range of concepts (LFR, SFR, GFR, VHTR, MSR, SCWR) with very diverse materials, temperatures, neutronic spectra,… The traditional approach for designing nuclear reactors would be to build prototypes for each of the concepts, and evolve these prototypes into industrial plants in parallel. While the cost of such a large number of prototypes will be spread over several countries, that have each strong interest in constructing their own prototype for their own “favourite” concepts, such an approach will likely results multiple adjusted (or calibrated) sets of nuclear data dedicated to each of the concepts. It is most likely that the nuclear data and models developed for one concept will not be adequate for the others because reliance on calibration will introduce error compensations. Those error

compensations could be strongly reduced if the validation perimeter of the models and data is expanded to a wider range of concepts, because the influence of local minima would be lessened by conflicting constraints. Another way of reducing error compensation is to validate the models and data on elementary experiments that are designed to unambiguously constrain only a small number of models/data at a time. Such experiments are different from scaled down demonstrators in the sense that they focus on constraining a well defined subset of model/data rather than testing the calculation of a whole reactor design, even if it is simplified to the extreme.
That shifting focus, by the simulation program, from reliance on calibration towards extensive modelling with elementary experimental validation could be emulated by the Gen IV project with the obvious benefits of getting more “universal” simulation tools, as well as much better physical knowledge of all the elementary physical processes involved. That knowledge is much more reusable than “calibrated” models and thus constitutes a better investment for future evolutions of fission reactor designs.

Future challenges

Both the simulation program of CEA DAM and the Gen IV project face the same challenges of estimating and optimising operating margins, and that challenge can only be tackled through quantification of all the model/data uncertainties and their propagation in simulation codes. In the field of nuclear data, uncertainty information is very sparse, and this is clearly a direction where a large effort is needed.

Evaluation of resonance neutron data for Am, Pb and Bi

N.V. Vassilev, M. J. Todorov, N. B. Janeva, N. T. Koyumdjieva

Institute for Nuclear Research and Nuclear Energy, Bulgarian Academy of Science,
72 Boul. Tzarigradsko chaussee 1784 Sofia, Bulgaria
pripesho@inrne.bas.bg

Abstract: A comprehensive overview of the available resonance data for Am, Pb and Bi has been performed by simultaneous analysis of the cross section files in actual evaluated data libraries and statistical properties of the resonances in resolved and unresolved region. There is large discrepancy between the data of different evaluated data files for ^{241}Am and ^{243}Am. The number of missed levels come out to be significant (neutron widths distributions) especially for ^{243}Am. For Pb and Bi there is only resolved resonance region in the evaluated libraries. The large discrepancies among libraries as well as significant deviation of level spacing distribution from Wigner law have been observed. Calculated point wise total cross section for ^{208}Pb with resolved resonance parameters (File2) from ENDF6.8 in comparison with the point-wise total cross section from File 3 and calculations with our code HARFOR with average resonance parameters were performed and results are presented as averaged cross sections in energy intervals of 100 keV.

Isotopes of americium

The improved nuclear data are needed for design and performance of reactor core parameters R dedicated to the transmutation of radioactive wastes. Data validation and uncertainty analysis are based on sensitivity approach considering the individual isotopes, cross sections and energy ranges. The data uncertainties expressed via variance and covariance matrices D are related to the sensitivity coefficients and R, as follows

$$\Delta R_0^2 = S_R^+ D S_R$$

We prepared a comprehensive overview of the available evaluated resonance data for Am isotopes accounting for the requirements of MA transmutation. These concern (n,gamma), fission and (n,xn) cross sections, resonance parameters, fission neutron spectrum, prompt and delayed neutron data of Am-241, -242m, -243.
The simultaneous analysis has been performed of the cross section files in actual evaluated data libraries and statistical properties of the resonances in resolved and unresolved region. There is large discrepancy between the data of different evaluated data files for ^{241}Am and ^{243}Am.

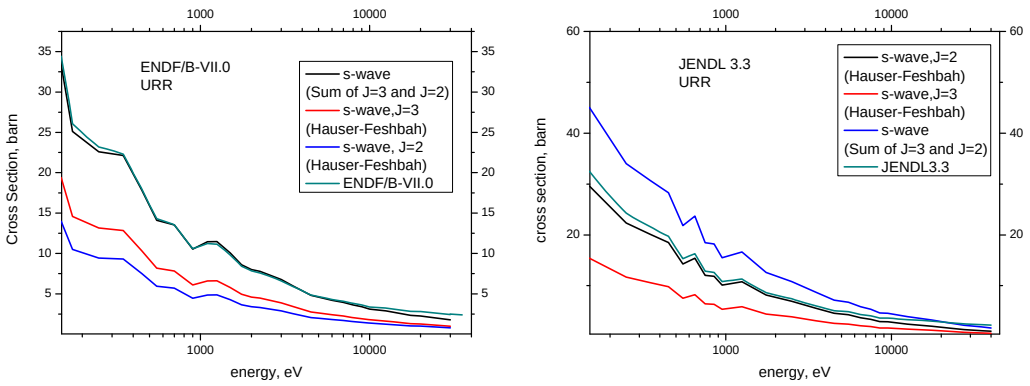

Figure 1. *Neutron capture in the URR of ^{241}Am*

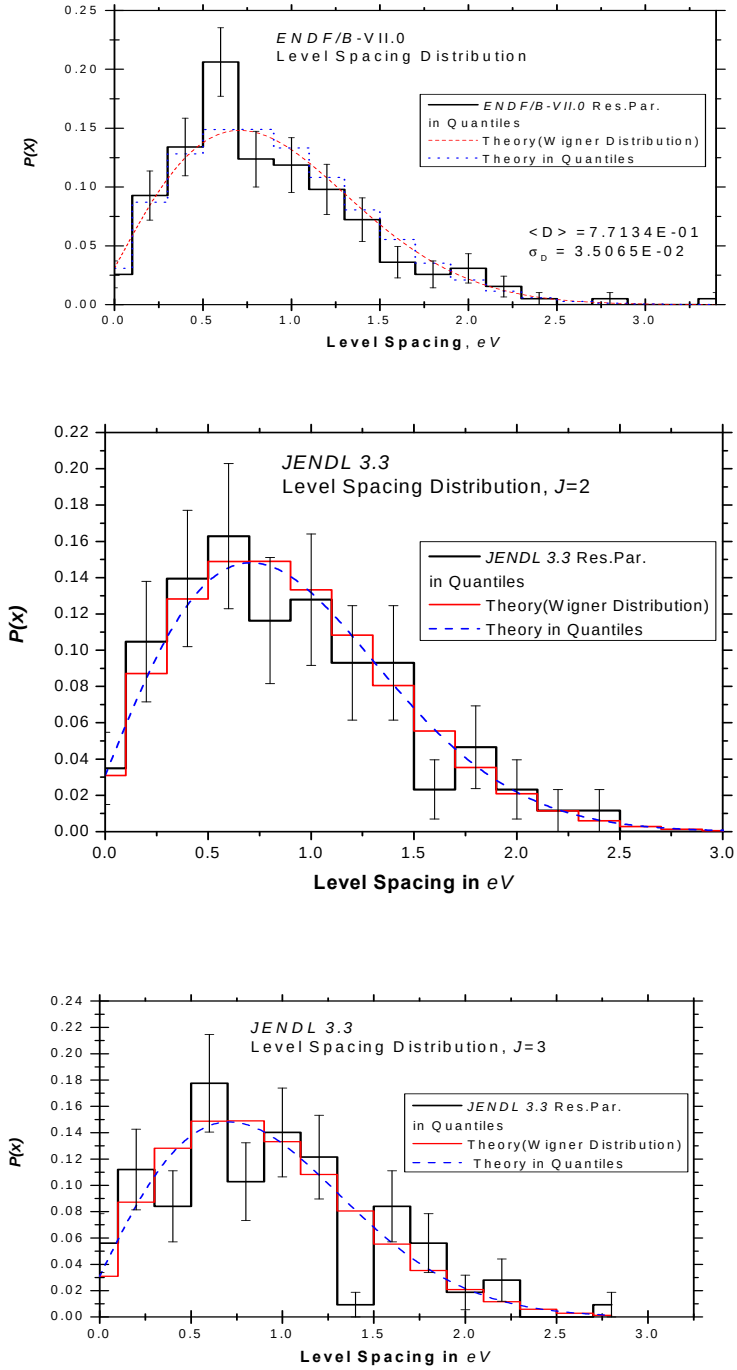

Figure 2. *Level spacing distribution of* ^{241}*Am*

The number of missed levels come out to be significant (neutron widths distributions) especially for ^{243}Am (Figure 3).

Conclusions for Am

Discrepancy between data of different evaluated data files

The number of missed level is significant (neutron widths distributions) especially for ^{243}Am.

The work on the analysis of the present status of 241Am and 243Am data file in the resonance region should be continued

recommendation - new top precision measurements of ^{241}Am and ^{243}Am capture cross section

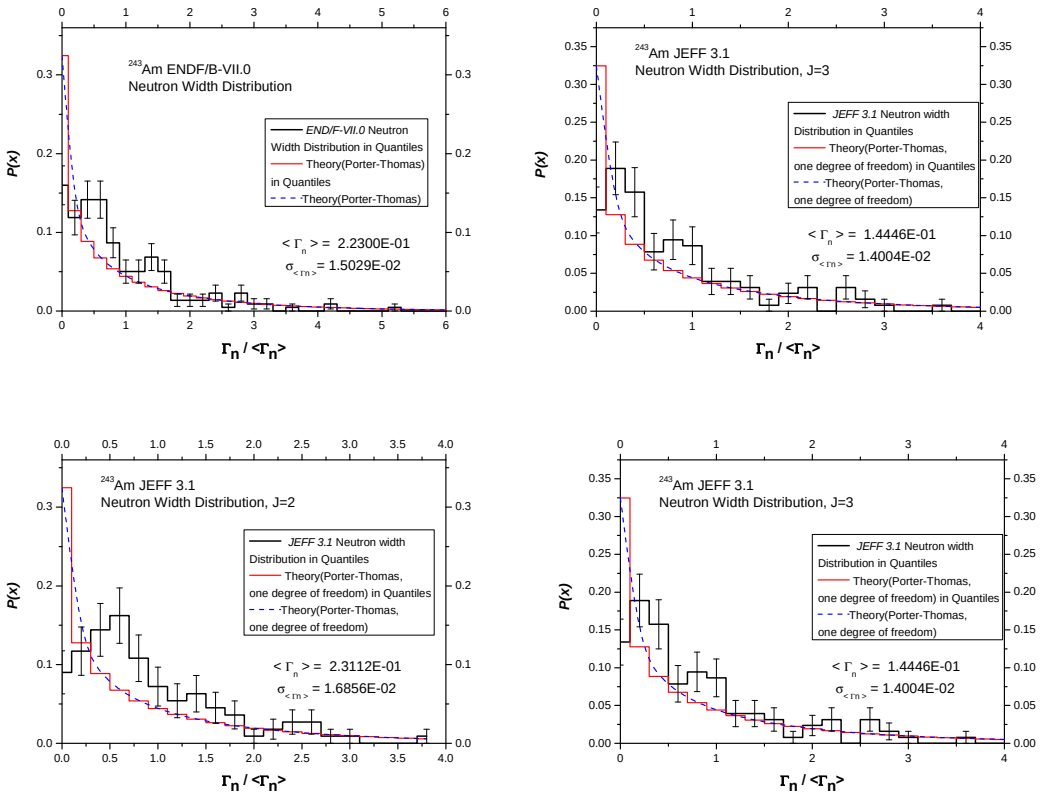

Figure 3. *Neutron widths distributions of ^{243}Am*

Isotopes of Pb and Bi

Many ADS designs that are currently under study consider a Pb/Bi eutectic for the core and coolant. The omnipresence of Pb and Bi in such a device entails that the simulation of the neutronic interactions with these materials have a considerable impact on the design parameters. The neutron multiplication in the target and the subsequent neutron scattering through the target and coolant determine neutronic power coefficients such as k_{eff} .When it comes to nuclear data evaluation, Pb and Bi have not yet received the same attention as the major actinides and common structural materials such as Fe, Si, etc. For incident neutrons, resonance parameters are adopted from the best possible library, where “best” denotes a combination of the most recent and complete of the resonances.

The resonance parameters of lead isotopes are obtained via Reich-Moore formalism; only for ^{204}Pb MLBW is used. The average resonance parameters for Pb isotopes deduced from RRR are summarized in Tables 1-3. There is no considerable difference between the values of the neutron strength function for the inspected Pb isotopes from different libraries. The radiative width for all nuclei is two-three or more times greater for variety of libraries. It is not possible at this point to take a decision are these values enough correct to reproduce the total cross section both in the resonance region and in higher energy region.

We tried to reproduce the total cross section of Pb-208 with the values from Tables 1-3. The results are shown on Figure 4 as averaged cross sections in energy intervals of 100 keV. We compare the calculated total cross sections with resolved resonance parameters from ENDF6.8 (File 2) with point-wise total cross sections from File 3. Also we show the results obtained with our code HARFOR. To reproduce the total cross section both in the resonance region and in higher energy region we had to use lower values of the neutron strength functions and effective scattering radius than those from Tables 1-3.

Table 1. *Resonance data for s-wave resonances*

	I	Library	$\overline{D}_l$, keV	$S_n^l .10^{-4}$	Γ_γ, eV	R^{eff}, fm
82 Pb 204	0^+	**RIPL**	**2.**	**1.1**	**0.77**	
		Jendl3.3 JEF3.1	2.267	0.85	0.702	8.5
82 Pb 206	0^+	**RIPL**	**32.**	**1.2**		
		Endf6.8	24.88	1.083	4.578	9.5*
		Jendl3.	28.01	1.53	1.462	8.042
82 Pb 207	0.5^+	**RIPL**	**38.**	**1.0**		
		Endf6.8	46.8	0.98	12.17	9.5*
		Jendl3.3	46.96	1.126	2.01	9.53
82 Pb 208	0^+	**RIPL**	**400.**			
		Endf7 Jendl3.3	246	1.15	0.166	9.69*

Table 2. Resonance data for p-wave resonances

	I_0	Library	$\overline{D}_l$, keV	$S_n^l .10^{-4}$	Γ_γ, eV	R^{eff}, fm
82 Pb 204	0^+	**RIPL**	**0.8**	**0.5**	**0.33**	
		Jendl3.3 JEF3.1	1.184	0.35	0.331	8.5
82 Pb 206	0^+	**RIPL**	**5.9**	**0.4**		
		Endf6.8	6.155	0.303	0.34	9.5*
		Jendl3.3	6. 626	0.353	0.248	8.042
82 Pb 207	0.5^+	**RIPL**	**5.0**	**0.6**		
		Endf6.8	4.727	0.63	0.489	9.5*
		Jendl3.3	4.93	0.623	0.2587	9.53
82 Pb 208	0^+	**RIPL**	**35.**	**0.5**		
		Endf7 Jendl3.3	38.04	0.357	0.276	9.69*

Table 3. *Resonance data for d-wave resonances*

	I_0	Library	$\overline{D}_l$, keV	$S_n^l .10^{-4}$	Γ_γ, eV	R^{eff}, fm
82 Pb 206	0^+	**RIPL**				
		Endf6.8	4.432	1.594	1.192	9.5*
		Jendl3.3	6.261	1.72	0.6356	8.042
82 Pb 207	0.5^+	**RIPL**				
		Endf6.8	17.12	1.292	1.422	9.5*
		Jendl3.3	18.2	1.4	0.5067	9.53
82 Pb 208	0^+	**RIPL**				
		Endf7 Jendl3.3	64.45	1.138	1.007	9.69*

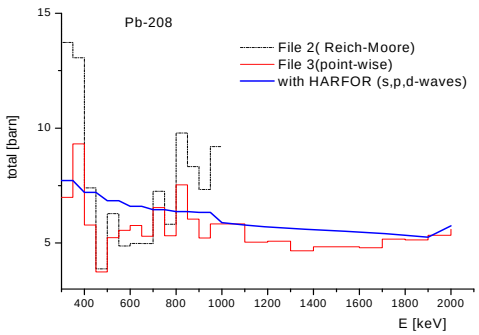

Figure 4. *Calculated total cross section for ^{208}Pb with resolved resonance parameters (File 2) from ENDF6.8 in comparison with the point-wise total cross section from File 3 and HARFOR calculations with the average resonance parameters*

$S_n^o = 0.93e^{-4}$ and $S_n^1 = 0.30e^{-4}$,

$R_0^{\,eff} = 9{,}5\ fm \quad R_1^{\,eff} = 7{,}88\ fm$

Uncertainty in displacement cross-section calculations at intermediate and high proton energies

A.Yu. Konobeyev, U. Fischer

Institut für Reaktorsicherheit, Forschungszentrum Karlsruhe GmbH, 76021 Karlsruhe, Germany
konobeev@irs.fzk.de

Abstract: The uncertainty in calculations of displacement cross-sections for proton irradiation at intermediate and high energies is analyzed. The calculation of cross-sections was performed using various types of screening functions, optical model parameters, and modifications of the intranuclear cascade evaporation model. The spread of calculated cross-sections is directly linked with the uncertainty of radiation damage rate calculations performed for materials of advanced nuclear energy systems.

Introduction

The study of the radiation damage rate in structural materials used in the design of spallation neutron sources and accelerators requires the detail knowledge about displacement cross-sections and their uncertainties in a wide energy range of primary particles. The present work discusses main factors resulting to the spread of calculated cross-sections.
The total displacement cross-section is calculated as the sum of the elastic ($\sigma_{d,el}$) and non-elasic components ($\sigma_{d,non}$)

$$\sigma_d = \sigma_{d,el} + \sigma_{d,non} \qquad (1)$$

Uncertainties for elastic and nonelastic components of σ_d are considered separately.

Elastic proton scattering

The displacement cross-section for elastic proton interactions with atoms is calculated as follows

$$\sigma_{d,el}(E_p) = \int_{E_d}^{T^{max}} \frac{d\sigma(E_p,T)}{dT} \nu(T)\, dT \ , \qquad (2)$$

where E_p is the incident proton energy; $d\sigma/dT$ is the cross-section of the energy transfer to recoil atom in the elastic proton scattering; $\nu(T)$ is the number of Frenkel pairs produced by the primary knock-on atom (PKA) with the kinetic energy T; T^{max} is the maximal energy transferred to PKA in elastic scattering; E_d is the effective threshold displacement energy.
In the present work the number of defects produced by the PKA in material $\nu(T)$ is calculated using the NRT model [1,2].
At low incident energies the screening effect plays an important role in the proton elastic scattering on atoms. The differential cross-section for the energy transfer from proton to the lattice atom can be written in the following form

$$d\sigma(E_p,T) = \pi a^2 f(t^{1/2}) \frac{dt}{2t^{3/2}} , \qquad (3)$$

where the $f(t^{1/2})$ is the screening function [3-7], “a” is the screening length, and “t” is the reduced energy.
Fig.1 illustrates the difference of $\sigma_{d,el}$ values calculated using various screening functions. It shows the ratio of elastic displacement cross-sections obtained using $f(t^{1/2})$ from Refs.[3,5-7] to $\sigma_{d,el}$ calculated using the screening function from Ref.[4] for copper.
The screening effect disappears with the increase of the proton energy. For copper the difference between $\sigma_{d,el}$ calculated by Eq.(2) with $f(t^{1/2})$ from Ref.[4] and the displacement cross-section estimated using the Rutherford formula is less than 10 % at proton energies above 150 keV, less 5 % at E_p > 0.65 MeV and less 1 % for the incident proton energy above 15 MeV.
Starting from several mega-electron volts of the incident proton energy the energy distribution of PKA is defined by the Coulomb scattering of protons, the nuclear scattering, and their

interference. For example, the difference between $\sigma_{d,el}$ calculated by Eq.(2) and correct calculations using optical model [8] for copper is more than 5 % at the proton energy above 6.5 MeV and more than 10 % at E_p above 10 MeV.
Fig. 2 illustrates the difference in elastic displacement cross-sections calculated using various sets of optical model parameters [8-14].

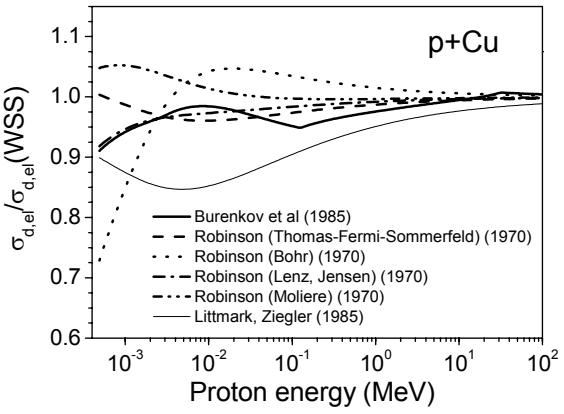

Figure 1. *The ratio of proton elastic displacement cross-sections obtained using various screening functions [3,5-7] to the elastic displacement cross-section calculated using $f(t^{1/2})$ from Ref.[3] for copper.*

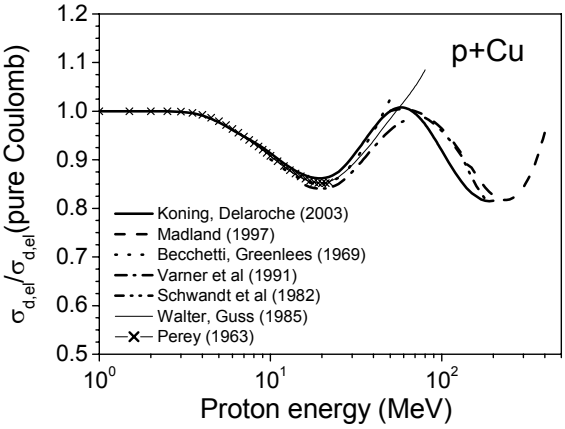

Figure 2. *The ratio of proton elastic displacement cross-sections calculated using different sets of optical model parameters [8-14] for copper to the elastic displacement cross-section obtained taking into account only Coulomb scattering of protons.*

The uncertainty in the elastic displacement cross-section is caused by

- the screening function calculation,
- the choice of optical model parameters,
- the value of the effective threshold displacement energy E_d.

In the present work the calculation of the variance of $\sigma_{d,el}$ was performed by the method from Ref.[15] using various $f(t^{1/2})$ functions, different sets of optical model parameters, and taking into account the uncertainty of the E_d value. Values of the effective threshold displacement energy from Ref.[16] were varied in the range $\pm$ 10 eV for each material.
Fig.3 shows ratios of the standard deviation to the average value of the elastic displacement cross-section $\delta\sigma_{d,el}/\langle\sigma_{d,el}\rangle$ for ^{27}Al, ^{63}Cu, ^{93}Nb and ^{181}Ta. Value of E_d used for calculations are equal to 27 eV for aluminum, 30 eV for copper, 78 eV for niobium, and 90 eV for tantalum.

Proton nonelastic interactions with nuclei

The displacement cross-section for nonelastic proton interactions with nuclei is equal to

$$\sigma_{d,non}(E_p) = \sum_i \int_{E_d}^{T_i^{max}} \frac{d\sigma(E_p, T_i, Z_T, A_T, Z_i, A_i)}{dT_i} \nu(T_i, Z_T, A_T, Z_i, A_i)\, dT_i \quad , \qquad (4)$$

where Z_i and A_i are the atomic number and the mass number of the recoil atom, correspondingly; Z_T and A_T are the same for the target material; $d\sigma/dT$ is the cross-section of the energy transfer to the recoil atom (Z_i,A_i); $\nu(T_i)$ is the number of Frenkel pairs produced by PKA with the kinetic energy T_i; T_i^{max} is the maximal kinetic energy of the residual atom produced in i-th reaction channel; the summing is for all open reaction channels.

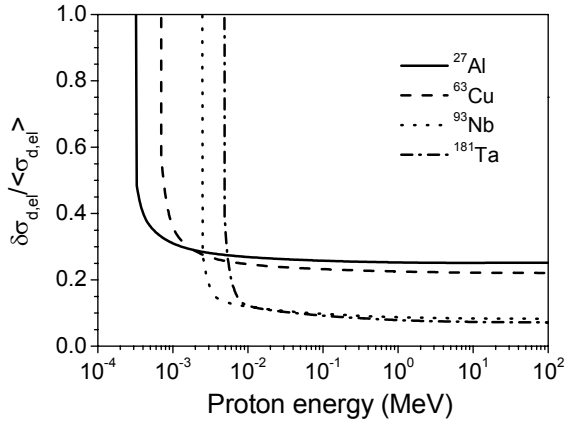

Figure 3. *Calculated ratios $\delta\sigma_{d,el}/\langle\sigma_{d,el}\rangle$ for ^{27}Al, ^{63}Cu, ^{93}Nb and ^{181}Ta.*

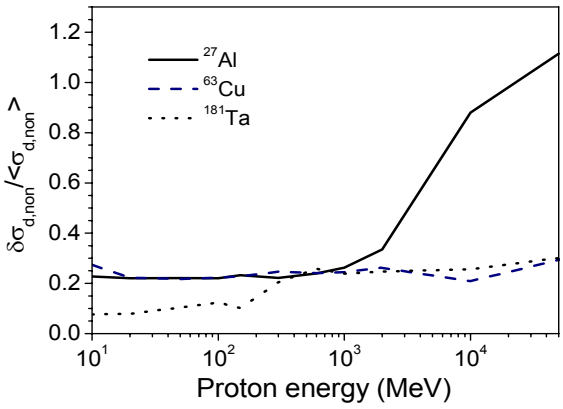

Figure 4. *Calculated ratios $\delta\sigma_{d,non}/\langle\sigma_{d,non}\rangle$ for ^{27}Al, ^{63}Cu, and ^{181}Ta.*

Table 1. *Proton nonelastic displacement cross-sections for ^{63}Cu calculated using various nuclear models and computer codes*

Model	Displacement cross-section for nonelastic proton interactions (b)				
	20 MeV	150 MeV	600 MeV	1 GeV	50 GeV
Bertini/Dresner	2597	3063	3578	3574	–
Bertini/ABLA	2758	3226	3826	3920	–
ISABEL/Dresner	2568	2950	3469	3607	–
ISABEL/ABLA	2670	3106	3703	3851	–
CEM03	2552	3045	3498	3529	–
INCL4/Dresner	–	3261	4099	4251	–
INCL4/ABLA	–	3409	4343	4544	–
FLUKA/Dresner	–	4045	4761	4768	1355
FLUKA/ABLA	–	4219	5202	5285	2130
CASCADE	2893	3002	3553	3743	2517
DISCA	3474	3502	3766	–	–
GNASH (ENDF/B-VI.8)	3317	3692	–	–	–
Average value	2850±360	3380±420	3980±570	4110±590	2000±590

Typical values of $\sigma_{d,non}$ calculated at various proton energies using different nuclear models and computer codes [17-20] are shown in Table 1 for ^{63}Cu. Results refer to the same nonelastic cross-section equal to 1120 mb for the proton energy 20 MeV, 734 mb for E_p=150 MeV, 753 mb for 600 MeV, 794 mb for 1 GeV, and 791 mb for the energy 50 GeV.

The spread in the calculated proton nonelastic displacement cross-section with the consideration of the uncertainty of the E_d value has been calculated by the analogy with previous Section. The adopted difference in E_d value was taken equal to 10 eV for each material. Fig.4 shows typical values $\delta\sigma_{d,non}/\langle\sigma_{d,non}\rangle$ for ^{27}Al, ^{63}Cu, and ^{181}Ta. One can see the growth of the uncertainty in proton nonelastic displacement cross-sections with the increase of the proton incident energy. High values of $\delta\sigma_{d,non}/\langle\sigma_{d,non}\rangle$ for ^{27}Al (Fig.4) result mainly from FLUKA calculations.

Conclusion

The uncertainty in the calculation of displacement cross-sections for proton interactions with atoms at various initial energies was discussed. The typical spread of cross-sections obtained using modern methods of calculations was demonstrated (Figs1, 2).
The main origin of the uncertainty of the elastic displacement cross-section is the scatter of the effective threshold displacement energy. The uncertainty of the nonelastic displacement cross-section results from the scatter of E_d and the method used for recoil energy distribution calculations.

References

[1] M.J. Norgett, M.T. Robinson, I.M. Torrens, “A proposed method of calculating displacement dose rates”, Nuclear Engineering and Design 33, 50 (1975).
[2] M.T. Robinson, ”Basic physics of radiation damage production”, J. Nucl. Mater. 216, 1 (1994).
[3] W. Eckstein, “Computer Simulation of Ion-Solid Interactions”, Springer-Verlag (1991).
[4] K.B. Winterbon, P. Sigmund, J.B.K. Sanders, “Spatial distribution of energy deposited by atomic particles in elastic collisions”, K. Dan. Vidensk. Selsk. Mat. Fys. Medd. 37, N14 (1970).
[5] A.F. Burenkov, F.F. Komarov, M.A. Kumahov, M.M. Temkin, “Spacial Distribution of Energy Deposited in Atomic Collision Cascades in Matter”, Energoatomizdat, Moscow. (1985).
[6] U. Littmark, J.F. Ziegler, “Handbook of Range Distributions”, Pergamon Press (1985).
[7] C.H.M. Broeders, A.Yu. Konobeyev, K. Voukelatou, “IOTA - a Code to Study Ion Transport and Radiation Damage in Composite Materials”, FZKA 6984 (2004); http://bibliothek.fzk.de/zb/ berichte/FZKA6984.pdf.
[8] A.J. Koning, J.P. Delaroche, “Local and global nucleon optical models from 1 keV to 200 MeV”, Nucl. Phys. A713, 231 (2003).
[9] F.G. Perey, “Optical-model analysis of proton elastic scattering in the range of 9 to 22 MeV”, Phys. Rev. 131, 745 (1963).
[10] F.D.Jr. Becchetti, G.W. Greenlees, “Nucleon-nucleus optical-model parameters, A>40, E<50 MeV”, Phys. Rev. 182, 1190 (1969).
[11] P. Schwandt, H.O. Meyer, W.W. Jacobs, A.D. Bacher, S.E. Vigdor, M.D. Kaitchuck, T.R. Donoghue, “Analyzing power of proton-nucleus elastic scattering between 80 and 180 MeV”, Phys. Rev. C26, 55 (1982).
[12] R.L. Walter, P.P. Guss, Rad. Effects 92, 1079 (1985); “A global optical model for neutron scattering for A > 53 and 10 MeV < E < 80 MeV”, Proc. Int. Conf. on Nucl. Data for Basic and Applied Science, Santa Fe (1985) p.1079.
[13] R.L. Varner, W.J. Thompson, T.L. McAbee, E.J. Ludwig, T.B. Clegg, “A global nucleon optical model potential”, Phys. Rep 201, 57 (1991).
[14] D.G. Madland, “Progress in the development of global medium-energy nucleon-nucleus optical model potentials”, Proc. OECD/NEA Spec. Meeting on the Nucleon Nucleus Optical Model up to 200 MeV, 13-15 November 1996, Bruyères-le-Chatel, France, p.129; http://www.nea.fr/html/science/om200/.
[15] D.L. Smith, “Covariance Matrices for Nuclear Cross Sections Derived from Nuclear Model Calculations”, ANL/NDM-159 (2004).
[16] C.H.M. Broeders, A.Yu. Konobeyev, “Defect production efficiency in metals under neutron irradiation”, J. Nucl. Mater. 328, 197 (2004).
[17] V.S. Barashenkov, “Monte Carlo simulation of ionization and nuclear processes initiated by hadron and ion beams in media”, Comp. Phys. Comm. 126, 28 (2000).
[18] P.G. Young, E.D. Arthur, M.B. Chadwick, “Comprehensive nuclear model calculations: theory and use of the GNASH code”, LA-12343-MS (1992).
[19] J.S. Hendricks, G.W. McKinney, J.W. Durkee, J.P. Finch et al, M.L. Fensin, M.R. James, R.C. Johns, D.B. Pelowitz, L.S. Waters, “MCNPX, Version 26C”, LA-UR-06-7991 Dec.7, 2006.
[20] C.H.M. Broeders, A.Yu. Konobeyev, Yu.A. Korovin, V.N. Sosnin, “DISCA - advanced intranuclear cascade cluster evaporation model code system for calculation of particle distributions and cross-sections at intermediate energies”, FZK 7221, June 2006, http://bibliothek.fzk.de/zb/berichte/FZKA7221.pdf.

On the need of microscopic models for evaluation of deuteron activation data

M. Avrigeanu, F. L. Roman, V. Avrigeanu

"Horia Hulubei" National Institute for Physics and Nuclear Engineering (IFIN-HH), P.O. Box MG-6, 077125, Bucharest-Magurele, Romania
mavrig@ifin.nipne.ro

Abstract: The angular distributions of the elastic-scattered deuterons on ^{27}Al at energies between 5 and 63 MeV as well as the total reaction cross section have been analyzed by using the double-folding model for a semi-microscopic optical model potential (OMP) calculation. The energy-dependent full phenomenological OMPs up to 60 MeV have been obtained as well, in order to assist the required applications. Next, the comparison between the elastic angular distributions calculated with the deuteron global potentials and those obtained from the present OMPs proved the latter as most reliable.

Introduction

The description of deuteron-nucleus interaction represents an important test for both the quality of semi-microscopic optical models and evaluation of nuclear data requested especially for fusion reactor technology. However, the difficulties to interpret the data in terms of the usual optical-model potential (OMP), e.g. the significant contributions of the break-up channel and the enhancement of a variety of reactions at low bombarding energy hampered such a comprehensive analysis (e.g., [1, 2]). Therefore, the deuteron elastic-scattering differential cross sections at incident energies lower than 20 MeV are not satisfactory described by any phenomenological global OMPs of Daehnick *et al.* [3], Lohr and Haeberli [4], Perey and Perey [5], or the most recent Haixia *et al*. [6]. Thus, strong differences could be found between the calculated results within the whole range of the scattering angles, i.e. from 0° to 180° obtained by using these potentials. In the absence of a global phenomenological optical potential able to describe the low-energy (E<20 MeV) deuteron elastic scattering data, a semi-microscopic optical potential remains the starting point of the deuteron-nucleus interaction analysis.

The semi-microscopic DF analysis

The present analysis involves a semi-microscopic OMP which consists of a Coulomb term, the real double-folding (DF) potential, a phenomenological imaginary surface potential, and a spin-orbit component [2, 7]. The direct and exchange components of the real microscopic optical potential U_{DF} [7] are given in terms of the projectile and target nuclear densities, which are folded with the Paris M3Y effective NN interaction. The nuclear density distributions of ^{27}Al target nuclei have been described by a Fermi form factor with the parameters provided by the electron scattering data analysis of Negele [8]. The deuteron density distribution has been obtained from the experimental charge form factors measured by Abbott et al [9]. It should be emphasized that no adjustable parameter or normalization constant was involved in this analysis for the microscopic real potential in order to couple it with the phenomenological imaginary and spin-orbit part of the OMP. In this respect the predictive power of the full potential – i.e. the semi-microscopic one – has been preserved (see also Refs. [10-12] for details).

As the first step of the present work it resulted a semi-microscopic *local* optical potential, with the DF real part and imaginary as well as spin-orbit potential parameters obtained from the fit of the whole body of elastic-scattering differential cross sections for ^{27}Al from 5 up to 63 MeV. The average energy dependence of these imaginary and spin orbit local parameters lead to the semi-microscopic OMP. Comparison of the experimental elastic-scattering angular distributions of deuterons on ^{27}Al from 5 to 63 MeV [4, 13-22] with semi-microscopic OMP calculations as well as by using the predictions given by the global OMPs of Daehnick *et al*. [3], Lohr-Haeberli [4] ,and Perey-Perey, respectively are shown in Fig. 1.

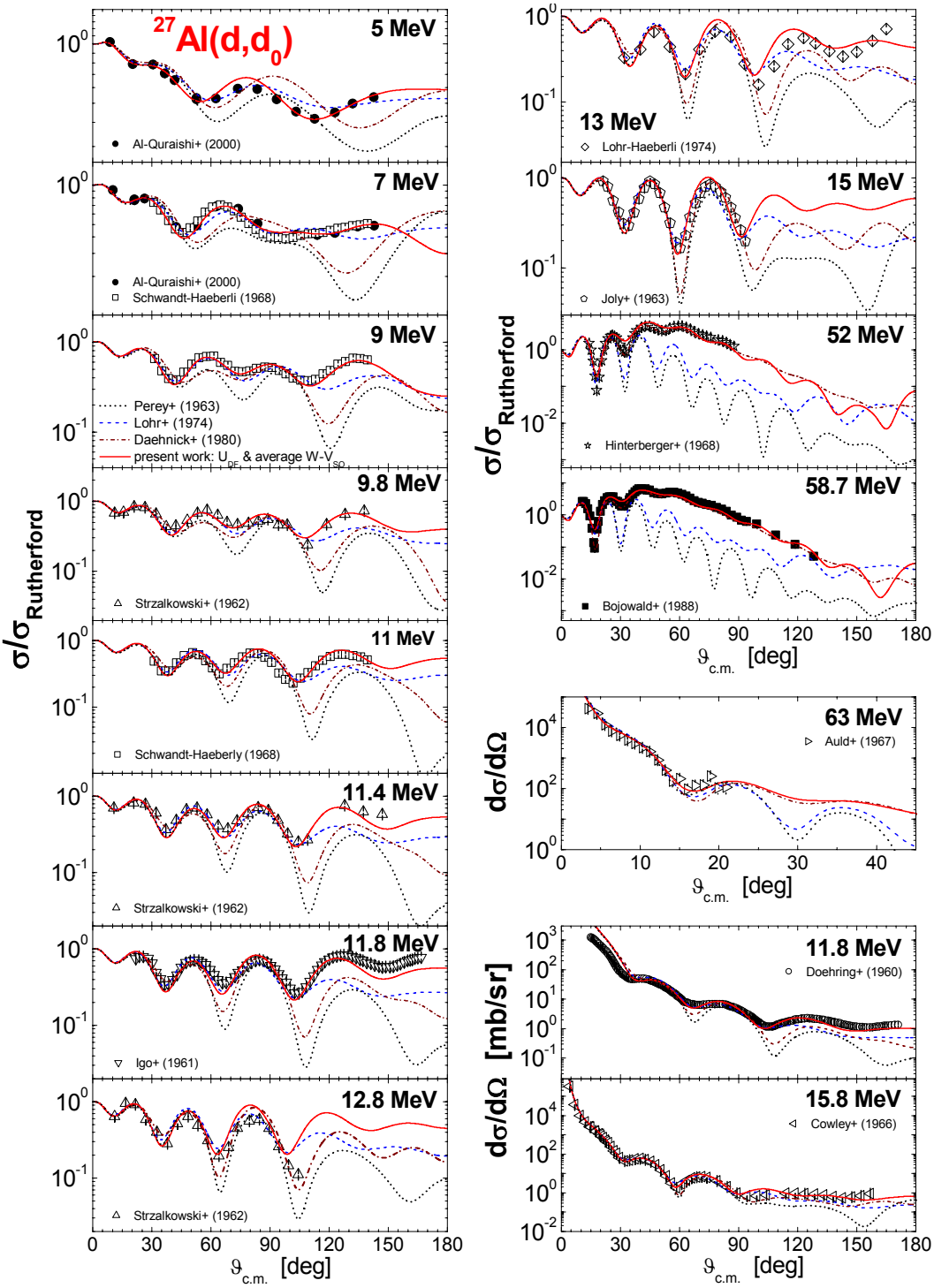

Figure 1. *Comparison of the experimental [4,13-22] and calculated elastic-scattering differential cross sections of the deuterons on ^{27}Al between 5 and 63 MeV using the semi-microscopic OMP (solid curves), as well as global parameter set of Daehnick et al. (dot-dashed curve), Lohr-Haeberli (dashed curves) and Perey-Perey (dotted curves).*

Average energy-dependent phenomenological OMP

The second step of our analysis has concerned the setting up of a real potential by keeping fixed the imaginary and spin-orbit potential parameters obtained previously within the semi-microscopic analysis, in order to obtain the full phenomenological OMP needed in applied calculations. The advantage of having well settled already at least half of the usual OMP parameters increases obviously the accuracy of fitting the data. Based on the corresponding local OMP parameters, the average energy-dependent OMP parameters have been obtained

and the corresponding average angular distributions are shown in Fig. 2 in comparison with those obtained with global OMP of Haixia at al[3], Bojowald *et al*.[20], as well as the default OMP of the TALYS code [23] .

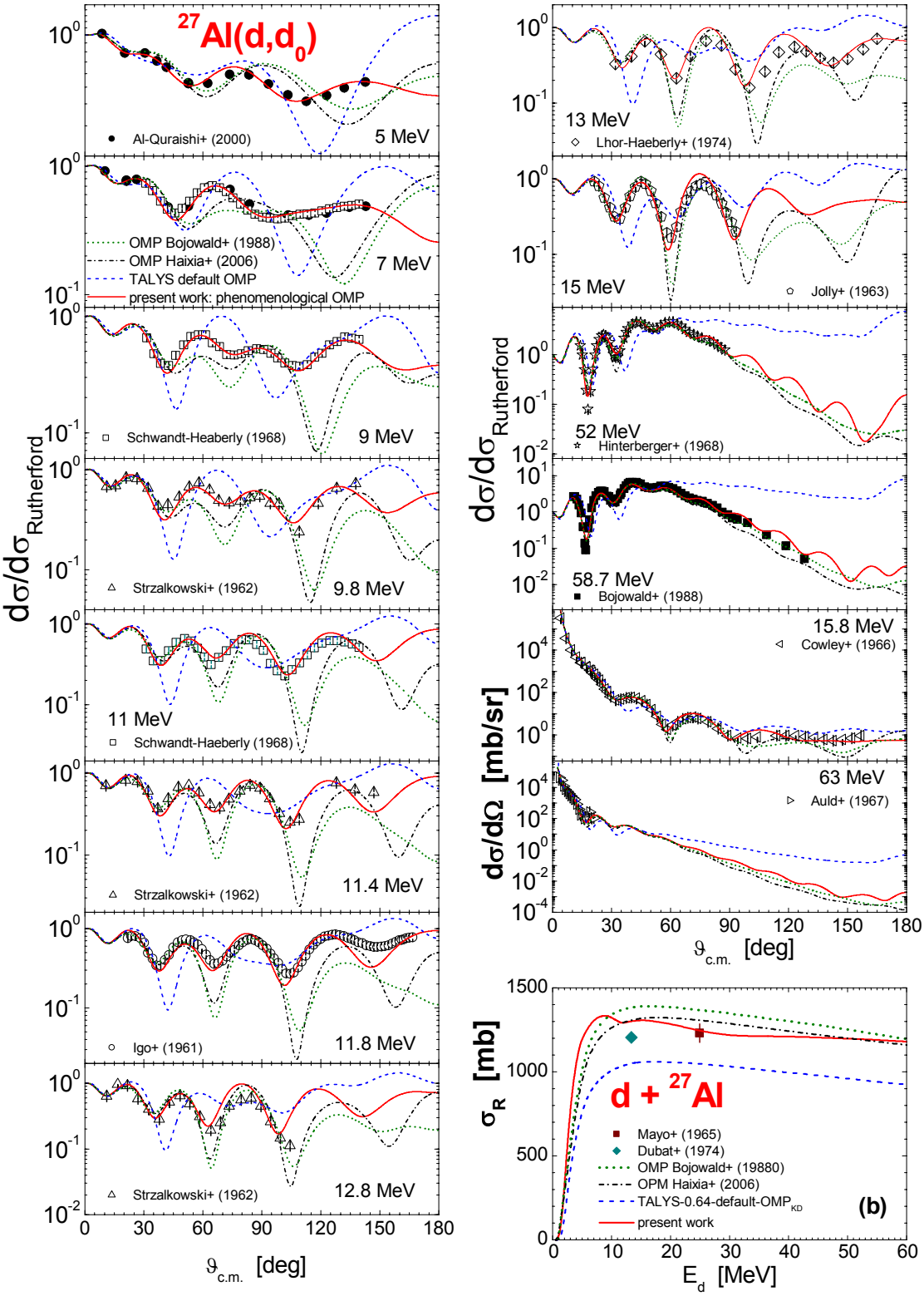

Figure 2. *Comparison of the experimental and calculated angular distributions of the elastic scattering of deuterons on ^{27}Al between 5 and 63 MeV by using the present phenomenological OMP as well as Haixie et al., Bojowald et al. and default TALYS code OMP parameters; (b) comparison between the experimental [24,25], and calculated total reaction cross sections for d+^{27}Al (see text for details).*

The measured total reaction cross sections [24,25] of deuterons are shown in the bottom part of Fig. 2 in comparison with the calculated values using the present phenomenological OMP for d+^{27}Al, the global [6,20] OMPs, and the default option of TALYS code [23] as well as the evaluated data of the ACSELAM library [26].

Conclusions

Based on a microscopic real potential, a phenomenological OMP for deuterons interaction with ^{27}Al at energies between 5 and 63 MeV have been obtained in order to assist the required applications. The available experimental angular distributions of the elastic-scattered deuterons on ^{27}Al, as well as the corresponding total reaction cross section have been analyzed with both the semi-microscopic and phenomenological OMP.
Finally, an improved description of the experimental data from 5 to 63 MeV is provided with respect to the predictions of Daehnick *et al*., Lohr-Haeberli, Perey-Perey, Bojowald *et al*., and Haixie *et al*. global OMPs, which can be considered a suitable validation of the actual OMPs.

Acknowledgements
Work supported under contract of Association EURATOM/MEdCT-Bucharest, and CNCSIS Contract No. PN2P3-2007-149.

References

[1] M Avrigeanu, W. von Oertzen, U. Fischer, V. Avrigeanu, Nucl. Phys. A 759, 327 (2005).
[2] M. Avrigeanu, H. Leeb, W. von Oertzen, F.L. Roman, V. Avrigeanu, Low energy deuteron elastic scattering on light and medium nuclei, in Int. Conf. on Nuclear Data for Science and Technology, April 22-27, 2007, http://www-dapnia.cea.fr/Sphn/nd2007/, #292.
[3] W.W. Daehnick, J.D. Childs, and Z. Vrcelj., Phys. Rev. C 21, 2253 (1980).
[4] J.M. Lohr and W. Haeberli, Nucl. Phys. A 232, 381 (1974).
[5] C.M. Perey and F.G. Perey, Phys. Rev. 132, 755 (1963).
[6] Haixia An and Chonghai Cai, Phys. Rev. C 73, 054605 (2006).
[7] M. Avrigeanu, H. Leeb, W. von Oertzen, F.L. Roman, and V. Avrigeanu, Proc. 11-th Int. Conf. on Nuclear Reaction Mechanisms, Varenna, edited by E. Gadioli, Ricercha Scientifica ed Educazione Permanente, Milano, Supplemento 126, p. 193 (2006).
[8] J.W. Negele, Phys. Rev. C 1, 1260 (1970).
[9] D. Abbott, A. Ahmidouch, H.Anklin, J. Arvieux et. al., Phys. Rev. Lett. 84, 5053 (2000).
[10] M. Avrigeanu, G.S. Anagnostatos, A.N. Antonov, and J. Giapitzakis, Phys. Rev.C 62, 017001, (2000).
[11] M. Avrigeanu, A.N. Antonov, H. Lenske, and I. Stetcu, Nucl. Phys. A 693, 616 (2001).
[12] M. Avrigeanu, W. von Oertzen, A.J.M. Plompen, and V. Avrigeanu, Nucl. Phys. A 723, 104 (2003).
[13] S.I.Al-Quraishi, C.E.Brient, S.M.Grimes et al., Phys. Rev. C 62, (2000) 044616.
[14] P.Schwandt and W.Haeberli, Nucl. Phys. A 110, 585 (1968).
[15] A.Strzalkowski, Phys. Lett. 2, 121 (1962).
[16] G.Igo, W.Lorenz and U.Schmidt-Rohr, Phys. Rev. 124, 832 (1961).
[17] A.Doehring, R.Jahr and H.Schmidt-Rohr, Z. Phys. 159, 149 (1960).
[18] R.K.Jolly, E.K.Lin and B.L.Cohen, Pys. Rev. 130, 2391 (1963).
[19] A.A.Cowley, G.Heymann, R.L.Keizer and M.J.Scott, Nucl. Phys. 86, 363 (1966).
[20] J.Bojowald, H.Machner, H.Nann, W.Oelert, M.Rogge, and P.Turek, Phys. Rev. C 38, 1153 (1988).
[21] E.G.Auld, D.G.Crabb, J.G.McEwen, L.Bird C.Whitehead, and E.Wood, Nucl. Phys. A101, 65 (1967).
[22] F.Hinterberger, G.Mairle, U.Schmidt-Rohr, G.J.Wagner, and P.Turek, Nucl. Phys. A111, 265 (1968).
[23] A.J. Koning, S. Hilaire, and M.C. Duijvestijn, ``TALYS: Comprehensive nuclear reaction modeling'', Proceedings of the International Conference on Nuclear Data for Science and Technology - ND2004, AIP vol. 769, eds. R.C. Haight, M.B. Chadwick, T. Kawano, and P. Talou, Sep. 26 - Oct. 1, 2004, Santa Fe, USA, p. 1154 (2005).
[24] L.V.Dubar, O.F.Nemets, L.I.Slyusarenko, and V.V.Tokarevskij, Yad. Fiz. 20, 624 (1974).
[25] S.Mayo, W.Schimmerling and M.J.Sametband, Nucl.Phys.62, 393 (1965).
[26] S. Tanaka et al., Development of IRAC code system to calculate induced radioactivity produced by ions and neutrons, in Proc. 8th Int. Conf. on Radiation Shielding, Arlington, April 1994, ANS, p. 965.

A proposal for an integral neutron data experiment in the 100-200 MeV region

J. Blomgren[1)], K. Chtioui[1,2)]

1) Department of Neutron Research, Uppsala University, Box 525, S-751 20 Uppsala, Sweden
2) Université de Caen, France
Jan.Blomgren@tsl.uu.se

Abstract: Cross section data for neutron-induced nuclear reactions at higher energies than for traditional applications of nuclear physics is required for the further development of sub-critical accelerator-driven systems (ADS) for transmutation of spent nuclear fuel. During the last decade, the situation on microscopic cross sections has improved significantly, to the extent that for the most important reactions, cross section data with uncertainties of about 10 % or less are available for a few key elements at some selected energies. Based on these data, nuclear data libraries up to about 200 MeV have been developed.
It is now motivated to make assessments of the predictive power of these libraries through integral experiments. In this paper, we present a pre-study of such a possible integral experiment on neutron data at two energies, 96 and 175 MeV. The reason for these two energies is the existence the high-intensity quasi-monoenergetic neutron source at The Svedberg Laboratory, Uppsala, Sweden. The envisaged experiment is on transmission and scattering of neutrons when passing blocks of iron or lead, with thicknesses ranging from 10 to 100 cm. Simulations of the proposed experiment have been performed with MCNP with two nuclear data libraries, JEFF-3.1 and ENDF/B-VI. The present project is part of the CANDIDE (Coordination Action on Nuclear Data for Industrial Development in Europe) project.

Introduction

As outlined in many places elsewhere in these proceedings, integral experiments are an indispensable activity in the evaluation and validation of nuclear data. Procedures for such validation are since long well established in the classical neutron energy range up to 20 MeV, i.e., the neutron energy range of relevance to critical fission reactors (thermal and fast), as well as fusion applications.
With the advent of accelerator-driven systems (ADS), the energy range in which information on neutron-induced nuclear reactions are required for design activities has been significantly increased. In a spallation-driven system, neutrons of energies all the way up to the incident proton energy, i.e., up to GeV energies, are present. Although relatively few neutrons reside at these high energies, their large capability to induce, e.g., materials damage necessitates the nuclear data libraries to be improved significantly above 20 MeV.
The ADS research activities funded by the EU have so far (FP 4, 5 and 6) been dominated by measurements of microscopic cross sections, a fact which has been motivated by the state of knowledge at the time these projects were launched. In particular the HINDAS project [1] in FP5 has resulted in fairly complete data bases on neutron elastic scattering and neutron-induced production of light ions up to about 100 MeV. In addition, fission total cross sections up to 200 MeV on a series of nuclei are now available, to a large extent thanks to ISTC projects. Total cross section data from LANL up to about 600 MeV on a series of nuclei complement the picture [2]. Thus, the most important microscopic cross sections are now available up to at least 100 MeV.
The recent achievements of these projects now motivate an increased attention to integral experiments, especially at ADS-relevant energies, i.e., above 20 MeV, where such experiments are almost absent. Thus, a few existing high-quality integral experiments should be identified. Above 20 MeV some shielding experiments exist, notably the 43 and 68 MeV TIARA transmission measurements for concrete and iron, which is mainly important for structural material studies [3].

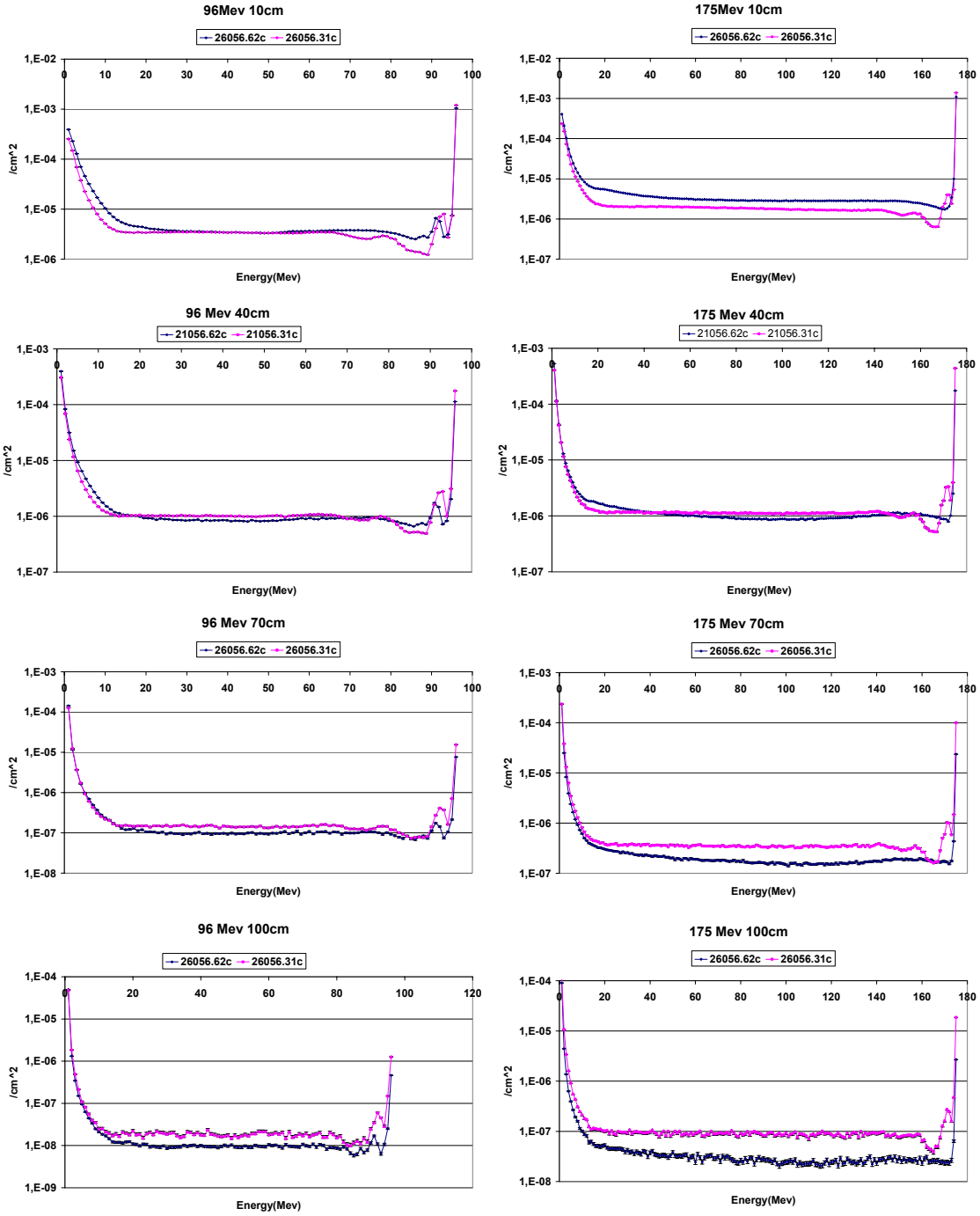

Figure 1. *Neutron transmission spectra for iron at 96 MeV (left column) and 175 MeV (right). From top to bottom, the spectra show transmission through 10, 40, 70 and 100 cm material thickness. The blue (dark) lines and the violet (light) lines show predictions by ENDF/B-VI and JEFF-3.1, respectively.*

What is missing is a clean experiment on core material that allows analysis of the impact of high-energy neutrons. An integral experiment of neutrons on a block of uranium would enable a thorough test of evaluated neutron data files above 20 MeV.

More complex systems, such as MEGAPIE [4], serve to test ADS calculations as a whole. The complex design of such target systems makes it, however, difficult to draw conclusions on the quality of the underlying nuclear data based on the performance of the full system.

The necessity and feasibility of integral experiments above the present maximum energy of 68 MeV will be investigated in the CANDIDE project [5]. In the present work, a first step towards this goal is presented. We have simulated the transmission of 96 and 175 MeV neutrons through slabs of iron and lead. The selections of materials have been dictated by the needs of ADS development. Iron is a representative construction material and lead is a candidate for coolant. Investigations of uranium constitute future work.

Simulation procedure

The transmission of neutrons through slabs of various thicknesses has been simulated using the MCNPX code [6]. We have used realistic dimensions of the neutron beam facility [7] at The Svedberg Laboratory (TSL), Uppsala, Sweden in all simulations. Neutrons are in reality produced by the ^{7}Li(p,n) reaction, which produces a quasi-monoenergy neutron spectrum, in which about half the neutrons have energies slightly below the energy of the incident proton beam, with a width of typically 1-2 MeV, and the remaining neutrons are spread out about equally on all energies from maximum down to zero energy. In our simulations, we have used strictly mono-energetic neutrons for simplicity and to accentuate the effects at high energies, where the nuclear data are the least well known. For proper detailed design of a realistic experiment, the neutron spectrum of the ^{7}Li(p,n) reaction should be used.
The neutron production is by all practical measures point-like. The neutrons are collimated to a narrow cone. At a distance of 401 cm from the production, the neutron beam impinges on a transmission target. At this position, the beam diameter is 10.9 cm. The transmission target is composed of slabs of target material, in our case iron or lead. We have simulated total thickness of 10, 40, 70 and 100 cm targets at two energies, 96 and 175 MeV. The choice of energies has been dictated by the maximum energies of the two operational modes of the TSL neutron beam facility.
In this exploratory study, we have used two nuclear data libraries, ENDF/B-VI [8] and JEFF-3.1 [9]. It is implicitly assumed that the differences in results between these two high-quality libraries reflect the underlying uncertainty in the knowledge of the true value of the cross section data.

Results

Results of transmission simulations on iron and lead are shown in Figs. 1 and 2, respectively. In both figures, results at 96 and 175 MeV are shown in the left and right panels, respectively. In general, all simulations show a similar pattern. There is a large peak at full energy, corresponding to neutrons transmitted without undergoing nuclear reactions. The compound peak at low energies is due to statistical decay, and the flat region in between is due to various types of pre-equilibrium reactions.
It was anticipated beforehand from basics physics considerations that the main differences should arise close to the full-energy peak, where the spectrum is sensitive to direct nuclear reactions. The reason for this is that calculations of cross sections for direct reactions are sensitive to nuclear physics details in the input. Thus, in the cases experimental data are absent, the evaluated data files have to rely on nuclear theory with fairly large uncertainties. In the other end of the spectrum, the compound peak at low energies should not display large deviations between the libraries, because it is governed by the well-known statistical emission. In between, some deviations can be found, manifesting differences in pre-equilibrium treatment.
These features are present in the results. It can be seen that there is indeed no significant differences between the libraries in the compound peak region. In both iron and lead, there are significant differences in the giant resonance region, i.e., at excitation energies of 5-20 MeV. One notable feature is that there are no visible giant resonance structures in lead at 175 MeV for any library, but there are such structures clearly predicted by ENDF/B-VI at 96 MeV, and to a lesser extent also by JEFF-3.1. It is difficult to identify a reason why such structures should not be present at 175 MeV, when they are clearly there at 96 MeV. Thus, this feature in the simulations is itself a reason for an experimental investigation. The libraries agree in general fairly well in the preequilibrium part of the spectrum, with the notable exception of iron at 175 MeV.

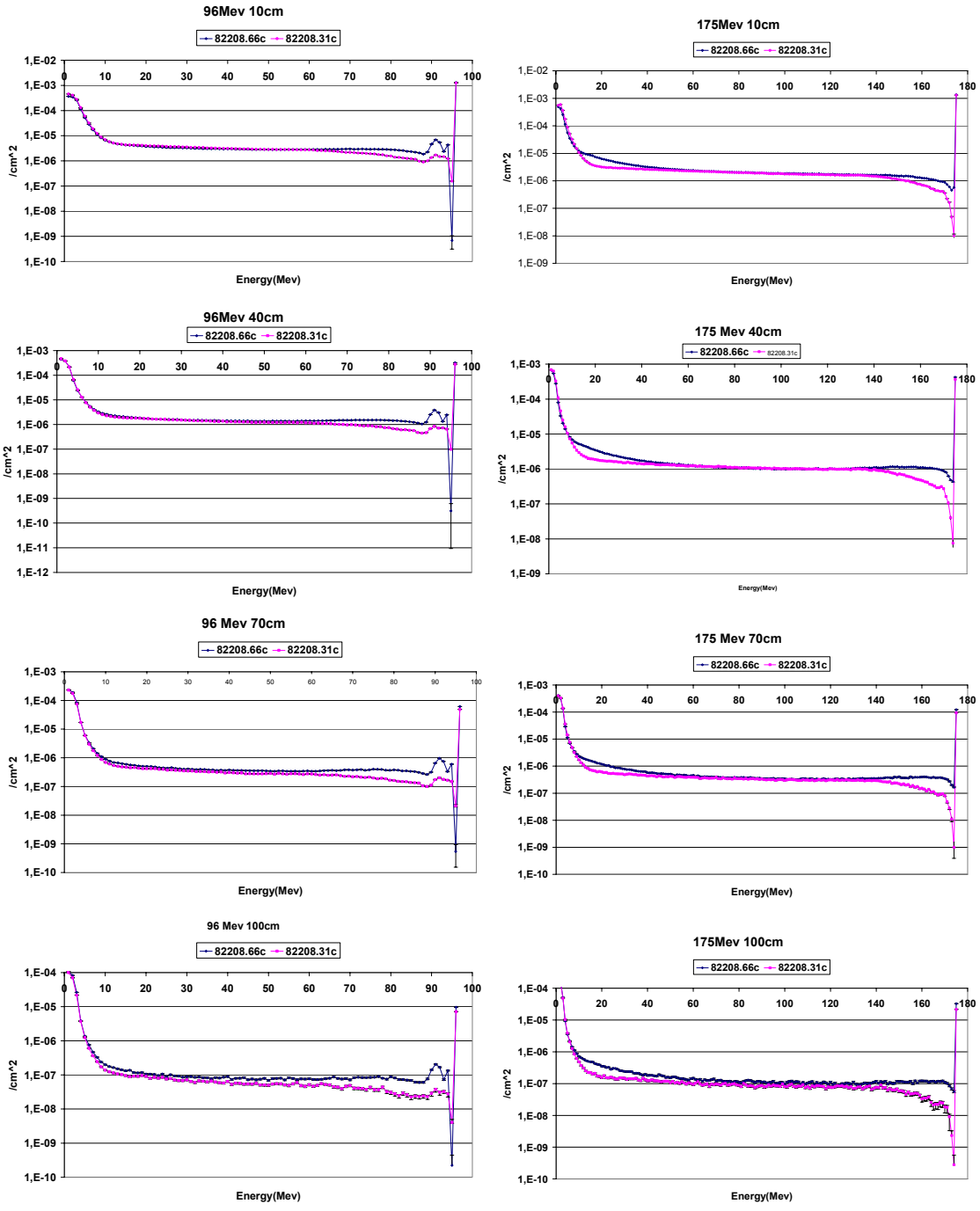

Figure 2. *Neutron transmission spectra for lead at 96 MeV (left column) and 175 MeV (right). From top to bottom, the spectra show transmission through 10, 40, 70 and 100 cm material thickness. The blue (dark) lines and the violet (light) lines show predictions by ENDF/B-VI and JEFF-3.1, respectively.*

Another important feature that might no be very obvious from the figures is the high-energy peak. It is especially notable in Figure 1 that the content in the high-energy peak for iron differs by a factor two at 96 MeV and almost a factor ten at 175 MeV for 100 cm target thickness. Measurement of this high-energy peak is a rather straight-forward procedure, with potential to yield valuable information.

In the case of lead, the differences in the high-energy peak are small. This does not necessarily reflect that the true value is well known. It could be the result of that these two evaluations use the same input. Thus, verifying the data on lead still has high priority.

It should be pointed out that in the case of lead, there are sharp dips in the spectra just below the high-energy peak. This is an artefact in the simulations. It just happens that there is no physical state in that particular bin. In reality, the experiment will be conducted with a resolution of, say, 5 MeV and then this dip will not appear.

Design of an integral experiment

The findings above are used as guidelines for a future integral experiment. Obviously, the expected differences are moderate or small at low neutron energies, whilst the most important discrepancies are found at fairly high energies, i.e., in the upper half of the energy range. This makes the detection easier in a gedanken experiment at TSL. The SCANDAL [7] neutron detector system at TSL is capable of detecting neutrons above 30-40 MeV with a resolution of typically 4 MeV. SCANDAL was originally designed for neutrons up to 130 MeV, but is presently being upgraded to work up to 180 MeV. Thus, SCANDAL can cover the maximum energy peak, the giant resonance region and most of the pre-equilibrium spectrum.
It would be valuable to cover also lower energies, preferably all the way down to zero energy. For these lower energies, other detectors have to be used. At present, a liquid scintillator for proton recoil detection and spectrum unfolding is being developed. This could possibly be used for these experiments. Another possibility is to use time-of-flight methods, but this is hampered by the relatively poor time structure of the beam. Moreover, wrap-around effects make part of the data ambiguous. Various detection schemes based on fission are also under consideration.

Outlook

What remains to be done is first to repeat these simulations also for uranium. Secondly, it would be interesting to test the sensitivity to individual cross sections in the libraries. Thus, it is planned to change one particular cross section and study in which way the transmission spectrum is changed.
These studies should be followed by detailed computations of experiment parameters. One crucial aspect is beam time. Already now, it is clear that with the differences displayed between the leading libraries in the present work, a well-designed experiment requires less than one week of beam time (i.e., a very realistic beam time) to reach sufficient accuracies for distinction between various libraries.

Acknowledgements
This work was financially supported by the European Union, contract 036397, Barsebäck Power AB, Forsmark AB, Ringhals AB, the Swedish Nuclear Power Inspectorate, the Swedish Nuclear Fuel and Waste Management, the Swedish Defense Research Agency and the Swedish Research Council.

References

[1] A. Koning, H. Beijers, J. Benlliure, O. Bersillon, J. Blomgren, J. Cugnon, M. Duijvestijn, Ph. Eudes, D. Filges, F. Haddad, S. Hilaire, C. Lebrun, F.-R. Lecolley, S. Leray, J-P. Meulders, R. Michel, R.-D. Neef, R. Nolte, N. Olsson, E. Ostendorf, E. Ramström, K.-H. Schmidt, H. Schuhmacher, I. Slypen, H.-A. Synal, R. Weinreich, J. Nucl. Sci. Tech., Suppl. 2 (2002) 1161.
[2] R.W. Finlay, W.P. Abfalterer, G. Fink, E. Montei, T. Adami, P.W. Lisowski, G.L. Morgan, R.C. Haight, Phys. Rev. C 47 237 (1993) 237.
[3] H. Nakashima, N. Nakao, S. Tanaka, T. Nakamura, K. Shin, S. Tanaka, H. Takada, S. Meigo, Y. Nakane, Y. Sakamoto, M. Baba, J. Nucl. Sci. Eng. 124 (1996) 243.
[4] W. Wagner, Y. Dai, H. Glasbrenner, M. Grosse, E. Lehmann, Nucl. Instr. Meth. A 562 (2006) 541.
[5] J. Blomgren, E. Bauge, D. Cano Ott, S. Csifrus, K. Dahlbacka, I. Gonçalves, E. González, H. Henriksson, R. Jacqmin, A. Koning, D. Lecarpentier, E. Malambu, A. Mengoni, R. Mills, A. Plompen, G. Rimpault, V. Starý, C. Trakas, P. Vaz, C. Zimmerman, in these proceedings.
[6] L.S. Waters, MCNPX Users' Manual – Version 2.1.5, Los Alamos National Laboratory, November 14, (1999).

[7] J. Klug, J. Blomgren, A. Atac, B. Bergenwall, S. Dangtip, K. Elmgren, C. Johansson, N. Olsson, S. Pomp, A.V. Prokofiev, J. Rahm, U. Tippawan, O. Jonsson, L. Nilsson, P.-U. Renberg, P. Nadel-Turonski, A. Ringbom, A. Oberstedt, F. Tovesson, V. Blideanu, C. Le Brun, J.F. Lecolley, F.R. Lecolley, M. Louvel, N. Marie, C. Schweitzer, C. Varignon, Ph. Eudes, F. Haddad, M. Kerveno, T. Kirchner, C. Lebrun, L. Stuttgé, I. Slypen, A. Smirnov, R. Michel, S. Neumann, U. Herpers, Nucl. Instr. Meth. A 489 (2002) 282.
[8] ENDF/B-VI, IAEA-NDS-100, Rev. 11 (1994). See also, e.g., www.nea.fr.
[9] JEFF-3.1, www.nea.fr.

Measurements of fission cross-sections of actinides at n_TOF

M. Calviani[1], N. Colonna[2], U. Abbondanno[26], G. Aerts[17], H. Álvarez[3], F. Álvarez-Velarde[4], S. Andriamonje[17], J. Andrzejewski[5], P. Assimakopoulos[6], L. Audouin[7], G. Badurek[8], P. Baumann[9], F. Becvar[10], E. Berthoumieux[17], F. Calviño[11], D. Cano-Ott[4], R. Capote[12,13], A. Carrillo de Albornoz[14], P. Cennini[15], V. Chepel[16], E. Chiaveri[15], G. Cortes[18], A. Couture[19], J. Cox[19], M. Dahlfors[15], S. David[7], I. Dillman[20], R. Dolfini[21], C. Domingo-Pardo[22], W. Dridi[17], I. Duran[3], C. Eleftheriadis[23], L. Ferrant[7], A. Ferrari[15], R. Ferreira-Marques[16], H. Frais-Koelbl[12], K. Fujii[26], W. Furman[24], I. Goncalves[16], E. González-Romero[4], A. Goverdovski[25], F. Gramegna[1], E. Griesmayer[12], C. Guerrero[4], F. Gunsing[17], B. Haas[27], R. Haight[28], M. Heil[20], A. Herrera-Martínez[15], M. Igashira[29], S. Isaev[7], E. Jericha[8], F. Käppeler[20], Y. Kadi[15], D. Karadimos[6], D. Karamanis[6], M. Kerveno[9], V. Ketlerov[25], P. Koehler[30], V. Konovalov[24], E. Kossionides[31], M. Krticka[10], C. Lampoudis[23],[17], H. Leeb[8], A. Lindote[16], I. Lopes[16], M. Lozano[13], S. Lukic[9], J. Marganiec[5], L. Marques[14], S. Marrone[2], T. Martínez[4], C. Massimi[32], P. Mastinu[1], A. Mengoni[12],[15], P.M. Milazzo[26], C. Moreau[2], M. Mosconi[20], F. Neves[16], H. Oberhummer[8], S. O'Brien[19], M. Oshima[33], J. Pancin[17], C. Papachristodoulou[6], C. Papadopoulos[34], C. Paradela[3], N. Patronis[6], A. Pavlik[35], P. Pavlopoulos[36], L. Perrot[17], M.T. Pigni[8], R. Plag[20], A. Plompen[37], A. Plukis[17], A. Poch[18], C. Pretel[18], J. Praena[1], J. Quesada[13], T. Rauscher[38], R. Reifarth[28], M. Rosetti[39], C. Rubbia[21], G. Rudolf[9], P. Rullhusen[37], J. Salgado[14], L. Sarchiapone[15], I. Savvidis[23], C. Stephan[7], G. Tagliente[2], J.L. Tain[22], L. Tassan-Got[7], L. Tavora[14], R. Terlizzi[2], G. Vannini[32], P. Vaz[14], A. Ventura[39], D. Villamarin[4], M.C. Vicente[4], V. Vlachoudis[15], R. Vlastou[34], F. Voss[20], S. Walter[20], H. Wendler[15], M. Wiescher[19], K. Wisshak[20]

The n_TOF Collaboration

1) Istituto Nazionale di Fisica Nucleare (INFN), Laboratori Nazionali di Legnaro, Italy
2) Istituto Nazionale di Fisica Nucleare (INFN), V. Orabona 4, 70126 Bari, Italy
3) Universidade de Santiago de Compostela, Spain
4) Centro de Investigaciones Energéticas Medioambientales y Tecnológicas CIEMAT, Madrid, Spain
5) University of Lodz, Lodz, Poland
6) University of Ioannina, Greece
7) Centre National de la Recherche Scientifique/IN2P3 - IPN, Orsay, France
8) Atominstitut der Österreichischen Universitäten,Techn. Universität Wien, Austria
9) Centre National de la Recherche Scientifique/IN2P3 - IReS, Strasbourg, France
10) Charles University, Prague, Czech Republic
11) Universidad Politecnica de Madrid, Spain
12) International Atomic Energy Agency (IAEA), Nuclear Data Sect., Vienna, Austria
13) Universidad de Sevilla, Spain
14) Instituto Tecnologico e Nuclear(ITN), Lisbon, Portugal
15) CERN, Geneva, Switzerland
16) LIP - Coimbra & Departamento de Fisica da Universidade de Coimbra, Portugal
17) CEA/Saclay - DSM/DAPNIA, Gif-sur-Yvette, France
18) Universitat Politecnica de Catalunya, Barcelona, Spain
19) University of Notre Dame, Notre Dame, USA
20) Forschungszentrum Karlsruhe GmbH (FZK), Institut für Kernphysik, Germany
21) Università degli Studi Pavia, Pavia, Italy
22) Instituto de Fısica Corpuscular, CSIC-Universidad de Valencia, Spain
23) Aristotle University of Thessaloniki, Greece
24) Joint Institute for Nuclear Research, Frank Lab. Neutron Physics, Dubna, Russia
25) Institute of Physics and Power Engineering, Kaluga region, Obninsk, Russia
26) Istituto Nazionale di Fisica Nucleare (INFN), Trieste, Italy
27) Centre National de la Recherche Scientifique/IN2P3 - CENBG, Bordeaux, France
28) Los Alamos National Laboratory, New Mexico, USA
29) Tokyo Institute of Technology, Tokyo, Japan
30) Oak Ridge National Laboratory, Physics Division, Oak Ridge, USA
31) NCSR, Athens, Greece
32) Dipartimento di Fisica, Università di Bologna, and Sezione INFN di Bologna, Italy
33) Japan Atomic Energy Research Institute, Tokai-mura, Japan
34) National Technical University of Athens, Greece

35) Institut für Isotopenforschung und Kernphysik, Universität Wien, Austria
36) Póle Universitaire Léonard de Vinci, Paris La Défense, France
37) CEC-JRC-IRMM, Geel, Belgium
38) Department of Physics and Astronomy - University of Basel, Basel, Switzerland
39) ENEA, Bologna, Italy
nicola.colonna@ba.infn.it

Abstract: Neutron-induced fission cross-sections of minor actinides have been recently measured at the n_TOF facility at CERN, Geneva, as part of a large experimental program aiming at collecting accurate new data relevant for Nuclear Astrophysics and for applications to emerging Nuclear Technologies. The measurements take advantage of the innovative features of the n_TOF facility, namely the wide energy range, high instantaneous neutron flux, and particularly low background. Preliminary results on the fission cross-sections of ^{233}U, ^{241,243}Am, and ^{245}Cm, from thermal to 3 MeV, are here reported. The measurements were performed with a Fast Ionization Chamber (FIC), relative to the standard cross-section of the ^{235}U(n,f) reaction. The fission cross-section ratio of ^{238}U/^{235}U up to 30 MeV is also presented.

Introduction

One of the problems in the development of nuclear energy production is the issue of nuclear waste treatment and storage. A significant fraction of the high-level nuclear waste is constituted by minor actinides, in particular Np, Am and Cm, built up as a result of multiple neutron captures and radioactive decays in current nuclear reactors. A possible solution to the problem of nuclear waste disposal could come from transmutation, via neutron induced fission of TRU's, in subcritical systems, such as an Accelerator Driven System (ADS), or in critical systems, such as future Gen-IV (fast) nuclear reactors [1]. Some isotopes, e.g. the fissile ^{233}U, are important for lighter fuel cycles, such as the Thorium Fuel Cycle, currently being considered for the lower production of minor actinides and non-proliferation issues.
In order to reduce calculation uncertainties in the design and operation of new generation reactors, high precision data on neutron-induced fission cross-sections from thermal energy to several tens of MeV are required for a variety of transuranic elements. In particular, there exist a pressing need for new measurements of neutron-induced fission for the long-lived isotopes of Am and Cm, for which available data are scarce or show large discrepancies.
With the aim of improving the accuracy of current databases, the n_TOF Collaboration has performed measurements of neutron-induced fission cross-sections for ^{233}U, ^{241,243}Am, and ^{245}Cm, as well as for the fission standards ^{235}U and ^{238}U. The measurements, performed at the innovative neutron facility n_TOF at CERN [2], allowed to collect data from thermal energy to several tens of MeV, with the full energy covered in one measurement only. The very high instantaneous neutron flux of n_TOF made possible, in some cases for the first time, to measure with good accuracy the fission cross-sections of isotopes with activity of hundreds of MBq. We report here the preliminary results on such measurements.

The neutron beam and experimental apparatus

The CERN n_TOF facility is a time-of-flight installation based on a spallation neutron source. Neutrons are produced by 20 GeV/c protons from the CERN Proton Synchrotron accelerator, impinging onto a 80x80x60 cm^3 lead block, surrounded by a 6 cm thick water layer acting as coolant and moderator of the neutron spectrum. The resulting energy spectrum spans over nine orders of magnitude, from thermal energy to approximately 1 GeV. Together with the wide energy range, the n_TOF facility is characterized by a very high instantaneous flux (1.5×10^7 n/pulse at the measuring station with the 8 cm diameter collimator used in fission measurements), and a low duty cycle (repetition rate of 0.4 Hz). At the measuring station, located at 187.5 m from the spallation target, the neutron beam presents a very high resolution in energy (1.1×10^{-3} at 30 keV), while a series of beam shaping collimators and thick shielding walls made of iron and concrete result in a very low ambient background [3].

The fission setup

The detection apparatus for the measurement of the neutron-induced fission cross-sections is based on a Fast Ionization Chamber (FIC) used for detecting the fission fragments. It is constituted by a stack of several parallel-plate chambers with 5 mm spacing between electrodes. It is operated with argontetrafluormethane (90% Ar+10% CF_4) at 720 mbar. The

whole detector is made of a stack of 17 ionization chambers, accommodating a total of 16 samples and 18 electrodes, for a total length of 50 cm. The setup allows to measure simultaneously the fission cross-sections of several isotopes. The samples are deposited on both sides of a 100 μm thick aluminum foil used as backing, mounted on a stainless steel holder. The diameter of the samples is 8 cm, and their thickness range from 4 to 450 μg/cm^2. Two different chambers have been used in the n_TOF measurements: FIC-0 was dedicated to low activity isotopes, whereas FIC-1 was used for highly radioactive species like ^{233}U, ^{241,243}Am and ^{245}Cm. This last chamber was qualified as a "sealed source" compliant with the ISO 2919 norm. The detector signals were acquired with a set of 8 bit Acqiris Flash Analog to Digital Converters (FADC) modules, at a sampling rate of 100 MS/s. The buffer memory of the FADC allows to record data for up to 80 ms, corresponding to neutrons in the thermal energy region. A detailed off-line analysis of the digitized signal allows to extract relevant information on the neutron time-of-flight and energy deposited by the fission fragments in the detector. The total mass of the samples are reported in Table 1, together with its uncertainty and the sample activity. These values along with the impurities in the various samples, have been obtained by alpha spectrometry using a silicon detector. The mass uncertainty is between 1 and 2 % for most samples. Since all cross-sections are measured relatively to the fission cross-section of ^{235}U (which is a standard at 0.0253 eV and from 0.15 eV to 200 MeV), the final overall uncertainty is expected to be ~3 %, in the whole energy region investigated.

Table 1. *Masses and uncertainties for the various TRU samples in FIC-1*

Sample	*Mass (mg)*	*Error (%)*	*Activity*
^{235}U	31.8	1.6	~0.2 kBq
^{233}U	28.8	1.7	~5 MBq
^{245}Cm	1.71	1.8	~0.2 GBq
^{241}Am	2.26	1.3	~76 MBq
^{243}Am	4.8	2.1	~7.4 MBq

Results

The first step in the analysis consists in determining for each signal the most relevant information, such as amplitude, total charge, time-of-flight and baseline value. Additionally, for each proton bunch, the beam intensity is extracted, together with the time of the initial γ-flash, used as a reference for the determination of the absolute neutron time-of-flight.
In Figure 1, left panel, the amplitude distributions for the various isotopes are presented. In the case of ^{235}U and ^{233}U a relatively low threshold on the amplitude is enough to reject electronic noise and background due to α-particles. On the contrary, for the ^{245}Cm sample, the presence of a large pile-up of α-particles complicates the analysis, since a higher threshold has to be applied which heavily affects the efficiency. As shown later, a subsequent normalization of the cross-section has to be performed in this case. For the time-to-energy conversion, the method developed in [4] was used. The main resonances in the ^{235}U(n,f) reaction were used for the energy calibration.

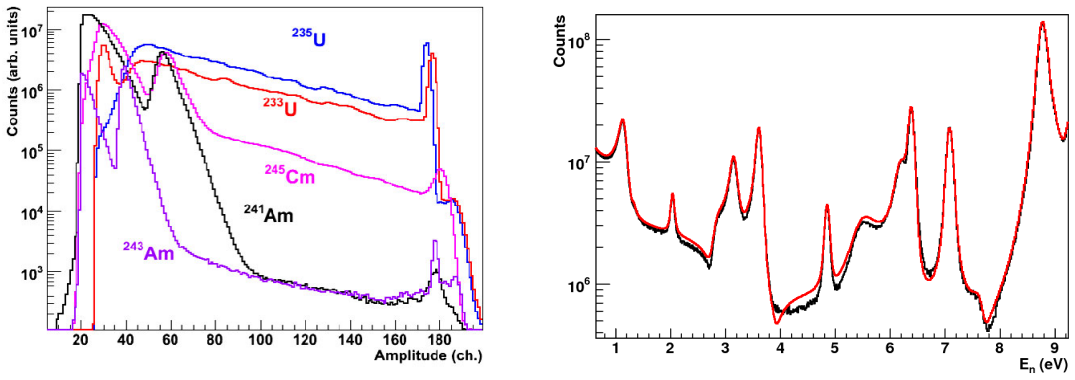

Figure 1. *Signal amplitude distribution for measured isotopes (left panel). The peak at channel ~180 is due to saturation in the FADC. Right panel: measured fission yield (in a.u.) for ^{235}U between 0.6 and 9.2 eV (black histogram), compared to ENDF/B-VII.0 (red).*

The right panel of Fig. 1 shows the extracted fission yield of ^{235}U, after calibration, and assuming an isolethargic neutron flux. A very good agreement between n_TOF and the evaluated library ENDF/B-VII.0 is observed, except in the resonance valleys. A comparison with previous data indicates that this discrepancy is due to a problem in the library. The figure also demonstrate the particularly low background of the present measurement. For the determination of the cross-sections of the measured actinides, the n_TOF neutron flux for the fission configuration (i.e. with the 8 cm diameter collimator) has to be extracted. To this end, the ^{235}U sample was used. In particular, the energy dependence of the neutron flux was derived from the ratio between the ^{235}U fission rate and the evaluated cross-section from ENDF/B-VII.0. MCNPX simulations have been performed in order to quantify the attenuation of the neutron beam in various materials (targets, backings and electrodes). This value has been evaluated to be at most of 0.1 %, so that no corrections need to be applied.

The ^{233}U(n,f) reaction

^{233}U(n,f) experimental cross section is shown in Fig. 2, together with the evaluated cross-section from ENDF/B-VII.0. For this isotope, a slightly higher threshold on the amplitude was applied, for α-background rejection. The resulting loss of efficiency was accounted for by extracting the flux from the ^{235}U sample, for the same threshold. The present analysis, still preliminary, shows a systematic discrepancy of the order of 5 % on average between the n_TOF data and the tabulated cross-sections. The origin of the systematic discrepancy is being investigated. Another possibility, however, would be to normalize the n_TOF data to the cross section from Deruytter and Wagemans [5,6] in the energy range between 8.1 and 17.6 eV, as suggested by Guber et al. in [7]. Small differences in the height of some ^{233}U(n,f) resonances are observed, while in the resonance dips the experimental cross section appears to be lower than the evaluated data, indicating a good rejection of the α-background.

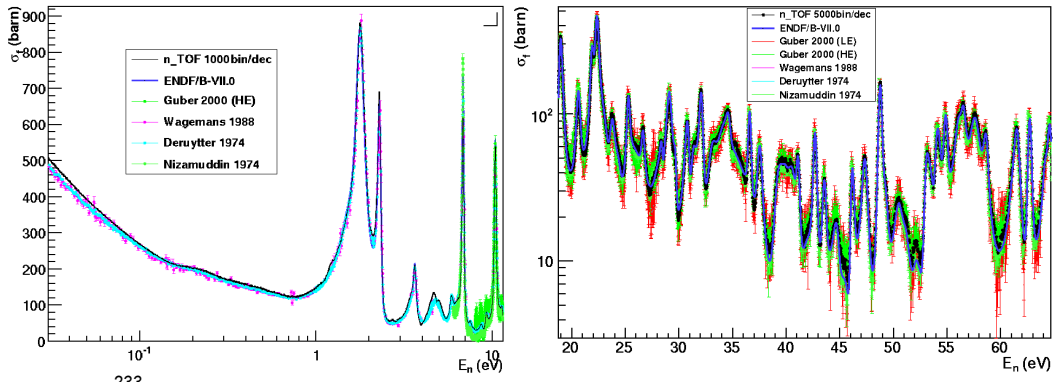

Figure 2. *^{233}U(n,f) cross section from thermal energies up to 70 eV together with ENDF/B-VII.0 data and other experimental results.*

The ^{241,243}Am(n,f) reactions

Accurate new data on fission cross-section of ^{241}Am are very important for ADS and Gen IV systems, since the present uncertainties, in particular above few hundreds of keV, are too high compared to the target accuracy required for the design of the new reactors. Measurements of the fission cross section of ^{241}Am are difficult to perform because of the extremely high α-particle activity of this nuclide. Its half-life against α-decay is 433 yr. For this reason, although several measurements have been performed on this isotope in the past, there are still large uncertainties. A measurement at n_TOF can improve the signal/noise ratio by a large factor, thanks to the very high instantaneous neutron flux. Figure 3, left panel, shows the preliminary results of the ^{241}Am(n,f) cross-section measured at n_TOF. The α-background was in large part suppressed with a high threshold on the signal amplitude. The residual contribution was estimated from the runs without beam and subtracted. While around and above threshold the cross-sections are in good agreement with previous experimental results and evaluated data, at low energy some differences are observed. In particular, a value higher than expected is observed in between resonances. Furthermore, the results show the presence of resonances that cannot be attributed to ^{241}Am. The most probable explanation for these observations is a possible contamination of ^{242m}Am, which is characterized by a fission cross-section up to 3 orders of magnitude higher than that of ^{241}Am, as shown in the figure. Even a very low contamination, around one part per thousand, is sufficient to account for the observed discrepancy. A more accurate analysis is now been

performed in order to get a more precise estimate of the ^{242m}Am contamination. It should be noticed that above a few hundreds keV, the effect of the contamination becomes negligible.

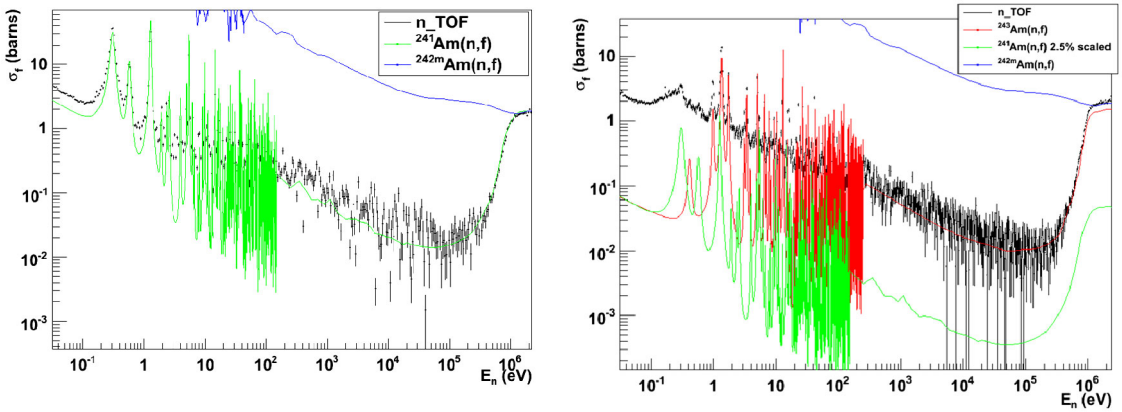

Figure 3. *^{241}Am(n,f) and ^{243}Am(n,f) cross-section measured at n_TOF are shown on the left and right panel respectively.*

In the case of ^{243}Am, the present situation of the experimental data below threshold is rather bad. Very few measurements exist for this isotope. The difficulty, in this case, is associated with the low fission cross-section, with a correspondingly poor signal-to-background ratio. In the present measurement, a complication arises from the declared contamination of ^{241}Am (2.5 %) and, possibly, from a very small presence of ^{242m}Am, which is expected as in the previous case. The right panel of Figure 3 shows the preliminary fission yield for this isotope, compared with the prediction of ENDF-B/VII.0 for ^{243}Am, ^{241}Am (scaled for the 2.5 % abundance in the sample) and ^{242m}Am (not scaled). In this case as well, even a very small contamination of ^{242m}Am represents a problem, given the low fission cross-section of ^{243}Am at low energy. Some discrepancy is also observed at high energy, still being investigated.

The ^{245}Cm(n,f) reaction

^{245}Cm is one of the most interesting minor actinides, for which only few and discordant experimental data exist, due to the relatively short half-life of this isotope ($t_{1/2}$ ~8500 yr). The very large α- background is evident in Fig. 1, where a second peak due to the pile-up of two α-particles can be seen. A further complication is related to the known contamination of 6.6 %, of ^{244}Cm, which presents a much higher rate of spontaneous fission.

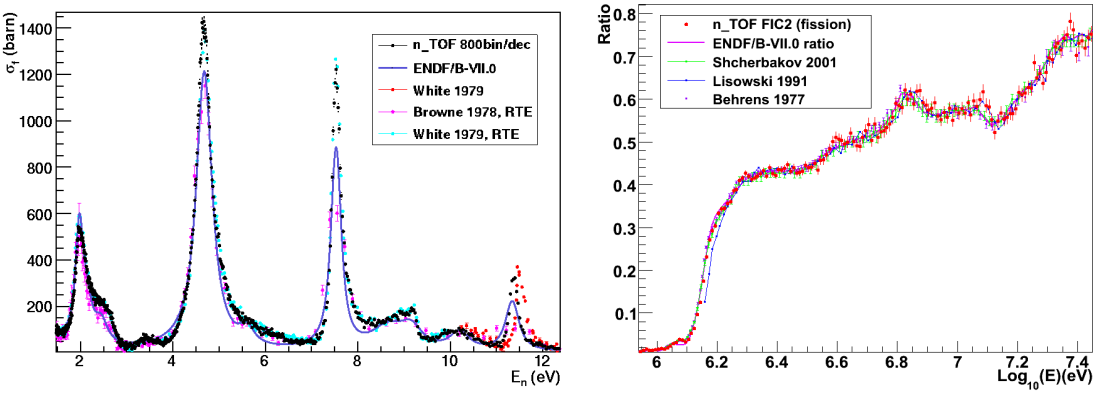

Figure 4. *Left panel: fission cross-section of 245Cm from 1.8 to 12 eV, measured at n_TOF (in black) compared with ENDF-B/VII and previous measurements. Right panel: ^{238}U/^{235}U fission cross-section ratio in the subthreshold region and from the threshold to 20 MeV.*

For this reason, in addition to a higher amplitude threshold, the experimental data have been corrected also for the residual α-background and spontaneous fission. The level to be subtracted was determined from measurements performed without the beam, for the same amplitude threshold. Due to an uncertainty in detection efficiency, a normalization to a known cross-section value is required. The present n_TOF data have been normalized to the ENDF/B-VII.0 cross-section at 0.03 eV, which agrees with Benjamin *et al.* [8] and Gavrilov *et*

al. [9] within 1 σ. The energy range of the n_TOF data is bigger than any previous measurement. The cross-sections in this case have been extracted in the range from 0.03 eV to 2 MeV (extension to an even higher energy is currently being performed). A previous measurement for this isotope with resolution comparable to n_TOF is from Moore *et al.* [10], obtained with an intense single neutron pulse of a nuclear explosion. These data, however, are only above 10 eV. The left panel in Figure 4 shows the ^{245}Cm(n,f) cross-sections for the first three resonances in the energy range between 1 and 10 eV. For all these resonances, the n_TOF data show a cross-section in the right tail higher by ~25 % relative to the evaluated ENDF/B-VII.0 cross-sections. In this case as well, the problem seems to be associated to the library, since a good agreement is observed between the n_TOF data and those from White et al. [11]. Moreover the 4.65 eV and 7.5 eV resonances are 15 % and 35 % higher than the ENDF/B-VII.0 evaluated data, respectively, in agreement with ref. [11].

The ^{238}U(n,f)/^{235}U(n,f) cross-section ratio

As previously pointed out the ^{235}U(n,f) cross section is a standard at 0.0253 eV and from 0.15 eV to 200 MeV, while the ^{238}U(n,f) cross section is a standard from 2 MeV to 200 MeV. The measurement of the ^{238}U/^{235}U fission cross section ratio is particularly important since it can be used by evaluators to test nuclear reaction codes and compile nuclear data evaluations. In the literature there are only two recent experimental results, Lisowski *et al.* [12] and Shcherbakov *et al.* [13], that cover a wide energy range. These two data sets are discordant above 64 MeV and partially below the threshold energy. We performed the analysis using two different chambers (FIC-1 and FIC-2) and adopting two different analysis strategies, obtaining comparable results. It should be noticed that the measured ratio does not depend on the shape and value of the neutron flux since the two samples have been measured simultaneously. As shown in Fig. 4, right panel, n_TOF data agree well with Shcherbakov's results, while confirming the discrepancy with the data of Lisowski around the threshold. The analysis is presently extended to extract the ratio up to a neutron energy of 300 MeV.

Conclusions

Neutron-induced fission cross-section measurements of ^{235,238}U, ^{233}U, ^{241,243}Am and ^{245}Cm have been performed at n_TOF, with a Fast Ionization Chamber (FIC). The first, preliminary results for ^{233}U and ^{245}Cm are consistent with databases in the resonance region, with no normalization required for ^{233}U. In the case of ^{245}Cm, after the subtraction of the background (α-particles and spontaneous fission of ^{244}Cm contaminant), very clean data are obtained. These results are among the first experimental data in the energy range between thermal energy and 20 eV, while at higher energy a good agreement with previous data is observed. For the ^{241}Am, and even more for the ^{243}Am samples, a further complication is most probably related to a very small contamination of ^{242m}Am. We have estimated that even a level of contamination of the order of 10^{-3} constitutes a problem, given the extremely high fission cross-section of this isotope. The determination of resonance parameters is now in progress with the SAMMY code for all minor actinides here presented. Finally, we have constructed the ^{238}U/^{235}U fission cross-section ratio up to an energy of 20 MeV. The n_TOF results are consistent with Shcherbakov's measurement, from the ^{238}U threshold to this energy.

References

[1] NEA-OECD, ed., Accelerator Driven Systems (ADS) and Fast Reactors (FR) in Advanced Nuclear Cycles (NEA-OECD, 2002).
[2] U. Abbondanno et al., Nucl. Instr. and Meth. A 538, 692, (2005).
[3] U. Abbondanno et al., n_TOF Performance Report, CERN/INTC-O-011, INTC-2002-037 (2002).
[4] G. Lorusso et al., Nucl. Instr. and Meth. A 532, 622 (2004).
[5] A.J. Deruytter, C. Wagemans, Nucl. Sci. Eng. 54, 423 (1974).
[6] C. Wagemans et al. in Conf. on Nucl. Data for Sci. and Techol. (Mito, Japan, 1988).
[7] K.H. Guber et al., Nucl. Sci. Eng., 135, 141 (2000).
[8] R.W. Benjamin et al., Nucl. Sci. Eng. 41, 203 (1972).
[9] V.D. Gavrilov et al., Atomnaya Energiya 41, 185 (1975).
[10] M.S. Moore et al., Phys. Rev. C 3, 1656 (1971).
[11] R.M. White et al. in Conf. on Nucl. Data for Sci. and Technol. (1979), p.496.
[12] P.W. Lisowski et al. in Conf. on Nucl. Data for Sci. and Technol. (1991), p.732.
[13] O.A. Shcherbakov et al. in Interaction of Neutrons with Nuclei (2001), p.288.

Neutron cross section analysis of ^{237}Np and ^{240}Pu between 1 eV and 2 keV

C. Guerrero[1], D. Cano-Ott[1] and The n_TOF Collaboration[2]

1) CIEMAT- Avda. Complutense, 22 28040 Madrid, Spain
2) www.cern.ch/ntof
carlos.guerrero@ciemat.es

Abstract: The neutron capture cross sections of ^{237}Np and ^{240}Pu were measured at the CERN n_TOF facility from 1 eV to 2 keV using the Total Absorption Calorimeter. The capture yields are calculated with a systematic uncertainty lower than 5% and are normalized to the most reliable transmission measurements, which are included in the resonance analysis with the SAMMY code. The resonance parameters and the associated covariance matrices obtained in this analysis are consistent with both, capture and transmission data.

Introduction

One of the solutions proposed for the management of radioactive nuclear waste is the transmutation of minor actinides and long-lived fission products by capture and fission reactions in dedicated devices such as Accelerator Driven Systems (ADS) or GEN-IV reactors. This technology could reduce substantially (by a factor of 100 or more) the radiotoxicity of the long lived component of the nuclear waste. The detailed engineering designs, safety evaluations and the accurate performance assessment of dedicated transmutation ADS and critical reactors require more precise and complete basic nuclear data [1] that should be measured with the required accuracy.
The capture cross sections of the most relevant minor actinides and fission products are being measured using the time-of-flight method at the n_TOF facility. The facility, with a high instantaneous neutron flux at a 185 m flight path, is especially well suited for measurements on low mass and/or radioactive samples. The n_TOF facility and its performance in terms of neutron fluence, energy resolution, sources of background, etc., is described in detail in Ref. [2], including the fully digital Data Acquisition System.
The neutron capture detection system consists of a segmented total absorption calorimeter (TAC) [3] made of 40 BaF_2 crystals with ^{10}B loaded carbon fiber as shown in Figure 1.

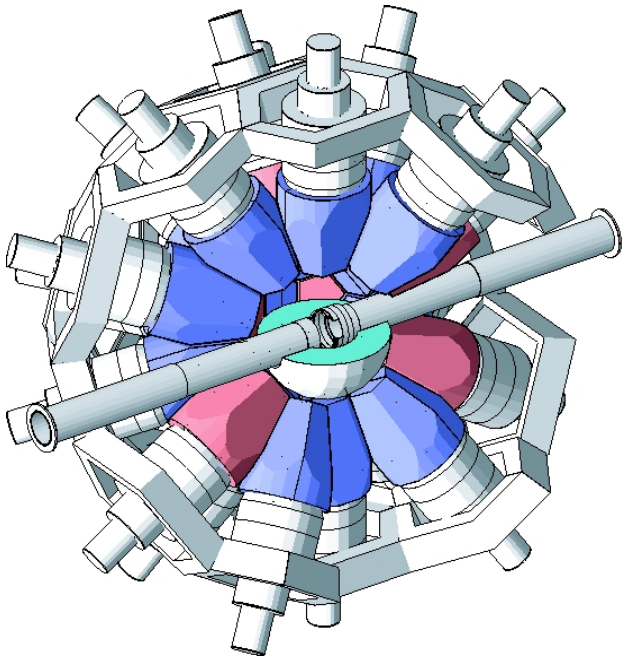

Figure 1. *The n_TOF TAC as it is implemented in the Monte Carlo simulations.*

The TAC has nearly 100% detection efficiency for capture events and good energy resolution (~14.4% at 662 keV). The neutron sensitivity and the sample activity are reduced by using a $C_{12}H_{20}O_4(^6Li)_2$ neutron absorber placed between the sample and the BaF_2 crystals.
In this work we present the measurement and analysis of the capture cross sections of ^{237}Np and ^{240}Pu between 1 eV and 2 keV. Final results will be published soon.

Experimental capture yield

The experimental capture yield, defined as the fraction of neutrons entering the sample, which undergo a capture reaction, is calculated from the number of detected events, the detection efficiency and the neutron flux intersecting the sample.
Under experimental conditions, the number of detected events is affected by several sources of background such as the activity of the samples, in-beam γ-rays, neutrons scattered in any material along the beam-line, etc. The segmentation of the TAC and its high total absorption efficiency can be used to apply specific conditions with respect to the deposited energy and multiplicity of the detected events to reduce most background components significantly.
The detection efficiency (including dead-time losses) is calculated [4] within 4% by means of Monte Carlo simulations with GEANT4 and the neutron flux intersecting the sample is calculated within 3% by the combination of on-line neutron monitors and of reference measurements, e.g. via the 4.9 eV resonance of ^{197}Au. The accuracy of the experimental capture yield is further improved by including transmission data in the cross section analysis, since these are less uncertain with respect to normalization and neutron flux.

Cross section analysis

The measured capture yields are analyzed together with transmission data using the SAMMY code [5]. Capture and transmission are analyzed sequentially using the resonance parameters and covariance matrix of the fit to one data set as input for the next one. The results are resonance parameters compatible with all data sets and a realistic covariance matrix.

^{237}Np cross section

The resolved resonance region (RRR) of ^{237}Np can be extended up to 500 eV. In this region the SAMMY fits were performed in ten energy intervals fitting all resonance parameters below 43 eV. At higher energies the radiative width was kept fixed to the average value (40.9$\pm$1.8 meV) found below 43 eV. Figure 2 shows an example of the SAMMY fits to capture data from n_TOF and to transmission data by Gressier et al. (GELINA, 1998) [6].
In the unresolved resonance region the yield was transformed into capture cross section using the thin target approximation. The code FITACS [7] included in SAMMY was used to fit the average capture cross section with average resonance parameters from a Hauser-Feshbach calculation with width fluctuations. The results agree within uncertainties with those found in the RRR.
In general, the ^{237}Np(n,γ) cross section from n_TOF agrees with the latest evaluations and the data of Weston et al. [8] (ORELA, 1981) and Scherbakov et al. [9] (RRI, 2005). However, they are in clear disagreement with the measurements by Esch et al.[10] (DANCE/LANL, 2004) in the URR and those of Kobayashi et al. [11] (RRI, 2002) in the complete energy range under study.

^{240}Pu cross section

The ^{240}Pu capture yield was analyzed up to 2 keV following the procedure of the ^{237}Np resonance analysis and using the transmission data of Kolar and Böckhoff [12] (GELINA, 1968), which are the basis of the latest evaluations [13]. In this case, the accuracy in the calculation of the capture yield for energies below 110 eV suffered from inhomogeneities in the capture sample, which caused sizable self-shielding effects.
The ^{240}Pu cross section from n_TOF differs significantly with respect to the evaluations, with differences ranging from +10% at 110 eV to -10% around 2 keV. It should be kept in mind that our analysis preserves the total cross section measured by Kolar and Böckhoff, Therefore the differences in σ(n,γ) appear from the fact that the correlation between Γ_γ and Γ_n is reduced when both capture and transmission are analyzed together. Indeed, the existing evaluations are only based on transmission data, which is not sufficient to calculate accurate partial cross sections because neither the condition σ(n,n)>>σ(n,γ) nor the opposite are satisfied.

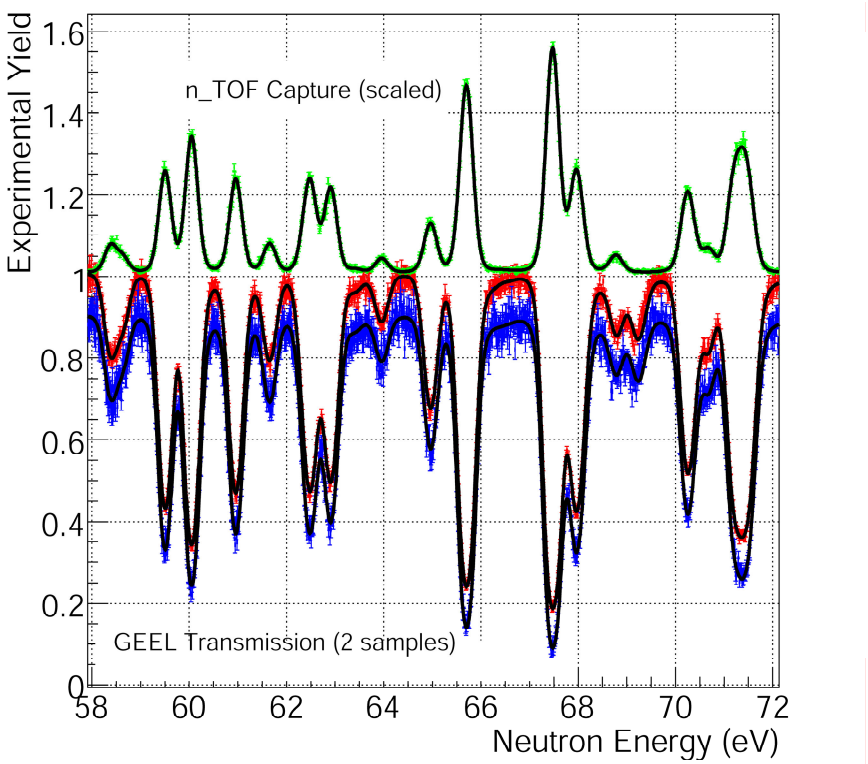

***Figure 2**. Example of the SAMMY fit (black line) to the n_TOF capture yield (green dots) and transmission at GELINA (red and blue dots) for the case of ^{237}Np.*

Conclusions

In this work we have presented the measurement and analysis of the (n,γ) cross sections of ^{237}Np and ^{240}Pu between 1 eV and 2 keV with the Total Absorption Calorimeter at the n_TOF facility.

The experimental capture yield, which has been briefly described, was analyzed together with the most reliable transmission data available using the SAMMY code in the resolved and unresolved resonance region. The results are in agreement with the evaluation for the case of ^{237}Np, but there are clear discrepancies between our ^{240}Pu capture cross section and those found in the evaluations. This underlines the importance of including all reaction channels in the evaluations, since otherwise the partial cross sections are highly correlated and it is not possible to calculate them with the required accuracy.

For this reason, the use of fission tagging samples for measuring in parallel neutron capture and fission cross sections is planned among the upgrades for the n_TOF-Ph2 project.

Acknowledgements

This work has been supported partially by the NTOF-ND-XADS project from the EU 5th Framework Programme, the CIEMAT-ENRESA Agreement on the "Transmutación aplicada a los residuos radiactivos de alta actividad" and the Spanish Plan Nacional de Física de Partículas under contract FPA2005-06918-C03-01.

References

[1] G. Aliberti et al., Nucl. Sci. Eng. 146 (2004) 13-50.
[2] U. Abbondano et al., CERN/INTC-O-011, INTC-2002-037.
[3] D. Cano-Ott et al., Proc. Int. Conf. on Nuclear Data for Science and Technology, Santa Fe, USA, AIP Conf. Proceedings, 769 (2004) 1442.
[4] C. Guerrero, Simulación Monte Carlo del Calorímetro de Absorción Total de n_TOF, Diploma Thesis, Universidad Complutense de Madrid (June 2005).
[5] N.M. Larsson, ORNL/TM-9179/R7 (2006).
[6] V. Gressier, DAPNIA/SPHN-99-04T.

[7] F.H. Fröhner, B. Goel and U. Fischer, Report ANL-83-4 (1983).
[8] L. W. Weston et al., Nuc.Sci.Eng. 79 (1981) 184.
[9] O. Scherbakov, K. Furutaka, S. Nakamura, H. Sakane, K. Kobayashi, S. Yamamoto, J. Hori and H. Harada, Nucl. Sci. and Eng. 42 (2005) 135-144.
[10] E.I. Esch, Los Alamos Scientific Lab. Reports 05 6885 (2005).
[11] K. Kobayashi, S. Lee, S. Yamamoto, H. J. Cho and Y. Fujita, Nucl. Sci. and Eng. 39 (2002) 111-119.
[12] W. Kolar and K. H. Böckhoff, Journal of Nuclear Energy 22 (1968) 299-320
[13] O. Bouland, H. Derrien, N. M. Larson and L. C. Leal, Nucl. Sci. and Eng., 127 (1997) 105-129.

Neutron inelastic scattering measurements using GAINS at GELINA

A. Negret[1], C. Borcea[1,2)], A.J.M. Plompen[1)]

1) European Commission, Joint Research Centre, Institute for Reference Materials and Measurements, Retieseweg 111, 2440 Geel, Belgium
2) IFIN "Horia Hulubei", P.O. Box MG-6, Bucharest-Magurele, Romania
alexandru-liviu.negret@ec.europa.eu

Abstract: A considerable effort was dedicated during last years to the upgrade of the setup used for measurements of neutron inelastic cross sections at GELINA. The completely renewed setup called GAINS (Gamma Array for Inelastic Neutron Scattering) is now operational at a 200 m flight path of the white neutron source GELINA.
GAINS consists of eight high-efficiency HPGe detectors placed at 110° and 150° in close geometry around the sample. The acquisition system is based on four 12 bits, 420 MHz digitizers with two input channels each.
The reliability of the system was already proven for ^{206}Pb data (based on a comparison with a former measurement). A ^{56}Fe(n,x$n'\gamma$) measurement is ongoing.
The present contribution describes the new system together with the analysis method. It further emphasizes the difficulties of a highly accurate ^{56}Fe(n,$n'\gamma$) measurement and shows the preliminary available results.

Introduction

A very successful program for measuring (n,x$n\gamma$) cross sections was running at GELINA during the last years. High resolution data were obtained for various isotopes (see, e.g., [1, 2]). However, the increased demand of highly accurate neutron inelastic data [3] represented the main motivation for upgrading the experimental setup and transforming it into a gamma spectrometer with increased detection efficiency.

Experimental setup and analysis algorithm

GELINA, the white neutron source of JRC-IRMM consists of a linac that sends 1 ns electron bursts on a ^{238}U target with a repetition rate of 800 Hz. The strong bremsstrahlung produced induces (γ,n) and (γ,f) reactions that produce a neutron burst of about 1 ns with an energy range from 0.2 MeV to about 25 MeV. A 200 m flight path is used in the present measurements. Each neutron burst is preceded by a very intense gamma flash from the original bremsstrahlung.
The flight path of 200 m is sufficient to allow time-of-flight measurements using HPGe detectors. The neutron flux is scattered on a sample with the thickness of the order of a few mm. The emerging gamma rays (mainly from inelastic excitation of the sample) are detected with HPGe detectors. The energy of the gamma rays allows the identification of the induced transition while the timing is related to the energy of the incoming neutron.
GAINS (Gamma Array for Inelastic Neutron Scattering) [4] was built as a gamma spectrometer dedicated to the (n,x$n\gamma$) measurements. It consists of 8 HPGe detectors (100% efficiency) placed at scattering angles of 110° and 150°. These angles (nodes of the fourth degree Legendre polynomial) allow a precise integration of the angular distribution for transition with multipolarities up to three. The acquisition system is based on four Acqiris DC440 (420 MS/s, 12 bits) digitizer cards.
A ^{235}U fission chamber is used to monitor the neutron flux in the 200 m cabin. All cross sections obtained with the present setup are therefore normalized to the ^{235}U(n,f) cross section.
The primary experimental result is represented by the gamma production cross sections for various transitions in a nucleus. Further, the level scheme of the studied nucleus from an external database is used in order to determine the total inelastic cross section (based on the sum of all gamma transitions to the ground state) and various level cross sections.

For the strongest transitions the total uncertainty of the cross sections is of the order of 5% and it is dominated by various systematic uncertainties.

Neutron inelastic cross sections on ^{56}Fe

The importance of iron as a structural material is obvious. ^{56}Fe is the main iron isotope, with a natural abundance of 91.75%. The accuracy studies for the design of all fast systems conclude that the uncertainty of neutron inelastic cross section of ^{56}Fe should be reduced from 7-25% to a level of 2% [3, 5].

Experimental considerations

A natural iron sample (99.5% purity) with a thickness of 3 mm was irradiated for about 6 weeks.

The total neutron inelastic cross section of ^{56}Fe is dominated by the contribution from the gamma transition from the first excited state (847 keV, 2^+) to the ground state. Two transitions could represent a source of background in that energy region:

- A gamma transition from ^{27}Al at 844 keV. The entire frame supporting the experimental setup, as well as the structural components of the detectors are made from aluminium. Therefore it is possible that neutrons scattered on the iron sample excite ^{27}Al generating the 844 keV gamma transition.
- The neutron inelastic excitation of ^{72}Ge produces a gamma ray of 834 keV. This energy is added to that of the recoil of the ^{72}Ge nucleus and produces a signal in the detector. This phenomenon results in a specific triangular shape in the spectrum produced by any HPGe detector exposed to a neutron flux with various energies.

In order to reveal the shape of the background under the 847 keV transition an additional measurement was performed with a Ni sample. Figure 1 compares the two time-integrated spectra.

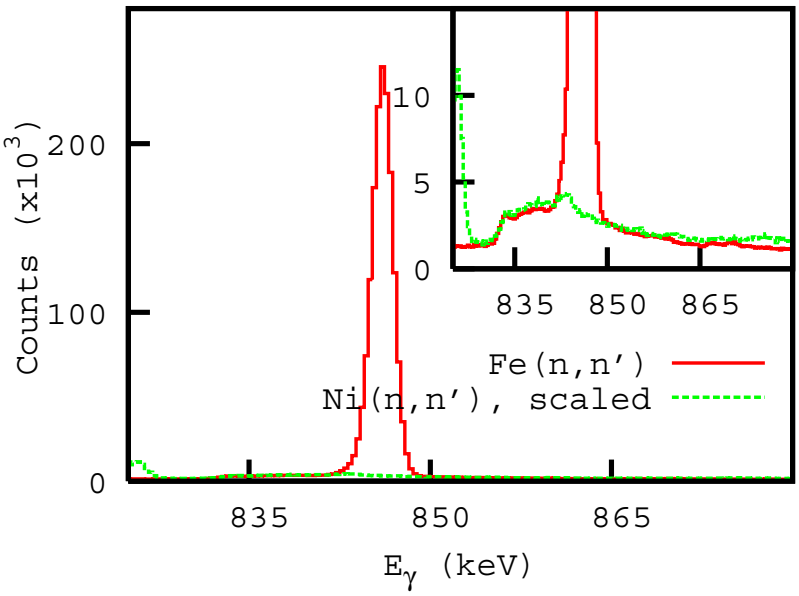

Figure 1. *Comparison of two time-integrated spectra in the 850 keV region. Red: spectrum obtained on the Fe sample; the 847 keV transition dominates the spectrum. Green: spectrum obtained with a Ni sample and scaled; the level of background in this region can be estimated from this comparison. The top-right box represents a zoom on the y axis.*

Preliminary results

^{56}Fe data are under analysis. Figure 2 displays the preliminary total inelastic cross section, deduced mainly from the gamma production cross section of the 847 keV transition.

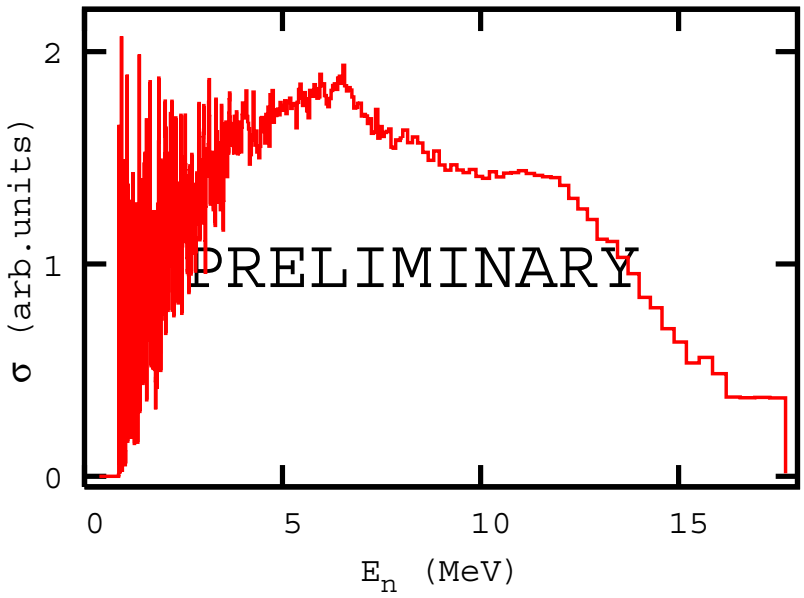

Figure 2. *Total neutron inelastic cross section of ^{56}Fe. Preliminary result.*

Further measurements are necessary before the absolute values of the cross section will be accurately determined. A dedicated experiment is foreseen in order to empirically analyse the effect of the neutrons on the germanium detector.

Conclusions

GAINS, the upgraded setup dedicated to neutron inelastic cross section measurements at GELINA is completely commissioned and the first set of data was taken for a ^{56}Fe sample. The analysis is under way and further consistency tests are necessary before final cross sections will be delivered.

References

[1] L.C. Mihailescu, C. Borcea, A.J. Koning and A.J.M. Plompen, "High resolution measurement of neutron inelastic scattering and (*n,2n*) cross-sections for ^{52}Cr", Nucl. Phys. A 786, 1 (2007)

[2] L.C. Mihailescu, C. Borcea, A.J. Koning, A. Pavlik, A.J.M. Plompen, "High resolution measurement of neutron inelastic scattering and (*n,2n*) cross-sections for ^{209}Bi", Nucl. Phys. A (2008), in print,

[3] G. Aliberti, G. Palmiotti and M. Salvatores, "Global target accuracy study", Proceedings of the Nemea 4 workshop (2007).

[4] A. Negret, C. Borcea, J.C. Drohe, L.C. Mihailescu, A.J.M. Plompen and R. Wynants, "A new setup for neutron inelastic cross section measurements", Proceedings of the ND2007 conference (2007).

[5] G. Aliberti, G. Palmiotti and M. Salvatores, "Target accuracy assessment for an ADS design", Proceedings of the Nemea 4 workshop (2007).

Neutron spectra measurement and calculations using different data libraries in iron benchmark assembly

B. Jansky[1)], Z. Turzik[1)], E. Novak[1)], M. Karac[1)], L. A. Trykov[2)], A.I. Blokhin[2)]

1) Nuclear Research Institute Řež plc, Czech Republic
2) Institute of Physics and Power Engineering, Obninsk, Russia
blokhin@ippe.ru

Abstract: The leakage neutron spectra measurements have been done on benchmark spherical assembly - iron sphere with diameter of 100cm. The Cf-252 neutron sources with different emissions were placed into the centre of iron sphere. The proton recoil method was used for neutron spectra measurement using stilbene crystals and hydrogen proportional counters. The neutron energy range of spectrometer was from 0.01 to 17MeV. The gamma pulse shape discrimination (PSD) method has been applied in stilbene measurements. The adequate MCNP neutron spectra calculations based on different data libraries (ENDF/B-VI.8, BROND-3, JENDL-3.3, JEFF-3.1) have been done and compared with measurements. Some aspects of presented benchmark are discussed in details including reproducibility of measurements, influence of group structure, smoothing of spectra, energy resolution of spectrometer, methodology of calculation (1-or 3-dimensional problem, results uncertainties), methodology of experiment (neutron background measurement using shadow cone). The results of analogous measurements and calculations performed on pure iron spheres of diameters 20, 30 and 50cm are also briefly discussed in the report.

Introduction

Neutron and gamma fields parameters behind iron and water layers corresponding to reactor pressure vessel were studied on benchmark iron spherical assemblies with diameter of 20, 30, 50 and 100cm, and on water spherical assemblies with diameter 30 and 50cm. The Cf-252 neutron sources were placed into the centre of iron sphere.

In this article the results of the leakage neutron spectrum measurement from the largest sphere of 100cm diameter are presented because of the discrepancies between calculation and experiment are the most significant.

The measurement results are compared with parallel calculations using four different data libraries in MCNP code. The following data libraries were used: ENDF/B-VI, BROND-3, JENDL-3.3, JEFF-3.1. In the following text the libraries are usually marked by shorted name ENDF, BROND etc. The measurement results can serve as integral verification of various data libraries.

Experimental assembly

The experimental assemblies is formed by the pure iron sphere with diameter of 100cm with neutron source in centre, see Fig.1. Neutron spectra were measured in two distances: R=150cm, abbrev. of assembly is FE DIA100, R150, shadow cone used (background is subtracted), spectrum was measured by stilbene and H-detector R=53cm, abbrev. of assembly is FE DIA100, R53, shadow cone not used, (background is included), spectrum was measured only by H-detector.

Methodology of calculation and measurement

The spherical shape of assemblies and spherical neutron source is used because this geometry represents the most simple one-dimensional (1D) calculation task. As a matter of fact, the assembly is a 3D object. The methodological 3D test-calculations (for Fe sphere of diam.50cm) was carried out and compared with simplified 1D results. The differences are not significant. The background of the measured field is determined by additional measurement performed with shielding cone. The shielding cone has to shield corresponding space angle to measure all unwelcome scattered neutrons and laboratory background neutrons.

Neutron spectrometers

The proton recoil method was used for neutron and gamma spectra measurement as well as main methods. Hydrogen proportional counters (0.01-1.3MeV) and scintillation detector of stilbene (0.1-17MeV) were used for neutron spectra measurement in the total energy range of 0.01-17MeV. The group structure used for H-detector is 40 or 200 group per decade (gpd). The group structure used for stilbene is the constant energy step in selected energy regions.

Spherical hydrogen detectors were of 4cm diameter and of 100, 400 and 1000kPa pressure. The dimension of stilbene was of diameter 3x1cm.

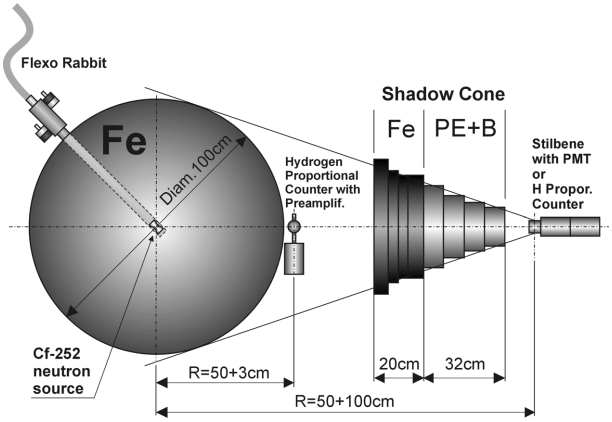

Figure 1. *Basic scheme of n-spectrum measurement. The sphere center is 200cm above the concrete floor.*

Calculation

The calculations were performed using Monte-Carlo program MCNP4c. As for geometry description, a simplified model [2] was used, which substitutes assembly elements with concentric spherical shells around the source. Also, the detector is represented by a 1cm thick spherical shell with radius equal to the real detector-source distance. In this way, considerable variance reduction has been achieved, while the results had remained essentially unperturbed in almost the whole energy range. Two detector shell radii have been dealt with: 53cm (which, in the case of a 100-cm-diameter sphere represents measurement of the spectrum close to the surface) and 150cm (which represents distant measurement).
For each calculation, 108 particle histories were computed. For JENDL3.3 library, 2x108 histories were calculated. The energy bin structure of resulting tallies was chosen to be logarithmic, either with 40 or with 200 groups per decade. Photon tallies start at 0.001MeV and end at 12.59MeV, while neutron tallies range from 1e-10MeV to 22.39MeV. However, only ten groups per decade scale are used up to 0.001MeV. The following nuclear data libraries were used in calculation: ENDF/B-VI.8, BROND-3, JENDL-3.3, JEFF-3.1. The evaluated nuclear data files were processed using NJOY-99.115.

Normalisation and smoothing of results

The result of spectra calculation and measurement φ(E) is normalised in the following way
$4\pi R2\ \varphi(E) / Q$ [1/MeV] (1)
where R is distance between detector and neutron source (centre to centre) and Q[1/s] is neutron source emission.
Quantity depicted in the figures has the following form and dimension
$4\pi R2\ E\ \varphi(E) / Q$ [1] (2)
The integral values presented in tables are also with dimension of 1.
The calculated spectra were smoothed by Gaussian with constant percentage resolution Δ of FWHM:
Δ=13% for 40gpd and Δ=4% for 200gpd.

Uncertainties

MCNP code gives only statistical uncertainties which are smaller then 5% for En<6MeV, 40gpd and 108 histories. Statistical uncertainties of H-detector measurements are calculated and represent the values about 3% for spectrum maximum for FE DIA100, R150 assembly and about 1% for FE DIA100, R53 assembly. These uncertainties were assessed for 40gpd. Statistical uncertainties of integral values are adequately calculated. Uncertainties based on methodology of measured spectra evaluation (like energy calibration etc.) are estimated by authors to be approx. 1-2% for energy range 0.15-0.8MeV and 3-7% for energy range 0.01-0.15MeV. Uncertainties of stilbene measurements are estimated by authors to be 7-15 % for energy range 1-17MeV. Estimation of another existing uncertainties (like of the source emission, efficiency of detectors etc.) is out of scope of this article.

Results of measurement and calculations

Two types of experimental results are presented: Assembly FE DIA100, R150, H-detector and stilbene measurement, binding energy for those methods is 1.2MeV,. Assembly FE DIA100, R53 (measurement on the surface), H-detector only. Comparison of measured and calculated results are presented in figures 2-8 and tables 1-3. The measurement on the surface in R=53cm seems to be reasonable for obtaining better statistics of experiment.

Table 1. *Assembly FE DIA100, R150; 40gpd, H-det and stillbene measurement - integral values (energy range is in MeV).*

	Energy Range		Libraries used for MCNP Calculation				
No.	from	to	EXP	ENDF	BROND	JENDL	JEFF
0	**0.01**	**17.00**	**8.397E-01**	**8.556E-01**	**8.459E-01**	**8.409E-01**	**8.796E-01**
1	**0.01**	**0.03**	1.289E-01	1.115E-01	1.105E-01	1.131E-01	1.210E-01
2	**0.03**	**0.10**	9.592E-02	8.575E-02	8.296E-02	8.934E-02	8.969E-02
3	**0.10**	**0.15**	1.112E-01	9.619E-02	9.608E-02	1.056E-01	1.156E-01
4	**0.15**	**0.20**	8.359E-02	7.546E-02	7.465E-02	7.965E-02	8.424E-02
5	**0.20**	**0.40**	2.534E-01	3.065E-01	3.090E-01	2.928E-01	2.872E-01
6	**0.40**	**0.80**	1.371E-01	1.543E-01	1.508E-01	1.393E-01	1.537E-01
7	**0.80**	**1.20**	2.231E-02	2.090E-02	1.733E-02	1.604E-02	2.264E-02
8	**1.20**	**1.70**	5.800E-03	3.853E-03	3.260E-03	3.999E-03	4.057E-03
9	**1.70**	**2.50**	1.203E-03	8.958E-04	9.618E-04	9.482E-04	1.108E-03
10	**2.50**	**4.00**	2.696E-04	1.676E-04	2.199E-04	1.456E-04	2.485E-04
11	**4.00**	**6.00**	5.125E-05	4.360E-05	4.369E-05	3.738E-05	4.680E-05
12	**6.00**	**8.00**	1.604E-05	1.546E-05	1.445E-05	1.220E-05	1.559E-05
13	**8.00**	**10.00**	6.455E-06	6.868E-06	6.946E-06	4.686E-06	6.707E-06
14	**10.00**	**17.00**	4.090E-06	2.984E-06	3.184E-06	2.599E-06	3.086E-06

Table 2. *Assembly FE DIA100, R53; 200gpd, H-det measurement - integral values (energy range is in MeV).*

	Energy Range		Libraries used for MCNP Calculation				
No.	from	to	EXP	ENDF	BROND	JENDL	JEFF
0	**0,01**	**1,29**	**1,044E+00**	**1,078E+00**	**1,064E+00**	**1,064E+00**	**1,114E+00**
1	**0,01**	**0,03**	1,533E-01	1,387E-01	1,374E-01	1,401E-01	1,505E-01
2	**0,03**	**0,08**	7,075E-02	6,358E-02	6,030E-02	6,529E-02	6,610E-02
3	**0,08**	**0,09**	4,185E-02	4,142E-02	4,100E-02	4,365E-02	4,300E-02
4	**0,09**	**0,15**	1,576E-01	1,326E-01	1,325E-01	1,460E-01	1,588E-01
5	**0,15**	**0,20**	1,047E-01	9,654E-02	9,498E-02	1,018E-01	1,071E-01
6	**0,20**	**0,25**	6,486E-02	6,643E-02	6,425E-02	6,559E-02	6,637E-02
7	**0,25**	**0,29**	7,799E-02	8,494E-02	8,211E-02	8,028E-02	8,013E-02
8	**0,29**	**0,33**	9,448E-02	1,354E-01	1,333E-01	1,241E-01	1,209E-01
9	**0,33**	**0,41**	8,185E-02	1,046E-01	1,154E-01	1,081E-01	1,043E-01
10	**0,41**	**0,52**	5,090E-02	5,296E-02	5,077E-02	4,867E-02	5,701E-02
11	**0,52**	**0,78**	1,146E-01	1,317E-01	1,279E-01	1,171E-01	1,271E-01
12	**0,78**	**1,06**	2,379E-02	2,257E-02	1,930E-02	1,665E-02	2,585E-02
13	**1,06**	**1,29**	7,426E-03	6,759E-03	5,311E-03	6,393E-03	6,690E-03

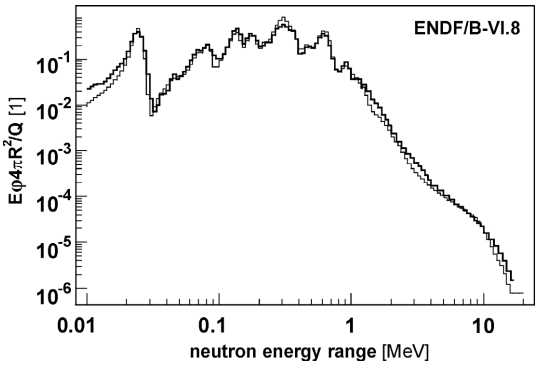

Figure 2. *Assembly: FE DIA100, R150, 40gpd. Measurement by H-det and stilbene - thick. Calculation by ENDF/B-VI.8 - thin.*

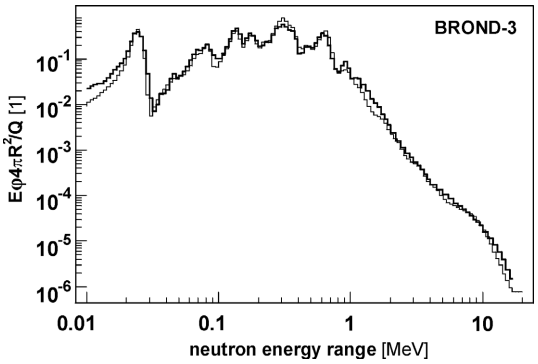

Figure 3. *Assembly: FE DIA100, R150, 40gpd. Measurement by H-det and stilbene - thick. Calculation by BROND-3 – thin.*

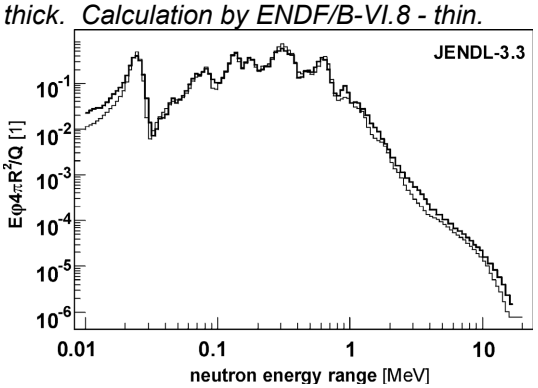

Figure 4. *Assembly: FE DIA100, R150, 40gpd. Measurement by H-det and stilbene - thick. Calculation by JENDL-3.3 – thin.*

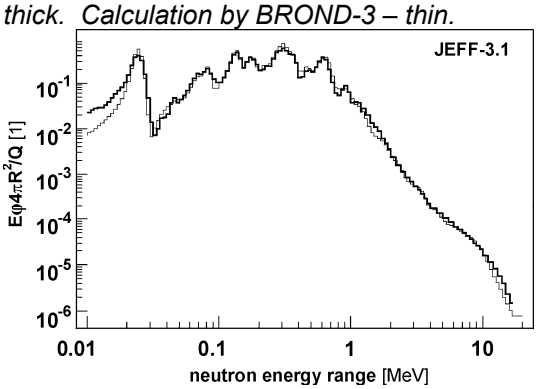

Figure 5. *Assembly: FE DIA100, R150, 40gpd. Measurement by H-det and stilbene - thick. Calculation by JEFF-3.1 – thin.*

Conclusion

The calculations performed in scale 40gpd overestimate measured spectra (by H-det and stilbene) in region around 0.3MeV by about 10-20% and also around 0.6MeV by about 10% (see Fig.8).

The calculations in the energy region above 1MeV underestimate measured spectrum (by stilbene) by about 20-40% depending on the library used (see Table 1 and Fig.8).

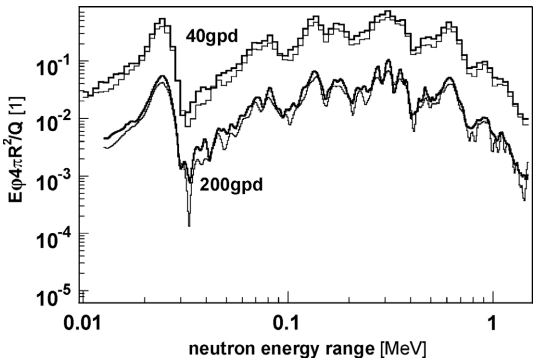

Figure 6. *Assembly: FE DIA100, R150 and R53, 40gpd and 200gpd. Measurement by H-det. R53-thick, 200gpd (diminished 10x).*

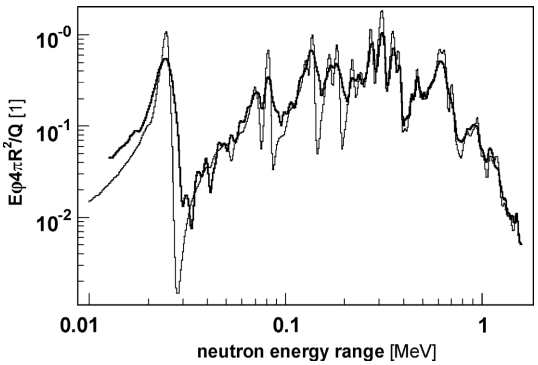

Figure 7. *Assembly: FE DIA100, R53, 200gpd. Measurement by H-det – thick. Calculation by ENDF/B-VI.8 – thin.*

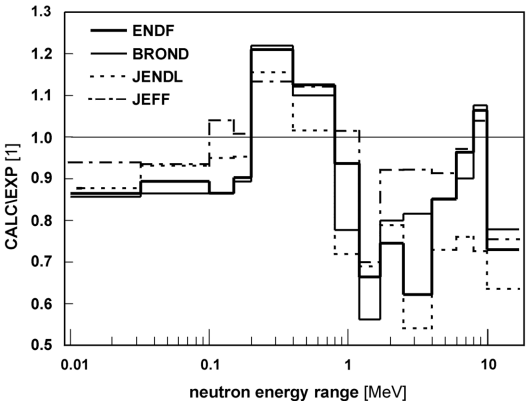

Figure 8. *Assembly: FE DIA100, R150, 40gpd. Measurement by H-det and stilbene. Comparison of calc. relative to EXP (Table 1).*

Table 3. *Assembly FE DIA100, R150 and R53; 200gpd, H-det measurement - integral values (energy range is in MeV). Data presented as the Calculation/Experiment*

	Energy Range			Library used for MCNP Calculation			
No.	**from**	**to**	**EXP**	**ENDF**	**BROND**	**JENDL**	**JEFF**
0	**0.01**	**1.29**	**R53**	**1.033**	**1.019**	**1.019**	**1.067**
			R100	**1.029**	**1.017**	**1.011**	**1.059**
1	**0.01**	**0.03**	**R53**	0.905	0.896	0.914	0.982
			R100	0.887	0.879	0.902	0.974
2	**0.03**	**0.08**	**R53**	0.899	0.852	0.923	0.934
			R100	0.907	0.860	0.930	0.942
3	**0.08**	**0.09**	**R53**	0.990	0.980	1.043	1.028
			R100	0.979	0.970	1.029	1.015
4	**0.09**	**0.15**	**R53**	0.841	0.841	0.926	1.007
			R100	0.831	0.832	0.916	1.000
5	**0.15**	**0.20**	**R53**	0.922	0.907	0.972	1.023
			R100	0.898	0.885	0.944	0.998
6	**0.20**	**0.25**	**R53**	1.024	0.991	1.011	1.023
			R100	1.102	1.070	1.082	1.095
7	**0.25**	**0.29**	**R53**	1.089	1.053	1.029	1.027
			R100	1.103	1.069	1.034	1.030
8	**0.29**	**0.33**	**R53**	1.433	1.411	1.314	1.280
			R100	1.423	1.401	1.289	1.255
9	**0.33**	**0.41**	**R53**	1.277	1.409	1.321	1.275
			R100	1.198	1.323	1.229	1.181
10	**0.41**	**0.52**	**R53**	1.041	0.997	0.956	1.120
			R100	1.065	1.024	0.976	1.141
11	**0.52**	**0.78**	**R53**	1.150	1.117	1.022	1.109
			R100	1.146	1.116	1.020	1.097
12	**0.78**	**1.06**	**R53**	0.949	0.811	0.700	1.086
			R100	0.968	0.812	0.712	1.091
13	**1.06**	**1.29**	**R53**	0.910	0.715	0.861	0.901
			R100	0.941	0.719	0.877	0.916

References

[1] Yu.I. Kolevatov, V.P. Semenov, L.A. Trykov, Neutron and gamma spectrometry in radiation physics, Energoatomizdat, Moscow, Russia, (1990) [in Russian].

[2] B. Jansky, P. Otopal, E. Novak, Data for calculation of the neutron and gamma leakage spectra from iron and water spheres with Cf-252 neutron source in centre, NRI report UJV-11506, NRI Rez, November 2000.

[3] B. Jansky, E. Novak, Z. Turzik, J. Kyncl, F. Cvachovec, P. Cuda, J. Kluson, L.A. Trykov, V.S. Volkov, Neutron and gamma leakage spectra measurements and calculations in pure iron benchmark assembly with Cf-252 neutron source, International Conference on Nuclear data for Science and Technology, ND 2001, Tsukuba, Ibaraki, Japan, 2001, Journal of nuclear Science and Technology, Supplement 2, August (2002).

The CTU subcritical assembly BLAŽKA driven by the NPI cyclotron-based external neutron source

J. Rataj [1], P. Bém [2], J. Dobeš [2], M. Honusek [2], M. Gotz, K. Katovský [1], A. Kolros [1], K. Matějka [1], E. Šimečková [2] and R. Škoda [1]

1) Czech Technical University in Prague, CZ-180 00 Czech Republic
2) Nuclear Physics Institute ASCR, CZ - 250 68 Řež, Czech Republic
rataj@troja.fjfi.cvut.cz

Abstract: The paper describes experiments with the subcritical assembly BLAŽKA driven by cyclotron-based external neutron source at the Nuclear Physics Institute, Řež.
Subcritical assembly "BLAŽKA" has been designed and fabricated at the CTU Prague. The assembly contains 232 fuel elements EK-10 (UO_2 + Mg alloy, 1856 g of ^{235}U in total), NaF (in polyethylene covers), graphite and polyethylene. All components are located in aluminium case with square shape hole in the central part. The hole is suitable for inserting external neutron source. Other channels in the blanket serve for an installation of various detectors.
Different high-power external neutron sources were developed for ADS investigations utilizing the NPI variable-energy cyclotron U-120M and liquid/solid target technique. The collimator-free beam-guide for the transport of accelerated ions to the neutron source targets minimizes the false neutron source. The dimensions of source chambers were set up to allow the insertion of the source to the central hole of the subcritical assembly. The pulse mode of produced white-spectrum neutron fields is predetermined by the cyclotron operation regime. The d(18MeV)+Be(thick target) neutron source reaction was used for the experiments with the subcritical assembly BLAŽKA.
The experiments were focused mainly on the investigation of the assembly responses to the neutron source changes and determination of the delayed neutron parameters. Three boron detectors were used for the "on-line" neutron detection. One part of the experiments was focused on the neutron spectrum analyses in subcritical assembly.
The acquired data are currently processed and analysed by OriginPro software. Preliminary results are compared with Monte Carlo simulations.

Introduction

Czech Technical University (CTU) in Prague, Department of Nuclear Reactors (DNR) has been studying transmutation technology from 1996 when CTU has became member of the national TRANSMUTATION consortium established in the Czech Republic.
The consortium has been established to study certain physical phenomenons of the transmutation technology. The main R & D works at CTU have been focused on study of the dynamics of subcritical system with external neutron source. CTU closely cooperates with the Nuclear Physics Institute (NPI) in Řež within these works.
Experiments with the subcritical assembly BLAŽKA driven by cyclotron-based external neutron source are a part of the Accelerator Driven System (ADS) project leaded by TRANSMUTATION consortium. The experiments were carried out in the spring 2007.

Figure 1. *Subcritical assembly with the cyclotron -based external neutron source*

Subcritical assembly Blažka

Subcritical assembly BLAŽKA has been designed and fabricated at CTU in Prague in 2001 [1]. The assembly consists of 232 fuel elements EK-10 type, NaF (in polyethylene covers), polyethylene and graphite. Fuel elements are grouped into the nine squares and surrounded by NaF, polyethylene plates and graphite blocks. All components are located in aluminium case with square shape hole in the central part. The hole is suitable for inserting external neutron source. Assembly contains channels for the detectors installation as well. Schematic set-up of the assembly is presented in Fig. 2. Basic parameters of the subcritical assembly are shown in Table 1.
Multiplication factor of the assembly was determined by monte carlo (MCNP) calculations [4]. The k_{eff} is 0.57 for the assembly surrounded by 10 cm thick polyethylene reflector.

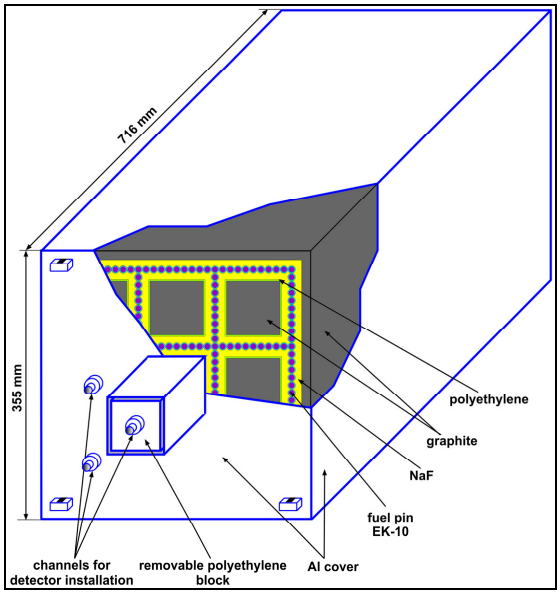

Figure 2. *Set-up of the subcritical assembly BLAŽKA*

Table 1. *Basic parameters of the subcritical assembly*

height [mm]	716
cross section [mm]	355x355
weight [kg]	120
fuel characterisation	232 fuel elements EK-10 type (UO_2 + Mg alloy in aluminium cladding), ^{235}U enrichment is 10%, assembly contains 1856 g of ^{235}U in total
another components	NaF, graphite, polyethylene, aluminum

Cyclotron-based external neutron source

The variable-energy cyclotron U-120M was operating in the negative-ion mode. Special collimator-free beam line was developed from extractor to the target station. Deuteron beam is focused by quadrupole triplet to a spot of 3 mm in diameter (FWHM of nearly Gaussian distribution) on the NG2 target. The energies of deuterons are varied from 11 to 20 MeV by an adjustment of the 30 μm carbon-foil extractor (which converts the accelerated D- ions to deuterons by stripping the electrons). The loss of beam intensity at the extractor and input hardware of the beam guide was suppressed to 10 % at most, which leads to an acceptably low contribution of produced fast neutron background (below about 0.3%) in the region of the irradiated samples (up to about 100 cm distance from the neutron source target). Both the long- and short-time fluctuation of the beam intensity during an operation of the accelerator is better than ± 10%.
The beams accelerated on the U-120M cyclotron are characterized by the *macrostructure* (150 Hz, duration of burst ranging from 0.2 to 2 ms – typically ~1 ms at filling of ~15%) and microstructure (14 MHz, duration of burst 3 ns). The beam is centred at the thick Be target of 40 mm in diameter and overall thick of 8 mm (enough to stop the incident deuteron beam within the target. For the beam-charge monitoring, the target was electrically isolated and equipped with a secondary electron suppressor by a repelling electrode biased to – 600 V.
The d(18 MeV)+Be(thick target) reaction provides white-spectrum neutron field with mean energy of about 6.8 MeV, extending up to cca 18 MeV (see Table 1). Together with charge symmetric d+Li reaction is most intensive source reaction of fast neutrons.

To the calculation of neutron transport characteristics in subcritical assembly, the basic data on both the integral and differential data on d+Be reaction were taken from EXFOR database. In these calculations, the detail data on energy-angular observables from symmetrical d+Li reaction were utilized as due to quantitative similarity of both reactions. The d+Li data were measured at NPI cyclotron in a set of experiments, described in the reference [2]. In these measurements, the angular distributions of the spectral neutron yield have been measured by the scintillation-detector technique in an open geometry arrangement of experiment. To subtract neutron-room background, the conventional shadow-bar method has been employed. Numerical data on the differential and integral cross sections are available on request

Table 2. *Characteristics of d+Be external neutron source at NPI Řež*

Integral yield Y_n (n/sr/μC)	3.3 E+10
Mean energy E_n (MeV)	6.8
Maximum energy (MeV)	17.8
Mean emmission angle (FWHM) θ_n	18°

Experimental setup and objectives of the experiment

Experimental works with subcritical assembly BLAŽKA were carried out at the cyclotron hall (Fig. 3) in NPI, Řež. The d(18MeV)+Be(thick target) reaction was used as a neutron source. The subcritical assembly was surrounded by polyethylene reflector during experiments. Measurements were performed for two different position of external neutron source towards subcritical assembly. Three boron chambers were used for on-line neutron detection.

Experiments were focused mainly on the study of the dynamics behavioural and determination of neutron properties of the subcritical assembly BLAŽKA with external neutron source. Main objectives of the experiments were:

- study of the subcritical assembly responses to the neutron source power changes,
- investigation of delayed neutrons production in assembly,
- measurement of neutron energy distribution inside and outside the assembly.

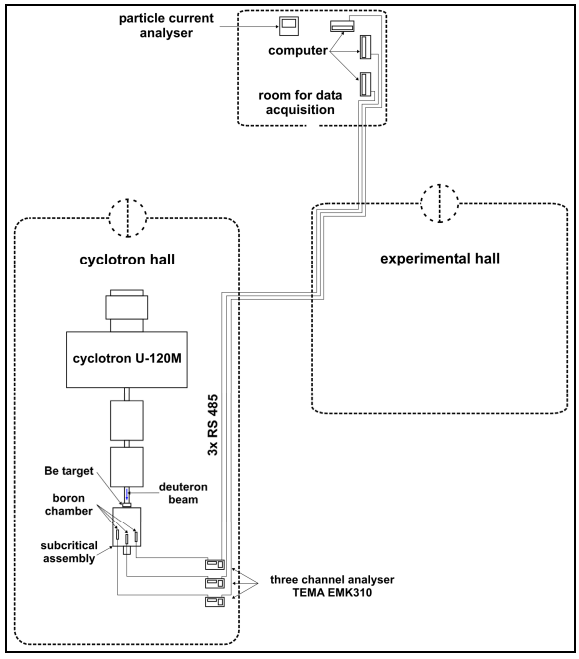

Figure 3. *Experimental set-up at the cyclotron hall*

Various sets of activation foils (Al, In, W, Fe, Au, Lu, Mn, Mo, Ni, U) were used for neutron energy distribution and Au wires were used for measurement of axial and radial distribution of neutrons. One of the configurations of the activation foils and Au wire outside the subcritical assembly is presented in Fig. 4.

Preliminary results of the determined reaction rates are shown in Fig. 5. One part of the measurements was focused on the observation of delayed neutrons production for various condition of the subcritical assembly irradiation (Fig. 6). Objective of these measurement was determination the delayed neutron parameters and comparison with the the well known delayed data (Keepin, Brady&England, Piksaikin).

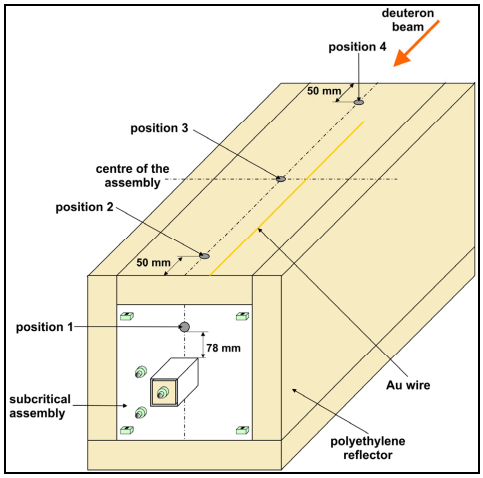

Figure 4. *Position of the foils for the reaction rates measurement*

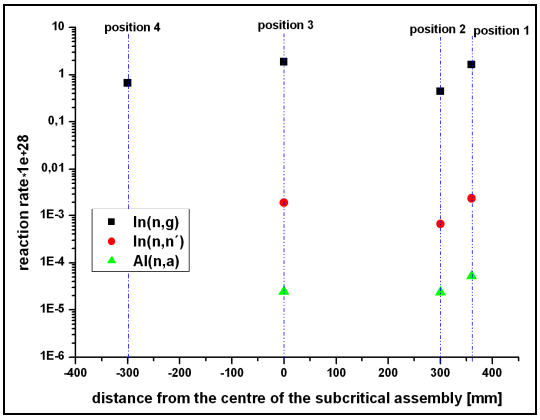

Figure 5. *Measured reaction rates outside the subcritical assembly for three different reactions*

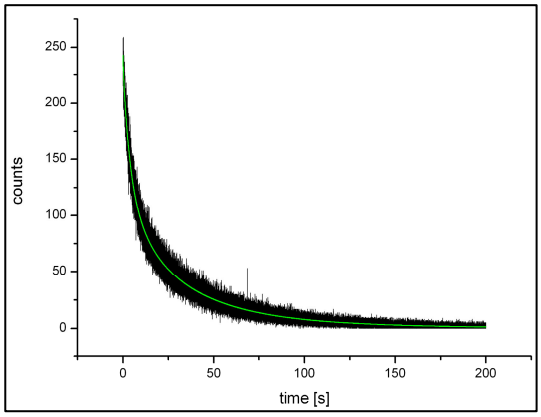

Figure 6. *Delayed neutrons production after irradiation of the subcritical assembly BLAŽKA*

Conclusions

Experiment with subcritical assembly BLAŽKA driven by NPI cyclotron-based external neutron source was carried out in spring 2007. The experiments were focused mainly on the investigation of the assembly responses to the neutron source changes and determination of the delayed neutron parameters. Large amounts of various experimental data were acquired during the measurements. Data are being currently processed and analysed. Verification calculations will be performed.

References

[1] J. Rataj, “Experimental study of neutronic parameters of developed modules of ADS blanket at the reactor VR-1”, diploma theses, DNR FNSPE CTU Prague, 2001

[2] J. Rataj, P. Bem, “Experimental Study of Subcritical Blanket Blažka with External Neutron Source NG2 at Nuclear Physics Institute, Řež“, Proceedings of the IYNC2004 conference, Canadian Nuclear Society, 2005,

[3] P. Bem et al., “D-Li reaction source term: Experimental verification of neutron yield based on thick and thin Li-targets”, Report NPI ASCR Řež, EXP(EFDA)-05/2004,

[4] J. F. Briesmeiter, "MCNP - A General Monte Carlo N-Particle Transport Code", Los Alamos National Laboratory, LA-12625-M, Los Alamos, New Mexico 87545, USA, March 1997,

Neutron production in Pb/U assembly irradiated by deuterons at 1.6 and 2.52 GeV

O. Svoboda[1,2], A. Krása[1,2], M. Majerle[1,2], V. Wagner[1,2]
for the "Energy plus Transmutation" collaboration

1) Nuclear Physics Institute of the Academy of Sciences of the Czech Republic PRI, 250 68 Řež near Prague, Czech Republic
2) Faculty of Nuclear Sciences and Physical Engineering, CTU in Prague, Břehová 7, 115 19 Prague, Czech Republic
svoboda@ujf.cas.cz

Abstract: "Energy plus Transmutation" is an international project that studies spallation reactions, neutron production and the following neutron transport in a thick lead target surrounded by sub-critical, natural uranium blanket. Relativistic light ions interacting with thick target induce spallation reactions and intense neutron fluxes are created. The high energy neutron field rising in the setup is measured by Al, Au, Bi, In, and Ta activation foils. Activated foils are measured with HPGe detector, yields of selected isotopes are determined with the respect to all necessary corrections. This setup was irradiated by protons in previous years. Experiments with deuterons are now in the centre of our interest, irradiations with energies 1.6 GeV and 2.52 GeV were carried out. First MCNPX simulations of deuterons were done and compared with the experiment.

Introduction and motivation

The international collaboration “Energy plus Transmutation” (E+T) designed a special setup for the study of spallation reactions, neutron production and transport, and transmutation of fission products and higher actinides in high-energetic neutron fields, see Fig.1 [1]. This experiment represents the next step in the spallation and transmutation studies that were performed at JINR (Dubna, Russia) during the last two decades. Our specific role in these studies is to measure the high energy neutron fields and perform Monte Carlo simulations of specific problems connected with this problematic.
The E+T setup was in previous years irradiated by protons with energies 0.7, 1.0, 1.5, and 2.0 GeV. Significant divergences in comparison with MCNPX simulations were observed at 1.5 and 2.0 GeV proton experiments [2]. These divergences cannot be explained by any systematic or statistical error. The detailed analysis shows that the most probable explanation is a problem in the MCNPX code, in the part describing the pre-equilibrium stage. In the paper both experimental and simulation results connected with deuteron experiments are discussed in more detail.

Experimental setup

E+T setup is build up of a thick (length 48 cm, 8.4 cm in diameter), lead target divided into 4 parts with 0.8 cm gaps between them. The target is surrounded with a natural uranium blanket. Uranium is packed in small rods coated with aluminum. Total weight of the lead target is 28.7 kg; total weight of the natural uranium is 206.4 kg. Construction materials holding together the target and blanket parts are of steel and aluminum. The whole setup is placed in a wooden box of approximately cubic size used as biological shielding. This box has walls filled with granulated polyethylene doped by a small amount of boron (5 ppm). 1 mm thick cadmium plates are fixed on inner walls of the wooden box to absorb thermal neutrons. The front and the back ends of the setup are without shielding. For more information about the E+T setup see [1].
The high energy neutron field produced in spallation and fission process was measured with neutron activation detectors. Neutrons induced various threshold reactions like (n,α) and (n,xn); Al, Au, Bi, Ta, and In materials in form of thin foils (mostly 2x2 cm^2) were used. Non-threshold (n,γ) reactions in Au and In were observed as a consequence of used biological shielding. Products of the threshold and non-threshold reactions were radioactive, emitting specific gamma-rays. Their activity was measured in HPGe detectors. All foils were put

through a short-time measurement, which took place a few hours after the irradiation. For some foils a long-time measurement was needed (typically Bi). Total amounts of observed isotopes were calculated with the respect to all spectroscopic corrections (see Specific spectroscopic corrections) and divided by the weight of the foil and by the total number of deuterons used during the irradiation to obtain the production rates B(A) (= yields) [1], which are comparable among all our experiments.
In our experiments activation foils were wrapped twice in the paper to avoid the radionuclide transport between the foils and to prevent the HPGe detector contamination. Foils in the paper enclosure were fixed on plastic plates and inserted into the gaps in E+T setup (Fig.2).

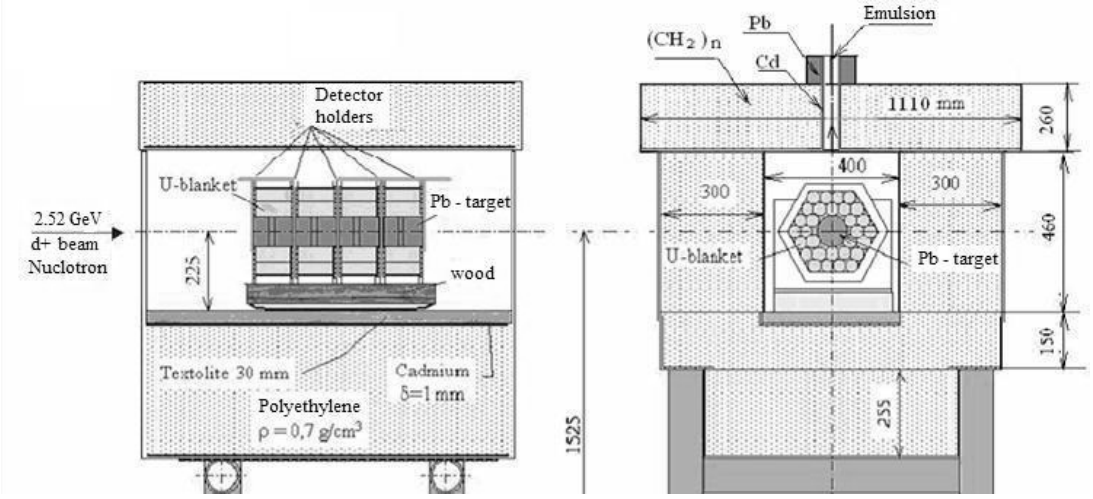

Figure 1. *Cross-sectional side view (left) and front view (right) of the E+T setup. All dimensions are in millimeters.*

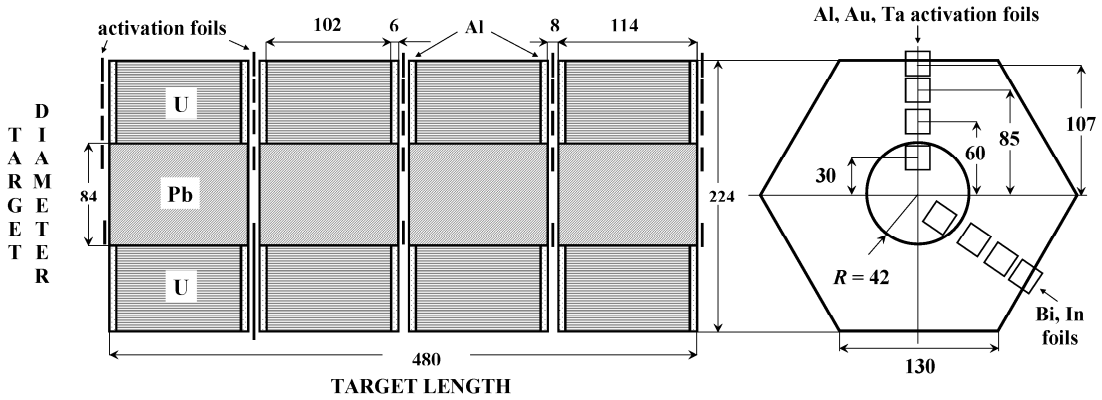

Figure 2. *The placement of activation foils, side view (on the left) and front view (on the right). Dimensions are in millimetres.*

Irradiations
Two deuterons irradiations of the setup with energies 2.52 and 1.6 GeV were performed as the continuation of previous experiments with protons. Both two irradiations lasted around 8 hours with the total flux in order 10^{13} and were performed at the Nuclotron accelerator at the Laboratory of High Energies, JINR. In both deuteron experiments the same systematics (foil placement, measurements on HPGe detectors, evaluation process, etc.) was maintained as in the proton experiments.

Beam monitors
Special set of Cu and Al beam monitors was needed to determine the beam properties (total flux, shape, and position). One 10x10 cm^2 Al foil placed 1 m in front of the target had measured the total deuteron flux, reaction $^{27}Al(d,3p2n)^{24}Na$ was observed. Total deuteron flux was determined to be $(6.4 \pm 0.7)x10^{12}$ for the 2.52 GeV deuteron experiment, cross-section value 15.25 ± 1.5 mbarn from [6] was used. Beam position and profile was measured with nine 2x2 cm^2 Cu foils placed directly in front of the target. A lot of reaction products were observed, due to unknown cross-section data only relative comparisons between the foils were done. Taking

into account the beam measurements from other collaboration members (mainly SSNTD) it was determined that the 2.52 GeV deuteron beam had an elliptical shape close to circle and was shifted 1.5 cm to the left and 0.3 cm down.
Beam evaluation for the 1.6 GeV deuteron experiment is still in progress.

Specific spectroscopic corrections
Wide range of specific spectroscopic corrections was studied.
- A correction for the non-point like emitters was studied using the MCNPX code. Point-like and the non-point-like emitters were in the simulation placed in various distances from the detector, and the efficiency ratios for non-point-like/point-like emitters were calculated. This correction strongly depends on the distance between the emitter and the detector. In our case for the 2x2 cm^2 activation foil placed in the closest position in the detector the correction is 2%.
- Because of non-stabile irradiation special correction was studied. The beam was divided in intervals with the same intensity and radioisotope production and decay in these intervals was calculated [3]. For more accurate correction evaluation a simple program was used. This program calculates the correction for every beam bunch. The correction strongly depends on the irradiation process and on the isotope half-life, and can be in our case up to 10% for the isotope with 1 hour half-life.
- Detector homogeneity was studied because of the non-symmetric activation of the foils. Standard laboratory point source - etalon ^{60}Co was placed step by step in the centre, 1 cm left, right, down, and up; and 1.5 cm left, right, down, and up. Activity ratios centre/outside were calculated and a map of the detector efficiency was done. Both two used HPGe detectors (in Dubna, Russia, and in Řež, Czech Republic) are non-symmetric with the differences in order of percents. Because the same orientation of the foils during the whole experiment (irradiation, measurements) could not be guaranteed, we involved this uncertainty in the total systematic error.

Experimental results

The products of threshold reactions with E_{thresh} from 5 to 52 MeV were observed. Examples of the yields of selected isotopes (proportional to the neutron field in the respective places of the setup) are shown in the Fig.3. These are similar for all our beam energies and particles. The maximum in longitudinal direction is located in the first gap between the target-blanket sections. In radial direction yields decrease almost exponentially with the increasing distance from the target axis. Comparison of the absolute values between the two deuteron experiments (2.52 and 1.6 GeV) shows a factor of ~ 1.5 (for gold threshold reactions).
The yields of the non-threshold reaction $^{197}Au(n,\gamma)^{198}Au$ are much higher and almost the same in the whole setup. This is caused due to homogenous field of 0.5 - 10^4 eV neutrons (originally fast neutrons, moderated in the biological shielding and reflected back to the target-blanket assembly) [5].

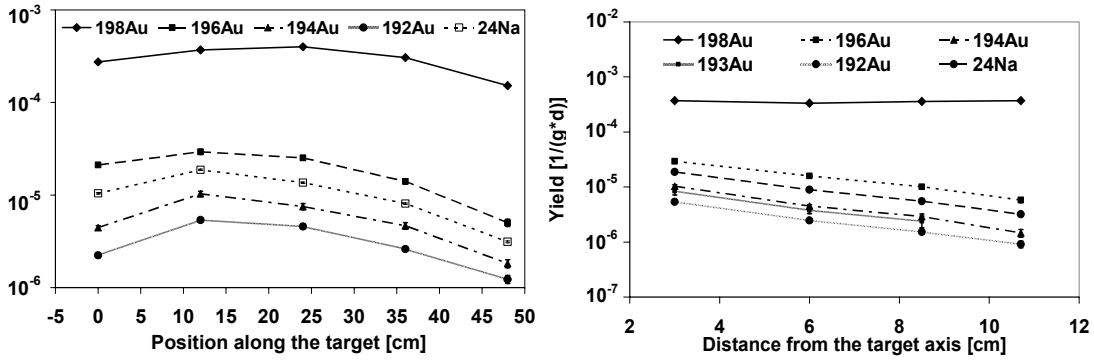

Figure 3. *Example of the yields of threshold and non-threshold reactions observed on Au and Al foils (longitudinal distribution on the left graph, radial on the right), 2.52 GeV deuteron experiment. The errors, in this semi-logarithmical scale hardly visible, are only statistical uncertainties (Gaussian fit of the gamma-peak).*

Monte Carlo simulations - MCNPX

Monte Carlo simulations of deuteron experiments were performed using the MCNPX 2.6.C [4] code with INCL4+Abla models. The geometry of the segmented lead target, the uranium rod blanket, the polyethylene shielding, metal frames, shells, and support structures were described in MCNPX [5]. The setup was simulated with the beam shape as it was determined in the experiment. The statistical errors of the simulation are mostly under 1% (at millions of histories) and are neglectable in comparison with the experimental ones.
The simulated yields of observed threshold reactions were determined by manual convolution of the cross-sections calculated in TALYS and of the protons, deuterons, and neutrons spectra in the detector volumes calculated with MCNPX. Computed yields were compared with the experimental ones (Fig.4) and good agreement in both directions was observed.

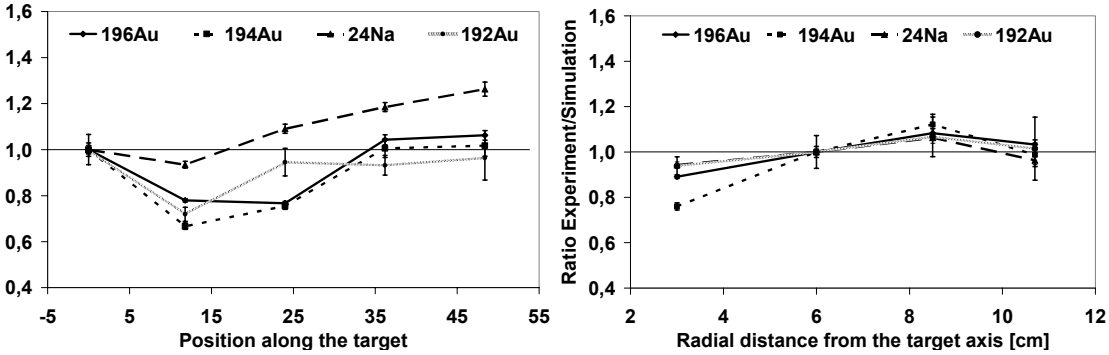

Figure 4. *The example of relative comparison of experimental and simulated yields of Au and Al isotopes in longitudinal and radial directions for the 2.52 GeV deuteron experiment (normalized to the first foil in the left graph and to the second foil in the right graph)*

Conclusion and outlook to the future

High energy neutron production and transport were studied in the setup made of thick lead target and natural uranium blanket irradiated by GeV deuterons. Activation foils from different materials were used as the neutron detectors; yields of selected isotopes were computed with the respect to various corrections. First experiment versus Monte Carlo simulation comparisons give satisfactory results, up to now no significant divergence as in the proton experiments was observed.
New experiments with deuterons (4.0 GeV) are planed to fill in the deuterons systematics.

Acknowledgements
We are grateful to the stuff of the LHE laboratory of the JINR, Dubna for using the Nuclotron accelerator and to the Agency of Atomic Energy of Russia for supply of material for the uranium blanket. This work was carried out under the support of the GA CR (grant No. 202/03/H043) and the GA AS CR (grant No. K2067107). We are also grateful for the computing help of the CESNET METACentrum.

References

[1] M. I. Krivopustov et al.: First Experiments with a Large Uranium Blanket within the Installation "Energy plus Transmutation" exposed to 1.5GeV Protons, Kerntechnik 68(2003)48
[2] O. Svoboda et al.: Neutron production in Pb/U assembly irradiated by protons and deuterons at 0.7-2.52 GeV, proceeding for International Conference on Nuclear Data for Science and Technology 2007, Nice, France
[3] H. Kumawat: Development of Cascade Programme and its Applications to Modelling Transport of Particles in Many Component System, dissertation, 51.7:539.17, Dubna 2004
[4] J. S. Hendricks et al., MCNPX - Version 26C, LANL report LA-UR-06-7991 (2006)
[5] M. Majerle et al.: MCNPX simulations of the experiments with relativistic protons directed to thick, lead targets, NIM A 580/1, p.110-113 (2007)
[6] J. Banaigs et al., Determination De L`Intensite D`Un Faisceau De Deutons Extrait D`Un Synchrotron Et Mesure Des Sections Efficaces Des Reactions C-12(D,P2N)C-11 Et Al-27(D,3P2N)Na-24 a 2.33 GeV, Nuclear Instruments and Methods in Physics Res. Vol. 95, p. 307, 1971

Determination of neutron energy spectrum in reactor core C1 of reactor VR-1 Sparrow

M. Vins, A. Kolros, K. Katovsky

Department of Nuclear Reactors, Faculty of Nuclear Sciences and Physical Engineering, Czech Technical University, V Holesovickach 2, 180 00, Prague 8, Czech Republic
vinsmiro@seznam.cz

Abstract: The contribution overviews neutron spectrum measurement, which was done in training reactor VR-1 Sparrow with a new type of nuclear fuel. Former nuclear fuel IRT-3M was changed for current nuclear fuel IRT-4M with lower enrichment of ^{235}U (enrichment was reduced from 36 % to 19.7 %) in terms of Reduced Enrichment for Research and Test Reactors (RERTR) Program. Neutron spectrum was acquired by irradiation of activation foils at the end of pipe of rabbit system and consecutive deconvolution of obtained reaction rates. Deconvolution was performed by iterative computer code SAND-II with 620 groups' structure. All gamma measurements were performed on Canberra HPGe detector. Activation foils were chosen according physical and nuclear parameters from the set of certificated foils. The final spectrum agreed well with typical spectrum of light water reactor. Measurement of neutron spectrum has brought better knowledge about new reactor core C1 and has improved methodology of activation measurement on reactor VR-1. It should also serve as base for future similar exercises for students.

Introduction

Training reactor VR-1 Sparrow is a unique nuclear facility in Czech Republic, which is managed by the Department of Nuclear Reactors, Faculty of Nuclear Sciences and Physical Engineering, Czech Technical University in Prague. Its task is to be used in preparation of students for future work in the field of nuclear engineering, to train inspectors for the IAEA, and to improve public knowledge about nuclear reactors and nuclear science generally. The VR-1 belongs to the class of pool light water reactors with natural cooling; its main advantage is possibility to do fast change in configuration of reactor core. The VR-1 is equipped by two horizontal and several vertical dry channels for experiments. Unfortunately, a small neutron fluency rate in the reactor core (in order of 1E13 m^{-2} s^{-1}) brings rather strong limitation to reactor applications. Maximum thermal power of reactor is 5 kW. In 2005 was former nuclear fuel IRT-3M replaced for current nuclear fuel IRT-4M with lower enrichment of ^{235}U (enrichment was reduced from former 36 % to 19.7 %) in terms of program RERTR. This change resulted in increase of uranium mass in reactor core and in change of neutron spectrum characteristic (as well as decrease of neutron fluency rate). Due to knowledge of neutron spectrum was needed for right evaluation of some experiments on VR-1 (mainly neutron activation analysis), the measurement of neutron spectrum was realised.

Measurement setup

Neutron spectrum measurement was performed using multi foils activation methodology with unfolding. Used foils were composed of almost pure elements and were chosen according their physical and nuclear properties. Nine different elements were measured (Table 1) and cadmium covers were used in another two cases for highlighting of fast and epithermal part of neutron spectrum. Foils were irradiated at the end of pipe of the rabbit system, which is the main position for irradiation of samples for neutron activation analysis. Position is indicated in Figure 1 (coordinates C3) and is situated approximately in the height centre of reactor core. Pipe transportation system is pneumatic equipment that enables fast transportation (in order of seconds) of irradiated samples from reactor to gamma spectroscopy laboratory. Unfortunately, it could not be used in measurement due to large size of foils. All activation foils were irradiated for time from 10 minutes to 1 hour at stable reactor levels from 100W to 1kW. After irradiation the samples were moved to the gamma spectroscopy laboratory equipped with HPGe detector (energy resolution 1.8 keV at energy 1173 keV; relative efficiency 25%) with software Genie-2000 v.3.0. Following measurement of activities lasted

from 5 minutes to tens of hours according to relevant decay constant. Energy and efficiency calibration of HPGe detector was done by certificated ^{137}Cs and ^{152}Eu etalons. Due to small fluency rate and dominance of thermal neutrons in reactor core mostly (n,γ) reactions (radiation capture) were observed. On base of data received from HPGe detector were computed reaction rates for each reaction consequently and then they were used as input data for deconvolution process.

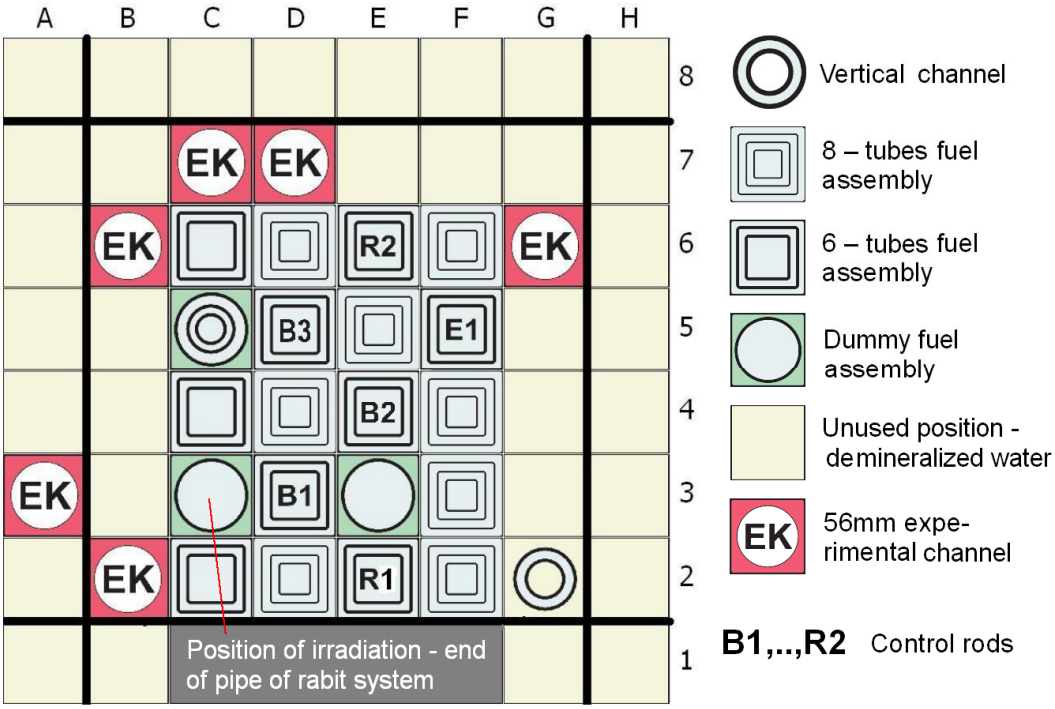

Figure 1. *Composition of reactor core, end of pipe of transportation system is in position C3*

Neutron spectrum calculation

Deconvolution was performed by computer iterative code SAND-II with 620 groups' structure. The code was newly acquired and it replaced an old version of SAND-II modified at Nuclear Research Institute at Rez. Former version worked in 113 groups' structure. Monte Carlo code MCNP4C was used for calculating of a first approximation of neutron spectrum, because the first approximation is another input data, which is needed by SAND-II (it is not possible to find unique solution from only measured reaction rates). A original reaction cross section library in SAND-II had not cover whole set of reactions chosen for measurement, therefore the original library was filled out by cross sections for following reactions: $^{64}Ni(n,\gamma)^{65}Ni$, $^{186}W(n,\gamma)^{187}W$ and $^{51}V(n,\gamma)^{52}V$. Values of new cross sections were processed by program NJOY99 from ENDF/B-VI.8 library. During the process were detected differences between cross sections from original SAND-II library and new cross sections for the same reactions, mainly in resonance area. Comparison with dosimetry library IRDF-2002 showed agreement between IRDF2002 and results of NJOY99 processing; therefore the original library was replaced. Comparison of calculations for both libraries was analysed. In Figure 2 can be seen cross sections for radiation capture at ^{197}Au gained from SAND-II library and NJOY99 processing.

Results

Summary of reaction rates is in Table 1 and resulting fluency rate for different energy area are showed in Table 2. Calculation was terminated after five iterations, because difference between results of two following steps did not exceed 1.5 %. Indium foil was discarded during SAND-II calculation due to excessive deviation. Failure in measurement is probably responsible. Mean standard deviation of result was 8.38% and deviation of single reaction did not exceed 15%, which illustrate a good consistency of experimental data.

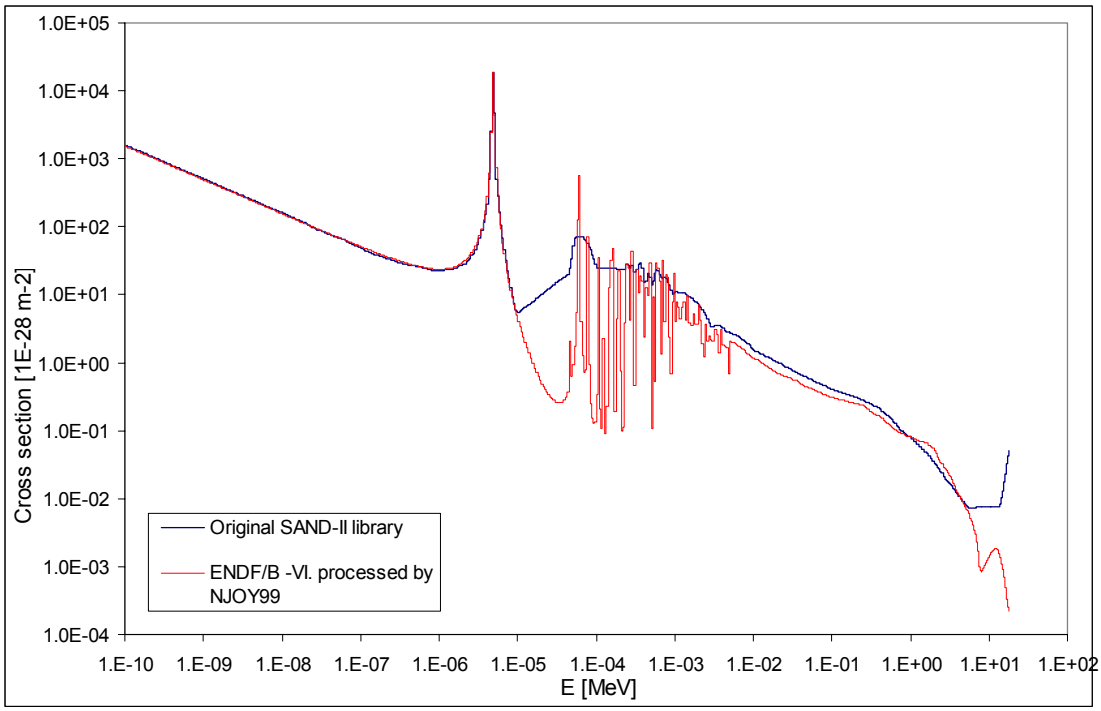

Figure 2. *Comparison of cross sections for ^{197}Au (n,g)^{198}Au reaction*

Table 1. *Summary of reaction rates*

Reaction	Measured reaction rate	Calculated reaction rate	Ratio of measured and calculated reaction rate	Deviation of measured to calculated reaction rate [%]
$^{197}Au(n,g)^{198}Au$ with Cd cover	5.28E-17	5.09E-14	1.0369	3.69
$^{55}Mn(n,g)^{56}Mn$ with Cd cover	9.71E-16	9.75E-16	0.9962	-0.38
$^{115}In(n,g)^{116}In^*$	Discarded			
$^{58}Ni(n,p)^{58}Co$	4.91E-17	4.92E-17	0.9968	-0.32
$^{45}Sc(n,g)^{46}Sc$	3.39E-14	3.18E-14	1.0688	6.88
$^{198}Au(n,g)^{197}Au$	1.43E-13	1.64E-13	0.8708	-12.92
$^{55}Mn(n,g)^{56}Mn$	1.72E-14	1.62E-14	1.0647	6.47
$^{63}Cu(n,g)^{64}Cu$	4.85E-15	5.34E-15	0.9075	-9.25
$^{186}W(n,g)^{187}W$	6.19E-14	6.34E-14	0.9765	-2.35
$^{51}V(n,g)^{52}V$	5.92E-15	6.00E-15	0.932	-6.8
$^{64}Ni(n,g)^{65}Ni$	2.05E-15	1.78E-15	1.1498	14.98
Average deviation				8.38

Table 2. *Summary of fluence rate*

Spectrum area	Energy	Fluency rate [cm^{-2} s^{-1}]
Thermal	1E-4eV – 0.5eV	1.38E+09
Epithermal	0.5eV – 0.1MeV	7.99E+08
Fast	> 0.1MeV	6.74E+08
All	> 1E-4eV	2.85E+9

Results are in good agreement with expectations based on former operational experience of reactor VR-1 Sparrow. Resulting differential spectrum is shown in Figure 3. Results for calculations with original and new libraries showed only slight differences in shape and

deviation (probably because of dominance in thermal area). Created “resonances” in the 1/E area of final spectrum is probably artificial and they are products of mathematical calculation of SAND-II.

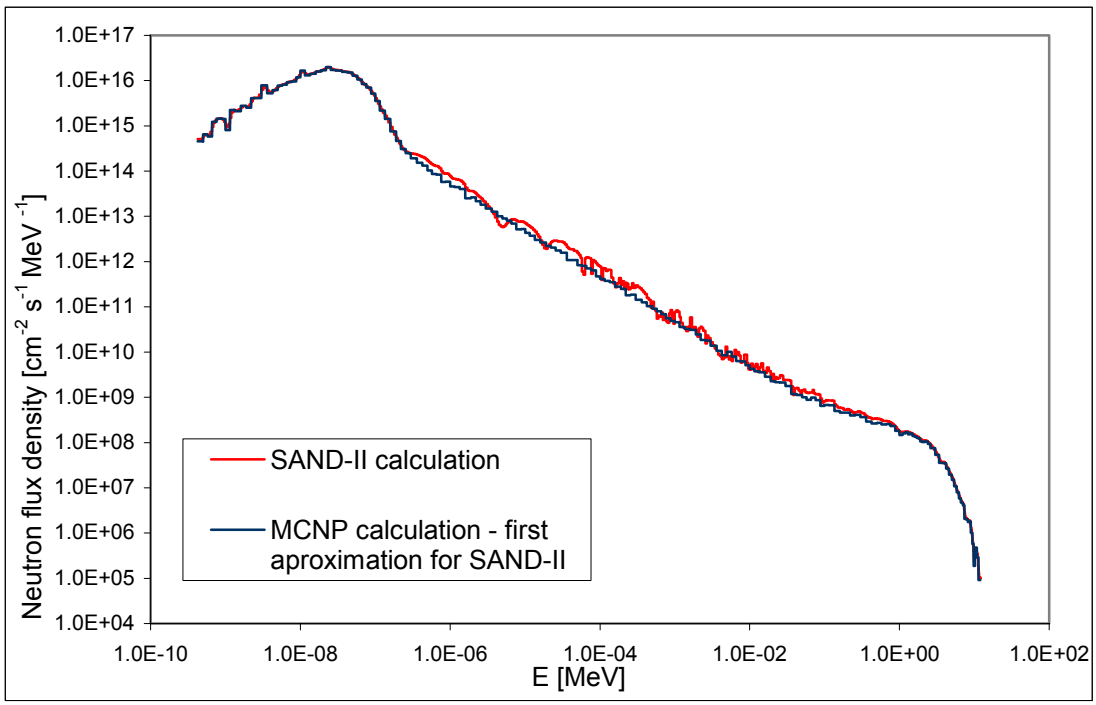

Figure 3. *Differential neutron spectra*

Conclusion

The differential neutron spectrum at the end of pipe of rabbit system agrees well with typical spectrum of well-moderated light water reactor. Result of SAND-II iterative procedure differs only slightly from its first step. It shows the suitability of first approximation (and worthiness of MCNP4C calculation) and agreement between theoretical and experimental results. In fact, the propriety of first approximation limited contribution of SAND-II de facto only to assessments of fluency rates, because SAND-II modification of spectrum is in question (1/E area). Although results are reasonable yet – there is still a space for improvement. The measurement provided suggestions for future experiments. The SAND-II will be replaced by other adjustment codes due to lack of any statistical evaluations of results (based on uncertainties of input data). Experience are gained with codes MAXED, GRAVEL, or i.e. STAY-SL nowadays and usage of other codes will be considered. Efforts will be also aimed at improving precision of model of reactor VR-1 for MCNP (new version 5) and improving precision of experiment measurement.

References

[1] M. Vins "Stanovení spektra neutronů v aktivní zóně C1 reaktoru VR-1“, master’s degree thesis, Prague, Czech Republic, 2007.
[2] K. Matejka et al., "Experimentální úlohy na školním reaktoru VR-1“, lecture notes, Prague, Czech Republic, 2004.
[3] K. Katovsky, A. Kolros, P. Paluska "Validation of experimental spectrum measurement on reactor VR-1“, research report, Prague, Czech Republic, 2005.

Systematic studies of neutrons produced in the Pb/U assembly irradiated by relativistic protons and deuterons

V. Wagner [1,2], A. Krása[1,2], M.Majerle[1,2], O. Svoboda[1,2]
for the "Energy plus Transmutation" collaboration

1) Nuclear Physics Institute of the Academy of Sciences of the Czech Republic PRI, 250 68 Řež near Prague, Czech Republic
2) Faculty of Nuclear Sciences and Physical Engineering, CTU in Prague, Břehová 7, 115 19 Prague, Czech Republic
wagner@ujf.cas.cz

Abstract: We studied the spatial and energetic distributions of neutrons produced by spallation reactions at different places around and inside the “Energy plus transmutation” installation, consisting of a thick lead target and uranium blanket surrounded by polyethylene shielding. Such setup was irradiated by relativistic protons and deuterons of different energies using JINR Dubna Nuclotron. The activation detectors were used for neutron field determination. The presence of polyethylene moderator helps us to determine changes of integral number of neutrons with beam energy. We compare our experimental results with MCNPX simulations and also with experimental systematic of neutron production on simple lead target. We see remarkable regularity of neutron production variation over studied incident energy range similar to regularity observed by K. van der Meer for thick lead target. While simulations describe well experimental data for proton beam energies below 1.5 GeV, significant discrepancies are found out for higher beam energies.

Introduction

The international collaboration “Energy plus Transmutation” (E+T) designed a setup for the study of spallation reaction, neutron production and transport, and transmutation of fission products and higher actinides in high-energetic neutron fields [1]. It uses interactions of relativistic protons and deuterons with a thick, lead target, which produce intensive neutron fields. Main tasks of our investigations are the study of the neutron field produced in the spallation target and the influence of subcritical blanket and moderators on the secondary neutron field. The aim of our experiments is to check the validity of the model descriptions and of the cross-section libraries used in the Monte-Carlo simulations of spallation reactions, and of the propagation of the produced high-energy neutrons.

Experimental setup

E+T setup is build up of thick (length 48 cm, 8.4 cm in diameter) lead target, divided into 4 parts with gaps 0.8 cm. It is surrounded by a natural uranium blanket. Total weight of the uranium is 206 kg. Whole setup is placed in a wooden container of approximately cubic size (used as biological shielding). This box has walls filled with granulated polyethylene. Cadmium plates (1 mm thick) are fixed on inner walls of the wooden box to absorb thermal neutrons. The front and the back ends of the setup are without shielding [1].
The high energy neutron field was measured by various threshold reactions like (n,α) and (n,xn). Al, Au, Bi, Ta, and In materials in form of thin foils were used. Non-threshold (n,γ) reactions in Au and In were used to measure yield of epithermal and resonance neutrons. Foils were placed in two main directions to measure both the longitudinal and radial distributions of the neutrons in the setup. Typical example of the foil placement is in [1].
The E+T setup was in previous years irradiated by protons with energies 0.7, 1.0, 1.5, and 2.0 GeV. Two deuterons irradiations of the setup with energies 2.52 and 1.6 GeV were performed as the continuation of previous experiments with protons.

Monte Carlo simulations - MCNPX

Monte Carlo simulations of spallation reactions, neutron production and transport, and material activation were performed using the MCNPX 2.6.C [3] code. In the input file the complex geometry of the segmented lead target, the uranium rod blanket, the polyethylene

shielding, all metal frames, shells, and support structures are described [4]. The simulated beam has a Gaussian profile, values of its horizontal and vertical FWHM and shift were used as the ones measured in the experiment. The statistical errors from the simulation can be neglected (are mostly under 1%) in comparison with the experimental ones.

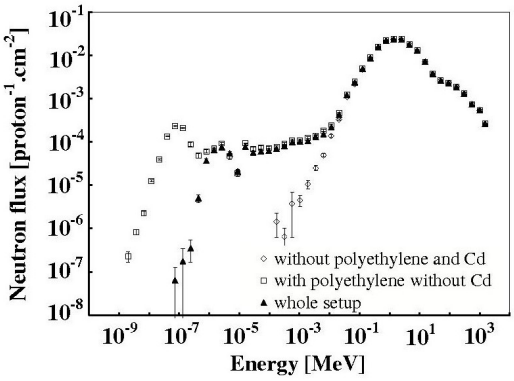

Figure 1. *Example of neutron spectra inside the E+T setup simulated by MCNPX code. Thermal, epithermal, and resonance neutrons are produced by polyethylene shielding neutron moderation. Thermal neutrons are absorbed by Cd layer.*

Determination of integral number of neutrons

We studied influence of container on neutron spectra inside and around our setup using MCNPX code to find out which parts of spectra are significantly changed and which are not influenced. The comparison of three types of simulation for neutron energy spectra on the top of U blanket is on Fig. 1. The spectra for these three simulations are the same for energy higher than 0.5 MeV. The spectrum for energy lower than 0.1 MeV starts to drop very quickly in the case of the set-up without container. Spectrum is constant and the same in the energy range from 1 eV up to 0.1 MeV for two simulated cases with container. Peak of thermal neutrons is not visible in the case with Cd layer (thermal neutrons are absorbed by Cd).

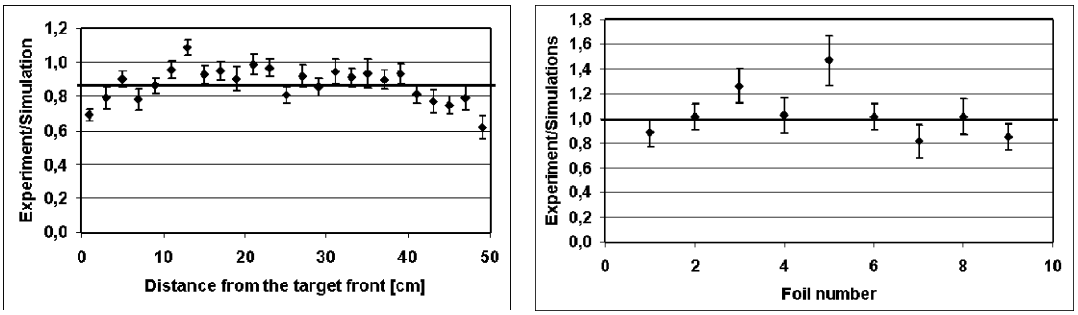

Figure 2. *Ratios between experimental and simulated ^{198}Au production yield for experiment with simple lead target (beam energy 0.885 GeV) and with E+T assembly (beam energy 1.5 GeV)*

The low energy neutron field (E < 0.1 MeV) inside shielding box is near to homogenous and it is completely done by the polyethylene moderation, see spectra in Fig. 1. The vast majority of such neutrons come from this shielding and intensity of this part of neutron spectra is done by total number of neutrons which are leaving target and blanket. The resonance and epithermal part of energy spectrum and intensity of moderated neutrons are significantly not dependent on energy spectra of neutrons produced by target and blanket but only on their total number. The dominating contribution of radioactive nuclei produced by non threshold neutron capture reactions in our experiment (set-up with container and Cd layer) is due to resonance neutrons. This is true also for very often used ^{197}Au(n,γ)^{198}Au reaction and then the ^{198}Au production depends only on total number of neutrons escaping the blanket. We can determine ratio between total neutron productions for different beam energies comparing the ^{198}Au production during corresponding experiments. This method is very similar to the water bath method very often used for determination of integral neutron number produced on thick target.

We used this method in the novel form showed at [2]. We determined the ratios between the experimentally obtained values of the ^{198}Au production per one beam nucleus and the simulated ones in different places, see Fig.2. The searched value of integral neutron number can be obtained by multiplying mean value of described ratios and the integral neutron number obtained using simulation [2]. The used method was tested on experimental data obtained during measurements with simple lead target inside the E+T shielding box irradiated by 0.885 GeV protons.

Neutron production on simple lead target

The dependency of neutron number produced per proton on beam energy for Pb was studied by a number of experiments, see review [2]. The used targets have different sizes. The number of produced neutrons depends on these sizes, but the yield saturated thickness and diameter exist, see Fig.2. It is possible to reach the maximal number of the produced neutrons for given beam energy, see Fig.3. The most of the experiments were carried out with target radius around 5 cm. Each data point from different experiments has been re-scaled to the yield-saturating target thickness and radius 5 cm for these reasons. Used corrections were mostly only a few percents. The obtained compilation is possible to fit by simple polynomial function, see Fig.4 left. The MCNPX simulation is shown and it overestimates integral neutron production. Our experimental point used by experiment with simple target and E+T shielding box for beam energy 0.885 GeV is in the good agreement with other experimental points.

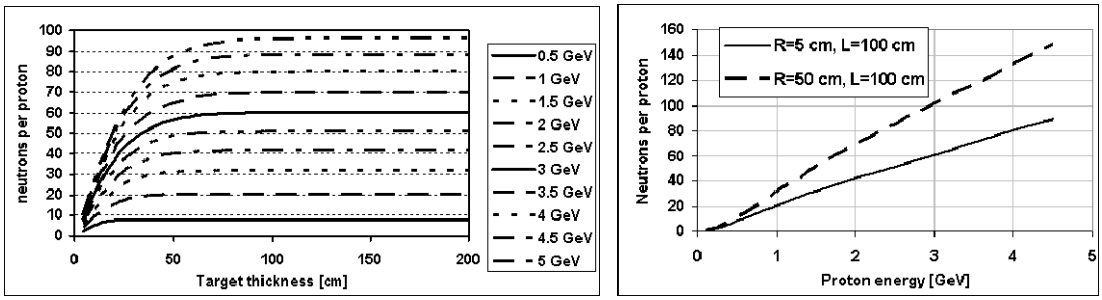

Figure 3. *The dependency of the integral neutron yield production on target thickness for the target radius 5 cm and different beam energies (left). Dependency of integral neutron yield produced on target with radius 5 cm (usual radius) and 50 cm (yield saturated radius) and thickness 100 cm (yield saturated thickness) on proton beam energy (right).*

Neutron production on E+T assembly

We obtained values of integral neutron number for different beam energies using the E+T assembly. These values can be compared with the data obtained using simple lead target. The dependency of total neutron production per beam particle on the beam energy is shown in the Fig. 4 right together with MCNPX simulations. Such dependency starts to be constant in the case of total neutron number per beam energy around 1 GeV.

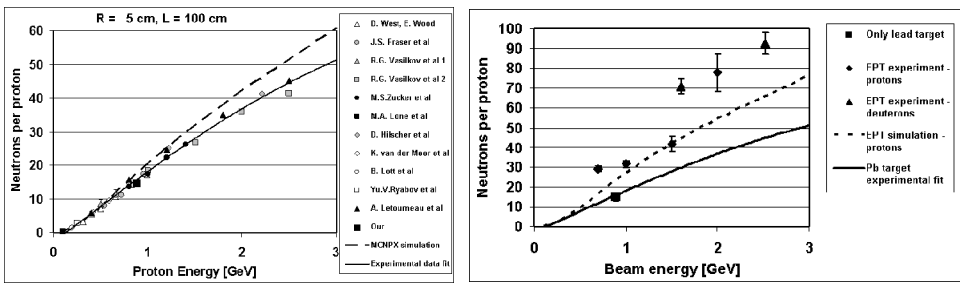

Figure 4. *Compilation of thick-target n/p values for p+Pb measured to date at all incident energies. Experimental data are re-scaled to the target thickness 100 cm and radius 5 cm (left). Dependency of total neutron production per one beam particle on beam energy for E+T assembly is shown on right figure. Experimental data are compared with MCNPX.*

Study of spatial distribution of high energy neutron field

We study spatial distribution of high energy neutrons (E > 1 MeV) produced at E+T assembly using neutron threshold reactions. The MCNPX simulations show that the influence of polyethylene shielding on neutron spectrum is negligible in the MeV energy range. It is possible to study neutron production of high-energy neutrons from lead target with uranium blanket without any disturbance of polyethylene shielding. Due to the hard part of the neutron spectrum in the U/Pb-assembly, isotopes produced in (n,*x*n)-reactions (the emission of up to x=7 neutrons) with high threshold energy (up to ~50 MeV) were observed [1]. The detailed description of obtained longitudinal and radial distributions of yields of isotopes produced in threshold reactions can be seen in [1].

The simulations describe the shape of longitudinal distribution of yields very well, see example of ^{194}Au in Fig.5. A quantitative agreement between experimental and simulated values is worse. The differences reach about 50 %. The trends of experimental data and simulations in the case of radial distributions are very good agreement for the 0.7 and 1.0 GeV experiments. Discrepancies in absolute values do not exceed 40 %. Absolutely different situation is for the experiment with the 1.5 GeV beam energy, the discrepancy between the experimental and simulated values increases quickly with growing perpendicular distance from the target axis up to more than two times. The results of 2.0 GeV experiment show similar tendency. Such great difference cannot be caused by experimental data uncertainties.

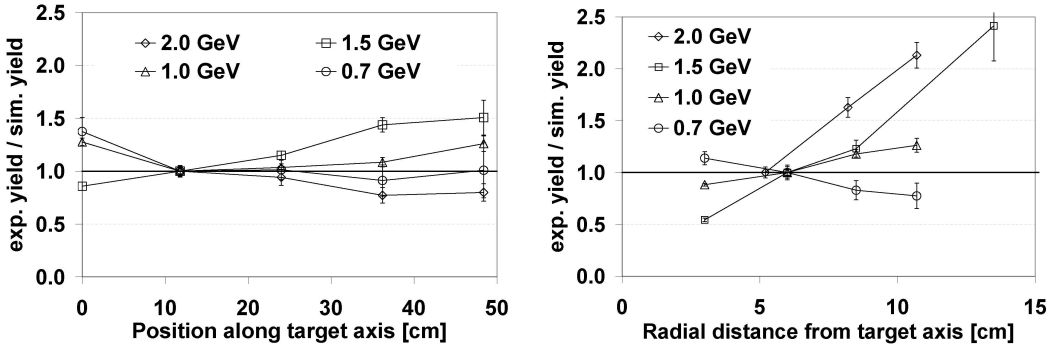

Figure 5. *Comparison of experimental and simulated yields of ^{194}Au in longitudinal (left) and radial (right) directions.*

Conclusion

Neutron production and transport was studied in the setup made of thick lead target and natural uranium blanket irradiated by GeV protons and deuterons. Activation foils from different materials were used as the neutron detectors. The dependency of integral neutron production on beam energy were obtained and compared with the production on simple lead target. The spatial distribution of neutron field is nicely described by MCNPX simulations for lower beam energies (E ≤ 1.0 GeV). We see significant discrepancies between experiment and simulations for higher beam energies (E ≥ 1.5 GeV). Our first two deuteron experiments had beam energy per nucleon lower than 1.5 GeV and spatial distribution data are nicely described by MCNPX simulations. New experiments with deuterons (4.0 GeV) are in plan to fill in the deuterons systematic.

Acknowledgements

We are grateful to the staff of the LHE laboratory of the JINR, Dubna for using the Nuclotron accelerator and to the Agency of Atomic Energy of Russia for supply of material for the uranium blanket. This work was carried out under the support of the GA CR (grant No. 202/03/H043) and the GA AS CR (grant No. K2067107).

References

[1] M. I Krivopustov. et al.: Kerntechnik 68(2003)48; Křížek F. et al.: Czech. J. of Physics 56 (2006) 243; O. Svoboda et al.: this conference contributions.
[2] K. van der Meer et al.: Nucl. Instr. and Meth. in Phys. Res. B217(2004)202.
[3] J. S Hendricks. et al., LANL report LA-UR-06-7991 (2006).
[4] M. Majerle et al.: Nucl. Instr. and Meth. in Phys. Res. A 580/1 (2007) 110.

Validation of simulation codes for future systems: motivations, approach and the role of nuclear data

G. Palmiotti[1)], M. Salvatores[1,2,3)], G. Aliberti[2)]

1) Idaho National Laboratory, NSE Division, 2525 Fremont Ave. P.O. Box 1625, Idaho Falls, ID 83415-3855 (USA)
2) Argonne National Laboratory, NE Division, Argonne, IL 60439 (USA)
3) CEA-Cadarache, 13108 St-Paul-Lez-Durance, France
massimo.salvatores@cea.fr

Abstract: The validation of advanced simulation tools will still play a very significant role in several areas of reactor system analysis. This is the case of reactor physics and neutronics, where nuclear data uncertainties still play a crucial role for many core and fuel cycle parameters. The present paper gives a summary of validation motivations, objectives and approach. A validation effort is in particular necessary in the frame of advanced (e.g. Generation-IV or GNEP) reactors and associated fuel cycles assessment and design.

Validation and verification

Validation of simulation codes is complementary to the "verification" process. In fact, "verification" addresses the question "are we solving the equations correctly" while validation addresses the question "are we solving the correct equations with the correct parameters"
Verification implies comparisons with "reference" equation solutions or with analytical solutions, when they exist. Most of what is called "numerical validation" falls in this category.
Validation strategies differ according to the relative weight of the methods and of the parameters that enter into the simulation tools. Most validation is based on experiments, and the field of neutronics where a "robust" physics description model exists and which is function of "input" parameters not fully known, will be the focus of this paper. In fact, in the case of reactor core, shielding and fuel cycle physics the model (theory) is well established (the Boltzmann and Bateman equations) and the parameters are the nuclear cross-sections, decay data etc.
Two types of validation approaches can and have been used:

a) Mock-up experiments ("global" validation): need for a very close experimental simulation of a reference configuration. Bias factors cannot be extrapolated beyond reference configuration;
b) Use of "clean", "representative" integral experiments ("bias factor and adjustment" method). Allows to define bias factors, uncertainties and can be used for a wide range of applications. It also allows to define "adjusted" application libraries or even "adjusted" data files.

The use of this last approach has been particularly successful in the design of SUPERPHENIX. In fact the prediction of the critical mass has been remarkably close to the experimental value observed at reactor start up (discrepancy of ~3 out of ~400 core sub-assemblies).

Validation: motivation and objectives

The recent extensive sensitivity/uncertainty studies, have allowed to preliminary quantify the impact of current nuclear data uncertainties on design parameters of the major Gen-IV and transmutation systems, and in particular on fast reactors with different coolants, with different fuels (oxide, metal, carbide, nitride), fuel composition (e.g. different Pu/TRU ratios), MA content and different conversion ratios. In general, innovative characteristics of future reactor cores will in fact imply new core architectures (e.g. without fertile blankets), reduced void reactivity coefficients, wide range of possible Pu vectors, significant presence of minor actinides in innovative fuels (metal, oxide, carbide, nitride) in burner or breeder core configurations.
These studies [1 to 4] have pointed out that present uncertainties on the nuclear data should be significantly reduced, in order to get full benefit from the advanced modeling and

simulation initiatives. Only a parallel effort in advanced simulation and in nuclear data improvement will enable to provide designers with more general and well validated calculation tools, that would be able to meet design target accuracies.
This point can be illustrated by the inspection of the review of current and targeted uncertainties for some SFR design parameters, as indicated in Tables 1-3 (consistent with the requirements of [5]):

Table 1. *Neutronics: Core*

Parameter	Current uncertainty (SFR)		Targeted Uncertainty
	Input Data Origin (A Priori)	Modeling Origin	
Multiplication Factor, k_{eff} ($\Delta k/k$)	1%	0.5%	0.3%
Power Peak	1%	3%	2%
Power Distribution	1%	6%	3%
Conversion Ratio (Absolute Value)	5%	2%	2%
Control Rod Worth: Element	5%	6%	5%
Control Rod Worth: Total	5%	4%	2%
Burnup Reactivity Swing ($\Delta k/k$)	0.7%	0.5%	0.3%
Reactivity Coefficients: Total	7%	15%	7%
Reactivity Coefficients: Component	20%	20%	10%
Fast Flux for Damage	7%	3%	3%
Kinetics Parameters	10%	5%	5%
Local Nuclide Densities: Major	5%	3%	2%
Local Nuclide Densities: Minor	30%	10%	10%
Fuel Decay Heat at Shutdown	10%	3%	5%

Table 2. *Neutronics: Shielding*

Parameter	Current uncertainty (SFR)		Targeted Uncertainty
	Input Data Origin (A Priori)	Modeling Origin	
Out of Core Coolant Activation	70%	70%	50%
Shield Dimensioning (Total Flux)	70%	30%	20%
Structural Damage Out of Core (Total Flux)	40%	30%	20%

Table 3. *Neutronics: Fuel Cycle*

Parameter	Current uncertainty (SFR)		Targeted Uncertainty
	Input Data Origin (A Priori)	Modeling Origin	
Neutron Dose at Fuel Fabrication	15%	15%	10%
Decay Heat of Spent Fuel at Repository	50%	15%	20%
Radiotoxicity at Repository	50%	15%	20%

These tight design target accuracies, which justified in a consolidated phase of design, in order to comply with safety and optimization requirements and objectives, can only be met if very accurate nuclear data are used for a large number of isotopes, reaction types and energy ranges.
The required accuracies on the nuclear data are such that it is difficult to meet them using only differential experiments, even if innovative experimental techniques are used.
The use of integral experiments has been essential in the past to insure enhanced predictions for power fast reactor cores. In some cases, these integral experiments have been documented in an effective manner and associated uncertainties are well understood.
A combined use of scientifically based covariance data and of integral experiments can be made using advanced statistical adjustment techniques (see, e.g., [6]). These techniques can provide in a first step adjusted nuclear data for a wide range of applications, together with new, improved covariance data and bias factors (with reduced uncertainties) for the required design parameters, in order to meet design target accuracies.
The method can be further improved to “adjust” physical parameters and to obtain in a second phase, a fully “adjusted” data file.

Uncertainty reduction needed to meet integral parameter target accuracies for <u>all</u> systems

As an example of the accuracy requirements to meet design target accuracies for innovative fast reactors, in [7] a study has been performed in order to quantify the requirements to meet simultaneously target accuracies such those indicated in Table 1 for a wide range of fast

reactors with different coolants, fuel type, MA content in the fuel, being iso-generators or burners and critical or sub-critical. In practice the following systems have been considered:

ABTR: Na-cooled Pu burner, with Conversion Ratio CR~0.5;
SFR: Na-cooled TRU burner with CR~0.25;
EFR: Na-cooled FR for homogeneous TRU recycle and CR~1;
GFR: Gas-cooled FR for homogeneous TRU recycle and CR~1;
LFR: Lead-cooled FR for homogeneous TRU recycle and CR~0.8;
ADMAB: Lead-cooled ADS with U-free fuel and Pu/MA~1/2.

A summary of the results is given in the following table:

Table 4. *ABTR, SFR, EFR, GFR, LFR, ADMAB: Uncertainty Reduction Requirements to Meet Integral Parameter Target Accuracies*

Isotope Cross-Section	Energy Range	Uncertainty (%)	
		Initial	Target
U238 σ_{inel}	19.6 - 6.07 MeV	29.3	9.0
	6.07 - 2.23 MeV	19.8	2.0
	2.23 - 1.35 MeV	20.6	2.1
	1.35 - 0.498 MeV	11.6	2.3
	498 - 183 keV	4.2	3.8
	183 - 67.4 keV	11.0	4.2
Pu241 σ_{fiss}	6.07 - 2.23 MeV	14.2	5.0
	2.23 - 1.35 MeV	21.3	3.9
	1.35 - 0.498 MeV	16.6	2.1
	498 - 183 keV	13.5	1.7
	183 - 67.4 keV	19.9	1.7
	67.4 - 24.8 keV	8.7	1.9
	24.8 - 9.12 keV	11.3	2.0
	9.12 - 2.03 keV	10.4	2.1
	2.03 - 0.454 keV	12.7	2.7
	454 - 22.6 eV	19.4	5.4
Cm244 σ_{fiss}	6.07 - 2.23 MeV	31.3	3.0
	2.23 - 1.35 MeV	43.8	2.6
	1.35 - 0.498 MeV	50.0	1.5
	498 - 183 keV	36.5	4.0
	183 - 67.4 keV	47.6	7.3
U238 σ_{capt}	24.8 - 9.12 keV	9.4	1.8
	9.12 - 2.03 keV	3.1	1.8
Fe56 σ_{inel}	6.07 - 2.23 MeV	7.2	2.6
	2.23 - 1.35 MeV	25.4	1.7
	1.35 - 0.498 MeV	16.1	1.5

Isotope Cross-Section	Energy Range	Uncertainty (%)	
		Initial	Target
B10 σ_{capt}	498 - 183 keV	15.0	2.9
	183 - 67.4 keV	10.0	2.7
	67.4 - 24.8 keV	10.0	3.3
	24.8 - 9.12 keV	8.0	3.9
	9.12 - 2.03 keV	8.0	6.0
Pu239 σ_{capt}	1.35 - 0.498 MeV	18.2	6.6
	498 - 183 keV	11.6	4.4
	183 - 67.4 keV	9.0	4.0
	67.4 - 24.8 keV	10.1	4.2
	24.8 - 9.12 keV	7.4	3.8
	9.12 - 2.03 keV	15.5	3.2
O16 σ_{capt}	19.6 - 6.07 MeV	100.0	37.9
	6.07 - 2.23 MeV	100.0	37.9
Am243 σ_{inel}	6.07 - 2.23 MeV	17.9	4.9
	2.23 - 1.35 MeV	35.3	3.9
	1.35 - 0.498 MeV	42.2	2.3
	498 - 183 keV	41.0	3.7
	183 - 67.4 keV	79.5	3.7
	67.4 - 24.8 keV	80.8	12.4
Am242m σ_{fiss}	1.35 - 0.498 MeV	23.4	21.4
	498 - 183 keV	16.5	6.3
	183 - 67.4 keV	16.6	4.7
	67.4 - 24.8 keV	16.6	4.8
	24.8 - 9.12 keV	14.4	5.6
	2.04 - 0.454 keV	11.8	5.9
Na23 σ_{inel}	1.35 - 0.498 MeV	28.0	10.5

Isotope Cross-Section	Energy Range	Uncertainty (%)	
		Initial	Target
Pu240 σ_{fiss}	6.07 - 2.23 MeV	4.8	2.9
	2.23 - 1.35 MeV	5.7	2.6
	1.35 - 0.498 MeV	5.8	1.6
	498 - 183 keV	3.9	3.7
	2.03 - 0.454 keV	21.6	11.8
Si28 σ_{capt}	19.6 - 6.07 MeV	52.9	7.2
Si28 σ_{inel}	6.07 - 2.23 MeV	13.5	3.9
	2.23 - 1.35 MeV	50.0	7.4
Pb206 σ_{inel}	6.07 - 2.23 MeV	5.5	4.2
	2.23 - 1.35 MeV	14.2	4.0
	1.35 - 0.498 MeV	9.2	4.7
Pb207 σ_{inel}	6.07 - 2.23 MeV	5.0	4.9
	2.23 - 1.35 MeV	13.8	6.0
	1.35 - 0.498 MeV	11.3	3.6
Pb σ_{inel}	6.07 - 2.23 MeV	5.4	3.0
Am243 σ_{fiss}	6.07 - 2.23 MeV	11.0	2.3
	2.23 - 1.35 MeV	6.0	1.9
	1.35 - 0.498 MeV	9.2	1.7
Bi209 σ_{inel}	2.23 - 1.35 MeV	34.1	2.8
	1.35 - 0.498 MeV	41.8	4.3
N15 σ_{el}	2.23 - 1.35 MeV	5.0	3.1
	1.35 - 0.498 MeV	5.0	1.2
	498 - 183 keV	5.0	1.9
	183 - 67.4 keV	5.0	2.3
Zr90 σ_{inel}	6.07 - 2.23 MeV	18.0	3.3

These results confirm the very significant uncertainty reduction needed to meet target accuracies on important design parameters. In some cases (e.g. inelastic of U-238), the required reduction seems hard to be met with differential measurements only.

The data statistical adjustment and bias factor method

The adjustment and bias factor method [6] makes use of:

- "a priori" nuclear data covariance information,
- integral experiments analysis to define C/E values,
- integral experiment uncertainties,

in order to evaluate "a priori" uncertainties on reference design performance parameters, to reduce these uncertainties using integral experiments ("a posteriori" uncertainties on performance parameters) and to define "adjusted" nuclear data and associated "a posteriori" covariance data.

A crucial step is the selection of a set of relevant experiments. This task can be performed using sensitivity analysis of selected configurations including reference design configurations for a wide range of integral parameters related to the core performances (critical mass, reactivity coefficients, control rod worth, power distributions etc), and fuel cycle parameters (reactivity loss/cycle, decay heat, transmutation rates, neutron sources and doses of spent fuel etc).

A second crucial step is the selection of science based covariance data for uncertainty evaluation and target accuracy assessment. Finally, the analysis of experiments should be performed using the best methods available, with some redundancy to avoid systematic errors. Finally the adjustment procedure allows to use calculation/experiment discrepancies (and associated uncertainties) in a statistical adjustment.
The "adjustment" procedure can be generalized and applied to the physical parameters that enter into the model description of a specific cross-section type. This generalized method is called "consistent method" [8], and is shortly described below.
If the cross-section is schematically described as:
$\sigma(E) = f(E, p_i)$
the sensitivity coefficients of the cross-section to the variations of the parameters p_i can be obtained from the model codes as:
$S_{pi} = (\delta f / \delta p_i)(p_i / f)$
These sensitivity coefficients can then be folded with standard sensitivity coefficients of integral parameters R to cross-section σ variations:
$(\delta R / \delta p_i)(p_i / R) = S_\sigma S_{pi}$
A correlation can now be established among integral parameters and basic physics parameters, and the adjustment procedure outlined previously, can be applied to the p_i parameters, if uncertainties (covariance data) are provided for the parameters.
Finally, if these parameters are part of the data file (e.g. the temperature values associated to the evaporation spectrum describing the secondary neutron distribution in inelastic scattering) the file itself can be in principle "adjusted".

Integral experiments

Integral experiments have been performed in large number in the past. Future experiments can be foreseen only on a few installations and at a later date (this is the case of the MASURCA critical facility at CEA-Cadarache).
Some of the most representative (and „clean") integral experiments are being collected within the NEA-NSC project IRPHEP [9]. In this respect, it should be stressed that documentation is essential: experimental conditions and environment, "credible" uncertainties, correlations among experiments.
Another very crucial point is the availability and share of power reactor experiments, e.g.

- Physics experiments at reactor start-up (e.g. SUPERPHENIX);
- Operation experiments (e.g. EBR-II, FFTF, PHENIX, JOYO);
- New experiments (e.g. at the future MONJU start-up);
- Irradiation experiments (e.g. PROFIL and TRAPU experiments in PHENIX).

Issues and perspectives

Innovative reactor system design and requirements for improved economy and safety, will require significant improvements beyond current simulation tools, associated to significant improvements in their validation, in particular in order to cope with very tight requirements on nuclear data uncertainties. In this respect, a robust validation approach can be used in the reactor core and fuel cycle physics field.
Powerful and flexible sensitivity analysis methods and tools are available (see [10]), and a large effort is underway to assess nuclear covariance data in very comprehensive way [11].
However, a choice of appropriate integral experiments has to be carefully made. There is the need for integral experiments with well documented uncertainty values and possible correlations among different experiment types. There is also the need for an increased role of power reactor integral experiments.
The experiment analysis should be performed with more than one reference methods, as far as possible independent from each other, in order to reduce or eliminate the risks of systematic method errors.
Since the result of the validation will provide bias factors and reduced uncertainties on most design parameters, together with statistically "adjusted" cross-sections with new associated covariance data, it will be needed to define the protocols for using them as application libraries. However, and more important, the "adjustments" will have to be interpreted as "trends" to be used by nuclear data evaluators, in order to improve current data files (such as ENDF/B-VII). We have also described in the present paper, how the statistical adjustment

procedure can be generalized to provide “adjustments” of physics parameters that enter into the models which describe the different cross-sections.
Finally, it should be stressed that the present data bases of integral experiments are relatively wide, even if not always documented in a satisfactory way. Future design studies, new core and fuel types, new core configurations, could require selected, high accuracy integral experiments, to be performed in the few adapted critical facilities, still available world-wide.

References

[1] M. Salvatores et al., “Nuclear Data Needs for Advanced Reactor Systems. A NEA Nuclear Science Committee Initiative,” Proc. Int. Conf. ND-2007, Nice, France (April 2007).
[2] G. Aliberti et al., “Nuclear Data Sensitivity, Uncertainty and Target Accuracy Assessment for Future Nuclear Systems”, Annals of Nucl. Energy, 33, 700-733 (2006).
[3] M. Salvatores, G. Aliberti and G. Palmiotti, “The Role of Differential and Integral Experiments to Meet Requirements for Improved Nuclear Data”, ND2007, Nice (France), April 2007.
[4] G. Aliberti et al., “Impact of Nuclear Data Uncertainties on Transmutation of Actinides in Accelerator-Driven Assemblies,” Nucl. Sci. Eng., 46, 13-50 (2004).
[5] G. Palmiotti, J. Cahalan, P. Pfeiffer, T. Sofu, T. Taiwo, T. Wei, A. Yacout, W. Yang, A. Siegel, Z. Insepov, M. Anitescu, P. Hovland, C. Pereira, M. Regalbuto, J. Copple, M. Williamson, “Requirements for Advanced Simulation of Nuclear Reactor and Chemical Separation Plants”, ANL-AFCI-168, May 2006.
[6] M. Salvatores, G. Aliberti, G. Palmiotti, “Nuclear Data Validation and Fast Reactor Design Performances Uncertainty Reduction”, ANS, Boston, June 2007.
[7] G. Aliberti, G. Palmiotti and M. Salvatores “Simultaneous Nuclear Data Target Accuracy Study for Innovative Fast Reactors, This Workshop.
[8] A. D’Angelo, A Oliva, G. Palmiotti, M. Salvatores, S. Zero “ Consistent Utilization of Shielding Benchmark Experiments”. Nuclear Science Engineering, 65, 477, 1978.
[9] “International Handbook of Evaluated Reactor Physics Benchmark Experiments”. NEA/NSC/DOC(2006).
[10] G. Palmiotti, M. Salvatores, G. Aliberti, “Methods in Use for Sensitivity Analysis, Uncertainty Evaluation, and Target Accuracy Assessment” This Workshop.
[11] P. Oblozinsky, This Workshop.

Methods in use for sensitivity analysis, uncertainty evaluation, and target accuracy assessment

G. Palmiotti[1)], M. Salvatores[1,2,3)], G. Aliberti[2)]

1) Idaho National Laboratory, NSE Division, 2525 Fremont Ave. P.O. Box 1625, Idaho Falls, ID 83415-3855 (USA)
2) Argonne National Laboratory, NE Division, Argonne, IL 60439 (USA)
3) CEA-Cadarache, 13108 St-Paul-Lez-Durance, France
Giuseppe.Palmiotti@inl.gov

Abstract: Sensitivity coefficients can be used for different objectives like uncertainty estimates, design optimization, determination of target accuracy requirements, adjustment of input parameters, and evaluations of the representativity of an experiment with respect to a reference design configuration. In this paper the theory, based on the adjoint approach, that is implemented in the ERANOS fast reactor code system is presented along some unique tools and features related to specific types of problems as is it is the case for nuclide transmutation, reactivity loss during the cycle, decay heat, neutron source associated to fuel fabrication, and experiment representativity.

Introduction

Sensitivity analysis and uncertainty evaluation are the main instruments for dealing with the sometimes scarce knowledge of the input parameters used in simulation tools. For sensitivity analysis, sensitivity coefficients are the key quantities that have to be evaluated. They are determined and assembled, using different methodologies, in a way that when multiplied by the variation of the corresponding input parameter they will quantify the impact on the targeted quantities whose sensitivity is referred to. Sensitivity coefficients can be used for different objectives like uncertainty estimates, design optimization, determination of target accuracy requirements, adjustment of input parameters, and evaluations of the representativity of an experiment with respect to a reference design configuration.
In uncertainty evaluation, the sensitivity coefficients are multiplied by the uncertainties of the input parameters in order to obtain the uncertainty of the targeted parameter of interest. The origin and quality of the uncertainties of the input parameters can be different and vary quite a lot. In some cases, they are provided by the expert judgment of qualified designer. In some other cases more useful information is available, for instance from experimental values, and they are cast in more rigorous formalism. This is the case, for instance, of covariance matrix for neutron cross-sections, where correlations in energy and among the different input parameters (reactions, isotopes) are also provided.
Target accuracy assessments are the inverse problem of the uncertainty evaluation. To establish priorities and target accuracies on data uncertainty reduction, a formal approach can be adopted by defining target accuracy on design parameter and finding out required accuracy on data. In fact, the unknown uncertainty data requirements can be obtained by solving a minimization problem where the sensitivity coefficients in conjunction with the existing constraints provide the needed quantities to find the solutions.
Sensitivity coefficients are also used in input parameter adjustments. In this case, the coefficients are used within a fitting methodology (e.g. least square fit, Lagrange multipliers with most likelihood function, etc.) in order to reduce the discrepancies between measured and calculational results. The resulting adjusted input parameters can be subsequently used, sometimes in combination with bias factors, to obtain calculational results to which a reduced uncertainty will be associated.
A further use of sensitivity coefficients is, in conjunction with a covariance matrix, a representativity analysis of proposed or existing experiments. In this case the calculation of correlations among the design and experiments allow to determine how representative is the latter of the former, and consequently, to optimize the experiments and to reduce their numbers. Formally one can reduce the estimated uncertainty on a design parameter by a quantity that represents the knowledge gained by performing the experiment.

In this paper we will brief summarize the sensitivity methodology that has been implemented in the ERANOS [1] code system and associated tools, and that make use of the so-called adjoint approach. The adjoint approach is based on the perturbation theory originally developed in the quantum mechanics field.
The ERANOS code system has been widely validated in the past and recently, it has been used for a very comprehensive analysis of the impact of cross-section uncertainties on the integral parameters of the selected GEN-IV systems, in order to define target accuracy requirement to meet expected design needs. The flexibility of the ERANOS systems has allowed to account for integral parameters related to the core neutronics (like reactivity coefficients, etc) and to the fuel cycle (neutron sources, decay heat, reactivity loss during the cycle, transmutation rates etc).
The present paper will summarize some of the most original features of the ERANOS system.

Historical notes

The perturbation theory has been introduced in reactor physics in the 50' and one can find a classical presentation in the Weinberg and Wigner book [2]. This is the perturbation theory applied to the k_{eff} of the critical reactor and L. N. Usachev gave a comprehensive development in an article published at the Geneva conference of 1955 [3].
It is interesting to note that the perturbation theory applied to reactor makes use of a definition of a function (the adjoint flux), that has a specific physical meaning if one is dealing with a non-conservative system as in the case of a nuclear reactor. This physical interpretation of the adjoint flux has been the focus of extensive studies, during the 60', in particular by J. Lewins [4, 5].
The perturbation theory, mostly developed and applied for reactivity coefficient studies, was readily used [6] for an application, sensitivity studies, that had a spectacular development in the 70' and 80'. This development was made possible by a generalization of the perturbation theory (thanks again to Usachev), that deals with the general problem of a variation of any kind of a neutron flux functional. Usachev derived an explicit formulation that relates the functional variation to any change of the Boltzmann operator [7].
This development, and its further generalization by Gandini, to the case of any kind of linear and bilinear functional of the real and adjoint flux [8], opened a new territory for the perturbation theory. It was now possible to relate explicitly the variation of any type of integral parameter (multiplication factor, reaction rates, reactivity coefficients, source values, etc.) to any kind of change of the operator that characterizes the system.
The application of the generalized perturbation theory to real life problems lead to new interesting developments that allowed to clarify specific characteristics of the new theory with implications for the computation of the generalized importance functions introduced by the theory [9].
Starting from the early 70' the generalized perturbation methods, which were essentially developed and used in Europe, became popular also in the rest of the world and in particular with new developments in several U. S. laboratories, ANL [10] and ORNL [11], and in Japan [12].
The perturbation methods, and their main application in the field of sensitivity analysis, have been used mostly in their first order formulation. Actually, as for any perturbation theory, the power of the method is particularly evident when one considers small perturbations (for instance for cross-sections σ) that therefore induce little changes of the functions (e. g. the neutron flux φ), that characterize the system, and for whom one can neglect the second order product (for instance $\delta\sigma\delta\varphi$). However, there have been theoretical developments that take into accounts higher order effects without losing all the advantages typical of the first order formulations [13, 14, and 15].
Among the theoretical developments after the 70' that had significant practical impact, one has to mention the extension of the perturbation theory to the nuclide field that allows to study the burn up due to irradiation in the reactor at the first order [16], and to higher orders [17]. Subsequently a new formulation, the "equivalent Generalized Perturbation Theory" EGPT [18], allowed to treat in a very simple and efficient way the perturbation and sensitivity analyses for reactivity coefficients.
Among the most recent development it is worth to mention those related to the ADS case with functionals that allow to calculate the sensitivity of the source importance (φ^*) and the inhomogeneous reactivity [19].

Finally, one should remind that, besides the neutronic field, there have been several studies for extending the perturbation theory developed for reactor physics to other domains (thermal-hydraulics, safety, etc.) with very interesting theoretical developments [20, 21, and 22].

Theory

Sensitivity coefficients and perturbation theories

The variations of any integral parameter Q due to variations of cross-sections σ can be expressed using perturbation theories [23], to evaluate sensitivity coefficients S:

$$\delta Q/Q = \sum_j S_j \frac{\delta\sigma_j}{\sigma_j} \tag{1}$$

where the sensitivity coefficients S_j are formally given by:

$$S_j = \frac{\partial Q}{\partial \sigma_j} \cdot \frac{\sigma_j}{Q} \tag{2}$$

For practical purposes, in the general expression of any integral parameter Q, the explicit dependence from some cross-sections (e.g. σ_i^e) and the implicit dependence from some other cross-sections (e.g. σ_j^{im}) are kept separated:

$$Q = f(\sigma_j^{im}, \sigma_i^e)\,. \tag{3}$$

As an example, we consider a reaction rate:

$$R = \left\langle \underline{\sigma}^e, \underline{\Phi} \right\rangle \tag{4}$$

where brackets $\langle , \rangle$ indicate integration over the phase space. In the case of a source-driven system, $\underline{\Phi}$ is the inhomogeneous flux driven by the external source, and the homogeneous flux in the case of critical core studies. In Eq. (4), $\underline{\sigma}^e$ can be an energy dependent detector cross-section; R is "explicitly" dependent on the $\underline{\sigma}^e$ and "implicitly" dependent on the cross-sections which characterize the system, described by the flux $\underline{\Phi}$. In other terms, R depends on the system cross-sections via $\underline{\Phi}$. Eq. (1) can be rewritten as follows:

$$\delta Q/Q = \sum_j S_j \frac{\delta\sigma_j^{im}}{\sigma_j^{im}} + \left(\frac{\partial Q}{\partial \sigma^e} \cdot \frac{\sigma^e}{Q} \right) \cdot \frac{\delta\sigma^e}{\sigma^e} \tag{5}$$

where we have the hypothesis of an explicit dependence of Q on only one σ^e. If we drop the index "im":

$$\delta Q/Q = \sum_j S_j \frac{\delta\sigma_j}{\sigma_j} + \left(\frac{\partial Q}{\partial \sigma^e} \cdot \frac{\sigma^e}{Q} \right) \cdot \frac{\delta\sigma^e}{\sigma^e} = I + D \tag{6}$$

where the term I is generally called "indirect" effect, and the term D is called "direct" effect. While the direct effects can be obtained with explicit expressions of the derivatives of Q, the indirect effect (i.e. the sensitivity coefficients S), can be obtained with perturbation expression, most frequently at the first order [23].

In what follows, we will explicit the formulations used by the ERANOS code system for the sensitivity coefficients at the first order for the indirect effects related to reactivity coefficients [18], reaction rates [23], nuclide transmutation (i.e., evolution in time [16]). The formulations related to other parameters of interest for critical or sub-critical systems will also be described (e.g. the reactivity loss during the irradiation, the decay heat etc). These examples are provided in order to highlight the wide extent of capabilities of the sensitivity algorithms of the ERANOS code system.

Reactivity coefficients [18]

A reactivity coefficient (like the Doppler effect) can be expressed as a variation of the reactivity of the unperturbed system (characterized by a value K of the multiplication factor, a Boltzman operator M, a flux $\underline{\Phi}$ and an adjoint flux $\underline{\Phi}^*$):

$$\Delta\rho = \left(1 - \frac{1}{K_p}\right) - \left(1 - \frac{1}{K}\right) = \frac{1}{K} - \frac{1}{K_p} \tag{7}$$

where K_p corresponds to a variation of the Boltzmann operator such that:

$$M \to M_p \left(= M + \delta M_p\right) \qquad \underline{\Phi} \to \underline{\Phi}_p \left(= \underline{\Phi} + \delta\underline{\Phi}_p\right)$$
$$\underline{\Phi}^* \to \underline{\Phi}_p^* \left(= \underline{\Phi}^* + \delta\underline{\Phi}_p^*\right) \qquad K \to K_p \left(= K + \delta K_p\right) \tag{8}$$

The sensitivity coefficients (at first order) for $\Delta\rho$ to variations of the σ_j are given as in [3]:

$$S_j^{\Delta\rho} = \frac{\partial(\Delta\rho)}{\partial\sigma_j} \cdot \frac{\sigma_j}{\Delta\rho} = \left\{ \frac{1}{I_f^p} \left\langle \underline{\Phi}_p^*, \sigma_j \underline{\Phi}_p \right\rangle - \frac{1}{I_f} \left\langle \underline{\Phi}^*, \sigma_j \underline{\Phi} \right\rangle \right\} \tag{9}$$

where $I_f = \left\langle \underline{\Phi}^*, F\underline{\Phi} \right\rangle$ and $I_f^p = \left\langle \underline{\Phi}_p^*, F\underline{\Phi}_p \right\rangle$, F being the neutron fission production part of the M (= F - A) operator.

Reaction rates

The classical formulations found e.g. in [23] can be applied to the case of e.g., damage rate or He-production in the structures, or to the power peak factor in the core:

$$R = \left\langle \underline{\Phi}, \underline{\Sigma}_R \right\rangle \tag{10}$$

The sensitivity coefficients are given by:

$$S_j^R = \left\langle \underline{\Psi}_R^*, \sigma_j \underline{\Phi} \right\rangle \tag{11}$$

where $\underline{\Phi}$ has been defined above, and $\underline{\Psi}_R^*$ is the solution of:

$$M^* \underline{\Psi}_R^* = \underline{\Sigma}_R \tag{12}$$

and M^* is the adjoint of the operator M. In the specific case of the power peak, this parameter can be expressed as the ratio:

$$R = \frac{\left\langle \Sigma_p \underline{\Phi} \right\rangle_{MAX}}{\left\langle \Sigma_p \underline{\Phi} \right\rangle_{Reactor}} \tag{13}$$

with Σ_p the power cross-section, essentially represented by $E_f \cdot \Sigma_f$, E_f being the average energy released per fission. The sensitivity coefficients are defined as:

$$S_j = \left\langle \underline{\Psi}^*, \sigma_j \underline{\Phi} \right\rangle \tag{14}$$

and $\underline{\Psi}^*$ is the importance function solution of:

$$M^* \underline{\Psi}^* = \frac{\Sigma_{p,MAX}}{\left\langle \Sigma_p \underline{\Phi} \right\rangle_{MAX}} - \frac{\Sigma_{p,Reactor}}{\left\langle \Sigma_p \underline{\Phi} \right\rangle_{Reactor}} \tag{15}$$

where $\Sigma_{p,MAX}$ is the Σ_p value at the spatial point where $\langle \Sigma_p \underline{\Phi} \rangle \equiv \langle \Sigma_p \underline{\Phi} \rangle_{MAX}$, and $\Sigma_{p,Reactor}$ is the Σ_p value at each spatial point of the reactor. In Eq. (15) effects due to $\Sigma_{p,MAX}$ and $\Sigma_{p,Reactor}$ variations are assumed to be negligible.

Nuclide transmutation [16]

The generic nuclide K transmutation during irradiation can be represented as the nuclide density variation between time t_0 and t_F. If we denote n_{Fi}^K the "final" density, the appropriate sensitivity coefficient is given by:

$$S_j^K = \frac{\partial n_F^K}{\partial\sigma_j} \cdot \frac{\sigma_j}{n_F^K} = \frac{1}{n_F^K} \int_{t_0}^{t_F} \underline{n}^* \sigma_j \underline{n} \; dt \tag{16}$$

where the time dependent equations to obtain $\underline{n}^*$ and $\underline{n}$, together with their boundary conditions, are defined in [16].

Reactivity loss during irradiation, $\Delta\rho^{cycle}$

At the first order, and neglecting the cross-section variation during irradiation (which is a good approximation for fast neutron systems), we can write:

$$\Delta\rho^{cycle} = \sum_K \Delta n^K \rho_K \tag{17}$$

where:

$$\Delta n^K = n_F^K - n_0^K \tag{18}$$

and ρ_K is the reactivity per unit mass associated to the isotope K.

The related sensitivity coefficients S_j^{cycle} associated to the variation of a σ_j, are given by:

$$S_j^{cycle} = \frac{\sigma_j}{\Delta\rho^{cycle}} \frac{\partial \Delta\rho^{cycle}}{\partial \sigma_j} = \frac{\sigma_j}{\Delta\rho^{cycle}} \left(\sum_K \frac{\partial n^K}{\partial \sigma_j} \cdot \rho_K + \sum_K \Delta n^K \frac{\partial \rho_K}{\partial \sigma_j} \right) \tag{19}$$

Using the formulations previously indicated., we obtain:

$$S_j^{cycle} = \sum_K \frac{\rho_K}{\Delta\rho^{cycle}} \int_{t_0}^{t_F} \underline{n}^* \sigma_j \underline{n} \; dt + \left\{ \frac{1}{l_f^p} \left\langle \underline{\Phi}_p^*, \sigma_j \underline{\Phi}_p \right\rangle - \frac{1}{l_f} \left\langle \underline{\Phi}^*, \sigma_j \underline{\Phi} \right\rangle \right\} \tag{20}$$

where the index "p" refers to the core state at $t = t_F$.

Case of a neutron source (e.g. at fuel fabrication)

A neutron source $NS_{t=tF}$ at $t = t_F$ can be defined as:

$$NS_{t=t_F} = \sum_i P_i n_{i,t=t_F} \tag{21}$$

where P_i is the neutron production cross-section (e.g. by spontaneous fissions). The sensitivity coefficients are:

$$S_j^i = P_i \cdot \frac{\partial n_F^i}{\partial \sigma_j} \cdot \frac{\sigma_j}{n_F^i} = \frac{P_i}{n_F^i} \int_{t_0}^{t_F} \underline{n}^* \sigma_j \underline{n} \; dt \tag{22}$$

where effects due to P_i cross-section variations are supposed to be negligible.

Decay heat

The decay heat is defined as:

$$H(t) = \sum_K \lambda_K Q_K n^K(t) \tag{23}$$

where for each isotope K, λ_K are the decay constants, Q_K the heat released in decay reaction and $n^K(t)$ are the nuclide densities at time t. The equations for $n^K(t)$ are the classical ones:

$$\frac{dn^K(t)}{dt} = \sum_F \gamma_{K,f} \tau_f + \sum_j n^K(t) \tau_j b_{j \to K} + \sum_i n^i(t) \lambda_i b_{i \to K} - \tau_K n^K(t) - \lambda_K n^K(t) \tag{24}$$

Or in a more compact form:

$$\frac{dn^K(t)}{dt} = b_k + \sum_{j=1}^{K-1} C_{kj} n^j(t) - C_{kk} n^K(t) \tag{25}$$

where $\gamma_{K,f}$ are the fission yields for fissionable isotope f, τ are microscopic reaction rates and $b_{j \to k}$ are branching ratios. This is an inhomogeneous Bateman-type equation that defines the appropriate nuclide field. The uncertainty on H(t) is obtained by combining the appropriate derivatives of H with respect to λ, Q and n, and accounting for possible correlations. As far as variations of the n^K terms, they can be evaluated using the perturbation techniques previously indicated. A specific feature is represented by the variation of the fission yields γ, i.e., by the variation of the "source" term b_K in Eq. (25).

The relative sensitivity coefficients corresponding to the decay heat at $t = t_x$ are given by:

$$S_K^\gamma = \tau_f \frac{\partial n_{t=t_x}^K}{\partial \gamma_{K,f}} \cdot \frac{\gamma_{K,f}}{n_{t=t_x}^K} = \frac{\tau_f}{n_{t=t_x}^K} \int_0^{t_x} \underline{n}^* \gamma_{K,f} dt \tag{26}$$

Calculational tools in the ERANOS code system

All the sensitivity calculations described above can be performed with the ERANOS code system, which allows to calculate homogeneous and inhomogeneous solutions of the Boltzmann equation and generalized importance functions, and to perform perturbation and uncertainty analysis. Specific modules in ERANOS allow generation of the source terms of the generalized importance equations and solution in two or three-dimensional of the finite-difference diffusion or S_n transport equation, or of nodal variational transport equations. A fundamental mode removal algorithm is applied when solving the generalized importance equations for sources that are orthogonal to the homogeneous solutions. Procedures that manipulate different perturbation modules are used to generate the sensitivity coefficients related to reactivity coefficients.

The discrete ordinate module BISTRO [24] in ERANOS can be used to perform flux and generalized importance function calculations. In order to avoid problems related to S_n negative solutions that are present for instance in the case of reaction rate ratios importance calculations, ERANOS uses a special procedure that allows separately calculating the generalized importance for the positive and negative contributions and combining them at the level of the perturbation or sensitivity coefficient computation .

Ancillary calculations: uncertainty analysis, experiment representativity, and target accuracy assessment

Uncertainty evaluation and experiment representativity factors are computed in ERANOS with covariance matrices provided in different general formats. The uncertainties associated to the cross-section can be represented in the form of a variance-covariance matrix:

$$D_\sigma = \begin{pmatrix} d_{11} & d_{12} & \Lambda & d_{1J} \\ d_{12} & d_{22} & \Lambda & d_{2J} \\ \Lambda & \Lambda & \Lambda & \Lambda \\ d_{1J} & d_{2J} & \Lambda & d_{JJ} \end{pmatrix} \tag{37}$$

where the elements dij represent the expected values related to the parameters σj, and σi.
The variance of Q can then be obtained as:

$$\mathrm{var}(Q) = \sum_{j,i}^{J} S_j S_i d_{ij}$$

In order to plan for specific experiments able to reduce uncertainties on selected design parameters, a formal approach, initially proposed by L. Usachev [25] has been applied by Palmiotti and Salvatores [26] and further developed in by Gandini [27]).
In the case of a reference parameter R, once the sensitivity coefficient matrix S_R and the covariance matrix D are available, the uncertainty on the integral parameter can be evaluated by the equation:

$$\Delta R_0^2 = S_R^{+} D S_R \tag{38}$$

We can consider an integral experiment conceived in order to reduce the uncertainty ΔR_0^2. Let us indicate by S_E the sensitivity matrix associated with this experiment. If we call "representativity factor" the following expression:

$$r_{RE} = \frac{\left(S_R^{+} D S_E\right)}{\left[\left(S_R^{+} D S_R\right)\left(S_E^{+} D S_E\right)\right]^{1/2}}, \tag{39}$$

it can be shown [25] that the uncertainty on the reference parameter R is reduced by:

$$\Delta R_0^{'\,2} = \Delta R_0^2 \cdot \left(1 - r_{RE}^2\right) \tag{40}$$

If more than one experiment is available, the Eq. (40) can be generalized. In the case of two experiments, characterized by sensitivity matrices S_{E1} and S_{E2} the following expression [27] can be derived:

$$\Delta R_0^{'\,2} = S_R^{+} D' S_R = \Delta R_0^2 \left[1 - \frac{1}{1 - r_{12}^2}\left(r_{R1} - r_{R2}\right)^2 - \frac{2}{1 + r_{12}} r_{R1} r_{R2}\right] \tag{41}$$

where D' is the new covariance matrix and

$$r_{12} = \frac{\left(S_{E1}^{+} D S_{E2}\right)}{\left[\left(S_{E1}^{+} D S_{E1}\right)\left(S_{E2}^{+} D S_{E2}\right)\right]^{1/2}} \tag{42}$$

$$r_{R1} = \frac{\left(S_R^{+} D S_{E1}\right)}{\left[\left(S_R^{+} D S_R\right)\left(S_{E1}^{+} D S_{E1}\right)\right]^{1/2}} \tag{43}$$

$$r_{R2} = \frac{\left(S_R^{+} D S_{E2}\right)}{\left[\left(S_R^{+} D S_R\right)\left(S_{E2}^{+} D S_{E2}\right)\right]^{1/2}} \tag{44}$$

The approach outlined here can be used to plan optimized integral experiments to reduce uncertainties on a set of integral parameters of a reference system.

A successive step is the assessment of target accuracy requirements. To establish priorities and target accuracies on data uncertainty reduction, a formal approach can be adopted by defining target accuracy on design parameter and finding out required accuracy on data. In fact, the unknown uncertainty data requirements d_l can be obtained (e.g. for parameters l not correlated among themselves), by solving the following minimization problem:

$$\sum_l \lambda_l / d_l^2 = \min \qquad l = 1K\ L \tag{45}$$

(L: total number of parameters) with the following constraints:

$$\sum_l S_{nl}^2 d_l^2 < \left(R_n^T\right)^2 \qquad n = 1K\ N \tag{46}$$

(N: total number of integral design parameters) where S_{nl} are the sensitivity coefficients for the integral parameter R_n and R_n^T are the target accuracies on the N integral parameters. λ_l are "cost" parameters related to each σ_l and should give a relative figure of merit of the difficulty of improving that parameter (e.g., reducing uncertainties with an appropriate experiment).

All the formulations shown above can be calculated with specific modules of the ERANOS code system.

References

[1] G. Rimpault et al., "The ERANOS Code and Data System for Fast Reactor Neutronics Analyses", Proc. PHYSOR 2002 Conference, Seoul (Korea), October 2002. see also G. Palmiotti, R.F. Burstall, E. Kiefhaber, W. Gebhardt, J.M. Rieunier, "New Methods Developments and Rationalization of Tools for LMFBR Design in the Frame of the European Collaboration", FR'91 International Conference on Fast Reactors and Related Fuel Cycles, Kyoto, Japan, October 28 – November 1,1991.

[2] A. Weinberg, E. Wligner, "The Physical Theory of Neutron Chain Reactors". The University of Chicago Press (1958). See also H. Brooks "Perturbation Theory for Boltzmann Equation", KAPL-304 (1950).

[3] L.N. Usachev., Proc. Int. Conf. on Peaceful Uses of Nucl. Energy, Vol 5, 503, Geneva (1955).

[4] J. Lewins.,Nucl. Sci. Eng. 7, 268, (1960).

[5] J. Lewins, "Importance - The Adjoint Function", Pergamon Press, (1965).

[6] A. Gandini, "Study of the sensitivity of calculations for Fast Reactors to Uncertainties in Nuclear Data" ANL-6608 (1962).

[7] L. N. Usachev, Atomn. Energ. 15, 472, (1963).

[8] A. Gandini, J. Nucl. Energy 21, 755, (1967).

[9] G.P. Cecchini, M. Salvatores, Nucl. Sci. Eng. 46, 304, (1971).

[10] W. M. Stacey, Jr., "Variational Methods in Nuclear Reactor Physics", Academic Press, See also W.M. Stacey, Nucl. Sci Eng. 48, 444, (1972).

[11] The Oak Ridge group has written a comprehensive volume on the subject: "Sensitivity and Uncertainty Analysis of Reactor Performance Parameters" Advances in Nucl. Sci. and Technology Vol. 14 (1982).

[12] See e.g.: M. Mitani, Nucl. Sci. Eng. 51, 180 (1973).

[13] A. Gandini. Nucl. Sci. Eng. 77, 316 (1981).

[14] E. Greenspan - D. Gilai - E. M. Oblow., Nucl. Sci. Eng. 68, 1 (1978).

[15] D. G. CACUCI et al. Nucl. Sci. Eng. 75, 88 (1980).

[16] A. Gandini, Technical Report CNEN RT/FI (75) 4, Rome, Italy (1975), See also J.M. Kallfelz, G. Bruna, G. Palmiotti and M. Salvatores, "Burn-up Calculations with Time-Dependent Generalized Perturbation Theory", Nucl. Sci. Eng. 62, 304 (1977), A. Gandini, M. Salvatores, L. Tondinelli, Nucl. Sci. Eng. 62, 333 (1977), M.L. Williams, Nucl. Sci. Eng. 70, 20 (1979).

[17] G. Palmiotti, M. Salvatores, J. C. Estiot, and G. Granget, "Higher Order Effects in Time-Dependent Sensitivity Problems," Nuclear Science Engineering 84, 150 (1983).

[18] A. Gandini, G. Palmiotti, and M. Salvatores, "Equivalent Generalized Perturbation Theory (EGPT)," Ann. Nuclear Energy 13, 109 (1986).

[19] G. Palmiotti, P.J. Finck, I. Gomes, B. Micklich and M. Salvatores, "Uncertainty Assessment for Accelerator-Driven Systems", Global `99, International Conference on Future Nuclear Systems, August 29-September 3, 1999, Jackson, Wyoming, USA

[20] E.M. Oblow, Nucl. Sci. Eng 68, 322 (1978).

[21] C.V. Parts - P.J. Maudlin.,Nucl. Technology, 54, 38 (1981), See also D.G. Cacuci - C.F. Weber, Trans. Am. Nucl. Soc. 34, 312 (1980).
[22] A. Gandini, Trans. Am. Nucl. Soc. 53, 265 (1986).
[23] See e.g. article by A. Gandini in “Uncertainty Analysis”, Y. Ronen Editor, CRC Press 1988 and article by E. Greenspan in “ Advances in Nuclear Science and Technology”, Vol. 14, J. Lewins and A. Becker Editors, Plenum Publishing Corporation, 1982.
[24] G. Palmiotti, J.M. Rieunier, C. Gho, M. Salvatores, “BISTRO Optimized Two Dimensional Sn Transport Code”, Nucl. Sc. Eng. 104, 26 (1990).
[25] L.N. Usachev and Y. Bobkov, “Planning on Optimum Set of Microscopic Experiments and Evaluations to Obtain a Given Accuracy in Reactor Parameter Calculations”, INDC CCP-19U, IAEA Int. Nucl. Data Committee, 1972.
[26] G. Palmiotti and M. Salvatores, “Use of Integral Experiments in the Assessment of Large Liquid-Metal Fast Breeder Reactor Basic Design Parameters”. Nucl. Sci. Eng. 87, 333 (1984).
[27] A. Gandini, “Uncertainty Analysis and Experimental Data Transposition Methods in Uncertainty Analysis”, Y. Ronen Editor, CRC Press (1988).

Simultaneous nuclear data target accuracy study for innovative fast reactors

G. Aliberti[1)], G. Palmiotti[2)], M. Salvatores[1,2,3)]

1) Argonne National Laboratory, NE Division, Argonne, IL 60439 (USA)
2) Idaho National Laboratory, NSE Division, 2525 Fremont Ave. P.O. Box 1625, Idaho Falls, ID 83415-3855 (USA)
3) CEA-Cadarache, 13108 St-Paul-Lez-Durance, France
aliberti@anl.gov

Abstract: The present paper summarizes the major outcomes of a study conducted within a NEA WPEC initiative aiming to investigate data needs for future innovative nuclear systems, to quantify them and to propose a strategy to meet them

Introduction

Within the NEA WPEC Subgroup 26 an uncertainty assessment has been carried out [1] using covariance data recently processed by joint efforts of several US and European Labs. In general, the uncertainty analysis shows that, in particular in the case of the wide selection of fast reactor concepts considered, the present integral parameters uncertainties resulting from the assumed uncertainties on nuclear data are probably acceptable both in the early phases of design feasibility studies. However, in the successive phase of preliminary conceptual designs and in later design phases of selected reactor and fuel cycle concepts, there will be certainly the need for improved data and methods, in order to reduce margins, both for economical and safety reasons. It is then important to define as soon as possible priority issues, i.e. which are the nuclear data (isotope, reaction type, energy range) that need improvement, in order to quantify target accuracies and to select a strategy to meet the requirements needed (e.g. by some selected new differential measurements and by the use of integral experiments). In this contest one should account for the wide range of high accuracy integral experiments already performed and available in national or, better, international data basis, in order to indicate new integral experiments that will be needed to account for new requirements due to innovative design features, and to provide the necessary full integral data base to be used for validation of the design simulation tools.
In previous studies [2,3], a target accuracy assessment has been performed separately for selected Gen-IV type of systems. In the present study, a simultaneous target accuracy study has been performed over an ensemble of fast neutron systems, with different coolants (Na, gas, lead, lead bismuth eutectic), different fuel types (oxides, metals, carbides, nitrides) and different Pu/TRU compositions, in different core volumes. These systems (ABTR, SFR, EFR, GFR, LFR and ADS), have been defined in [2,4,5,6] and their characteristics are summarized in Table 1.

Table 1*. Features of the Investigated Systems*

System	Fuel	Coolant	TRU/(U+TRU)	MA[(a)]/(U+TRU)	Power (MWth)
ABTR	Metal	Na	0.162	~0	250
SFR	Metal	Na	0.605	0.106	840
EFR	MOX	Na	0.237	0.012	3600
GFR	Carbide	He	0.217	0.050	2400
LFR	Metal	Pb	0.233	0.024	900
ADS	Nitride	Pb-Bi	1.0	0.680	380

[(a)] Minor Actinides

Data target accuracies

To be consistent with the target accuracy study presented in [3], the guidelines that will be provided in the present paper for data improvements will refer to the analysis of the following parameters: multiplication factor, power peak, Doppler and coolant void reactivity coefficient, burnup Δk/k, nuclide density at end of cycle. Within the Subgroup 26, a preliminary list of design target accuracies for fast reactor systems (at first, independently of the coolant and

fuel type) has been established as presented in Table 2. These target accuracies reflect the perceived status of the art, even if they are not yet the result of a systematic analysis, which should necessarily involve industrial partners. The target accuracy requirements presented in Table 2 have also been extended to the ADS system.

Table 2. *Fast Burner Reactor and ADS Target Accuracies (1σ)*

Multiplication factor (BOL)	300 pcm	Reactivity coefficients (Coolant void and Doppler)	7%
Power peak (BOL)	2%	Major nuclide[(a)] density at end of irradiation cycle	2%
Burnup reactivity swing	300 pcm	Other nuclide density at end of irradiation cycle	10%

[(a)] U-235, U-238, Pu-238, Pu-239, Pu-240, Pu-241, Pu-242

Moreover, the same covariance data have been used as in [3]. These data have been produced by a major joint effort within Subgroup 26 of BNL, LANL, ORNL and NRG [7 to 16]

Theoretical approach and reference calculations

As already discussed in the introduction, in addition to the selected fast systems analyzed in [2,4], the ADS system investigated in [5,6] has been also considered.
Sensitivity and uncertainty coefficients are consistent with the results presented in [1,6] and calculated at ANL with the ERANOS code system [17].
As reminder, once the sensitivity coefficient matrix S_R for each integral parameter R and the covariance matrix D are available, the uncertainty on the integral parameter can be evaluated as: $\Delta R_0^2 = S_R^+ D S_R$.
A successive step is the assessment of target accuracy requirements. To establish priorities and target accuracies on data uncertainty reduction, a formal approach can be adopted by defining target accuracy on design parameters and finding out the required accuracy on the nuclear data σ_i. In fact, the unknown uncertainty data requirements d_i can be obtained (e.g. for parameters i not correlated among themselves), by solving the minimization problem:
$\sum_i \lambda_i / d_i^2 = \min$, (i = 1…I, I: total number of parameters), with the following constraints:

$\sum_i S_{R_n i}^2 d_i^2 < \left(R_n^T\right)^2$ (n = 1…N, N is the total number of integral design parameters),

where $S_{R_n i}$ are the sensitivity coefficients for the integral parameter R_n, and R_n^T are the target accuracies on the N integral parameters; λ_i are "cost" parameters related to each σ_i and should give a relative figure of merit of the difficulty of improving that parameter (e.g., reducing uncertainties with an appropriate experiment).
The cross-sections uncertainties required for satisfying the target accuracies have been calculated by a minimization process that satisfies the nonlinear constraints with bounded parameters. The SNOPT code [18] has been used for this purpose. To avoid the introduction of meaningless parameters, as unknown "d" parameters (i.e., as cross-sections for which target accuracies are required), only those which globally account at least for 98% of the overall uncertainty for each integral parameter have been chosen. Concerning the cost parameters, as already done in previous work [2,3], a constant value of one for all λ_i is initially taken. Additionally, at the first stage it was decided to not account for correlations between data. This assumption is of course rather arbitrary, but it is consistent with standard requirements for reactor designs in early phases of development.

Uncertainty results

The uncertainties on the major integral parameters due to diagonal values of the BOLNA covariance matrix are provided in Table 3 (see values only associated to the label "With initial uncertainties"). For the ADS, the Doppler reactivity coefficient has not been considered due the its small calculated value. In Table 3, in italic font are the initial parameter uncertainties out of the required accuracies summarized in Table 2. In general, it can be observed that the power peak, the Doppler and void reactivity coefficients, meet the accuracy requirements in all cases with the only exception of the ADS for the three parameters and of the SFR for the void coefficient. The worst situation is represented by the ADS, where all integral parameter uncertainties (with the only exception of the nuclide densities at end of irradiation, due to the

short burn up) do not meet the accuracy requirements. As for the nuclei densities at the end of irradiation, most of the target accuracies are already met.

Table 3. *Integral Parameter Uncertainties (%) with Initial and Required Cross-Section Uncertainties*

		ABTR	SFR	EFR	GFR	LFR	ADS
k_{eff} BOC [pcm]	**With initial uncertainties**	*643*	*1108*	*877*	*1270*	*890*	*1882*
	With required uncertainties	291	348	322	326	320	279
Power Peak BOC	**With initial uncertainties**	0.3	0.3	0.8	1.2	0.4	*14.2*
	With required uncertainties	0.2	0.1	0.3	0.3	0.2	2.2
Doppler BOC	**With initial uncertainties**	2.9	3.6	2.5	3.6	2.8	-
	With required uncertainties	1.4	1.7	1.1	1.4	1.4	-
Void	**With initial uncertainties**	5.1	*15.7*	6.7	5.5	5.0	*13.1*
	With required uncertainties	2.8	6.0	3.3	3.1	1.9	3.5
Burnup [pcm]	**With initial uncertainties**	-37	-152	*-584*	254	-128	*-603*
	With required uncertainties	-14	-45	-201	92	-45	-207

Target accuracy results

Tables 4 and 5 show the relevant target accuracy results for the ensemble of only Na-cooled and all fast systems respectively. The required nuclear data accuracies, obtained from the optimization procedures, are such that the design target accuracies are fulfilled in most cases. Besides the initial integral parameter uncertainties, Table 3 shows the calculated residual uncertainties on the major integral parameters when one uses the required cross-section uncertainties, as obtained with the minimization procedure applied to all fast systems. Note that the required parameter accuracies are not exactly met because of the cross-sections not accounted in the minimization procedures which give as consequence a residual uncertainty going to be added to the specified accuracy.

In the two cases (i.e. only Na-cooled or all fast reactor types), the major requirements are related to the same type of data (Pu-241 fission, U-238 inelastic and capture, Pu-240 fission) and to approximately the same level of accuracy. Specific requirements can show up in the two cases according to the cooling type or to the specific structural materials. Minor actinide data needs become more evident if the ADS case (i.e. with MA dominated fuel) is considered. There are however some general requirements, whatever is the type of system, as e.g. for Cm-244 and Am-242m fission data.

Table 4. *ABTR, SFR, EFR: Uncertainty Reduction Requirements to Meet Integral Parameter Target Accuracies*

Isotope Cross-Section	Energy Range	Uncertainty (%)		Isotope Cross-Section	Energy Range	Uncertainty (%)		Isotope Cross-Section	Energy Range	Uncertainty (%)	
		Initial	Target			Initial	Target			Initial	Target
U238 σ_{inel}	19.6 - 6.07 MeV	29.3	20.1	**Fe56 σ_{inel}**	19.6 - 6.07 MeV	13.0	8.9	**Am242m σ_{fiss}**	6.07 - 2.23 MeV	23.4	8.0
	6.07 - 2.23 MeV	19.8	4.6		6.07 - 2.23 MeV	7.2	4.1		2.23 - 1.35 MeV	19.7	8.2
	2.23 - 1.35 MeV	20.6	4.5		2.23 - 1.35 MeV	25.4	3.3		1.35 - 0.498 MeV	16.5	4.3
	1.35 - 0.498 MeV	11.6	5.5		1.35 - 0.498 MeV	16.1	3.2		498 - 183 keV	16.6	3.1
Pu241 σ_{fiss}	6.07 - 2.23 MeV	14.2	6.5	**Pu239 σ_{capt}**	1.35 - 0.498 MeV	18.2	10.1		183 - 67.4 keV	16.6	3.1
	2.23 - 1.35 MeV	21.3	5.8		498 - 183 keV	11.6	6.5		67.4 - 24.8 keV	14.4	4.1
	1.35 - 0.498 MeV	16.6	3.4		183 - 67.4 keV	9.0	5.6		24.8 - 9.12 keV	11.8	4.3
	498 - 183 keV	13.5	2.6		67.4 - 24.8 keV	10.1	6.3		9.12 - 2.03 keV	12.4	6.5
	183 - 67.4 keV	19.9	2.6		24.8 - 9.12 keV	7.4	5.5		2.03 - 0.454 keV	12.2	5.2
	67.4 - 24.8 keV	8.7	3.3		9.12 - 2.03 keV	15.5	6.7	**Pu240 σ_{fiss}**	19.6 - 6.07 MeV	9.6	8.6
	24.8 - 9.12 keV	11.3	3.5	**O16 σ_{capt}**	19.6 - 6.07 MeV	100.0	62.3		6.07 - 2.23 MeV	4.8	2.8
	9.12 - 2.03 keV	10.4	5.4		6.07 - 2.23 MeV	100.0	39.5		2.23 - 1.35 MeV	5.7	2.6
	2.03 - 0.454 keV	12.7	4.4	**Na23 σ_{inel}**	2.23 - 1.35 MeV	12.6	9.3		1.35 - 0.498 MeV	5.8	1.8
	454 - 22.6 eV	19.4	8.6		1.35 - 0.498 MeV	28.0	4.0		498 - 183 keV	3.9	3.9
U238 σ_{capt}	24.8 - 9.12 keV	9.4	3.8	**Cm244 σ_{fiss}**	6.07 - 2.23 MeV	31.3	8.2		2.03 - 0.454 keV	21.6	12.4
					2.23 - 1.35 MeV	43.8	8.2				
					1.35 - 0.498 MeV	50.0	5.1				
					498 - 183 keV	36.5	12.1				

Table 5. *ABTR, SFR, EFR, GFR, LFR, ADMAB: Uncertainty Reduction Requirements to Meet Integral Parameter Target Accuracies*

Isotope Cross-Section	Energy Range	Uncertainty (%)	
		Initial	Target
U238 σ_{inel}	19.6 - 6.07 MeV	29.3	9.0
	6.07 - 2.23 MeV	19.8	2.0
	2.23 - 1.35 MeV	20.6	2.1
	1.35 - 0.498 MeV	11.6	2.3
	498 - 183 keV	4.2	3.8
	183 - 67.4 keV	11.0	4.2
Pu241 σ_{fiss}	6.07 - 2.23 MeV	14.2	5.0
	2.23 - 1.35 MeV	21.3	3.9
	1.35 - 0.498 MeV	16.6	2.1
	498 - 183 keV	13.5	1.7
	183 - 67.4 keV	19.9	1.7
	67.4 - 24.8 keV	8.7	1.9
	24.8 - 9.12 keV	11.3	2.0
	9.12 - 2.03 keV	10.4	2.1
	2.03 - 0.454 keV	12.7	2.7
	454 - 22.6 eV	19.4	5.4
Cm244 σ_{fiss}	6.07 - 2.23 MeV	31.3	3.0
	2.23 - 1.35 MeV	43.8	2.6
	1.35 - 0.498 MeV	50.0	1.5
	498 - 183 keV	36.5	4.0
	183 - 67.4 keV	47.6	7.3
U238 σ_{capt}	24.8 - 9.12 keV	9.4	1.8
	9.12 - 2.03 keV	3.1	1.8
Fe56 σ_{inel}	6.07 - 2.23 MeV	7.2	2.6
	2.23 - 1.35 MeV	25.4	1.7
	1.35 - 0.498 MeV	16.1	1.5

Isotope Cross-Section	Energy Range	Uncertainty (%)	
		Initial	Target
B10 σ_{capt}	498 - 183 keV	15.0	2.9
	183 - 67.4 keV	10.0	2.7
	67.4 - 24.8 keV	10.0	3.3
	24.8 - 9.12 keV	8.0	3.9
	9.12 - 2.03 keV	8.0	6.0
Pu239 σ_{capt}	1.35 - 0.498 MeV	18.2	6.6
	498 - 183 keV	11.6	4.4
	183 - 67.4 keV	9.0	4.0
	67.4 - 24.8 keV	10.1	4.2
	24.8 - 9.12 keV	7.4	3.8
	9.12 - 2.03 keV	15.5	3.2
O16 σ_{capt}	19.6 - 6.07 MeV	100.0	37.9
	6.07 - 2.23 MeV	100.0	37.9
Am243 σ_{inel}	6.07 - 2.23 MeV	17.9	4.9
	2.23 - 1.35 MeV	35.3	3.9
	1.35 - 0.498 MeV	42.2	2.3
	498 - 183 keV	41.0	3.7
	183 - 67.4 keV	79.5	3.7
	67.4 - 24.8 keV	80.8	12.4
Am242m σ_{fiss}	1.35 - 0.498 MeV	23.4	21.4
	498 - 183 keV	16.5	6.3
	183 - 67.4 keV	16.6	4.7
	67.4 - 24.8 keV	16.6	4.8
	24.8 - 9.12 keV	14.4	5.6
	2.04 - 0.454 keV	11.8	5.9
Na23 σ_{inel}	1.35 - 0.498 MeV	28.0	10.5

Isotope Cross-Section	Energy Range	Uncertainty (%)	
		Initial	Target
Pu240 σ_{fiss}	6.07 - 2.23 MeV	4.8	2.9
	2.23 - 1.35 MeV	5.7	2.6
	1.35 - 0.498 MeV	5.8	1.6
	498 - 183 keV	3.9	3.7
	2.03 - 0.454 keV	21.6	11.8
Si28 σ_{capt}	19.6 - 6.07 MeV	52.9	7.2
Si28 σ_{inel}	6.07 - 2.23 MeV	13.5	3.9
	2.23 - 1.35 MeV	50.0	7.4
Pb206 σ_{inel}	6.07 - 2.23 MeV	5.5	4.2
	2.23 - 1.35 MeV	14.2	4.0
	1.35 - 0.498 MeV	9.2	4.7
Pb207 σ_{inel}	6.07 - 2.23 MeV	5.0	4.9
	2.23 - 1.35 MeV	13.8	6.0
	1.35 - 0.498 MeV	11.3	3.6
Pb σ_{inel}	6.07 - 2.23 MeV	5.4	3.0
Am243 σ_{fiss}	6.07 - 2.23 MeV	11.0	2.3
	2.23 - 1.35 MeV	6.0	1.9
	1.35 - 0.498 MeV	9.2	1.7
Bi209 σ_{inel}	2.23 - 1.35 MeV	34.1	2.8
	1.35 - 0.498 MeV	41.8	4.3
N15 σ_{el}	2.23 - 1.35 MeV	5.0	3.1
	1.35 - 0.498 MeV	5.0	1.2
	498 - 183 keV	5.0	1.9
	183 - 67.4 keV	5.0	2.3
Zr90 σ_{inel}	6.07 - 2.23 MeV	18.0	3.3

These results should be used with precaution. They indicate trends and general priority needs. In fact, these quantitative values have been obtained considering only diagonal (variance) uncertainty values, that represent an underestimation of the real uncertainty. Moreover, and certainly more important, the accuracy requirements and priorities are strongly dependent on the assumed initial uncertainty variance-covariance data, and in particular on the very low initial uncertainty values on the fission cross-section of Pu-239. This work however provides a clear indication for future work: a) Improvement of the present covariance data: b) Selection of a few priority differential measurements, where the expected experimental uncertainties can match the data required uncertainty; c) Definition of a strategy of combined use of high quality integral experiments, sophisticated analysis tools, scientifically based covariance data within a statistical data adjustment, in order to fully validate calculation tools for the design of future innovative systems. This approach is discussed in a companion paper at this workshop [19].

Acknowledgments

Argonne National Laboratory's work was supported by the U.S. Department of Energy, Office of Nuclear Energy, under contract DE-AC02-06CH11357.

References

[1] M. Salvatores et al., "Nuclear Data Needs for Advanced Reactor Systems. A NEA Nuclear Science Committee Initiative," Proc. Int. Conf. ND-2007, Nice, France (April 2007).

[2] G. Aliberti et al., "Nuclear Data Sensitivity, Uncertainty and Target Accuracy Assessment for Future Nuclear Systems", Annals of Nucl. Energy, 33, 700-733 (2006).

[3] M. Salvatores, G. Aliberti and G. Palmiotti, "The Role of Differential and Integral Experiments to Meet Requirements for Improved Nuclear Data", ND2007, Nice (France), April 2007.

[4] Y. I. Chang, P. J. Finck, C. Grandy, "Advanced Burner Reactor Preconceptual Design Report", ANL-ABR-1 (Argonne National Laboratory, September 2006).

[5] G. Aliberti et al., “Impact of Nuclear Data Uncertainties on Transmutation of Actinides in Accelerator-Driven Assemblies,” Nucl. Sci. Eng., 46, 13-50 (2004).
[6] G. Aliberti, G. Palmiotti, M. Salvatores, “New Covariance Data and Their Impact on ADS Designs,” in Proc. of AccApp Conference, Pocatello, ID, USA, (July-August 2007).
[7] D. Rochman et al., “Preliminary Cross-Section Covariances for WPEC Subgroup 26,” Tech. Rep. BNL-77407-2007-IR, Brookhaven National Laboratory, (2007).
[8] D. Rochman et al., “Preliminary nu-bar Covariances for 238; 242Pu and 242; 243; 244; 245Cm,” Tech. Rep. BNL-77407-2007-IR-Suppl.1, Brookhaven National Laboratory, (2007).
[9] M. Chadwick et al., “ENDF/B-VII.0: Next Generation Evaluated Nuclear Data Library for Nuclear Science and Technology,” Nuclear Data Sheets, 107, pp. 2931 (December 2006).
[10] S. F. Mughabghab, “Atlas of Neutron Resonances: Resonance Parameters and Thermal Cross-Sections,” Amsterdam: Elsevier, (2006).
[11] M. Herman et al., “EMPIRE Nuclear Reaction Model Code, Version 2.19 (Lodi),” www.nndc.bnl.gov/empire219/ (March 2005).
[12] T. Kawano, Tech. Rep. JAERI-Research, 99-009, JAERI, (1999).
[13] N. M. Larson, “Updated Users’ Guide for SAMMY: Multilevel R-Matrix Fits to Neutron Data Using Bayes’ Equations,” ORNL/TM-9179/R7 (2007).
[14] L. Leal, H. Derrien, N. Larson, G. Arbanas, and Royce Sayer, “ORNL Methodology for Covariance Generation for Sensitivity/Uncertainty Analysis,” in Proc. of International Conference on Nuclear Criticality Safety, St. Petersburg, Russia, (May 2007).
[15] J. Koning, “Generating Covariance Data with Nuclear Models,” in Proceedings of the International Workshop on Nuclear data Needs for Generation IV Nuclear energy systems, Antwerpen, (April 5-7, 2005), ed. P. Rullhusen, World Scientific (2006), p. 153.
[16] J. Koning, S. Hilaire and M. C. Duijvestijn, “TALYS: Comprehensive Nuclear Reaction Modeling,” in Proc. of Int. Conf. on Nuclear Data for Science and Technology - ND2004, AIP vol. 769, Santa Fe, NM, USA, (Sep. 26 - Oct. 1, 2004), p. 1154, (2005).
[17] G. Rimpault, et al., “The ERANOS Code and Data System for Fast Reactor Neutronic Analyses,” in Proc. of PHYSOR 2002 Conference, Seoul, South Korea, (October 2002).
[18] P.E. Gill et al., “SNOPT: An SQP algorithm for Large-Scale constrained programming”, Technical Report SOL 97-3, Systems Optimization Laboratory, Department of Operations Research, Stanford University, Stanford, California 94305-4022, 1997.
[19] G. Palmiotti, M. Salvatores, G. Aliberti “Validation of simulation codes for future systems: motivations, approach and the role of nuclear data”, this workshop.

Sodium cross sections and covariance data for the assessment of SFR neutronic characteristics

G. Rimpault, W. Khamakhem, R. Jacqmin, J.C. Sublet, J. Tommasi

Commissariat à l'Energie Atomique (CEA), Cadarache Centre, 13108 Saint-Paul-lez-Durance Cedex, France
gerald.rimpault@cea.fr

Abstract: The sodium evaluated data in the recent ENDF/B-VII.0, JENDL3.3 and JEFF3.1 files exhibit significant differences. These evaluations are based on a rather limited number of differential measurements, complemented in some cases by theoretical information coming from optical model codes, and by integral experiments. In this paper, we review these evaluations in relation with previous file versions. The impact of the data changes on Sodium Fast Reactor (SFR) void coefficients is discussed. Also, recent covariance data for sodium, compiled for the OECD/WPEC Subgroup 26 by Brookhaven National Laboratory, are discussed in relationship with the SFR safety margins. Finally, a request for improved sodium cross-section and covariance data, compatible with the SFR design expectations, is presented for consideration by the OECD High Priority Request List (HPRL) review group.

Introduction

One of the driving forces for improving nuclear data is their impact on reactor design parameters, as system performance, and sometimes even feasibility issues, can be dependent on such data. Sodium is a rather transparent material; hence it has little impact on most of the SFR characteristics, *except* the sodium void coefficient and neutron attenuation in shields.
The sodium void coefficient is positive in standard designs, and its reduction is part of the improved safety objectives assigned to future reactors [1]. Neutron shields tend to be more compact in innovative designs for economical reasons and hence, transmission through sodium has to be well predicted, since it affects the level of activation in heat exchangers and vessel damage. An improved prediction of these two characteristics is therefore required for innovative SFRs, and this is very much linked to the quality of the sodium cross sections and their associated covariances.
In Section 1, we review the latest Na-23 evaluations and comment on the differences between the files. Section 2 describes the impact of these data on the SFR design characteristics. The paper concludes on the needs for improved sodium data.

Review of sodium evaluations

Comparisons of current evaluations

The main sets of neutron transmission and inelastic scattering measurements on Na-23 are:
- S. Cierjacks' transmission data (Karlsruhe, 1970) [2],
- D. Larson's transmission data (ORNL, 1976) [3], which are somewhat higher than Cierjacks',
- H. Märten's high-resolution inelastic scattering measurements, from 450 keV to 2 MeV (IRMM Geel, 1994) [4].

The ENDF/B-VII.0 evaluation is essentially identical to the ENDF/B-V evaluation made by D. Larson (1977). It may be noted that the covariance information which was in ENDF/B-VI.8 was not carried forward into ENDF/B-VII.0.
The JENDL-3.3 file contains a recent evaluation made by K. Shibata (2000), using nuclear model calculations [5]. The total cross section is unchanged with respect to JENDL-3.2. The latter was based on an earlier Japanese evaluation of Cierjacks and Larson's data (1987). However, the inelastic scattering cross section is revised in the range from threshold to 1st excited level (~ 400 keV to 2.15 MeV), using Märten's measurements and a scaling factor of 1.25 "derived from a benchmark test". Inelastic data are kept identical to JENDL-3.2 between 2.15 and 4.0 MeV. The elastic scattering cross section is taken as the difference between the total and the non-elastic reactions. The JENDL-3.3 file contains covariance data, which are directly taken from JENDL-3.2.

The JEFF-3.1 sodium evaluation is based on JEF-2.2, which was itself adopted from JENDL-3.2. The JEFF-3.1 data are identical to JEF-2.2 below 350 keV, but different above. The inelastic scattering and total cross sections are derived from Kopecky's simultaneous analysis [6] of Larson's and Märten's measurements, between 450 MeV and 2 MeV. Above 2 MeV, the JEF-2.2 data have been simply scaled: the inelastic scattering cross section is multiplied by a factor 0.69, while the elastic cross section is scaled by a factor 1.32. These values were taken so as to match Kopecky's data under 2 MeV and to be consistent with integral validation tests (see below). We note a slight, non-physical drop in the total cross section (5%) at 350 keV.
The main differences between the files are:

- Below 350 keV: The JEFF-3.1 and JENDL-3.3 evaluations are identical, while the ENDF/B-VII.0 total cross section is higher (4%) at low energy in the smooth part but the 2.8 keV resonance is narrower;
- Above 350 keV: the ENDF/B-VII.0 and JENDL-3.3 total cross section files are very similar. In the 500 keV to 2 MeV region, the JEFF-3.1 evaluation is higher than the other two evaluations by 8-10%, and also higher than Larson's data. Yet, JEFF-3.1 matches the Larson's measurements above 2.1 MeV (see Figures 1 and 2);
- The JEFF-3.1 and JENDL-3.3 total inelastic scattering cross sections are similar functions of energy between 500 keV and ~ 2.1 MeV, but the JEFF-3.1 value is 20% lower (see Figure 3). This lower value tends to be supported by Trykov and Sinin's independent work [10] for BROND-3, although no file is available for comparisons. The older Na23 evaluation used in ENDF/B-VII.0 has poorer resolution. Above 2.1 MeV, it is interesting to note that the scaling factors independently applied in JENDL-3.3 and JEFF-3.1 lead to very different inelastic cross sections, differing by more than 30%.

The integral trends that led from JEF-2.2 to JEFF-3 included the analysis of a limited number of sodium void experiments in two different fast reactor configurations. These experiments consisted in reactivity measurements of voided zones located in the central part of the core leading to information to the only non-leakage component of the sodium void. The conclusion of this work was that the JEF-2.2 sodium inelastic scattering cross section had to be decreased in the MeV range, while the elastic scattering cross section had to be increased by about the same magnitude [8-9]. This led to the JEFF-3.0 (= JEFF-3.1) file.

Uncertainties in sodium evaluations

The discrepancies between the various files in the 500 keV to 5 MeV range are substantially larger than the *a priori* 1-σ uncertainties quoted in the JENDL-3.3 file (~ 2% in both the total and inelastic scattering cross sections), suggesting that the latter are underestimated. On the other hand, these discrepancies are consistent with the uncertainties provided in the ENDF/B-VI.8 file: ~ 6% and 20% around 1 MeV, for the total and inelastic cross sections, respectively.
It is interesting to compare these values with covariance files recently produced through an international collaboration of Sub Group 26 of the OECD/WPEC [11]. These files (also known as BOLNA) consist of a preliminary set of group covariances for ENDF/B-VII evaluations, although some of the covariance information used is directly taken from JENDL-3.3. Values have been produced for inelastic, elastic, capture, fission and (n,xn) reactions, and ν. These group covariances have been generated for assessing the impact of nuclear data uncertainties on Gen-IV reactor characteristics.
As the BOLNA data are preliminary and still incomplete, they should be used with caution. In particular, no value is given for the total cross section. Since this value is generally measured while the elastic cross section is deduced from it and from the other reactions, the covariance data should reflect that. It is not the case in BOLNA, and no cross correlation exists between values from different reactions. In the case of sodium, since inelastic and elastic cross sections are the dominant partial cross sections, negative correlations should exist between these two reactions down to the inelastic threshold.
Tables 1, 2 and 3 compare different evaluations of the Na-23 total, elastic, and inelastic cross sections, respectively. The tables actually show differences with respect to JEF-2.2. Simple average values are shown, over a 15-group structure routinely used for sensitivity studies.

Tables 1 to 3 provide a quantitative summary of the discrepancies shown in Figures 1 to 3. They suggest that the BOLNA uncertainties are a bit too low, in view of the dispersion between the evaluated files.

Table 1. *Na-23 total cross section compared to JEF-2.2*

Upper Energy (MeV)	JEFF-3.1	ENDF/B-VII	JENDL-3.3	BOLNA 1-σ Uncertainties
1.96E+01	0.4%	2.9%	2.8%	N/A
6.12E+00	3.8%	5.5%	5.2%	N/A
2.23E+00	16.0%	2.8%	2.8%	N/A
1.35E+00	8.6%	1.4%	1.4%	N/A
4.98E-01	-0.6%	-0.7%	0.6%	N/A
1.83E-01	0.0%	-0.4%	0.0%	N/A
6.74E-02	-0.1%	0.0%	-0.1%	N/A
2.48E-02	-0.3%	-1.5%	-0.3%	N/A
9.12E-03	0.0%	-5.8%	0.0%	N/A
2.03E-03	0.1%	-9.9%	0.0%	N/A
4.54E-04	0.0%	1.0%	0.0%	N/A
2.25E-04	0.0%	2.8%	0.0%	N/A
4.08E-05	0.0%	3.5%	0.0%	N/A
5.62E-06	0.0%	5.0%	0.0%	N/A
1.12E-06	0.8%	7.8%	1.0%	N/A

Table 2. *Na-23 elastic cross section compared to JEF-2.2*

Upper Energy (MeV)	JEFF-3.1	ENDF/B-VII	JENDL-3.3	BOLNA1-σ Uncertainties
1.96E+01	26.7%	-2.7%	0.6%	1.8%
6.12E+00	26.8%	1.7%	5.4%	4.6%
2.23E+00	29.7%	7.6%	7.0%	3.7%
1.35E+00	11.4%	3.0%	1.5%	3.0%
4.98E-01	-0.5%	-0.6%	0.7%	3.3%
1.83E-01	0.0%	-0.4%	0.0%	3.3%
6.74E-02	-0.1%	0.0%	-0.1%	2.4%
2.48E-02	-0.3%	-1.5%	-0.3%	2.9%
9.12E-03	0.0%	-5.8%	0.0%	3.2%
2.03E-03	0.1%	-10.0%	0.0%	4.9%
4.54E-04	0.0%	1.0%	0.0%	4.8%
2.25E-04	0.0%	2.8%	0.0%	4.7%
4.08E-05	0.0%	3.6%	0.0%	4.7%
5.62E-06	0.0%	5.1%	0.0%	4.7%
1.12E-06	0.9%	8.5%	1.1%	4.6%

Table 3. *Na-23 inelastic cross section compared to JEF-2.2*

Upper Energy (MeV)	JEFF-3.1	ENDF/B-VII	JENDL-3.3	BOLNA1-σ Uncertainties
1.96E+01	-25.8%	4.2%	6.6%	18.8%
6.12E+00	-31.0%	11.2%	5.0%	8.9%
2.23E+00	-32.2%	-14.1%	-11.9%	12.6%
1.35E+00	-19.6%	-15.3%	0.5%	28.0%
4.98E-01				

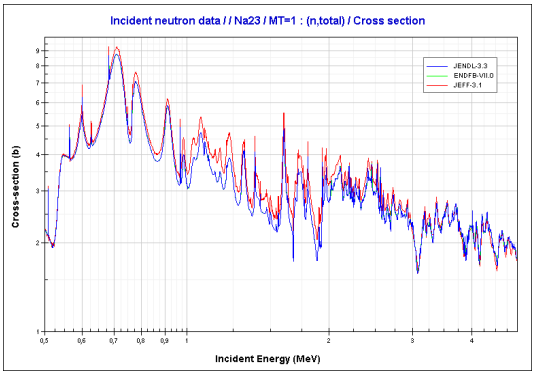

Figure 1. *The sodium total cross section between 500 keV and 5 MeV*

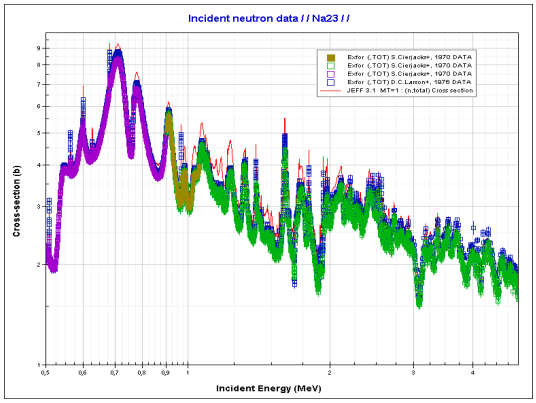

Figure 2. *The JEFF-3.1 total cross section and measurements between 500 keV and 5 MeV*

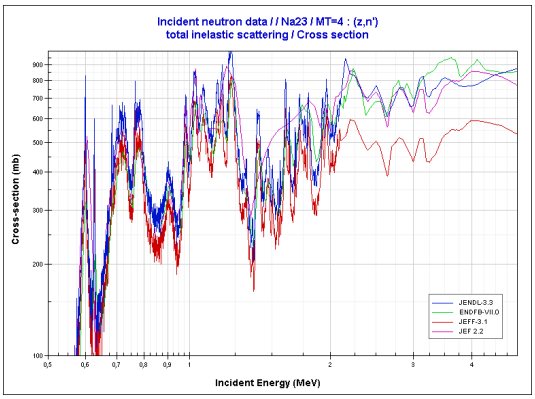

Figure 3. *The sodium total inelastic cross section between 500 keV and 5 MeV*

From these comparisons, we conclude that significant differences exist between the latest evaluated files. These differences are mainly the consequence of changes made in the JEFF and JENDL files to reflect average trends derived from some fast integral experiments. As the benchmarking trends were not all consistent between each other, and as *a priori* cross correlations between reactions were (and are still) missing, the net result is a rather large dispersion in the 500 keV to 6 MeV range. These differences are larger than the uncertainties of the BOLNA files. This situation calls for a revision of the files, together with a consistent re-analysis of some benchmarks.

Impact of sodium nuclear data on SFR characteristics

The SFRs currently under study differ from past concepts as design criteria are now those of Gen-IV reactors. The main expected SFR improvements are in the area of plant safety behaviour and fuel economy, but achieving the other fundamental criteria of Gen-IV systems, such as the ability to minimize waste production, get the maximum energy from the fuel and improve the proliferation resistance, are also considered.
These criteria, in a first conceptual phase, translate into a search for breakeven cores (i.e., zero net breeding gain) and enhanced safety features. An improved safety for a sodium cooled reactor requires revisiting many aspects of the design and is a rather lengthy process. As a first step, studies have focussed on the reduction of the sodium voiding reactivity effect, together with an increase in the Doppler Effect. This is essential to achieve a satisfactory transient behaviour, as well as to reduce the risk of getting into a generalized core fusion.
In the following, the main neutronic characteristics of SFR cores are presented, together with their calculated uncertainties as inferred from the BOLNA covariances. These values are compared to target accuracies. Finally, different sodium evaluations are tested and the differences in the results are compared.

SFR and EFR-like core characteristics

In design studies, it is customary to distinguish two categories of core concepts, depending on the required Research & Development efforts:

- Concepts called “innovative”, based on variations around established technologies, such as oxide fuel pins inserted in a hexagonal wrapper.
- Concepts called “highly innovative”, based on more radical changes, such as the use of dense carbide fuel, and very innovative fuel forms and sub-assembly geometries.

These concepts have been compared to a European Fast Reactor (EFR-like) type design.

Once defined, the core designs have to be checked for their viability. This typically includes calculating the following neutronic characteristics at Beginning of Life (BOL) and End of Life (EOL): sodium void worth, $\Delta\rho_{\text{Void Na}}$, Doppler effect, $\Delta\rho_{\text{Dop (T° Nom -> Fusion)}}$, and control rod worth, $\Delta\rho_{\text{2 CR rings}}$.
Table 4 shows that the three cores exhibit significantly different neutron characteristics, reflecting differences in neutron spectra. In particular, the SFR sodium void is approximately 40% lower than the EFR-like sodium void, while the Doppler Effect is 70% larger.

Table 4. *Sodium void, Doppler effect and control rod worth at BOL for SFR oxide, SFR carbide and EFR-like*

Values in $	SFR Carbide	SFR Oxide	EFR-like
$\Delta\rho_{\text{Void Na}}$	3.3	2.9	4.7
$\Delta\rho_{\text{Dop (T° Nom -> Fusion)}}$	-2.8	-1.9	-1.1
$\Delta\rho_{\text{2 CR rings}}$	-32.7	-17.1	-25.4

Impact of sodium uncertainties on reactor core characteristics
Values of uncertainties at BOL for the SFR oxide, SFR carbide and EFR-like main neutronic characteristics have been calculated using the BOLNA covariances. The results are presented in Table 5. The last column in the table shows the target uncertainties for the Gen-IV feasibility phase.

Table 5. *BOL uncertainties (% at 1-σ) for SFR oxide, SFR carbide and EFR-like reactor main neutronic characteristics, as computed from the BOLNA covariances*

	SFR Carbide	SFR Oxide	EFR-like	Target Uncertainties
k_{eff}	± 2.16	± 1.80	± 1.46	± 0.30
$\Delta\rho_{\text{Void Na}}$	± 11.8	± 12.4	± 8.0	± 7.0
$\Delta\rho_{\text{Dop (T° Nom -> Fusion)}}$	± 6.0	± 5.1	± 4.7	± 7.0
$\Delta\rho_{\text{2 CR rings}}$	± 4.7	± 2.9	± 3.6	± 4.0

Uncertainties in k_{eff} due to nuclear data are significantly larger than the corresponding target uncertainty.
Regarding the Doppler effect, uncertainties are within the required bound. However, it should be mentioned that the sensitivity calculation in this case does not take into account the resonance uncertainties. Studies are underway within WPEC/SG26 group to evaluate how much this might account for.
For control rod worths, the situation appears to be satisfactory for the EFR-like and the SFR Oxide, although the situation of the SFR Oxide would have to be checked once the exact number and position of the control elements are known.
Finally, for the sodium void worth, while the computed uncertainties for the EFR-like reactor are almost acceptable, the values are much larger for the SFR cores, exceeding the target uncertainties. This is due to the larger spectrum change occurring in these cores when sodium is removed. The smaller amplitude of the void effect comes from the smaller Na volume fraction.
In Table 6, the contribution of the sodium cross section variances (BOLNA values) to the uncertainty in the void effect is shown.

Table 6. *Contribution of the sodium cross section uncertainties (BOLNA) to the BOL uncertainties in the SFR oxide, SFR carbide and EFR-like reactor sodium void*

	SFR Carbide	SFR Oxide	EFR-like	Target Uncertainties
Total uncertainty (%)	± 11.8	± 12.4	± 8.0	± 7.0
Na contribution (%)	± 7.0	± 7.3	± 5.5	

Table 6 shows that the contribution from the sodium data is important with respect to the total uncertainty. The other contribution comes from nuclides (other than Na) which affect the neutron importance shape as a function of energy. This contribution depends mainly on the ratio of neutron production to neutron capture. Variations or errors in the major nuclide concentrations or cross section shape may thus lead to large variations in the Na void worth.

Impact of different evaluated files on reactor core characteristics

The contribution arising from the importance shape may be reduced by using improved actinide cross sections, such as those of the ERALIB1 adjusted library [8, 12].

In order to appreciate this effect, the sodium void worth was calculated with the JEF-2.2, ERALIB1, and JEFF-3.1 libraries, and different sodium files. The results are presented in Tables 7 and 8. The two components of the sodium void worth are indicated separately in the tables.

Table 7. *SFR oxide Na void effect with different data sets*

SFR oxide, 0 EFPD	**JEF-2.2**	**ERALIB1**	**JEFF-3.1**	**ERALIB1 + Na23 JEFF-3.1**	**ERALIB1 + Na23 ENDF/B-VII.0**
$\Delta\rho_{Void}$ (pcm)	1406	1207	1252	1234	1359
Non-leakage Term (pcm)	2712	2405	2617	2563	2618
Leakage Term (pcm)	-1306	-1198	-1366	-1329	-1259

Table 8. *EFR-like reactor Na void effect with different data sets*

EFR-like, 0 EFPD	**JEF-2.2**	**ERALIB1**	**JEFF-3.1**	**ERALIB1 + Na23 JEFF-3.1**	**ERALIB1 + Na23 ENDF/B-VII.0**
$\Delta\rho_{Void}$ (pcm)	1955	1729	1839	1804	1898
Non-LeakageTerm (pcm)	2837	2620	2866	2805	2835
Leakage Term (pcm)	-882	-891	-1027	-1001	-938

For the SFR (Table 7), the use of JEF-2.2 yields the largest sodium void worth. ERALIB1 and JEFF-3.1 give similar results, but for different reasons as they are compensating effects between the leakage and non-leakage terms.

For the EFR-like (Table 8), the use of JEF-2.2 still yields the largest sodium void worth. However, ERALIB1 and JEFF-3.1 no longer lead to similar results, as the leakage and non-leakage components do not compensate as much. JEFF3.1 yields a sodium void worth which is 6% larger than with ERALIB1.

Additional calculations were performed, with the JEFF-3.1 and ENDF/B-VII.0 sodium data substituted for the corresponding ERALIB-1 data. When the ENDF/B-VII.0 sodium data are used, the sodium void worth increases significantly, mainly because of the change in the non-leakage term. The differences with the ERALIB1 results are 12% (SFR) and 10% (EFR-like).

These reactivity variations resulting from differences in evaluated files are much larger than the uncertainties computed from the BOLNA covariances (Table 6). This suggests that the use of the latter will lead to underestimates of the sodium void worth uncertainties.

Conclusion

The latest sodium data available in the JEFF-3.1, ENDF/B-VII.0 and JENDL-3.3 nuclear data files contain significant differences in the 500 keV to 6 MeV range. The discrepancies between the files are larger than some of the published *a priori* uncertainties.

When computing SFR and EFR-like reactor sodium void worths using the above files, relatively large differences in the results were found, exceeding the 7% target accuracy required for the design of Gen-IV innovative reactors.

It is recommended that sodium inelastic and total cross sections be re-evaluated in the 500 keV to 2 MeV range, with the help of new measurements. A ~ 5% target uncertainty in the inelastic data should be aimed for, in order to satisfy the Gen-IV design criteria in both the viability and performance phases. Correlations between reactions should be introduced in the updated file, mainly between the elastic and inelastic reactions.

It is also suggested that integral experiments sensitive to sodium data be re-analysed to explain some inconsistencies in the trends derived from past studies. The experiments to be considered are first the reactivity measurements of voided zones of various sizes, so as to vary the relative importance of the leakage and non-leakage components of the sodium void.

A two-term linear formula, representing the contributions from these two components, was used to fit the experimental data [7]. This work would lead to sodium elastic and inelastic scattering cross section information in the MeV range (impacting the non-leakage component), but also to the total scattering cross section information (impacting the leakage component). Also, the analysis of JANUS experiments studying neutron attenuation in Na shields should be performed since they are very sensitive to the Na total cross section and hence brings a bound to the variation changes that can be applied to sodium elastic and inelastic scattering cross sections.

References

[1] L. Buiron, Ph. Dufour, G. Rimpault, G. Prulhiere, C. Thevenot, J. Tommasi, F. Varaine, A. Zaetta, "Innovative Core Design For Generation IV Sodium-Cooled Fast Reactors", Proc. ICAPP 2007 Int. Conf., Nice, France May 13-18, 2007.

[2] S. Cierjacks, P. Forti, D. Kopsch, L. Kropp, J. Nebe, H. Unseld, "High Resolution Total Neutron Cross Section for Na, Cl, K, V, Mn and Co between 0.5 and 30 MeV", KFK-1000, 1969.

[3] D. C. Larson, et al., "Measurement of the Neutron Total Cross Section of Sodium from 32 keV to 37 MeV", ORNL-TM-5614,. Oak Ridge National Laboratory, 1976.

[4] H. Märten, J. Wartena, and H. Weigmann, IRMM Report GE/R/ND/02/94, 1994.

[5] K. Shibata, "Evaluation of Neutron Nuclear Data for Sodium-23", Journal of Nuclear Science and Technology, Vol. 39, N°10, pp. 1065-1071, October 2002.

[6] S. Kopecky, R. Shelley, H. Märten, H. Weigmann, "High Resolution Inelastic Scattering Cross Sections of 23Na and 27Al", Proc. Intern. Conf. on Nuclear Data for Science and Technology, Trieste, Italy, 19-24 May, 1997.

[7] G. Rimpault, H. Oigawa, P. Smith, "Assessment of Latest Developments in Sodium Void Reactivity Worth Calculations," Proc. Int. Conf. on the Physics of Reactors, Mito, Japan, Vol. 2, E-11, Sept. 16-20, 1996.

[8] E. Fort, et al., "Improved performance of the fast reactor calculational system ERANOS-ERALIB1 due to improved a priori nuclear data and consideration of additional specific integral data", Annals of Nuclear Energy, 30, pp. 1879-1898, 2003.

[9] The JEF-2.2 Nuclear Data Library, OECD/NEA, JEF Report 17, April 2000.

[10] E. L. Trykov and I. R. Svinin, "Analysis and Reevaluation of the Neutron Cross Sections for 23Na", INDC(CCP)-425, May 2000.

[11] D. Rochman, et al., BNL Report BNL-77407-2007-IR, prepared for OECD/WPEC SG26, January 2007.

[12] E. Fort, et al.: "Realisation and Performance of the Adjusted Nuclear Data Library ERALIB1", Proc. of Int. Conf. on the Physics of Reactors (PHYSOR-1996), Session F03, Mito, Japan, 1996.

[13] G. Rimpault, "The ERANOS Code and Data System for Fast Reactor Neutronic Analyses", Proceedings of the PHYSOR-2002 International Conference on the New Frontiers of Nuclear Technology: Reactor Physics, Safety and High Performance Computing, Seoul, Korea, October 7-10, 2002.

Target accuracy assessment for an ADS design

G. Aliberti[1)], G. Palmiotti[2)], M. Salvatores[1,2,3)]

1) Argonne National Laboratory, NE Division, Argonne, IL 60439 (USA)
2) Idaho National Laboratory, NSE Division, 2525 Fremont Ave. P.O. Box 1625, Idaho Falls, ID 83415-3855 (USA)
3) CEA-Cadarache, 13108 St-Paul-Lez-Durance, France
aliberti@anl.gov

Abstract: Nuclear data uncertainties and their impact on a very wide range of reactor systems, including their associated fuel cycles, have to be assessed in order to consolidate preliminary design studies for new innovative systems. One specific class of systems is the so-called “dedicated waste transmuters”, that are fast neutron systems (critical or sub-critical, i.e. ADS), loaded with a Minor Actinide (MA) dominated fuel and potentially Uranium-free. The availability of very general tools for sensitivity and uncertainty analysis together with new variance-covariance matrix data, produced in a joint effort under the auspices of the OECD-NEA by the world leading nuclear data evaluation groups, makes that endeavor particularly significant. In this report major results of interest for dedicated ADS are discussed and the most important fields and data types are pointed out, where priority improvements are required.

Introduction

The potential impact of nuclear data uncertainties on a large number of performance parameters of an ADS dedicated to the transmutation of radioactive wastes was presented in [1,2]. An uncertainty study was performed based on sensitivity analyses, which did underline the cross-sections, the energy range, and the isotopes that were responsible for the most significant uncertainties. In particular, in [2], the uncertainty assessment was performed with the use of the new covariance data recently developed within the WPEC Subgroup 26 [3] by joint efforts of several laboratories. The new set of uncertainties [4 to 13] is called BOLNA (standing for BNL, ORNL, LANL, NRG, ANL, from the Labs where the covariances were produced). The integral parameters analyzed in [2] were all the ADS parameters potentially most sensitive to nuclear data uncertainties: multiplication factor, power peak, defined as the point maximum power value normalized to the total power, burnup Δk/k, coolant void reactivity coefficient, nuclide density at end of cycle (transmutation potential), the ratio φ* of the average external source importance to the average fission neutron importance, the values of the displacements per atom (dpa), He production, H production and the ratio (He production)/dpa at the spatial point where they reach their maximum value (Max dpa, Max (n,α), Max (n,p), Max (n,α)/dpa). The Doppler reactivity coefficient has not been considered due the its small calculated value.
The uncertainty analysis carried out in [2] lead to the following conclusions. The overall uncertainties on the selected integral parameters are quite significant. Pu-241 and some of the higher Pu isotopes contribute to the uncertainties, while the Pu-239 contribution is always very small, in agreement with what was already pointed out in [1]. However, the major contributions are due to MA data and in particular to Cm-244 data uncertainties. Am-241, Am-243, Cm-245 give also some noteworthy contributions. As for structural materials, Fe-56 and Bi-209 show not negligible effects. Concerning the isotope reactions that are the most important contributors to the uncertainties, the role of fission cross-section uncertainties is found remarkable for most parameters. In fact, uncertainties in the fission cross-sections have an effect both on the reactivity and in the hardness of the spectrum. This last effect can be seen both on the power peak and on the Max (n,α)/dpa ratio. With respect to the previous study [1], there is much less impact of (n,2n) cross-sections, due to lower values of uncertainty in the present variance-covariance data (~10%, to be compared to the 100% value used in [1]). On the contrary, the significant impact of the Fe-56 inelastic cross-section is confirmed, in particular on the void reactivity coefficient.
To provide guidelines on priorities for new evaluations or experimental validations, in the present paper required accuracies on specific nuclear data have been derived. This analysis is similar to the work performed in [1]. However, the present results account for the target

accuracies on major design parameters, recently established within the NEA WPEC Subgroup 26, and are consistent with the uncertainty assessment carried out with the BOLNA covariance matrix. Additionally, the present study involves the use of more sophisticated computational tools.

Data target accuracies

To be consistent wit the target accuracy study presented in [14], the guidelines that will be provided in the present paper for data improvements are based on the analysis of the following parameters: multiplication factor, power peak, coolant void reactivity coefficient, burn up Δk/k, nuclide density at end of cycle. Within the Subgroup 26, a preliminary list of design target accuracies for fast reactor systems (at first, independently of the coolant and fuel type) has been established as presented in Table 1. These target accuracies reflect the perceived status of the art, even if they are not yet the result of a systematic analysis, which should necessarily involve industrial partners. Moreover, it has to be kept in mind that no final, well defined "images" for any of the dedicated transmuter (critical or sub critical) systems exist at present. This means that the target accuracies shown in Table 1 reflect the current hypothesis for transmutation systems with innovative fuels and core configurations as described in [15,16] (i.e. fast spectrum Na-cooled "burner" systems), and are applied to the LBE cooled ADS under study as well.

Table 1. *Fast Burner Reactor and ADS Target Accuracies (1σ)*

Multiplication factor (BOL)	300 pcm	Reactivity coefficients (Coolant void and Doppler)	7%
Power peak (BOL)	2%	Major nuclide density at end of irradiation cycle	2%
Burnup reactivity swing	300 pcm	Other nuclide density at end of irradiation cycle	10%

Theoretical approach and reference calculations

The chosen ADS system has some general features (e.g., the mass ratio between plutonium and MA, the americium-to-curium ratio, etc.) that are representative of the class of MA transmuters with a fast neutron spectrum and a Uranium-free fuel. The target and the coolant material of the core consist of Pb-Bi eutectic (LBE), and the model is very close to the sub-critical core, which has been analyzed in the framework of an international OECD-NEA benchmark [17].
Sensitivity and uncertainty coefficients are consistent with the results presented in [2] and calculated at ANL with the ERANOS code system [18].
As reminder, once the sensitivity coefficient matrix S_R for each integral parameter R and the covariance matrix D are available, the uncertainty on the integral parameter can be evaluated as follows:

$$\Delta R_0^2 = S_R^+ D S_R \qquad \text{Eq. 1}$$

A successive step is the assessment of target accuracy requirements. To establish priorities and target accuracies on data uncertainty reduction, a formal approach can be adopted by defining target accuracy on design parameters and finding out the required accuracy on the nuclear data σ_i. In fact, the unknown uncertainty data requirements d_i can be obtained (e.g. for parameters i not correlated among themselves), by solving the following minimization problem:

$$\sum_i \lambda_i / d_i^2 = \min \qquad \text{(i = 1…I, I: total number of parameters)} \qquad \text{Eq. 2}$$

with the following constraints:

$$\sum_i S_{R_n i}^2 d_i^2 < \left(R_n^T\right)^2 \quad \text{(n = 1…N, N: total number of integral design parameters),}$$

where $S_{R_n i}$ are the sensitivity coefficients for the integral parameter R_n, and R_n^T are the target accuracies on the N integral parameters; λ_i are "cost" parameters related to each σ_i and should give a relative figure of merit of the difficulty of improving that parameter (e.g., reducing uncertainties with an appropriate experiment).
The cross-sections uncertainties required for satisfying the target accuracies have been calculated by a minimization process that satisfies the nonlinear constraints with bounded parameters. The SNOPT code [19] has been used for this purpose. To avoid the introduction

of meaningless parameters, as unknown “d” parameters (i.e., as cross-sections for which target accuracies are required), only those which globally account at least for 98% of the overall uncertainty for each integral parameter have been chosen. Concerning the cost parameters, as already done in previous work [15], a constant value of one for all λ_i is initially taken. Additionally, at the first stage it was decided to not account for correlations between data. This assumption is of course rather arbitrary, but it is consistent with standard requirements for reactor designs in early phases of development.

Results

The most relevant cross-section accuracy requirements are presented in Table 2. It can be observed that tight requirements are found for MA cross-sections, in particular for σ_{fiss} of Cm-244, Am241, Cm-245, Am-243, Cm-242, Am-242m, for σ_{inel} of Am-243 and for ν of Cm-244. For these reactions, the required accuracies are an order of magnitude below the present uncertainties. Concerning the major actinides, improvements are required for σ_{fiss} of Pu-241 (again ~factor 10), for σ_{fiss} of Pu-238 (~factor 5) and for ν of Pu-238 (~factor 3). Finally, important requirements are also found for structural materials, particularly for σ_{inel} of Fe-56, Bi-209, Pb and Zr-90.

Table 2. *Uncertainty Reduction Requirements Needed to Meet Integral Parameter Target Accuracies*

Isotope	Cross-Section	Energy Range	Uncert. (%)		Isotope	Cross-Section	Energy Range	Uncert. (%)	
			Initial	Target				Initial	Target
Cm244	σ_{fiss}	6.07 - 2.23 MeV	31.3	3.0	Bi209	σ_{inel}	2.23 - 1.35 MeV	34.1	2.8
		2.23 - 1.35 MeV	43.8	2.6			1.35 - 0.498 MeV	41.8	4.2
		1.35 - 0.498 MeV	50.0	1.5	Am243	σ_{fiss}	6.07 - 2.23 MeV	11.0	2.3
Fe56	σ_{inel}	6.07 - 2.23 MeV	7.2	2.5			1.35 - 0.498 MeV	9.2	1.6
		2.23 - 1.35 MeV	25.4	1.6	Cm244	ν	6.07 - 2.23 MeV	11.1	2.5
		1.35 - 0.498 MeV	16.1	1.5			1.35 - 0.498 MeV	5.5	1.3
Am243	σ_{inel}	1.35 - 0.498 MeV	42.2	2.3	N15	σ_{el}	1.35 - 0.498 MeV	5.0	1.2
		498 - 183 keV	41.0	3.6	Pb	σ_{inel}	6.07 - 2.23 MeV	5.4	2.9
		183 - 67.4 keV	79.5	3.7	Zr90	σ_{inel}	6.07 - 2.23 MeV	18.0	3.3
Pu241	σ_{fiss}	1.35 - 0.498 MeV	16.6	2.1	Pu238	σ_{fiss}	2.23 - 1.35 MeV	33.8	6.0
		498 - 183 keV	13.5	1.7			1.35 - 0.498 MeV	17.1	3.4
		183 - 67.4 keV	19.9	1.7			498 - 183 keV	17.1	3.9
Am241	σ_{fiss}	6.07 - 2.23 MeV	11.7	1.7	Cm242	σ_{fiss}	6.07 - 2.23 MeV	52.6	26
		2.23 - 1.35 MeV	9.8	1.4			498 - 183 keV	66.0	28.4
		1.35 - 0.498 MeV	8.3	1.2	Pu238	ν	1.35 - 0.498 MeV	7.0	2.8
Cm245	σ_{fiss}	1.35 - 0.498 MeV	49.4	3.3			498 - 183 keV	7.0	3.4
		498 - 183 keV	37.2	2.9	Am242m	σ_{fiss}	498 - 183 keV	16.6	4.8
		183 - 67.4 keV	47.5	2.9			183 - 67.4 keV	16.6	4.8
		67.4 - 24.8 keV	26.5	3.2					

The required nuclear data accuracies, obtained from the optimization procedures, are such that the design target accuracies are fulfilled in most cases. Table 3 shows the initial integral parameter uncertainties (using the “BOLNA diagonal” covariance matrix) and the calculated uncertainties with the required cross-section uncertainties, as obtained with the minimization procedure. Note that the required parameter accuracies are not exactly met because of the cross-sections not accounted in the minimization procedures which give as consequence a residual uncertainty going to be added to the specified accuracy. In Table 3, in italic font are the initial parameter uncertainties out of the required accuracies summarized in Table 1. Besides the parameters listed in Table 1 (e.g. the parameters for which accuracy requirements have been defined), uncertainties on the additional integral quantities investigated in [2] have been recalculated. Uncertainties on nuclide densities at end of irradiation have not been reported because low values are found in general due to the short burn up.

***Table 3**. Integral Parameter Uncertainties (%) with Initial and Required σ Uncertainties*

	k_{eff} [pcm]	Power Peak	Void	Burnup [pcm]	φ*	Max dpa	Max (n,α)	Max (n,p)	Max (n,α)/ dpa
Initial	*1882*	*14.2*	*13.1*	*603*	1.43	20.53	9.71	16.29	13.12
With required uncertainties	283	2.2	3.5	216	0.34	3.18	5.29	3.47	5.16

Acknowledgments
Argonne National Laboratory's work was supported by the U.S. Department of Energy, Office of Nuclear Energy, under contract DE-AC02-06CH11357.

References

[1] G. Aliberti et al., "Impact of Nuclear Data Uncertainties on Transmutation of Actinides in Accelerator-Driven Assemblies," Nucl. Sci. Eng., 46, 13-50 (2004).
[2] G. Aliberti, G. Palmiotti, M. Salvatores, "New Covariance Data and Their Impact on ADS Designs," in Proc. of AccApp Conference, Pocatello, ID, USA, (July-August 2007).
[3] M. Salvatores et al., "Nuclear Data Needs for Advanced Reactor Systems. A NEA Nuclear Science Committee Initiative," Proc. Int. Conf. ND-2007, Nice, France (April 2007).
[4] D. Rochman et al., "Preliminary Cross-Section Covariances for WPEC Subgroup 26," Tech. Rep. BNL-77407-2007-IR, Brookhaven National Laboratory, (2007).
[5] D. Rochman et al., "Preliminary nu-bar Covariances for 238; 242Pu and 242; 243; 244; 245Cm," Tech. Rep. BNL-77407-2007-IR-Suppl.1, Brookhaven National Laboratory, (2007).
[6] M. Chadwick et al., "ENDF/B-VII.0: Next Generation Evaluated Nuclear Data Library for Nuclear Science and Technology," Nuclear Data Sheets, 107, pp. 2931 (December 2006).
[7] S. F. Mughabghab, "Atlas of Neutron Resonances: Resonance Parameters and Thermal Cross-Sections," Amsterdam: Elsevier, (2006).
[8] M. Herman et al., "EMPIRE Nuclear Reaction Model Code, Version 2.19 (Lodi)," www.nndc.bnl.gov/empire219/ (March 2005).
[9] T. Kawano, Tech. Rep. JAERI-Research, 99-009, JAERI, (1999).
[10] N. M. Larson, "Updated Users' Guide for SAMMY: Multilevel R-Matrix Fits to Neutron Data Using Bayes' Equations," ORNL/TM-9179/R7 (2007).
[11] L. Leal, H. Derrien, N. Larson, G. Arbanas, and Royce Sayer, "ORNL Methodology for Covariance Generation for Sensitivity/Uncertainty Analysis," in Proc. of International Conference on Nuclear Criticality Safety, St. Petersburg, Russia, (May 2007).
[12] A. J. Koning, "Generating Covariance Data with Nuclear Models," in Proceedings of the International Workshop on Nuclear data Needs for Generation IV Nuclear energy systems, Antwerpen, (April 5-7, 2005), ed. P. Rullhusen, World Scientific (2006), p. 153.
[13] A. J. Koning, S. Hilaire and M. C. Duijvestijn, "TALYS: Comprehensive Nuclear Reaction Modeling," in Proc. of Int. Conf. on Nuclear Data for Science and Technology - ND2004, AIP vol. 769, Santa Fe, NM, USA, (Sep. 26 - Oct. 1, 2004), p. 1154, (2005).
[14] M. Salvatores, G. Aliberti and G. Palmiotti, "The Role of Differential and Integral Experiments to Meet Requirements for Improved Nuclear Data", ND-2007, Nice, France, (April 2007).
[15] G. Aliberti et al., "Nuclear Data Sensitivity, Uncertainty and Target Accuracy Assessment for Future Nuclear Systems", Annals of Nucl. Energy, 33, 700-733, (2006).
[16] Y. I. Chang, P. J. Finck, C. Grandy, "Advanced Burner Reactor Preconceptual Design Report", ANL-ABR-1, Argonne National Laboratory, (September 2006).
[17] "Comparison Calculations for an Accelerator-Driven Minor Actinides Burner," OECD Nuclear Energy Agency, (2001).
[18] G. RIMPAULT et al., "The ERANOS Code and Data System for Fast Reactor Neutronic Analyses," in Proc. of PHYSOR 2002 Conference, Seoul, South Korea, (October 2002).
[19] P.E. Gill et al., "SNOPT: An SQP algorithm for Large-Scale constrained programming", Technical Report SOL 97-3, Systems Optimization Laboratory, Department of Operations Research, Stanford University, Stanford, California 94305-4022, (1997).

Uncertainties on spent fuel inventories in the application of nuclear fuel cycles

R.W. Mills, C.H. Zimmerman, R.G. Moore

Nexia Solutions Ltd, B170, Sellafield, Seascale, Cumbria, CA20 1PG, UK
robert.w.mills@nexiasolutions.com

Abstract: The nuclear industry utilises nuclear data in many ways. These range from dose rate calculations for irradiated fuel transport to inventory calculations for waste consignment. In all of these cases the calculation uncertainties are highly dependent on the nuclear data used in calculating the spent fuel inventory. As an example of this, the calculation of decay heat in the context of the current fuel reprocessing plants is discussed. The radiogenic heating is calculated using the atoms present, half-lives and energy released per decay for each nuclide. There are thus two sources of error in the resultant decay heat the error on the nuclide number densities and the uncertainties on the nuclear data. Nexia Solutions has developed a validation database over a number of years which can be used to indicate uncertainty in the calculation of radionuclide number density. This database includes PWR, BWR, and the UK's Advanced Gas Cooled and Magnox Reactor fuel measurements of important nuclides and some direct decay heat measurements of PWR fuel. It should be noted that decay heat after a few days of cooling is dominated by only a few nuclides (less than 20 contribute greater than 99%) many of which have been measured in spent fuels. At shorter times over a hundred nuclides contribute significantly and thus an alternative method is demonstrated to calculate the uncertainty on the decay heat on the timescale of seconds to days. A series of current and possible fuel cycle scenarios are considered and using the decay heat results an analysis is attempted to determine which nuclear data contributes most to the uncertainty on the final result and where future measurements are required.

Fuel cycles

Nuclear data is important in the design and operation of nuclear fuel cycles. While accurate nuclear data is clearly required, what is much more important is an accurate estimate of the systematic and random uncertainties of nuclear data and its effects on engineering parameters required to develop bounding cases for the design and safe operation of plants. Current reprocessing operations carried out, for example, in France or the UK use the Purex fuel cycle. This fuel cycle is well understood and involves operations associated with the transport of irradiated nuclear fuel, chemical processing of dissolved fuel, storage or use of uranium and plutonium and the disposal of the various waste streams from the cycle. In general, each of these stages have design requirements or operational safety case requirements which require the use of nuclear data in their specification. For example, the transport of irradiated nuclear fuel requires a safety case which specifies the radiation shielding to be used and sets a limit on the heat capacity of the transport cask. It is clear that uncertainty in the raw nuclear data which contributes to the calculated limits of these safety cases needs to be determined. As an example of this, the specific case of determining the uncertainties in the heat produced by the irradiation of nuclear fuel in LWRs will be discussed in this paper.

The Purex based thermal reactor fuel cycle can be regarded as a subset of some advanced cycles. For example, the "double strata" fuel cycle proposed by the Japanese and French [1] comprises thermal reactor systems using UOX with single recycle MOX fuel, plutonium burning fast reactors (FR) which recycle plutonium and multiple recycling accelerator driven systems (ADS) which burn minor actinides, plutonium and uranium. The same arguments concerning the accuracy of nuclear data hold for these advanced systems as they do for the current Purex based thermal reactors systems. A representation of the "double strata" fuel concept is shown in figure 1. The difficulty here is that much less validation data are available for fast neutron systems in FR or ADS than for thermal systems and consequently the determination of systematic and random uncertainties is much more difficult.

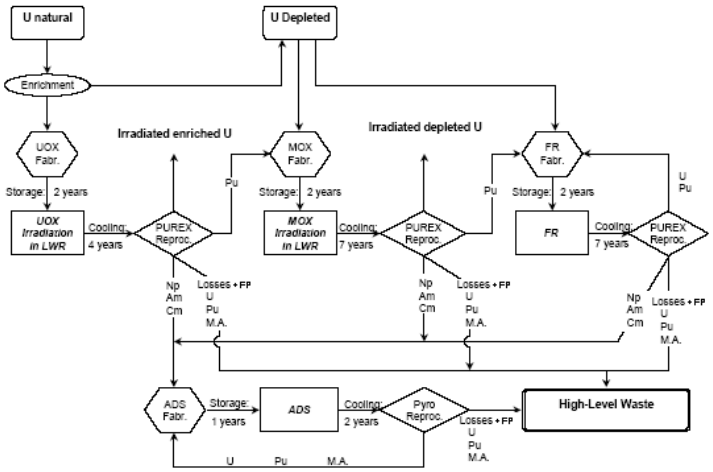

Figure 1. *Diagram of a "double strata" fuel cycle*

The calculation of spent fuel inventories

All engineering quantities, such as decay heat and radiation emission depend, on the composition of the spent fuel. The general form of the differential equation governing the number density of a nuclide with time is given by:

$$\frac{dN_i}{dt} = -\lambda_i N_i + \sum_j \lambda_j N_j B_{j,i} + \sum_k N_k \sigma_{f,k} \phi Y_{k,i} - \sum_l N_i \sigma_{i,l} \phi + \sum_m N_m \sigma_{m,i} \phi$$

The first two terms of this equation are those developed by Bateman [2] to describe a chain of radio-active decays. Here the first term is the decay of the nuclide i and the second term is the decay of direct precursor nuclides (given as the set of nuclides j) to i. Here N_x is the number density of a nuclide x, λ_x is the decay constant of x, $B_{x,y}$ is the branching fraction of decays of x that lead to y. The following three terms describe the general form of neutron reactions. The third term is the production of fission product nuclides i from the neutron induced fission of nuclides, k, where $\sigma_{f,k}$ is the fission cross-section of nuclide k, ϕ is the scalar neutron flux and $Y_{k,i}$ is the independent yield of nuclide i from the fission of nuclide k. The fourth term is the destruction of nuclide i by all possible neutron reactions to a set of nuclides l, where $\sigma_{i,l}$ is the cross-section of i leading to l. The fifth term describes the product of nuclide i by neutron reactions on all nuclides that lead to i by one reaction step given as the set of nuclides m.

To carry out a full error analysis of such a calculation would require a complete set of covariances for the cross-sections and other parameters. As these are not available, an alternative is to estimate the accuracy of the FISPIN inventory by comparing with experimental measurements. Within Nexia Solutions a large database of measurements has been collected over the last 30 years for UK nuclear fuels (most Magnox and Advanced Gas Cooled reactors), and also including some BWR and PWR data. The database has comparisons with calculations using JEF-2.2 based libraries using the WIMS, TRAIL and FISPIN10 code route [3]. These data are being contributed to the NEA Expert Group on Assay Data of Spent Nuclear Fuel.

So far JEFF-3.1 has only been applied to a small subset of the assay data in the Nexia Solutions database. One set of data compared with JEFF-3.1 calculations is 3 UOX samples from the Gösgen PWR that was part of the ARIANE programme. These were analysed at the Institute for Transuranium Elements (ITU) and the Belgian Nuclear Research Centre (SCK.CEN) during the late 1990s [4, 5]. The samples are referred to as GU1 (analysed at SCK.CEN), GU3 and GU4 (ITU). The liquor solution derived from sample GU3 was divided and analysed at both laboratories. These results are identified as GU3' (SCK.CEN) and GU3 (ITU). Enrichments were 3.5% and 4.1%, and sample irradiations ranged from 29 to 60 GWd/t. The calculated to experiment ratios (C/E) for these samples using the WIMS, TRAIL, FISPIN10 route using JEFF-3.1 based libraries are shown in table 1.

Table 1. *Gösgen nuclide inventory C/E ratios using JEFF-3.1 data.*

Nuclide	Sample				JEFF-3.1	Nuclide	Sample				JEFF-3.1
	GU1	GU3'	GU3	GU4	Mean ; SD		GU1	GU3'	GU3	GU4	Mean ; SD
Sr90	0.77	1.03	0.98	0.99	0.94 ; 0.12	Sm152	1.02	1.15	1.14	1.12	1.11 ; 0.06
Mo95	1.00	0.88	0.94	0.97	0.95 ; 0.05	Sm154	0.97	1.08	1.09	1.12	1.07 ; 0.07
Tc99	1.03	0.91	1.03	1.27	1.06 ; 0.15	Eu151	0.57	0.76			0.67 ; 0.14
Ru101	1.06	0.87	0.95	0.97	0.96 ; 0.08	Eu153	1.13	1.11	1.03	1.10	1.09 ; 0.04
Ru106	1.08	0.87	0.47	0.85	0.82 ; 0.25	Eu154	2.27	1.80	1.57	1.60	1.81 ; 0.32
Rh103	1.14	1.16	1.19	0.96	1.11 ; 0.10	Eu155	1.05	0.99	0.86	0.96	0.96 ; 0.08
Ag109	2.18	1.09			1.64 ; 0.77	Gd155	1.12	1.23	1.00	0.68	1.01 ; 0.24
Sb125	1.90	1.98			1.94 ; 0.05	U234	1.17	1.39	1.43	1.39	1.35 ; 0.12
I129		0.99	0.97	0.90	0.96 ; 0.05	U235	1.41	1.14	1.26	1.06	1.21 ; 0.15
Cs133	1.02	1.04	0.95	0.99	1.00 ; 0.04	U236	1.02	1.01	0.99	1.01	1.01 ; 0.01
Cs134	1.05	1.03	0.84	1.01	0.98 ; 0.10	U238	1.00	1.00	1.00	0.99	0.996 ; 0.001
Cs135	1.05	1.07	1.01	1.14	1.07 ; 0.05	Np237		0.90	0.84	0.74	0.82 ; 0.08
Cs137	0.97	0.99	0.95	1.06	0.99 ; 0.05	Pu238	1.03	0.97	0.90	1.04	0.98 ; 0.06
Ce144	1.06	1.07	1.06	1.08	1.07 ; 0.01	Pu239	1.18	1.04	1.04	1.07	1.08 ; 0.07
Nd142	0.93	0.97	1.02	1.11	1.01 ; 0.08	Pu240	1.02	0.98	0.96	0.99	0.99 ; 0.03
Nd143	1.14	1.05	1.11	0.98	1.07 ; 0.07	Pu241	1.15	1.09	1.06	1.09	1.10 ; 0.03
Nd144	0.95	0.97	0.97	0.94	0.95 ; 0.02	Pu242	0.92	1.00	0.91	1.02	0.96 ; 0.06
Nd145	1.01	1.00	1.03	0.98	1.00 ; 0.02	Pu244	0.69	0.55			0.62 ; 0.10
Nd146	1.00	0.99	0.99	0.98	0.990 ; 0.008	Pu	1.09	1.03	1.01	1.05	1.05 ; 0.04
Nd148	1.00	1.00	1.00	1.00	1.000 ; 0.000	Am241	1.23	1.28	1.25	1.06	1.20 ; 0.10
Nd150	0.98	0.98	0.93	1.01	0.97 ; 0.03	Am242m	1.24	0.93			1.08 ; 0.22
Pm147	1.46	1.16	0.85	0.94	1.10 ; 0.27	Am243	1.01	1.08	0.83	1.08	1.00 ; 0.12
Sm147	0.94	1.02	0.98	1.05	1.00 ; 0.05	Cm242	0.98	0.93			0.96 ; 0.03
Sm148	0.91	0.90	0.82	1.00	0.91 ; 0.07	Cm243	3.13	1.18			2.16 ; 1.38
Sm149	1.16	1.37	0.97	1.14	1.16 ; 0.16	Cm244	0.89	0.84	0.57	0.81	0.78 ; 0.14
Sm150	1.03	1.06	1.01	1.07	1.04 ; 0.03	Cm245	1.05	0.87	0.57	0.87	0.84 ; 0.20
Sm151	1.34	1.30	1.25	1.26	1.29 ; 0.04	Cm246	0.68	0.73			0.71 ; 0.03

Validation of decay heat

Schmittroth reported measurements of the decay heat from irradiated PWR assemblies together with comparisons against ORIGEN2 [6]. This included 20 measurements with cooling times between 2.4 and 8.2 years for irradiations between 25 and 40 GWd/t; note that 4 measurements reported as suspect were ignored. The assemblies came from the San Onofre, Point Beach and Turkey Point reactors. The stainless steel cladding from San Onofre did not have a measured value for the cobalt impurity and, as this results in 10 to 20% of the heat in these cases, they could not be used for validation. Decay heat calculations were carried out using the FISPIN10 with JEFF-3.1 based libraries. The reactor physics models were based on design data reported in World Nuclear Industry Handbook [7]. The experimental decay heats and the FISPIN results are compared in table 2.

Table 2. *Comparison of PWR assembly decay heat measurements with JEFF-3.1 calculations.*

Reactor	Initial ^{235}U (Wt%)	Burnup (GWd/t)	Cooling (d)	Measured heat (W)	JEFF-3.1 decay heat C/E
Point Beach	3.397	31.914	1635	724	0.97
		31.914	1635	723	0.97
		38.917	1634	921	1.00
		39.384	1633	931	1.00
		35.433	1630	846	0.96
		38.946	1629	934	0.99
		37.057	1630	874	0.99
Turkey Point	2.556	28.430	962	1423	1.04
		28.430	2077	625	1.01
		26.485	963	1284	1.05
		27.863	864	1550	1.05
	2.559	25.595	1782	637	0.98
Mean and Standard Deviation of C/E values				Point Beach	0.98 ± 0.02
				Turkey Point	1.02 ± 0.03
				All	1.00 ± 0.03

These results show good agreement between experiment and calculations, all within ±5%. The overall mean C/E was 1.00 ± 0.03. It is noted that the uncertainties on the measurements

were ± 2%. However, this type of analysis is only valid for fuels measured.

Calculation of decay heat using the C/E from assay predictions

An alternative method to calculate the biases and uncertainities on decay heat for more general cases is to use the nuclide concentration biases and uncertainities given in table 1. In the following work, we consider a FISPIN calculation for a 4% UOX assembly irradiated in a PWR to 40 GWd/t and cooled in steps to $1x10^6$ years. It was necessary to assume that shorter lived daughters in equilibrium with parents had the same C/E values as their parents, that U239 and Np239 has a C/E the same as Pu239 and that the Ba140/La140 had the same C/E as Cs137. Nuclides not in table 1 were assumed to have no bias but a 100% uncertainity. Also if no errors were quoted for nuclear data then a 50% value was assumed.

Table 3. *Expected decay heat calculated from FISPIN and C/E of assay data.*

Cooling time (Years unless stated)	FISPIN heat (kW/tUi)	Expected bias (%)	Expected uncertainty (%)	Fraction of heat from measured nuclides (%)	Expected heat (kW/tUi)	Expected heat uncertainty (kW/tUi)	Bounding heat (bias + 2 * uncertainty)
Shutdown	2.45E+03	0.26	93.49	7.83	2.45E+03	2.29E+03	7.02E+03
3 days	1.58E+02	0.74	49.43	52.43	1.56E+02	7.73E+01	3.11E+02
5	2.18E+00	-0.31	4.76	99.35	2.19E+00	1.04E-01	2.40E+00
10	1.38E+00	0.50	4.79	99.31	1.37E+00	6.58E-02	1.51E+00
15	1.19E+00	0.27	4.74	99.42	1.18E+00	5.61E-02	1.30E+00
20	1.07E+00	0.23	4.58	99.54	1.07E+00	4.89E-02	1.16E+00
25	9.74E-01	0.35	4.43	99.63	9.71E-01	4.30E-02	1.06E+00
30	8.93E-01	0.62	4.31	99.71	8.87E-01	3.82E-02	9.64E-01
100	3.50E-01	7.32	4.79	100.00	3.27E-01	1.56E-02	3.58E-01
1000	6.48E-02	12.35	5.82	100.00	5.77E-02	3.36E-03	6.44E-02
50000	3.39E-03	7.05	6.31	99.56	3.17E-03	2.00E-04	3.57E-03
100000	1.26E-03	5.07	5.06	98.78	1.20E-03	6.08E-05	1.32E-03
1000000	4.58E-04	-8.59	4.90	97.87	5.02E-04	2.46E-05	5.51E-04

This technique leads to large uncertainities where the measured components make up little of the heat due to the 100% uncertainity assumed for the unmeasured component. However, after 5 years the decay heat is dominated by nuclides for which assay data exists, or where reasonable assumptions can be made. Here the uncertainities are around 5% which is only slightly larger than the comparison shown for the measured assemblies above. A large positive bias exists on decay heat between 100 and 50000 years from the biases for ^{241}Am (+20%) and ^{239}Pu (+8%) and their daughters. At one million years the underprediction of ^{237}Np (-18%) and its daughters lead to a -9% underprediction of the heat.

It can be concluded that decay heat from LWR spent fuel can be adequately determined using existing codes and data. However, as no such nuclide measurements are published for spent fuels from fast reactors and ADS systems this analysis cannot be repeated for these systems and thus biases and uncertainities on their decay heat cannot be determined.

Acknowledgements

The authors gratefully acknowledge support from the UK Nuclear Decommissioning Authority and the European Commission's Euratom FP6 CANDIDE project.

References

[1] "Accelerator-driven Systems (ADS) and Fast Reactors (FR) in Advanced Nuclear Fuel Cycles: A Comparative Study", NEA report 3109, OECD Nuclear Energy Agency, Paris, ISBN 92-64-18482-1 (2002).

[2] H. Bateman, "The solution of a system of differential equations occurring in the theory of radio-active transformations," Proc. Cambridge Phil. Soc., 15, p. 423 (1910).

[3] The WIMS, TRAIL and FISPIN10 codes are available from the ANSWERS software development group of Serco Assurance Ltd. The FISPIN10 code is developed by Nexia Solutions with funding from the UK Nuclear Decommissioning Authority.

[4] Boulanger D and Lippens M, "ARIANE International Program, Final Report", AR 2000/15, BELGONUCLEAIRE, December 2000.

[5] Aoust T, "ARIANE International Program, Irradiation Data Report Parts 1,2 and 3", AR 99/13, Belgonucleaire, July 1999.

[6] F. Schmittroth, "ORIGEN2 Calculations of PWR spent fuel decay heat compare with calorimeter data." HEDL-TME 83-32 UC-85 (1984).

[7] Nucl. Eng. Int. World Nuclear Industry Handbook 1987 (ISSN 0029-5507).

Fission spectrum related uncertainties

G. Aliberti[1)], I. Kodeli[2)], G. Palmiotti[3)] and M. Salvatores[1,3,4)]

1) Argonne National Laboratory, NE Division, Argonne, IL 60439 (USA)
2) OECD/NEA, Paris, France
3) Idaho National Laboratory, NSE Division, 2525 Fremont Ave. P.O. Box 1625, Idaho Falls, ID 83415-3855 (USA)
4) CEA-Cadarache, 13108 St-Paul-Lez-Durance, France
aliberti@anl.gov

Abstract: The paper presents a preliminary uncertainty analysis related to potential uncertainties on the fission spectrum data. Consistent results are shown for a reference fast reactor design configuration and for experimental thermal configurations. However the results obtained indicate the need for further analysis, in particular in terms of fission spectrum uncertainty data assessment.

Introduction

Sensitivity coefficients for the multiplication factor associated to the fission spectrum are calculated according to the formula:

$$S_{k_{eff}(\chi),i,g,d} = \frac{\int_d \chi^*_{i,g,d}\Phi^*_{g,d} \times \left[\nu_{i,g',d}\Sigma_{f_{i,g',d}}\Phi_{g',d}\right]dr}{\int \sum_i \left[\chi_{i,g'}\Phi^*_{g'}\right] \times \left[\nu_{i,g'}\Sigma_{f_{i,g'}}\Phi_{g'}\right]dr}\Bigg|_{\substack{i=\text{isotope}\\ g,g'=\text{energy group}\\ d=\text{domain}}}, \qquad (1)$$

where $\chi^*_{i,g,d} = \chi_{i,g,d}\frac{\left\langle \nu\Sigma_{f_{i,d}}\Phi_d \right\rangle}{\left\langle \nu\Sigma_{f_d}\Phi_d \right\rangle}$, [ ] denotes the integration over the energy (summation over the groups g'), while $\langle\ \rangle$ denotes the integration over energy and space. After computing the sensitivity coefficients, the fission spectrum related uncertainties are successively determined using the classical formula $\Delta R_0^2 = S^+_{k_{eff}(\chi)} D S_{k_{eff}(\chi)}$, where D is the dispersion matrix containing the covariance data.

Table 1. *$\Delta k/k$[2]: Sensitivity Coefficients for ABTR*

		Pu-239: Breakdown by Energy Group						
Gr.	**Energy [(a)]**	**σ_{capt}**	**σ_{el}**	**ν**	**σ_{inel}**	**σ_{fiss}**	**χ**	**Total**
1	**19.6 MeV**	0.00	0.00	0.45	-0.01	0.30	3.24	3.98
2	**6.07 MeV**	-0.01	0.01	4.51	-0.13	3.03	29.49	36.90
3	**2.23 MeV**	-0.03	0.02	4.62	-0.08	3.08	18.80	26.41
4	**1.35 MeV**	-0.21	0.09	15.02	-0.05	10.42	20.08	45.36
5	**498 keV**	-0.58	0.17	20.32	-0.01	14.31	6.01	40.22
6	**183 keV**	-0.74	0.13	16.15	-0.02	11.68	1.37	28.57
7	**67.4 keV**	-0.55	0.03	8.00	-0.01	5.99	0.28	13.75
8	**24.8 keV**	-0.59	0.02	5.32	0.01	4.04	0.06	8.87
9	**9.12 keV**	-0.34	0.00	1.67	0.00	1.24	0.02	2.58
10	**2.03 keV**	-0.51	0.00	2.19	0.00	1.56	0.00	3.24
11	**454 eV**	-0.21	0.00	0.79	0.00	0.49	0.00	1.06
12	**22.6 eV**	-0.03	0.00	0.11	0.00	0.06	0.00	0.14
13	**4 eV**	0.00	0.00	0.04	0.00	0.03	0.00	0.07
14	**0.54 eV**	0.00	0.00	0.01	0.00	0.00	0.00	0.01
15	**0.1 eV**	0.00	0.00	0.00	0.00	0.00	0.00	0.00
Total		-3.80	0.47	79.20	-0.29	56.24	79.35	211.17

[(a)] Upper energy boundary

	Total Sensitivity - Breakdown by Isotope							
Isotope	**σ_{capt}**	**σ_{el}**	**ν**	**σ_{inel}**	**σ_{fiss}**	**$\sigma_{n,2n}$**	**χ**	**Total**
U235	-0.04	0.00	0.56	-0.01	0.37	0.00	0.56	1.44
U238	-13.84	2.72	12.22	-4.20	7.42	0.08	12.08	16.50
Pu238	-0.01	0.00	0.16	0.00	0.11	0.00	0.16	0.42
Pu239	-3.80	0.47	79.20	-0.29	56.24	0.00	79.35	211.17
Pu240	-0.62	0.07	2.65	-0.05	1.80	0.00	2.65	6.51
Pu241	-0.07	0.01	1.51	0.00	1.09	0.00	1.51	4.04
Pu242	-0.03	0.00	0.10	0.00	0.07	0.00	0.10	0.24
Np237	-0.08	0.00	0.10	0.00	0.07	0.00	0.10	0.18
Am241	-0.12	0.00	0.11	0.00	0.08	0.00	0.10	0.17
Am242m	0.00	0.00	0.02	0.00	0.02	0.00	0.02	0.07
Am243	-0.02	0.00	0.02	0.00	0.01	0.00	0.01	0.02
Cm242	0.00	0.00	0.01	0.00	0.01	0.00	0.01	0.02
Cm244	0.00	0.00	0.01	0.00	0.01	0.00	0.01	0.02
Cm245	0.00	0.00	0.00	0.00	0.00	0.00	0.00	0.01
Fe56	-1.38	5.18	0.00	-1.59	0.00	0.00	0.00	2.22
Cr52	-0.17	1.25	0.00	-0.17	0.00	0.07	0.00	0.98
Ni58	-0.05	0.12	0.00	-0.01	0.00	0.00	0.00	0.06
Zr90	-0.14	0.49	0.00	-0.21	0.00	0.00	0.00	0.14
Na23	-0.12	2.03	0.00	-0.42	0.00	0.00	0.00	1.49
B10	-0.52	0.01	0.00	0.00	0.00	0.00	0.00	-0.52
Total	-21.01	12.37	96.66	-6.96	67.29	0.16	96.66	245.18

Sensitivity coefficient results

The following sensitivity coefficients have been calculated for the ABTR [1] multiplication factor with the ERANOS code system [2]. Table 1 gives the breakdown by energy group for Pu-239 and the total values by isotope. The sensitivity coefficients shown in the tables are the total over the reactor. It can be observed that, as expected, the total isotope sensitivity for the fission spectrum has the same value of v; the distribution by energy group is however different for each isotope (see case of Pu-239). Additionally, the overall k_{eff} sensitivity to the fission spectrum (and to v) is practically 100% (NT Table 1 gives $\Delta k/k^2$ sensitivities and for the ABTR under study k_{eff} = 1.034472).

Fission spectra covariance matrices

The information on the fission spectra covariance matrices is available in the DOSCOV package [3] and in the JENDL-3.2 and -3.3 [4,5] evaluations. In the DOSCOV package, dating back to ~1980, the covariance data for the U-235 fission spectrum were obtained assuming the standard deviations of 1.2% and 5.9% for the Watt spectrum parameters *a* and *b*, respectively, and the correlation of -0.21 between them. For the purpose of these studies the covariance matrices were converted from the DOSCOV 24-group structure to those needed using the ANGELO code [6]. More recently, the covariance matrices for several isotopes, including U-235, U-238, Pu-239, were prepared in the JENDL-3.2 and -3.3 [2,3] evaluations. The data were processed using the ERROR-J 2.3 code [7].

Table 2. *Pu-239 JENDL3.3 Variance/Covariance Data (ABTR)*

			Convariances														
		Group	1	2	3	4	5	6	7	8	9	10	11	12	13	14	15
Variances (%)	Gr.	Energy [(a)]	19.6 MeV	6.07 MeV	2.23 MeV	1.35 MeV	498 keV	183 keV	67.4 keV	24.8 keV	9.12 keV	2.03 keV	454 eV	22.6 eV	4 eV	0.54 eV	0.1 eV
9.58	**1**	**19.6 MeV**	1.000	0.787	-0.323	-0.905	-0.665	-0.608	-0.592	-0.589	-0.589	-0.590	-0.594	-0.595	-0.595	-0.596	-0.596
7.12	**2**	**6.07 MeV**	0.787	1.000	0.329	-0.975	-0.984	-0.968	-0.963	-0.962	-0.962	-0.963	-0.964	-0.964	-0.964	-0.964	-0.964
1.03	**3**	**2.23 MeV**	-0.323	0.329	1.000	-0.110	-0.491	-0.554	-0.571	-0.574	-0.574	-0.574	-0.569	-0.568	-0.568	-0.568	-0.568
5.03	**4**	**1.35 MeV**	-0.905	-0.975	-0.110	1.000	0.919	0.888	0.879	0.877	0.877	0.877	0.880	0.880	0.881	0.881	0.881
6.62	**5**	**498 keV**	-0.665	-0.984	-0.491	0.919	1.000	0.997	0.996	0.995	0.995	0.995	0.996	0.996	0.996	0.996	0.996
8.92	**6**	**183 keV**	-0.608	-0.968	-0.554	0.888	0.997	1.000	1.000	1.000	1.000	1.000	1.000	1.000	1.000	1.000	1.000
8.21	**7**	**67.4 keV**	-0.592	-0.963	-0.571	0.879	0.996	1.000	1.000	1.000	1.000	1.000	1.000	1.000	1.000	1.000	1.000
7.30	**8**	**24.8 keV**	-0.589	-0.962	-0.574	0.877	0.995	1.000	1.000	1.000	1.000	1.000	1.000	1.000	1.000	1.000	1.000
12.59	**9**	**9.12 keV**	-0.589	-0.962	-0.574	0.877	0.995	1.000	1.000	1.000	1.000	1.000	1.000	1.000	1.000	1.000	1.000
12.16	**10**	**2.03 keV**	-0.590	-0.963	-0.574	0.877	0.995	1.000	1.000	1.000	1.000	1.000	1.000	1.000	1.000	1.000	1.000
25.09	**11**	**454 eV**	-0.594	-0.964	-0.569	0.880	0.996	1.000	1.000	1.000	1.000	1.000	1.000	1.000	1.000	1.000	1.000
0.61	**12**	**22.6 eV**	-0.595	-0.964	-0.568	0.880	0.996	1.000	1.000	1.000	1.000	1.000	1.000	1.000	1.000	1.000	1.000
0.05	**13**	**4 eV**	-0.595	-0.964	-0.568	0.881	0.996	1.000	1.000	1.000	1.000	1.000	1.000	1.000	1.000	1.000	1.000
0.00	**14**	**0.54 eV**	-0.596	-0.964	-0.568	0.881	0.996	1.000	1.000	1.000	1.000	1.000	1.000	1.000	1.000	1.000	1.000
0.00	**15**	**0.1 eV**	-0.596	-0.964	-0.568	0.881	0.996	1.000	1.000	1.000	1.000	1.000	1.000	1.000	1.000	1.000	1.000

[(a)] Upper energy boundary

Table 3. *U-235 DOSCOV Variance/Covariance Data (ABTR)*

			Convariances														
		Group	1	2	3	4	5	6	7	8	9	10	11	12	13	14	15
Variances (%)	Gr.	Energy [(a)]	19.6 MeV	6.07 MeV	2.23 MeV	1.35 MeV	498 keV	183 keV	67.4 keV	24.8 keV	9.12 keV	2.03 keV	454 eV	22.6 eV	4 eV	0.54 eV	0.1 eV
11.33	**1**	**19.6 MeV**	1.000	1.002	-0.674	-1.011	-1.002	-0.991	-0.991	-0.991	-0.991	-0.991	-0.991	-0.991	-0.991	-0.991	-0.991
2.85	**2**	**6.07 MeV**	0.969	1.000	-0.590	-1.012	-1.003	-0.991	-0.991	-0.991	-0.991	-0.991	-0.991	-0.991	-0.991	-0.991	-0.991
0.31	**3**	**2.23 MeV**	-0.770	-0.620	1.000	0.649	0.616	0.618	0.614	0.613	0.612	0.612	0.612	0.612	0.612	0.612	0.612
1.93	**4**	**1.35 MeV**	-0.992	-1.000	0.596	1.000	1.002	1.010	1.010	1.010	1.010	1.010	1.010	1.010	1.010	1.010	1.010
2.98	**5**	**498 keV**	-0.974	-0.999	0.564	0.998	1.000	1.009	1.009	1.009	1.009	1.009	1.009	1.009	1.009	1.009	1.009
3.46	**6**	**183 keV**	-0.952	-0.990	0.559	0.990	0.991	1.000	1.000	1.000	1.000	1.000	1.000	1.000	1.000	1.000	1.000
3.64	**7**	**67.4 keV**	-0.950	-0.990	0.559	0.990	0.991	1.000	1.000	1.000	1.000	1.000	1.000	1.000	1.000	1.000	1.000
3.71	**8**	**24.8 keV**	-0.950	-0.990	0.559	0.990	0.991	1.000	1.000	1.000	1.000	1.000	1.000	1.000	1.000	1.000	1.000
3.73	**9**	**9.12 keV**	-0.949	-0.990	0.559	0.990	0.991	1.000	1.000	1.000	1.000	1.000	1.000	1.000	1.000	1.000	1.000
3.74	**10**	**2.03 keV**	-0.949	-0.990	0.559	0.990	0.991	1.000	1.000	1.000	1.000	1.000	1.000	1.000	1.000	1.000	1.000
3.74	**11**	**454 eV**	-0.949	-0.990	0.559	0.990	0.991	1.000	1.000	1.000	1.000	1.000	1.000	1.000	1.000	1.000	1.000
3.74	**12**	**22.6 eV**	-0.949	-0.990	0.559	0.990	0.991	1.000	1.000	1.000	1.000	1.000	1.000	1.000	1.000	1.000	1.000
3.74	**13**	**4 eV**	-0.949	-0.990	0.559	0.990	0.991	1.000	1.000	1.000	1.000	1.000	1.000	1.000	1.000	1.000	1.000
3.74	**14**	**0.54 eV**	-0.949	-0.990	0.559	0.990	0.991	1.000	1.000	1.000	1.000	1.000	1.000	1.000	1.000	1.000	1.000
3.74	**15**	**0.1 eV**	-0.949	-0.990	0.559	0.990	0.991	1.000	1.000	1.000	1.000	1.000	1.000	1.000	1.000	1.000	1.000

[(a)] Upper energy boundary

The JENDL3.3 fission spectrum covariance matrix for Pu-239 is presented in Tables 2 in a 15 energy group structure. The DOSCOV fission spectrum covariance matrix is presented in Table 3 for U-235 in a 15 energy group structure. In the present study, as demonstrative example, the same matrix has been used for Pu-239.

Uncertainty results

Table 4 shows the breakdown of the calculated uncertainty coefficients by energy group for Pu-239 and the total uncertainties by isotope. Results for the fission spectrum are obtained with the JENDL3.3 covariance data (only U-235 and Pu-239 matrices were available), while for other cross-sections the BOLNA dispersion matrix [8] is used. It is observed that the total uncertainty associated to the fission spectrum is dramatically important, an order of magnitude higher than the v total contribution. As consequence, the overall uncertainty on the multiplication factor significantly increases (from 0.92% to 4.01%) becoming desperately out of the required accuracies (0.3%).

Table 4. *$\Delta k/k^2$: Uncertainty Coefficients (ABTR)*

		Pu-239: Breakdown by Energy Group						
Gr.	**Energy [(a)]**	**σ_{capt}**	**σ_{el}**	**ν**	**σ_{inel}**	**σ_{fiss}**	**χ**	**Total**
1	**19.6 MeV**	0.00	0.00	0.00	0.01	0.01	1.01	1.01
2	**6.07 MeV**	0.02	0.01	0.01	0.04	0.05	2.87	2.87
3	**2.23 MeV**	0.03	0.01	0.01	0.03	0.05	0.34	0.35
4	**1.35 MeV**	0.06	0.02	0.02	0.03	0.10	1.96	1.97
5	**498 keV**	0.11	0.02	0.05	0.01	0.13	1.21	1.22
6	**183 keV**	0.11	0.01	0.09	0.01	0.13	0.66	0.69
7	**67.4 keV**	0.09	0.00	0.06	0.01	0.08	0.29	0.32
8	**24.8 keV**	0.09	0.00	0.04	0.01i	0.06	0.13	0.17
9	**9.12 keV**	0.07	0.00	0.02	0.00	0.02	0.09	0.12
10	**2.03 keV**	0.01	0.00	0.00	0.00	0.02	0.03	0.04
11	**454 eV**	0.00	0.00	0.00	0.00	0.01	0.01	0.02
12	**22.6 eV**	0.00	0.00	0.00	0.00	0.00	0.00	0.00
13	**4 eV**	0.00	0.00	0.00	0.00	0.00	0.00	0.00
14	**0.54 eV**	0.00	0.00	0.00	0.00	0.00	0.00	0.00
15	**0.1 eV**	0.00	0.00	0.00	0.00	0.00	0.00	0.00
Total		0.23	0.03	0.13	0.06	0.24	3.90	3.92

	Total Uncertainty - Breakdown by Isotope							
Isotope	**σ_{capt}**	**σ_{el}**	**ν**	**σ_{inel}**	**σ_{fiss}**	**$\sigma_{n,2n}$**	**χ**	**Total**
U235	0.01	0.00	0.00	0.00	0.00	0.00	0.02	0.02
U238	0.26	0.20	0.14	0.69	0.04	0.00	0.00	0.77
Pu238	0.00	0.00	0.01	0.00	0.01	0.00	0.00	0.02
Pu239	0.23	0.03	0.13	0.06	0.24	0.00	3.90	3.92
Pu240	0.06	0.00	0.08	0.01	0.09	0.00	0.00	0.13
Pu241	0.01	0.00	0.00	0.00	0.12	0.00	0.00	0.12
Pu242	0.01	0.00	0.00	0.00	0.01	0.00	0.00	0.01
Np237	0.00	0.00	0.00	0.00	0.00	0.00	0.00	0.01
Am241	0.01	0.00	0.00	0.00	0.01	0.00	0.00	0.01
Fe56	0.07	0.08	0.00	0.24	0.00	0.00	0.00	0.27
Cr52	0.01	0.06	0.00	0.00	0.00	0.01	0.00	0.06
Zr90	0.01	0.01	0.00	0.03	0.00	0.00	0.00	0.04
Na23	0.02	0.05	0.00	0.07	0.00	0.00	0.00	0.08
B10	0.04	0.00	0.00	0.00	0.00	0.00	0.00	0.04
Total	0.36	0.23	0.20	0.73	0.29	0.01	3.90	4.01

[(a)] Upper energy boundary

Table 5. *$\Delta k/k^2$: Uncertainty Coefficients (ABTR)*

		Pu-239: Breakdown by Energy Group						
Gr.	**Energy [(a)]**	**σ_{capt}**	**σ_{el}**	**ν**	**σ_{inel}**	**σ_{fiss}**	**χ**	**Total**
1	**19.6 MeV**	0.00	0.00	0.00	0.01	0.01	0.83	0.83
2	**6.07 MeV**	0.02	0.01	0.01	0.04	0.05	1.26	1.26
3	**2.23 MeV**	0.03	0.01	0.01	0.03	0.05	0.26	0.27
4	**1.35 MeV**	0.06	0.02	0.02	0.03	0.10	0.86	0.86
5	**498 keV**	0.11	0.02	0.05	0.01	0.13	0.58	0.60
6	**183 keV**	0.11	0.01	0.09	0.01	0.13	0.30	0.36
7	**67.4 keV**	0.09	0.00	0.06	0.01	0.08	0.14	0.19
8	**24.8 keV**	0.09	0.00	0.04	0.01i	0.06	0.07	0.13
9	**9.12 keV**	0.07	0.00	0.02	0.00	0.02	0.03	0.08
10	**2.03 keV**	0.01	0.00	0.00	0.00	0.02	0.01	0.02
11	**454 eV**	0.00	0.00	0.00	0.00	0.01	0.00	0.01
12	**22.6 eV**	0.00	0.00	0.00	0.00	0.00	0.00	0.00
13	**4 eV**	0.00	0.00	0.00	0.00	0.00	0.00	0.00
14	**0.54 eV**	0.00	0.00	0.00	0.00	0.00	0.00	0.00
15	**0.1 eV**	0.00	0.00	0.00	0.00	0.00	0.00	0.00
Total		0.23	0.03	0.13	0.06	0.24	1.87	1.91

	Total Uncertainty - Breakdown by Isotope							
Isotope	**σ_{capt}**	**σ_{el}**	**ν**	**σ_{inel}**	**σ_{fiss}**	**$\sigma_{n,2n}$**	**χ**	**Total**
U235	0.01	0.00	0.00	0.00	0.00	0.00	0.01	0.02
U238	0.26	0.20	0.14	0.69	0.04	0.00	0.00	0.77
Pu238	0.00	0.00	0.01	0.00	0.01	0.00	0.00	0.02
Pu239	0.23	0.03	0.13	0.06	0.24	0.00	1.87	1.91
Pu240	0.06	0.00	0.08	0.01	0.09	0.00	0.00	0.13
Pu241	0.01	0.00	0.00	0.00	0.12	0.00	0.00	0.12
Pu242	0.01	0.00	0.00	0.00	0.01	0.00	0.00	0.01
Np237	0.00	0.00	0.00	0.00	0.00	0.00	0.00	0.01
Am241	0.01	0.00	0.00	0.00	0.01	0.00	0.00	0.01
Fe56	0.07	0.08	0.00	0.24	0.00	0.00	0.00	0.27
Cr52	0.01	0.06	0.00	0.00	0.00	0.01	0.00	0.06
Zr90	0.01	0.01	0.00	0.03	0.00	0.00	0.00	0.04
Na23	0.02	0.05	0.00	0.07	0.00	0.00	0.00	0.08
B10	0.04	0.00	0.00	0.00	0.00	0.00	0.00	0.04
Total	0.36	0.23	0.20	0.73	0.29	0.01	1.87	2.09

[(a)] Upper energy boundary

Table 6. *Fission Spectra Related Uncertainties for the KRITZ benchmarks.*

	Impact of fission spectra uncertainty [%]				
	KRITZ-2.1c	KRITZ-2.1h	KRITZ-2.13c	KRITZ-2.13h	KRITZ-2.19c
^{235}U (DOSCOV)	1.59	1.58	1.62	1.61	0.09
^{235}U (JENDL3.3)	4.06	4.03	4.14	4.11	0.24
^{238}U (JENDL3.3)	0.61	0.71	0.48	0.53	0.19
^{239}Pu (JENDL3.3)	-	-	-	-	3.68
Total (JENDL3.3)	4.10	4.09	4.16	4.14	3.70

Table 5 shows the results with the DOSCOV covariance matrix for the fission spectrum (only U-235 and Pu-239 matrices were available). The fission spectrum related uncertainties are lower than in the previous case but still very high.

KRITZ critical light water benchmark analysis

Cross-section sensitivity and uncertainty analyses of several KRITZ UO_2 and MOX critical configurations [9] were performed in the scope of the OECD international benchmark exercise. These studies, based on the SUSD3D [10] cross-section sensitivity and uncertainty package, addressed among other sources of uncertainty also those linked to the fission spectra [11]. The calculated uncertainties in k_{eff} due to the uncertainties in the fission spectra of U-235, U-238 and Pu-239 are presented in Table 6.
It can be observed that the uncertainties vary only slightly between different KRITZ configurations. Subsequently it seems that the discrepancy between the calculated and measured k_{eff}, largely varying with the configuration and the temperature, cannot be explained by the fission spectra uncertainties. Furthermore, compared to the observed discrepancies between the calculations and experiments, of the order of ~0.5 %, these uncertainties seem largely overestimated, indicating either some error compensation effects, or too-conservative covariance matrix estimations.

Conclusions

The impact of the uncertainties in the fission spectra was evaluated for an actinide burner Na-cooled fast reactor (ABTR) as well as for several KRITZ critical benchmark configurations. The information on the fission spectra covariance matrices was taken from the JENDL-3.3 [4,5] evaluation and the DOSCOV package [3]. Large differences were observed between the two with the uncertainties in k_{eff} as high as 1.5 – 4 %. The results show rather small differences between different reactor systems (fast, light water) and different configurations (UO_2, MOX). Furthermore, compared to the observed discrepancies between the calculations and experiments for KRITZ, of the order of ~0.5 %, these uncertainties seem largely overestimated, indicating either some error compensation effects (due to cross-section adjustments involving nu-bar, absorption etc.), or too-conservative covariance matrix estimations.
Possible inconsistencies in correlation matrix were observed.

References

[1] Y. I. Chang, P. J. Finck, C. Grandy, “Advanced Burner Reactor Preconceptual Design Report”, ANL-ABR-1 (Argonne National Laboratory, September 2006).
[2] G. Rimpault, et al., “The ERANOS Code and Data System for Fast Reactor Neutronic Analyses”, in Proc. of PHYSOR 2002 Conference, Seoul, South Korea, (October 2002).
[3] R.E. Maerker, J.J. Wagschal and B.L. Broadhead, “Development and Demonstration of an Advanced Methodology for LWR Dosimetry Applications. (Section 7)”, EPRI NP-2188 (December 1981), report available in “ZZ DOSCOV, 24-Group Covariance Data Library from ENDF/B-V for Dosimetry Calculation”, DLC-0090 package of NEA Data Bank collection (http://www.nea.fr/abs/html/dlc-0090.html).
[4] K. Shibata et al., JENDL-3.2 Covariance File, Proc. Nuclear Data Covariance Workshop, BNL, April 22-23, 1999, ORNL/TM-2000/19.
[5] T. Kawano, K. Shibata, “Evaluation of Covariances for Resolved Resonance Parameters of 235U, 238U and 239Pu in JENDL-3.2”, JAERI-Research 2003-001, Feb. 2003.
[6] I. Kodeli, Manual for ANGELO2 and LAMBDA codes, NEA-1264/05 package (2003).
[7] G. Chiba: ERRORJ Manual, JNC TN9520 2003-008, Sept. 2003.
[8] M. Salvatores et al., “Nuclear Data Needs for Advanced Reactor Systems. A NEA Nuclear Science Committee Initiative”, Proc. Int. Conf. ND-2007, Nice, France (April 2007).
[9] I. Remec, J.C. Gehin, R.J. Ellis, "KRITZ-2 and KRITZ-1 Experiments on Regular H2O/Fuel Pin Lattices with Low Enriched Uranium Fuel at Temperatures up to 245 C", ORNL, Sept. 2000.
[10] I. Kodeli, “Multidimensional Deterministic Nuclear Data Sensitivity and Uncertainty Code System, Method and Application,” Nucl. Sci. Eng., 138, 45-66 (2001).
[11] I. Kodeli, Sensitivity and Uncertainty Analysis of The Kritz-2 Benchmarks, in “Benchmark on the KRITZ-2 LEU and MOX Critical Experiments, Final Report”, NEA/NSC/DOC(2005)24, OCDE 2006.

Approximating large resonance parameter covariance matrices with group-wise covariance matrices for advanced nuclear fuel cycle applications

M.E. Dunn, G. Arbanas, L.C. Leal, D. Wiarda

Oak Ridge National Laboratory, P.O. Box 2008, MS6170, Oak Ridge, TN
dunnme@ornl.gov

Abstract: The large size of resonance parameter covariance matrices (RPCMs) in the actinide region often renders them problematic for dissemination via ENDF. Therefore, a method of approximating the RPCM by a much smaller group-wise covariance matrix (GWCM) is described, implemented, and examined. In this work, ^{233}U RPCM is used to generate GWCMs for the 44-group AMPX, 100-group GE, 171-group VITAMIN-C, and 240-group CSWEG. Each of these GWCMs is then used to compute group-wise uncertainties for the groups of the remaining group structures. The group-wise uncertainties thus obtained are compared with those obtained from a full RPCM, that is, without the approximation. A systematic comparison of group-wise uncertainties based on GWCMs vs RPCM, for a variety of group structures, will shed light on the validity of this approximation and may suggest which group structure(s) yield a GWCM that could be used in lieu of the RPCM.

Introduction

Complete RPCMs of ^{235}U, ^{238}U, ^{233}U, ^{239}Pu and other actinides have recently been evaluated at the Oak Ridge National Laboratory, for example [1]. Due to the large size of these RPCMs, their inclusion into ENDF files, renders these problematic for dissemination via ENDF. To illustrate, the sizes of ^{235}U, ^{238}U, ^{239}Pu, and ^{233}U RPCMs are ≈ 1.7 GB, 0.7 GB, 0.2 GB, and 0.1 GB, respectively; while the entire ENDF database is ≈ 0.5 GB in size. The proposed RPCM-to-GWCM conversion scheme is an attempt to compress the RPCM while preserving its essential information.

Methodology

A compression scheme that converts the RPCM into a group-wise covariance matrix (GWCM) is investigated for four (relatively arbitrary) group-structures: 44-group AMPX, 100-group GE, 171-group VITAMIN-C, and 240-group CSWEG. The energy boundaries of these group structures are plotted in Fig. 1. ^{233}U was chosen for this study because it has relatively few resonances, thus making computations amenable to a repetitive numerical study, and because its RPCM was recently evaluated. The analysis consists of these four steps:

1. Group-wise cross-sections and uncertainties are computed for each of the four group-structures using the ^{233}U RPCM. These computations are used as a reference for the purpose of estimating the deviations introduced by the compression scheme.
2. ^{233}U RPCM is converted into a GWCM for each of the four group structures.
3. For each group structure, cross-sections and uncertainties (standard deviations) are computed from the GWCMs of the three remaining group-structures. Namely, the 44-group GWCM is used to compute uncertainties on the 100-, 171-, and 240-group structures, the 100-group GWCM is used to do the same on the 44-, 171-, and 240-group structure, and so on.
4. Uncertainties obtained in Step 3 are compared to the reference uncertainty obtained in Step 1; large deviations would be a sign of inadequacy of a particular GWCM.

A modified PUFF-IV [2] was used to convert the RPCM, stored in ENDF File 32, into a GWCM and then to seamlessly join the GWCM with the high-energy File 33. All computations assumed a constant neutron flux. It was verified that the uncertainties obtained from GWCMs are identical to those obtained from RPCMs for the same group structure.

Results

For each group structure the total cross-section and its uncertainty were computed using RPCM and the GWCMs of the remaining three group-structures.
For each group-structure, a total cross section is plotted in the first row of Figs. 2 and 3, its standard deviations are plotted in the second row, its relative standard deviations (RSDs) are plotted in the third row, and the *relative* RSD deviations from the RPCM's RSD are plotted in the fourth row. Each group structure occupies one of the columns in Figs. 2 and 3: 44-group AMPX and the 100-group GE structures are in the left and right columns in Fig. 2, respectively; while the 171-group VITAMIN-C and the 240-group CSWEG structures are in the left and right columns in Fig. 3, respectively.
We use the RPCM computation of RSDs as a reference for determining the deviation introduced by GWCMs. This deviation is introduced when a GWCM is used to compute group-wise RSD for a group structure that is *different* from the group structure on which the GWCM was originally created. A large deviation from the RPCM RSD indicates that a GWCM may not be suitable for computations on that group structure.
The largest relative deviations of the RSD are seen when 44- and 100-group GWCMs are used to compute RSDs for the remaining three group structures: a 40–60% deviation from the RPCM RSD can be seen in narrow groups between 0.1 and 10 eV in the bottom row of plots. This may indicate that 44-group structure may not be a good candidate for a reliable GWCM.
Overall, the 240-group GWCM outperformed its counterparts on the 100- and 171-group structures. This may not be surprising because it has more grid points, which (usually) means a better approximation to the RPCM. Details of distribution of energy boundaries of a given structure may also affect the quality of GWCM computations in a specific energy range. This may explain why the 240-group GWCM had deviations comparable to those of other GWCMs on the 44-group structure, because the 44-group structure is denser than the other three below 1 eV, as seen in Fig. 1.

Conclusions

It appears that a judicious choice of energy group structure could make the RPCM-to-GWCM compression scheme viable for computations of group-wise uncertainties. A group structure with a dense grid across the entire energy range is a likely candidate. It is conceivable that a new group structure could be designed specifically to retain the most RPCM information for all common group structures. Effects of this method on uncertainties in resonance integrals and thermal cross sections, as well as on off-diagonal covariance elements, require further study.

References

[1] L. Leal et al., "ORNL Methodology for Covariance Generation for Sensitivity /Uncertainty Analysis", p.25-29 in Proceedings of the 8th Int. Conference on Nuclear Criticality Safety (ICNC 2007), Vol. II, May 28-June 1, 2007, St. Petersburg, Russia.
[2] D. Wiarda and M. E. Dunn, *PUFF-IV: A Code for Processing ENDF Uncertainty Data into Multigroup Covariance Matrices*, ORNL/TM-2006/147, Oak Ridge National Laboratory (October 2006).

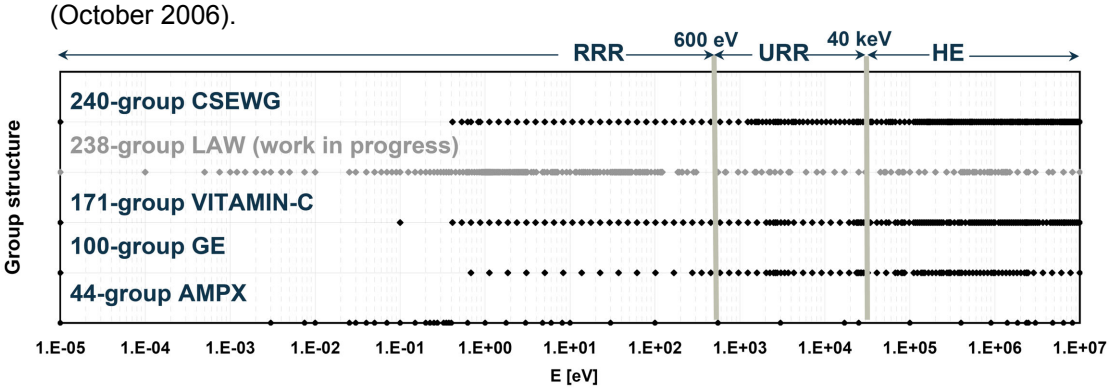

***Figure 1**. Energy grids of the four group-structures. ^{233}U energy regions are noted.*

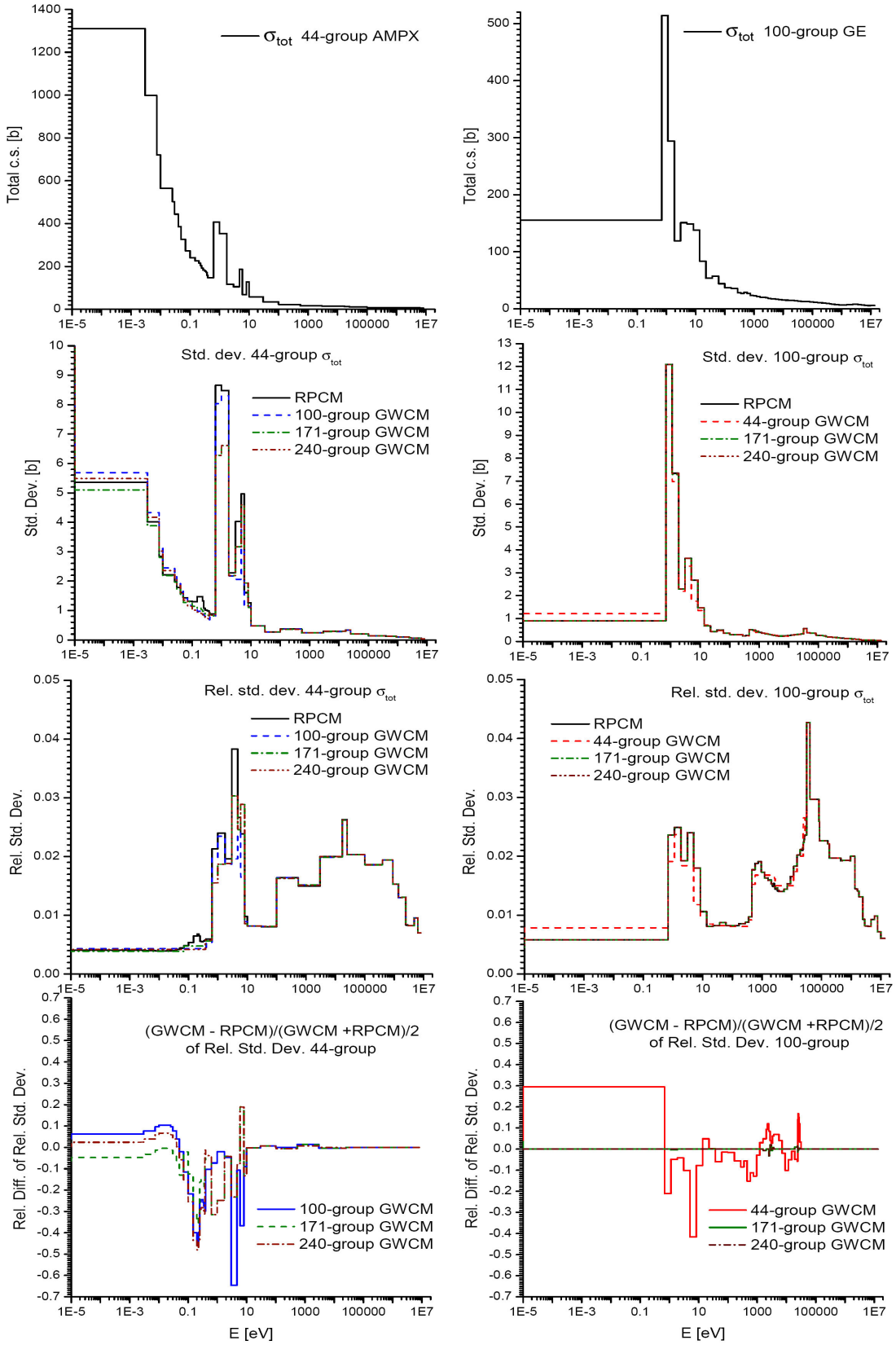

Figure 2. *Total cross section, its standard deviation, its RSD, and relative deviations from the RPCM RSD for the 44-group (left column) and the 100-group (right column).*

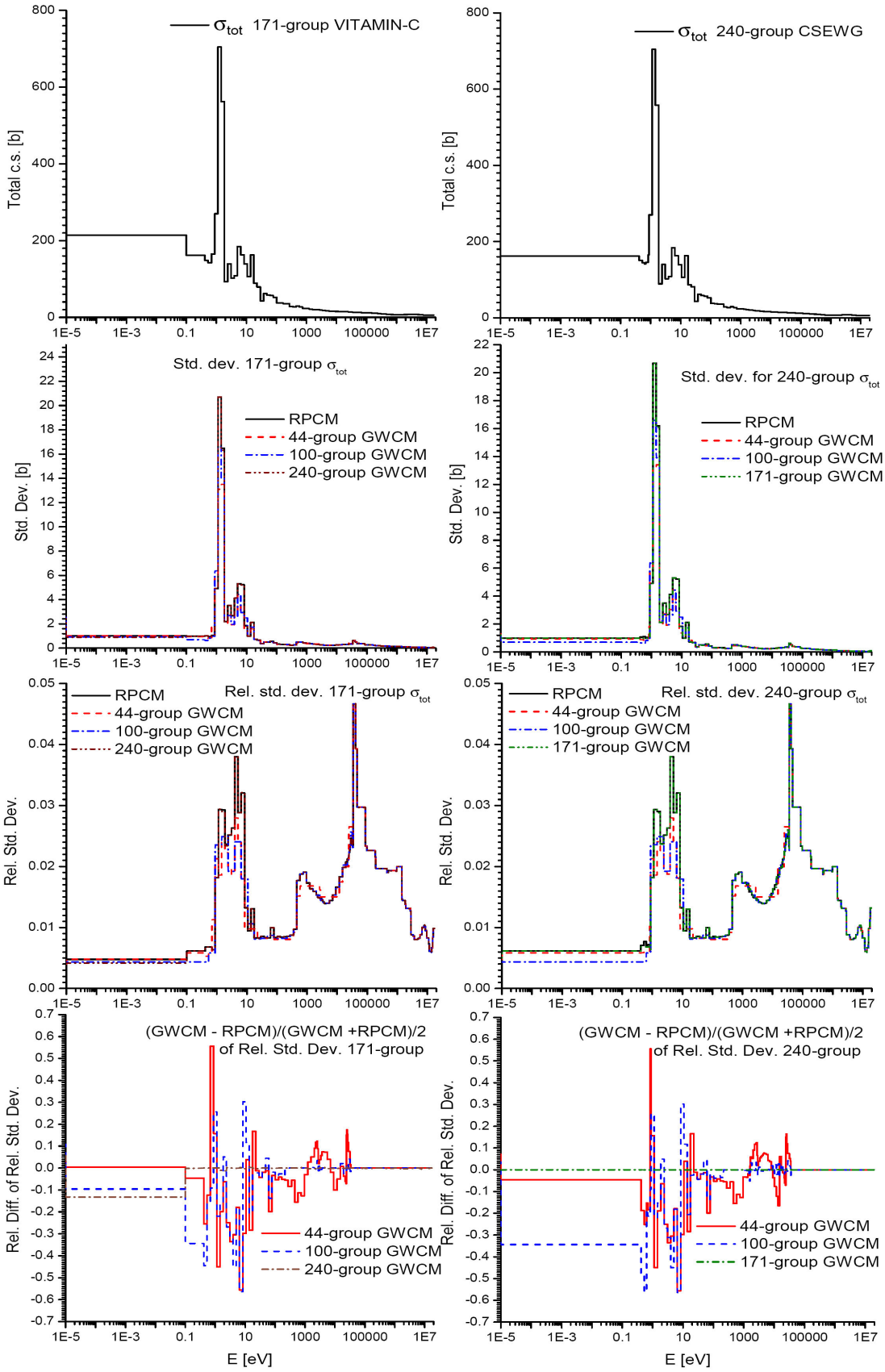

Figure 3. *Total cross section, its standard deviation, its RSD, and relative deviations from the RPCM RSD for the 171-group (left column) and the 240-group (right column).*

Neutron total and capture cross sections for Sn and Te isotopes

V. Avrigeanu, M. Avrigeanu, F.L. Roman

"Horia Hulubei" National Institute for Physics and Nuclear Engineering (IFIN-HH), P.O. Box MG-6, 077125, Bucharest-Magurele, Romania
vavrig@ifin.nipne.ro

Abstract: An analysis of the neutron total cross sections for the Sn and Te isotopes and the neutron energies up to 30 MeV, as well as of the neutron capture on the same target nuclei for the neutron energies up to 3 MeV is described. On this basis a consistent method has been adopted for the calculation of the electric dipole γ-ray strength functions $f_{E1}(E_\gamma)$ to be further involved within the study of (α,γ) reaction on Cd and Sn isotopes and the α-potential revision.

Introduction

Recent investigations of the (α,γ) reaction on Cd and Sn isotopes, of large astrophysical interest, have shown substantial discrepancies of the model predictions compared to the only few measured cross sections at sub-Coulomb energies [1-3]. While it is obvious the high sensitivity of α-particle capture reactions to the α-particle optical model potential (OMP), the analysis at the same time of the concurrent (α,n) and (α,p) reactions [2,3] might indicate that the deviation of the Hauser-Feshbach (HF) statistical-model calculations from the experimental data is not only caused by the α-potential. Therefore, before further study of the particular points of a regional α-particle OMP recently developed [4], we have looked for a better knowledge of the neutron OMP and γ-ray strength functions based on the analysis of neutron total cross sections for the Sn and Te isotopes as well as of the neutron capture on the same target nuclei.

Neutron total cross sections

First, the more recent data of the total neutron cross sections on Sn and Te isotopes [5-7] have especially been involved for the check of the corresponding predictions of the global and local neutron OMPs of Koning and Delaroche [9] at energies around and below 1 MeV (Fig. 1). While a very good agreement is found for the odd tin isotopes, an underestimation of ~15% has been found for Te isotopes.
In order to describe also the corresponding neutron resonance data [10], the local OMP parameter set for the isotope ^{128}Te has been adopted at the same time with the use of global values of the Fermi energy for each Te isotope [9]. A better agreement has thus been obtained also between the measured and calculated neutron total cross sections for the Te isotopes.

Neutron capture cross sections

Second, the already proved neutron OMP has been involved within the neutron capture analysis for the all stable isotopes of Sn and Te. The HF calculated capture cross sections have been now fully determined by the γ-ray strength functions used for the calculation of the γ-ray transmission coefficients (e.g., Refs. [11,12]). Thus the electric dipole γ-ray strength functions $f_{E1}(E_\gamma)$, of main importance for calculation of these transmission coefficients, have been obtained by means of a modified energy-dependent Breit-Wigner (EDBW) model [13,14]. The systematic correction factors F_{SR} within the EDBW formula were obtained by using the experimental average radiative widths $\Gamma_{\gamma 0}^{exp}$ of the *s*-wave neutron resonances [10] for various nuclei, and assuming that $F_{SR}=\Gamma_{\gamma 0}^{exp}/\Gamma_{\gamma 0}^{EDBW}$. Moreover, the γ-ray strength functions $f_{E1}(E_\gamma)$ thus obtained have been checked within the calculations of capture cross sections of Sn and Te isotopes for neutron energies from keV to 2–3 MeV (Fig. 2), using the OMP described above, nuclear level density parameters obtained recently within this mass region [12], and global estimations of the γ-ray strength functions for multipoles $\lambda \leq 3$ [15]. Thus

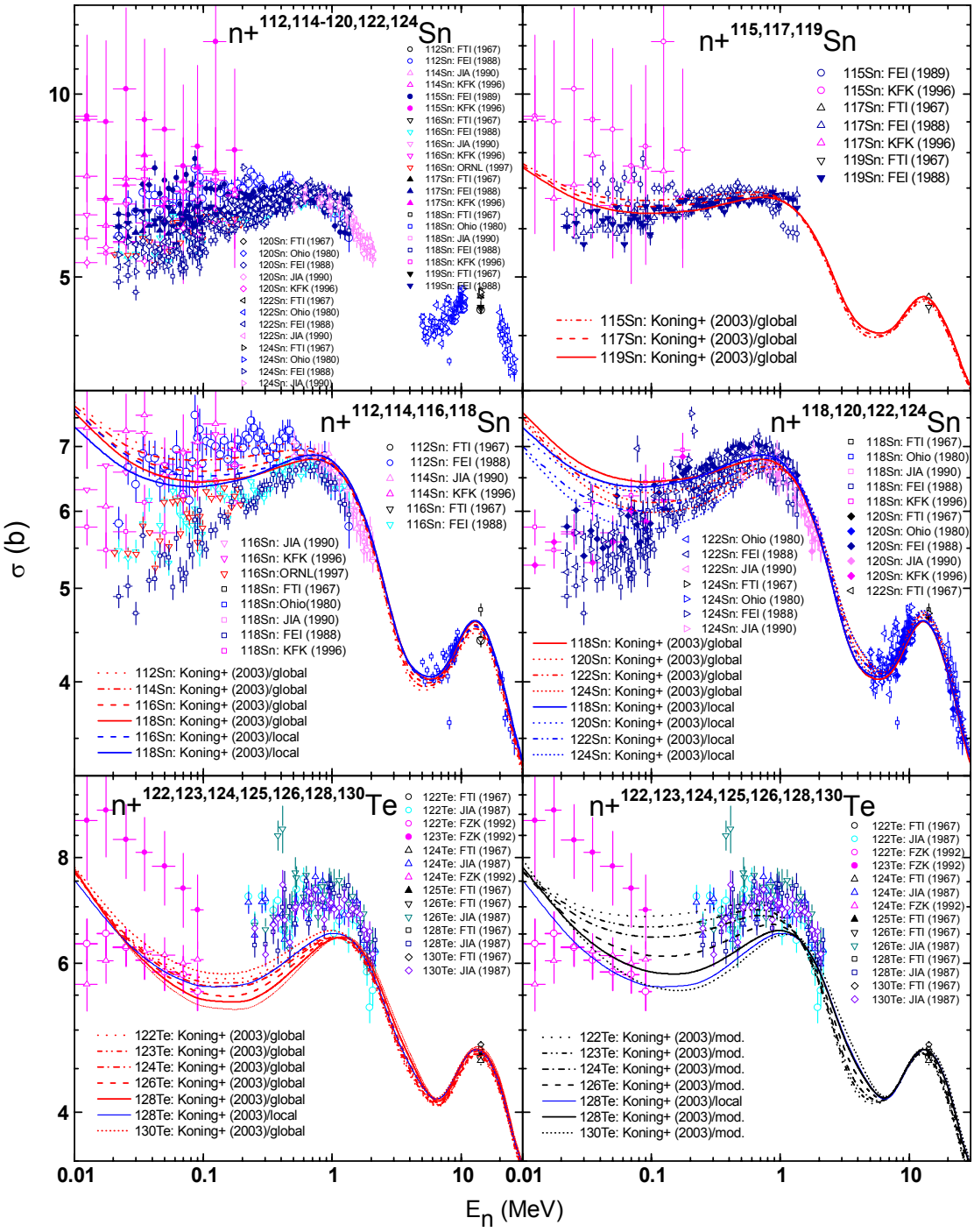

Figure 1. *Comparison of experimental [5-8] and calculated neutron total cross sections for ^{112,114,115,116,117,118,119,120,122,124}Sn and ^{122,123,124,125,126}Te isotopes with emphasis of the lower energy region.*

we have found that, unlike the case of the mass region A~90 [12] where the RIPL-2 values [10] for the experimental average radiative widths $\Gamma_{\gamma 0}$ are related to γ-ray strength functions providing a suitable descriptions of the capture data, the RIPL radiative widths correspond in the present case to calculated capture cross sections that are too large with respect to the experimental data (a similar case has been found in the mass ranges A~60 [11] and A~180 [16]). In Fig. 2 are shown also the average radiative widths corresponding to good agreement with the capture data, leading to an appropriate estimation of the EDBW model correction factors, while in Fig. 3 is shown a systematics of the capture cross sections analyzed in this work change, in relation with the variation of the neutron binding energy of de-exciting nuclei.

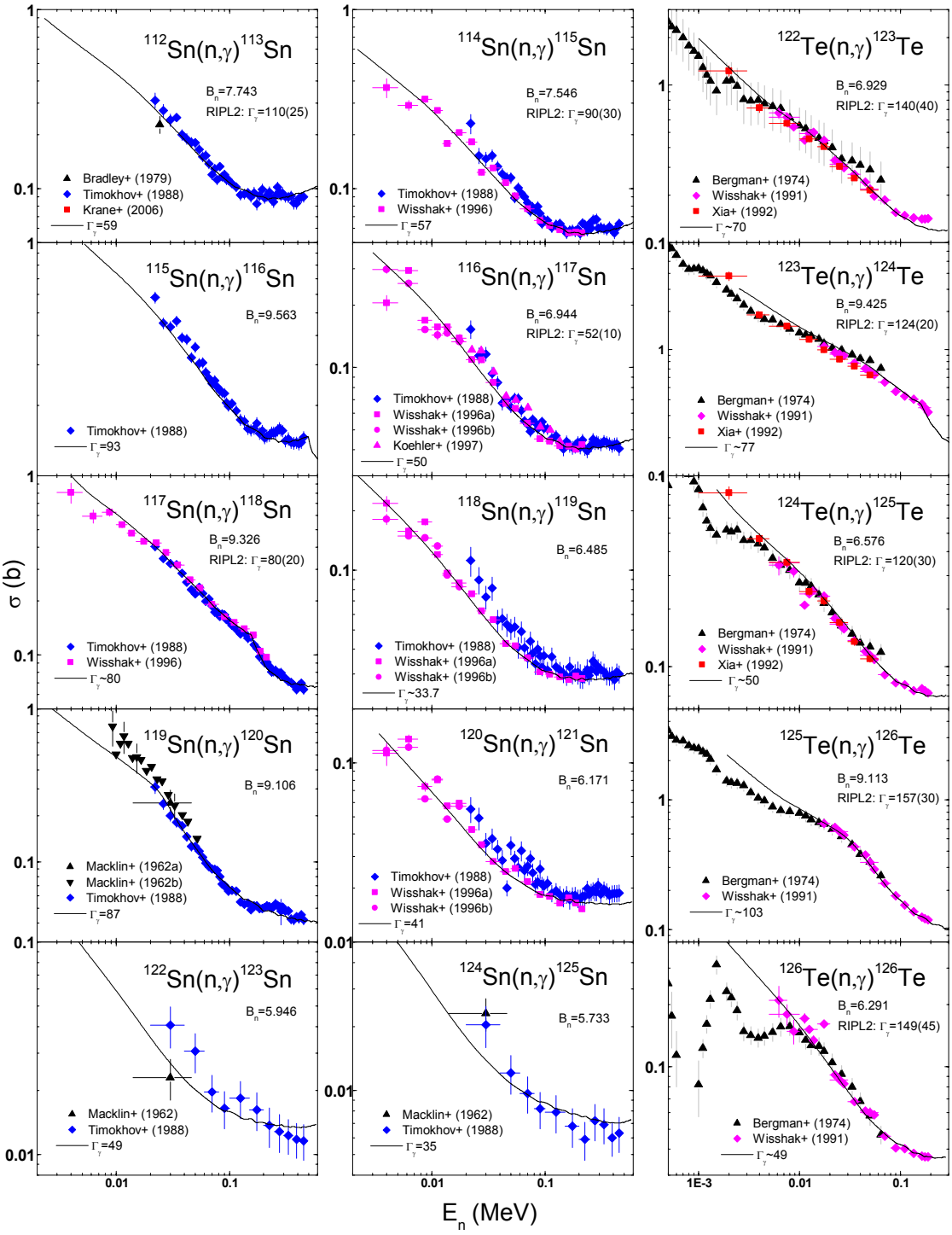

Figure 2. *Comparison of experimental [5-8] and calculated neutron capture cross sections for the ^{112,114,115,116,117,118,119,120,122,124}Sn and ^{122,123,124,125,126}Te isotopes corresponding to the calculated average radiative widths (in meV) at the neutron binding energies (in MeV) shown for each target isotope.*

Finally, based on this analysis, a consistent method has been adopted also for the calculation of the electric dipole γ-ray strength functions $f_{E1}(E_\gamma)$ to be further involved within the study of (α,γ) reaction on Cd and Sn isotopes and the α-potential revision without additional effects due to eventually less appropriate γ-ray transmission coefficients.

Acknowledgements
Work supported under contract of Association EURATOM/MEdCT-Bucharest, and MEdCT Contract No. CEEX-05-D10-48.

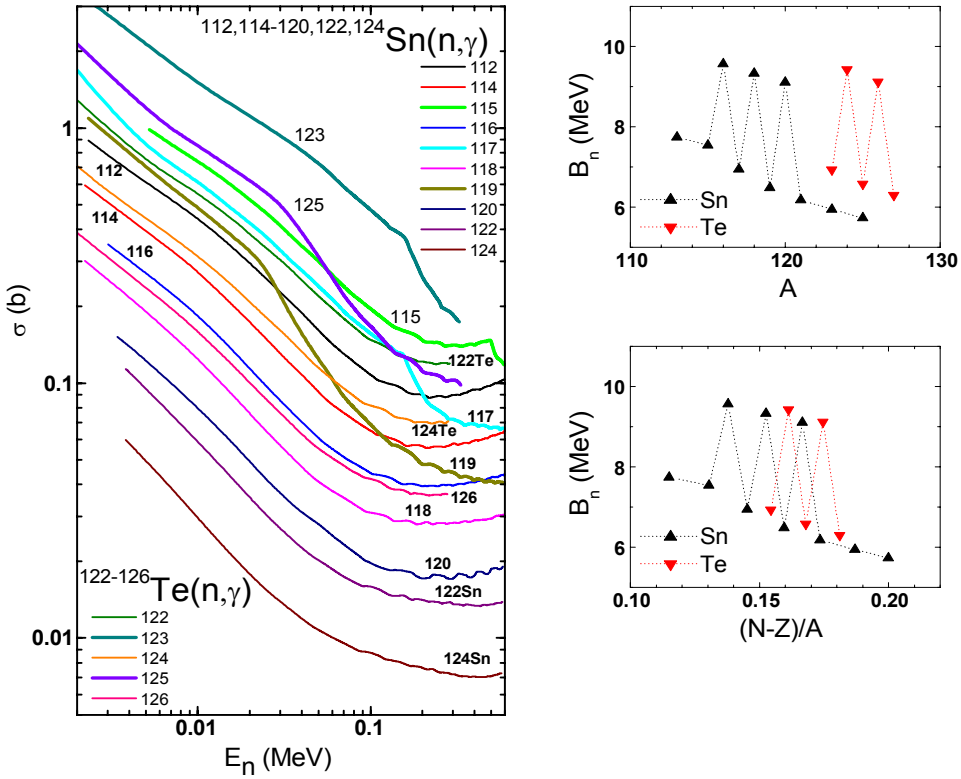

Figure 3. *(left) Systematics of the calculated neutron capture cross sections for the Sn and Te stables isotopes, and (right) the change of the neutron binding energy corresponding to each residual nucleus with the atomic mass number (top) and nuclear asymmetry (bottom).*

References

[1] S. Harissopulos, A. Lagoyannis, A. Spyrou, Ch. Zarkadas, S. Galanopoulos, G. Perdikakis, H-W. Becker, C. Rolfs, F. Strieder, R. Kunz, M. Fey, J.W. Hammer, A. Dewald, K-O. Zell, P. von Brentano, R. Julin, and P. Demetriou, J. Phys. G: Nucl. Part. Phys. 31, S1417 (2005).

[2] Gy. Gyürky, G.G. Kiss, Z. Elekes, Zs. Fülöp, E. Samorjai, A. Palumbo, J. Görres, H.Y. Lee, W. Rapp, M. Wiescher, N. Özkan, R.T. Güray, G. Efe, and T. Rauscher, Phys. Rev. C 74, 025805 (2006).

[3] N. Özkan, G. Efe, R.T. Güray, A. Palumbo, J. Görres, H.Y. Lee, L.O. Lamm, W. Rapp, E. Stech, M. Wiescher, G. Gyürky, Zs. Fülöp, E. Samorjai, Phys. Rev. C 75, 025801 (2007).

[4] M. Avrigeanu, W. von Oertzen, A.J.M. Plompen, V. Avrigeanu, Nucl. Phys. A 723**,** 104 (2003); M. Avrigeanu, W. von Oertzen, and V. Avrigeanu, Nucl. Phys. A 764**,** 246 (2006).

[5] K. Wisshak, F. Voss, Ch. Theis, F. Käppeler, K. Guber, L. Kazakov, N. Kornilov, and G. Reffo, Phys. Rev. C 54, 1451 (1996).

[6] P.E. Koehler, J.A. Harvey, R.R. Winters, K.H. Guber, and R.R. Spencer, Phys. Rev. C 64, 065802 (2001).

[7] Y. Xia, T.W. Gerstenhöfer, S. Jaag, F. Käppeler, and K. Wisshak, Phys. Rev. C 45, 2487 (1992).

[8] *EXFOR Nuclear reaction data*, http://www-nds.iaea.or.at/exfor/.

[9] A.J. Koning and J.P. Delaroche, Nucl. Phys. A 713, 231 (2003).

[10] IAEA-CRP Reference Input Parameter Library (RIPL-2), http://www-nds.iaea.org/RIPL-2/.

[11] V. Semkova, V. Avrigeanu, T. Glodariu, A.J. Koning, A.J.M. Plompen, D.L. Smith, S. Sudar, Nucl. Phys. A 730, 255 (2004).

[12] P. Reimer, V. Avrigeanu, S. Chuvaev, A.A. Filatenkov, T. Glodariu, A.J. Koning, A.J.M. Plompen, S.M. Qaim, D.L. Smith, H. Weigmann, Phys. Rev. C 71, 044617 (2005).

[13] D.G. Gardner and F.S. Dietrich, Report UCRL-82998, LLNL-Livermore, 1979.

[14] M. Avrigeanu, V. Avrigeanu, G. Cata, and M. Ivascu, Rev. Roum. Phys. 32, 837 (1987).

[15] C.H. Johnson, Phys. Rev. C 16, 2238 (1977).

[16] V. Avrigeanu, S.V. Chuvaev, R. Eichin, A.A. Filatenkov, R.A. Forrest, H. Freiesleben, M. Herman, A.J. Koning, K. Seidel, Nucl. Phys. A 765, 1 (2006).

Neutron- vs. proton-induced reactions in pre-equilibrium models

E. Běták[1,2)]

1) Institute of Physics, Slovak Academy of Sciences, 84511 Bratislava, Slovakia
2) Fac. of Philosophy and Sci., Silesian University, 74601 Opava, Czech Republic
betak@savba.sk

Abstract: The pre-equilibrium exciton model is deeply based on the use of level densities and (some form of) effective interactions. Very frequently, the one-component description (not distinguishing between the neutrons and the protons) is used, and the charge differences are introduced by means of effective charge factors. The relative strength of the neutron-proton interaction with respect to that of the proton-proton (or neutron-neutron) pairs is either considered to be irrelevant or it is approximated by that of the free nucleon-nucleon scattering. However, recent experiments indicate that the interaction between the neutron and the proton is much stronger than between two neutrons or two protons in real nuclei than it is for free nucleons. This fact influences the relative strengths of the neutron and the proton channels, and therefore it makes some difference on other calculated cross sections as well.

Introduction

The pre-equilibrium exciton model entered its fifth decade and with the appearance of th new-generation "do-all" codes, like EMPIRE-II [1] or TALYS [2, 3], the model gains certain popularity and its second youth. Typically, the pre-equilibrium description is an one-component one, i.e. not distinguishing between the neutrons and the protons. To compensate this handicap, an effective charge factor is introduced into the one-component formulation, which is doing majority of the effect. Introduction of such charge factor into the equations is not without problems, and - in fact – all such factors introduced till now can be easily shown to be incorrect in one or another aspect (see Ref. [4] for more detailed discussion). In some (very infrequent) cases, however, a real two-component formulation is applied, what is physically more justified. Two questions remain open in this approach:
First, we do not have enough reliable information about the two-component exciton level densities and those which we use, are strongly dependent on model assumptions.
Second, whereas there is just one squared effective matrix $|M|^2$ element responsible for the equilibration process in the one-component case, we have three matrix elements in the two-component formulation, namely $|M_{\pi\pi}|^2$, $|M_{\nu\nu}|^2$ and $|M_{\pi\nu}|^2$. The two first of them, describing proton-proton and neutron-neutron scatterings, are equal, whereas the third one can be written as [2, 5]

$$|M_{\pi\nu}|^2 = R \,.\, |M_{\nu\nu}|^2 \,. \qquad (1)$$

In the first detailed pre-equilibrium study of two-component formulation of the exciton model [5], this factor was taken to be 2.89, what corresponds to the free neutron-proton scattering [6 - 8]. The typical value used in the code TALYS – which is fully two-component formulation of the problem – is 1.5 [2]. However, several very recent experiments [9 - 11] indicate that - at least at somewhat higher energies - the neutron-proton correlations in nuclei are much stronger than would correspond to this usually adopted value. To the best of our knowledge, there are no data (yet) directly applicable to energies and nuclei typical for the pre-equilibrium exciton model. But if such effect appears to be confirmed also for heavier nuclei and energies of just few tens of MeV, the predictions of the pre-equilibrium model calculations should be modified. Below, we try to see how and in which aspect one can expect the change.

Nucleon emission rates

Following the general philosophy and ignoring the even-odd effects, the exciton model calculation of nucleon-induced reactions should start from an 1-exciton state, $n_0=1$. However, if we consider the nucleon emission only, the full strength of the 1-exciton state is transferred via a particle-hole pair creation into a 3-exciton state, $n=3$, and the nucleon emission can start only from here. This is a reason why the earlier analyses considered the 3-exciton state to be the initial configuration for the pre-equilibrium decay.

Let us illustrate the effect using simple considerations, applicable (to some extent) also to the one-component formulation with the effective charge factors (cf. also [5, 12, 13]), and consider e.g. the reactions induced by neutrons. The initial stage contains just 1 particle, which is obviously the neutron. The 3-exciton state is of 2 excited particles; one of them is neutron, and the other one is – if we ignore the differences of interaction between the like and that of the unlike pairs and if we assume that all nucleons of the composite system can be excited with equal probability – a (further) neutron with a probability ~N, and a proton with a probability ~Z. Thus, the ratio of the charge-dependent parts of the neutron to the proton emission from the 3-exciton state (which is essentially responsible for the hardest part of the emission) are

$$(1+N/A) / (Z/A) = 1 + 2N/Z \qquad (2)$$

(yielding a value of 3 for the extremely simplified case of $Z=N$ and $g_\pi=g_\nu$), whereas if we introduce the different strength of the interaction between the like and the unlike pairs of nucleons, this ratio becomes

$$(1 + (RZ+AN)/(A(RZ+N)) \ / \ (ARZ/(RZ+N)) \ , \qquad (3)$$

what gives a value of 1.15, i.e. nearly 3x less than in the "old" approach, if we adopt the value of $R=10$. Thus, the ratio of the neutron-to proton emissions, and especially its hard part, is sensitive to the new findings of the relative strengths of the nucleon interaction, if the reported effect takes place also at energies of several tens of MeV and in nuclei heavier than carbon. Of course, we have illustrated the effect on its most pronounced case – it becomes weaker as we attain equilibrium. One has to remind here that there is still less success to reproduce the absolute values of the unlike nucleon emission in the pre-equilibrium model than it is from other reactions (cf. [14]).

Equilibration rates

Influencing the neutron-to-proton emission ratio is not the only possible manifestation of unexpectedly strong neutron-proton interaction observed in some reactions. The other way is the modification of the transition rates, i.e. those leading towards equilibrium. As in the preceding chapter, the strength of this effect decreases with increasing complexity of the stage of the reaction, and it is expected to be most pronounced for the $n=1$ state. As derived in [5] (though R was taken from free nucleon-nucleon scattering there only), the ratio of the proton particle-hole pair creation to that of neutron for the $n=1$ configuration is

$$\lambda_\pi^+ / \lambda_\nu^+ = 2 R \ . \qquad (4)$$

Usually, the absolute value of the squared transition matrix element $|M|^2$ is fixed by the emission from the $n=3$ state, which is the dominant one for the hard portion of nucleon spectra in nucleon-induced reactions, so that one cannot expect much effect for the nucleon emission (which itself is impossible from the $n=1$ state).

However, there is a completely different situation for γ's. There, the essential part of hard γ spectra comes out from the $n=1$ state, whose lifetime is determined just by the transition to the $n=3$ state (the influence on the γ emission was not considered in [5]). As the γ emission is weak, it does not influence significantly that of nucleons, but the reverse statement is not true. If we change the (total) transition rates from $n=1$ to $n=3$ significantly, the hardest portion of the γ emission changes by the same factor in the reversed direction.

If we now add the fact that a great majority of stable or semi-stable nuclei (which serve as targets for nuclear reactions) has both more neutrons than protons, and in addition they often have some neutron skin (even if not very thick – e.g., the typical thickness for ^{208}Pb is close to 0.15 - 0.20 fm [15 - 17]), we come to a conclusion that there is a significant and principal difference of the γ emission from proton- with respect to the neutron-induced reactions.

Conclusions

Recent experiments (though in light nuclei and at energies of several hundred MeV) showed that the neutron-proton interaction is much stronger with respect to that between the neutron or between the proton pairs than it is for free nucleons. If this effect is confirmed also for heavier nuclei and somewhat lower energies, it should have significant influence on the neutron-to-proton emission rate and it should also create a clear distinction between the γ emisison in proton and neutron radiative capture. We have indicated how the most sensitive quantities should behave and what size of the effect may be expected.

Acknowledgements
The work has bee supported by VEGA Grant No. 2/7115/27. The subsidy of the participance of the author at the NEMEA-4 workshop is cordially accepted.

References

[1] M. Herman, P. Obložinský, R. Capote, A. Trkov, V. Zerkin, M. Sin, B. Carlson, "EMPIRE modular system for nuclear reaction calculations (version 2.19 Lodi)", Report NNDC-BNL, Upton, USA 2005.
[2] A.J. Koning, M.C. Duijvestijn, Nucl. Phys. A744, 15 (2004).
[3] A. Koning, S. Hilaire, M. Duijvestijn, "TALYS: A nuclear reaction program", Report 21297/04.62741/P FAI/AK/AK, NRG Petten 2004.
[4] E. Běták, P.E. Hodgson, Rep. Prog. Phys. 61, 483 (1998).
[5] J. Dobeš, E. Běták, Z. Phys. A310, 329 (1983).
[6] N. Metropolis, R. Bivins, M. Storm, A. Turkevich, J.M. Miller, G. Friedlander, Phys. Rev. 110, 185 (1958).
[7] K. Kikuchi, M. Kawai, "Nuclear Matter and Nuclear Reactions", North-Holland 1968.
[8] I. Kumabe, K. Fukuda, M. Matoba, Phys. Lett. 92B, 15 (1980).
[9] A. Tang et al., Phys. Rev. Letts. 90, 042301 (2003).
[10] E. Piasetzky, M. Sargsian, L. Frankfurt, M. Strikman, J.M. Watson, Phys. Rev. Letts. 97, 162504 (2006).
[11] R. Subedi, "Large study of short-range correlations in 12C(e,e'pn)", APS Meeting Abstracts, Div. Nucl. Phys., Oct. 25-28, 2006, abstract BC.005.
[12] C.K. Cline, Nucl. Phys. A193, 417 (1972).
[13] C. Kalbach, Z. Phys. A283, 401 (1977).
[14] M.B. Chadwick, T. Kawano, "Off-stability nuclear reaction theory predictions for actinides", FINUSTAR-2 conference, Agios Nikolaos, Greece, 10-14 September 2007.
[15] G. Shen, J. Li, G.C. Hillhouse, J. Meng, Phys. Rev. C71, 015802 (2005); E C76, 029902(E) (2007).
[16] B. Klos et al., Phys. Rev. C76, 014311 (2007).
[17] B. Alex Brown, G. Shen, G.C. Hillhouse, J. Meng, A. Trzcinska, Phys. Rev. C76, 034305 (2007).

Characterisation of delayed gammas for detection of U-235 in nuclear waste barrels

P.M. Dighe[1)], E. Berthoumieux[1)], D. Doré[1)], J.M. Laborie[2)], X. Ledoux[2)], V. Macary[1)] and D. Ridikas[1)]

1) CEA/DSM Saclay, DAPNIA/SPhN, 91191 Gif-sur-Yvette, France
2) CEA/DAM Ile-de-France, DPTA/SPN, 91680 Bruyères-le-Châtel, France
priyamvada.dighe@cea.fr

Abstract: High penetrating property of delayed gammas above 3MeV can be very useful to detect nuclear materials in shielded waste packages. At present no information is available on the lumped decay groups of delayed gammas after fission of actinides. Therefore, under the INPHO project (INterrogation PHOtonique), the experimental work is being carried out to deduce gamma decay parameters for various nuclear materials. In this work the delayed gamma spectra produced after photo fission have been examined for the detection and quantification of U-235. For this purpose the highly enriched U-235 target was irradiated by high energy bremsstrahlung photons. The decay gamma spectra were measured using two BGO detectors right after the irradiation in cycles to increase the statistics. The delayed gamma groups were analysed with the support of theoretical yield of precursors (fission products) obtained from the ABLA code predictions. The experimental decay spectra then were globally fitted to extract the lumped decay group parameters for U-235. These new data are extremely important for the non-destructive characterization of the waste barrels and complement our experiments already performed with Th-232 and U-238 targets.

Introduction

For the non destructive assessment of nuclear waste barrels, a photo fission method can be very powerful for detection and quantification of the content of fissile material. The β-delayed γ rays and neutrons emitted form the fission products can be used for the assessment of fissile material. High energy (> 3MeV) decay gammas might offer better sensitivity to the detection of fissile material as compared to the delayed neutrons. The delayed gammas produced after fission have specific energy and decay time characteristics. Some reports are available on the detection of delayed gammas for interrogation of fissile materials [1], [2], [3]. However, the systematic studies of both relative and absolute yields of delayed photons above 3MeV and construction of lumped decay groups in particular are not yet established. Within the INPHO project we performed a number of experiments with Th-232 and U-238 targets, and some efforts were already made to extract the lumped decay groups [4]. Nevertheless, at the same time the information produced was not sufficient. In the present paper we report on the innovative approach how the lumped decay groups with unique weight factors for delayed gammas can be obtained in the case of the U-235 target. We also show that these decay groups are reproducing the experimental decay spectra after different irradiation conditions, what ultimately helps in optimisation of the method in detection and quantification of fissile materials using high energy decay photons.

Experiment

The experiment was conducted with highly enriched U-235 target at ELSA electron accelerator facility of CEA/DIF/DPTA located in Bruyères-le-Châtel. The electron beam of 15 MeV energy, 300mA peak current, 70μs pulse duration and 1Hz pulse repetition rate was impinged on Tantalum target-converter to produce bremsstrahlung photons. The bremsstrahlung beam was collimated using the lead collimator. The high energy photons (> 6 MeV) induced photo-fission in the U-235 target. The delayed gammas emitted from the decaying fission fragments were measured with the help of two Saint-Gobain BGO detectors (ref. 76576), known for their high efficiency to high energy gamma photons and resistance to neutron radiation. Fig. 1 represents the schematic of experimental set-up. The U-235 target was placed at 234 cm distance from the Tantalum converter. The fissile target was enclosed in cadmium box to avoid further fission reactions caused by the scattered thermal neutrons. The BGO detectors were placed at 37cm distance from the target and were enclosed in

paraffin wax of 10cm thickness to reduce the background. The energy calibration of BGO's was carried out with the Y-88 source. To ensure correctness of energy calibration, the drift in the energy peak (mainly due to the temperature variations) was monitored periodically during the course of experiments. The irradiations were repeated over a number of cycles and the histograms were plotted by summing the data for better statistics.

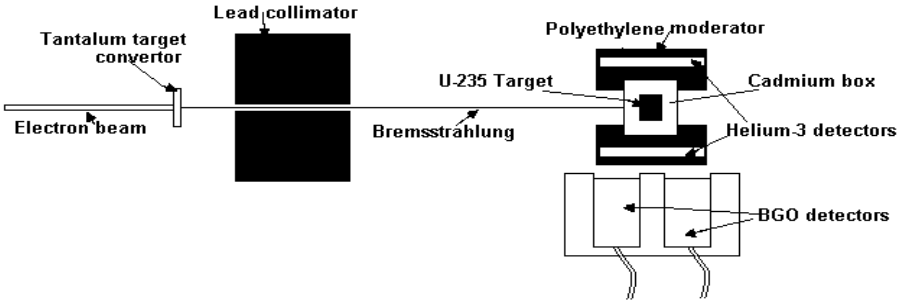

Figure 1. *Schematic diagram of the experimental set-up for delayed photon measurements after photofission of U-235.*

Results and discussions

The experimental decay spectra was obtained for 300s, 60s, 10s and 1macro irradiation durations. The energy cut was set at 3MeV. Therefore the decay spectra were composed of gamma photons above 3MeV energy emitted from decaying nuclides after photo fission. In addition to signal counts some high energy background counts were also present due to induced activity produced in surrounding material and also from natural background, which was quantified during irradiations without target.

The decay spectra of delayed photons in equilibrium can be represented as a sum of exponentials as given in the following equation:

$$F(t) = \sum_{i=1}^{N} Ai \exp(-\lambda_i t) \qquad \text{Eq.(1)}$$

where, *Ai* is weight factor, λi is decay constant and *t* is time elapsed after infinite irradiation. However, since the target irradiation was finite and cyclic due to pulsed beam, correction for the pulsed and repetitive beam in equation 1 had to be carried out as presented below:

$$F(t) = \sum_{i=1}^{N} Ai \ \exp(-\lambda_i t)\, T^{i}_{const}\ T^{i}_{pulse}\ T^{i}_{rep}$$

$$T^{i}_{const} = 1 - \exp(-\lambda_i T_{irr})$$

$$T^{i}_{pulse} = \frac{T_{irr}}{n\,\tau} \frac{1 - \exp(-\lambda_i T_{irr})}{1 - \exp(-\lambda_i T_{period})} \qquad \text{Eq. (2)}$$

$$T^{i}_{rep} = \left(\frac{1}{1 - \exp\left(-\lambda_i T_{cycle}\right)} \right) \left(1 - \frac{1 - \exp(-\lambda_i T_{cycle}\ N_{cycle})}{N_{cycle}\ (1 - \exp(-\lambda_i T_{cycle}))} \right)$$

where, T_{irr}, T_{period}, T_{cycle} are irradiation time, period time and cycle time respectively. N_{cycle} is a number of pulses and τ is the duration of pulse.

The delayed gamma spectra are composed of decay of a huge number of precursors with variable half lives. Therefore it is more convenient to group the half lives of precursors into small numbers which can independently reproduce the experimentally obtained decay curve with desired accuracy. In this context our aim was to extract the minimum necessary decay groups λi with corresponding weight factors *Ai* using equation 2 from experimental decay spectra of U-235 target.

We found that nearly more than 500 known precursors with half lives in the range from ~0.2 sec to ~2000 sec are contributing to the decay spectrum ($E\gamma$ > 3MeV). Due to almost uniform spread in half lives (see Fig. 2A) it is very difficult to lump them into several groups using weighted sum technique. At the same time, we realized that in the absence of any initial parameters it is not feasible to extract groups from the experimental curves. This difficulty was

addressed with the help of theoretical decay groups of delayed photons. The photofission fragment yields of beta delayed precursors were initially calculated [5] using the ABLA fission-evaporation code (GSI). Afterwards, cumulative yields were obtained using the CINDER90 evolution code (LANL). Out of these isotopes most contributing isotopes with half lives less than 1000 sec were selected to extract theoretical decay groups. In this way the *Ai*'s were theoretically estimated by multiplying the yield of the isotopes obtained from the code and photon intensity above 3MeV obtained from nuclear data tables. With the help of these selected precursors theoretical decay spectra were derived as shown in Fig. 2B. The lumped decay groups *Ai* were then extracted by fitting this theoretical curve using Eq. 1 by least square method. The decay groups with weight factors were finalised for minimum χ^2 value. These groups (see Table 1) were then used as initial guess parameters to finally obtain decay groups from the experimental decay spectra.

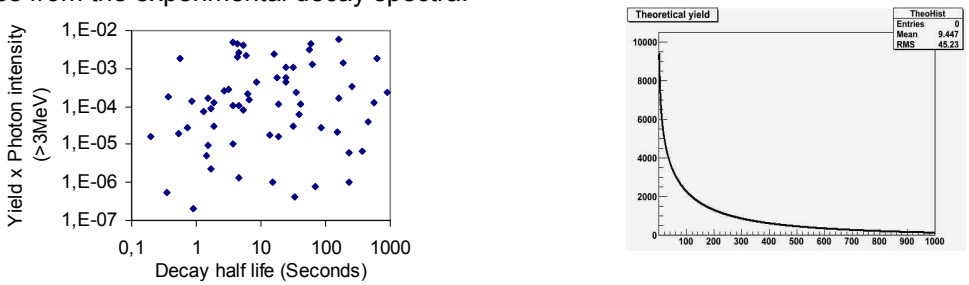

(A) (B)

Figure 2. *(A) Selected most contributing precursors with the fission fragment yields obtained using ABLA predictions [5]; (B) Constructed theoretical decay spectra from the most contributing precursors.*

The goal being reproduce all measured decay spectra, therefore the data from all four irradiations were fitted simultaneously (see Fig. 3). The histograms were filled with variable bin width with 5% error to retain the time information of shortest decay group. The fit to the curve was carried out by reduced χ^2 method and goodness of fit was deduced from χ^2 to degree of freedom ratio close to one.

Table 1. *The delayed photon decay groups (preliminary) for the photofission on the U-235 target: both values extracted from theoretical and experimental decay curves are shown.*

	Decay groups (theory)		Decay groups (experiment) by keeping $T_{(1/2)}$ constant (as obtained from theory)
	$T_{(1/2)}$	*Ai* (%)	*Ai* (%)
	446.0	7.5	15.6
	120.6	19.6	16.4
	38.6	19.3	29.2
	10.8	9.9	7.0
	4.3	38.7	21.5
	0.7	4.4	10.0
χ^2/NDF	1.56		1.01

Some attempts were made to extract different numbers of decay groups. The best fit was obtained using the six decay group approach. The theoretically obtained six decay group curves were compared to experimental spectra without any variation. For this analysis the χ^2/NDF ratio was close to 1.5 with the relative error below 10%. This indicates that the theoretically obtained parameters are very close to the experimental values and can reproduce the decay spectra in very close proximity.

Finally the fit was enhanced by varying the weight factor *Ai* only and keeping the theoretically obtained half lives $T_{1/2}$ constant. The final fit was obtained with χ^2/NDF ratio as 1.01 (Fig. 3).

We note that the values of *Ai* obtained using the theoretical curve differ from the experimentally obtained values. This variation could be partly explained that in our model predictions only the most contributing nuclides were selected to evaluate theoretical decay spectra. Table 1 summarises the values of six decay groups obtained from the fit on both theoretical and experimental decay spectra.

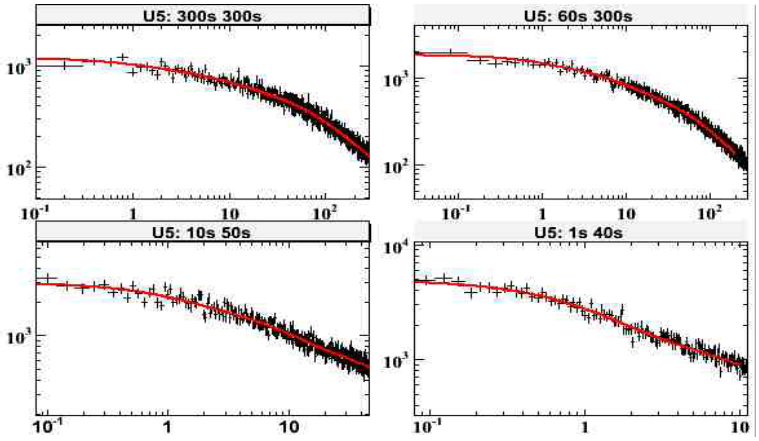

Figure 3. *Final global fit to the experimental delayed gamma decay curves (counting rate versus decay time) of U-235 after photofission.*

Finally we note that the background spectra due to the activation of cadmium box were independently measured for all the irradiations without target. From these background spectra time dependent decay parameters were deduced and were employed to eliminate the interfering background effect.

Conclusions

There is an urgent need for characterization of high energy delayed gammas emitted after photofission for the non-destructive characterization of the waste barrels. Our experiment performed with the U-235 target complements our earlier work already reported with Th-232 and U-238 targets. The experimental strategy was conducted with great care to minimise the interfering background counts produced due to surrounding material and thermal neutron induced fission. The irradiations were repeated over a number of cycles to reduce the statistical errors. The energy calibration was done continuously during the experiment to ensure correctness of 3MeV energy cut. The measurements were done with two identical high efficiency BGO detectors.
In this work the complexity of evaluation of lumped decay groups for delayed photons emitted above 3MeV has been greatly solved with the support of theoretical decay groups. The unique global decay group parameters for U-235 were obtained for the 1st time with a good accuracy. We note separately that already theoretical decay groups were able to reproduce the experimental decay spectra within 10% uncertainty. In the future experiment, the highly enriched Np-237 and Pu-239 target will be analysed using similar method to deduce the decay parameters of high-energy delayed photons.

Acknowledgements
The authors are grateful to the ELSA facility team for providing us a high quality beam and to the CEA DEN/DPA for their financial support within the INPHO project.

References

[1] C.L. Hollas, D.A. Close and C.E. Moss, “Analysis of fissionable material using delayed gamma rays from photofission” NIM. B24/B25 (1987) 503.
[2] M. Gmar and J. M. Capdevila “Use of delayed gamma spectra for detection of actinides (U,Pu) by photofission” NIM A, Volume 422, Issues 1-3, 11 February 1999.
[3] E.B. Norman et al., “Signatures of fissile materials: high-energy gammas rays following fission”, NIM A 521 (2004) 608-610.
[4] S. Boyer et al., "Delayed gammas detection technique for nuclear waste characterization", Proc. of NEMEA-3, Borovets, Bulgaria, October 25-28, 2006.
[5] D. Doré et al.,”Delayed neutron yields and spectra from photofission of actinides with bremsstrahlung photons below 20 MeV”, Journal of Physics: Conference Series 41 (2006) 241.

High sensitivity prompt neutron method for bulk hydrogen analysis

R. Dóczi[1)], J. Csikai[1,2)]

1) Institute of Nuclear Research of the Hungarian Academy of Sciences, 4001 Debrecen, Pf. 51, Hungary
2) Institute of Experimental Physics, University of Debrecen, 4010 Debrecen-10, Pf. 105, Hungary
drita@atomki.hu

Abstract: Previous methods developed for bulk hydrogen analysis completed with the determination of C/H atomic ratio were improved by prompt detection of thermal neutrons in both cases using small-size BF_3 proportional counters. Results indicate not only the advantages in the routine use of the two methods but also their higher sensitivities as compared to the activation technique applied in our previous investigations. These results render the industrial applications also possible.

Experimental procedure

The importance of the bulk hydrogen analysis and the related techniques and methods have been described in detail elsewhere [1,2]. The principle and the comparison of the neutron slowing down and the neutron reflection techniques can be found in several references [3-6].
In the present experiment the neutron slowing down method was used. Neutrons thermalized by the hydrogenous samples have been detected by a small BF_3 counter (see Figure 1) instead of a set of activation foils. The experimental arrangements for the Dy foil activation and the new prompt method based on the detection of thermalized epithermal neutrons in the samples by a BF_3 tube can be seen in Figure 2.

Figure 1. *Devices and experimental arrangement for the high sensitivity prompt method using BF_3 counter.*

a)

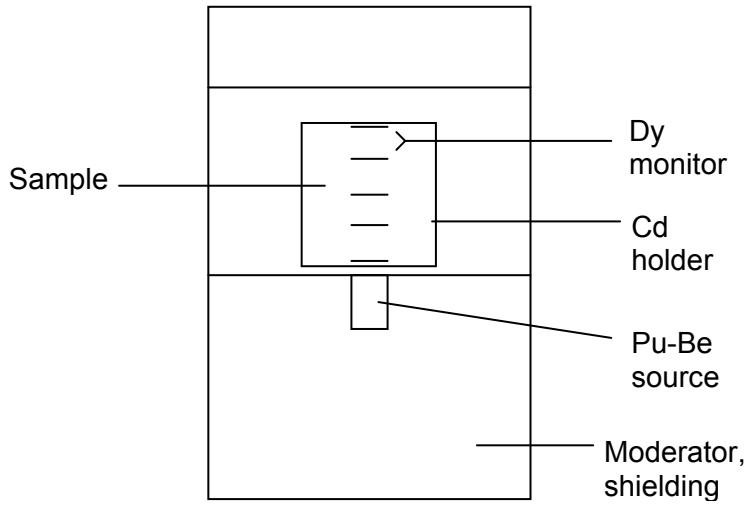

b)

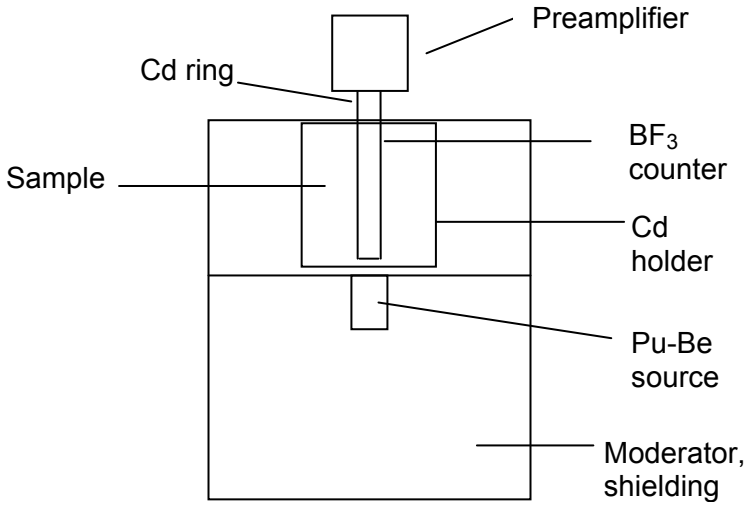

Figure 2. *Experimental arrangements for the activation (a) and prompt (b) measurements.*

The samples were placed in Cd holders of 10.2 cm diameter and 8 cm height assuring the analysis of a sample dimension of about 1 litre. Considering the prompt method an empty tube of 2 cm diameter is necessary along the central line of the samples in order to introduce the BF_3 counter for the measurements of solid samples. The high sensitivity of the BF_3 tube renders the use of a Pu-Be neutron source of much lower activity (18.5 GBq) possible as compared to that (185 GBq) used in activation measurements.

Results and discussion

The axial flux distributions measured (see Figure 2a) along the central line of the samples by Dy foils using the $^{164}Dy(n,\gamma)^{165}Dy$ reaction have been approximated by a second order polynomial. The flux values averaged over the sample, <F> were determined by the way [3] developed previously. The relative excess flux values, $R_F=(<F>-<F_0>)/<F_0>$ are based on the experiments performed with <F> and without $<F_0>$ a sample. A strong correlation was found between the relative excess flux and the hydrogen content of the given sample.

In our new experimental arrangement (see Figure 2b) the relative excess counts, $R=(I-I_0)/I_0$ were determined by measuring the neutron counts with (I) and without (I_0) a sample for the

same time using the BF_3 tube. In this case also a strong correlation was found between the relative excess counts, R, and the hydrogen content of the samples which can be described by a third order polynomial. The numerical details of the correlation and the parameters of the polynomial can be seen in Figure 3. This calibration curve of the system was measured using different types of hydrogen standards, such as polyethylene (CH_2), polystyrene (C_8H_8), ammonium-nitrate (NH_4NO_3), and melamine ($C_3H_6N_6$). The calibration curve shown in Figure 3 renders the determination of hydrogen concentration for example in oils and coals of different origins also possible.

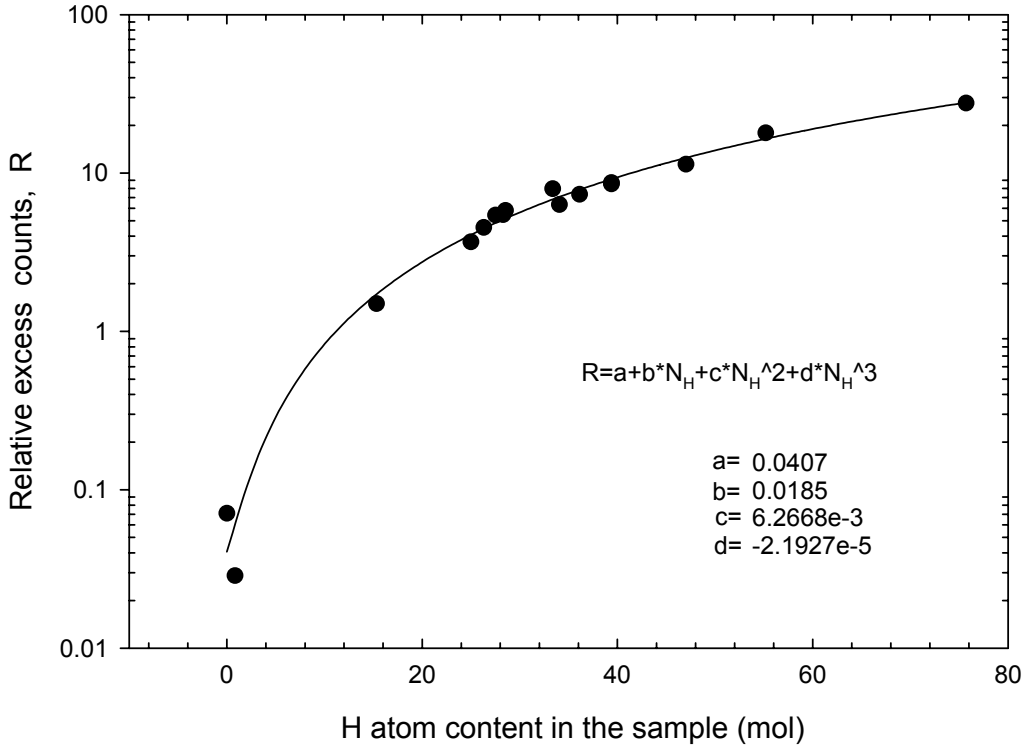

Figure 3. *R vs. N_H function measured by a BF_3 counter.*

Results indicate not only the advantages in the routine use of the prompt method but also its higher sensitivity as compared to the activation technique used in our previous investigations, which means that replacing the activation foils with prompt neutron counters (e.g. BF_3) can assure a routine application of the slowing down method for bulk hydrogen analysis needed in different fields of science and technology.

The simultaneous application of the slowing down and the neutron reflection [7] methods using BF_3 proportional counters render the determination of both the hydrogen concentration and the C/H atomic ratio for the samples of unknown composition possible.

Acknowledgements

This work was supported in part by the Hungarian Academy of Sciences (2007).

References

[1] Bulk Hydrogen Analysis Using Neutrons, Final report of the First Co-ordinating Meeting, IAEA/PS/RCM97-1, Vienna, Austria, 1997.

[2] Bulk Hydrogen Analysis Using Neutrons, Report of the Third Research Co-ordinating Meeting 23-26 October 2000, F1-RC-655.3, IAEA, Vienna, Austria, 2001.

[3] B. Király, T. Sanami, J. Csikai, Advantages and limitations od thermal and epithermal neutron activation analysis in bulk samples. Appl. Radiat. Isot. 58. (2003) 691.

[4] J. Csikai, R. Dóczi, B. Király, Investigations on landmine detection by neutron-based techniques. Appl. Radiat. Isot. 61. (2004) 11.

[5] R. Dóczi, M. A. Ali, M. Fayez-Hassan, J. Csikai, Determination of hydrogen content in bulk samples using the neutron activation method, Applied Radiation and Isotopes 63 (2005) 137-140.
[6] R. Dóczi, J. Csikai, T. Sanami, M. Fayez-Hassan, Bulk Hydrogen Analysis Using Epithermal Neutrons, Journal of Radioanalytical and Nuclear Chemistry, Vol.266, No 1 (2005) 11-17.
[7] J. Csikai, R. Dóczi, A comparison of the neutron thermalization and reflection methods used for bulk hydrogen analysis, Applied Radiation and Isotopes 65 (2007) 764-768.

Neutron geophysical tool response in complex realistic borehole geometry – Monte Carlo calculations

A. Drabina[1)], M. Bała[2)], U. Woźnicka[1)], T. Zorski[2)]

1) The Henryk Niewodniczański Institute of Nuclear Physics Polish Academy of Sciences, ul. Radzikowskiego 152, 31-342 Kraków , Poland
2) AGH University of Science and Technology, Faculty of Geology, Geophysics and Environmental Protection, al. Mickiewicza 30, 30-059 Kraków, Poland

Andrzej.Drabina@ifj.edu.pl

Abstract: Monte Carlo simulation of the neutron transport is a powerful tool in complex downhole geophysical investigations. One of the problems in well logging not yet analyzed completely is an influence of the invaded zone on the tool reading. The brine present in the borehole migrates into the surrounding rock due to the difference in pressure of the borehole and formation fluids. In the invaded zone the mud filtrate displaces formation fluids in rock pores. The radial dimension of the invaded zone depends mostly on permeability of the rock. The higher permeability and pressure difference, the deeper invasion. High porosity and permeability characterize rocks in which hydrocarbons reservoirs can be found. This situation makes the problem of the invaded zone of special importance. In our work we have tried to estimate the influence of the invaded zone on the geophysical neutron logging tool response. Two invasion models have been analyzed – one of deep invasion and the second of shallow invasion. The problem has been solved using Monte Carlo simulations. The MCNP5 code with the continuous-energy neutron data library ENDF/BVI.8 (ACTIA) has been used.

Introduction

The problem of the influence of the invaded zone on the nuclear well logging tool responses is recently thoroughly analyzed both for vertical and horizontal wells [1], [2]. The problem is of great importance, as the presence of the invaded zone can reduce, or even eliminate the effect of gas on neutron-tool measurements [1]. On the other hand, taking into account and quantifying the influence of invasion on the geophysical measurements is very complicated. Correcting the measurements requires detailed information about the invasion depth, filtrate saturation, etc., which are unknown in most circumstances [2]. At present, one of the best ways to analyze and quantify the problem of invasion is to use the simulation methods, where all needed parameters of formation, fluids and invasion are well known. In our work we used the MCNP5 code [3] to simulate the answer of the prototype neutron logging tool NNTE. The tool is devoted for neutron porosity and for thermal neutron absorption cross-section Σ_a measurements. It is equipped with the Am-Be neutron source and 3 detectors [4]. Two of them (NEAR and FAR detectors) measure epithermal neutrons and the third one (second NEAR detector) measures thermal neutrons. We have analyzed the influence of the shallow and deep invasion in the Miocene sandstone formation typical of the Carpatian Foredeep in Poland.

Input data for the calculations

The chemical composition of the Miocene sandstone standard is as follows [4]: SiO2: 72.4983682%, Al2O3: 7%, Fe2O3: 2%, CaO: 7.5%, K2O: 1.8%, CO2: 8%, H2O: 1.2%, B-10: 0.0016318%.
The thermal neutron absorption cross-section for the Miocene sandstone standard: Σ_a=15 c.u.
Rock matrix density of the Miocene formation assumed for the calculations (according to the laboratory analysis for the Jasionka-4 well): ρ_{ma}= 2.692 g/cm3.
Four values of formation porosity were taken into account: 10, 20, 25 and 30 p.u..
The rock pores of the uninvaded (virgin) zone were filled with gas CH_4 (density of gas: ρ_g=0.1 g/cm^3) and with formation water (salinity of formation water: 50 kppm NaCl, density ρ_w = 1.03591 g/cm^3). Water saturation for the uninvaded zone (fraction of the pore space filled with formation water) was equal to 0.4.

The formation was intersected with the borehole of diameter 216 mm. The borehole was filled with mud (more precisely – brine) of salinity 15 kppm NaCl, and density ρ_m=1.0108 g/cm^3. Between borehole wall and the virgin zone, the invaded zone was assumed. The rock matrix and porosity of the invaded zone was the same as of the virgin zone, in our case – the Miocene sandstone standard of porosities 10, 20, 25 or 30 p.u.. The water saturation of the zone decreased with the distance from the borehole wall in the hyperbolic manner, starting from 0.9 at the borehole wall, ending with 0.4 at the uninvaded zone. Two models of water saturation distribution were assumed in the calculations: case 1 – model of shallow invasion, and case 2 – model of deep invasion (Fig. 1). In the "case 1", the thickness of the invaded zone was 13 inches and in the "case 2" – 22 inches. In each case, the zone was divided by the 1-inch layers [5].

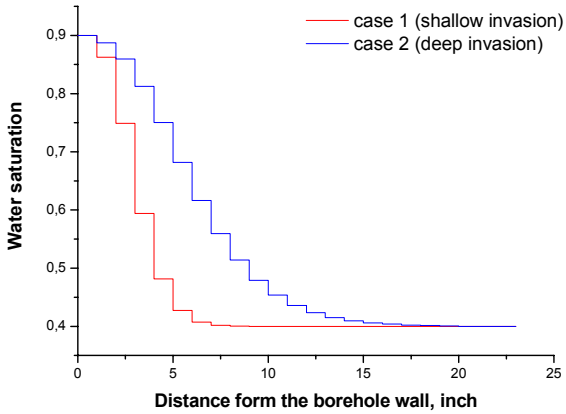

Figure 1. *Water saturation distribution in the 1 inch cylindrical layers around the borehole.*

In the invaded zone, the liquid filling the rock pores was the mixture of formation water and mud filtrate, where the mud filtrate was assumed to be the same as the mud filling the borehole.

Fluid distribution in the pore space as a function of the distance from the borehole wall for both analyzed cases is presented in Fig.2.

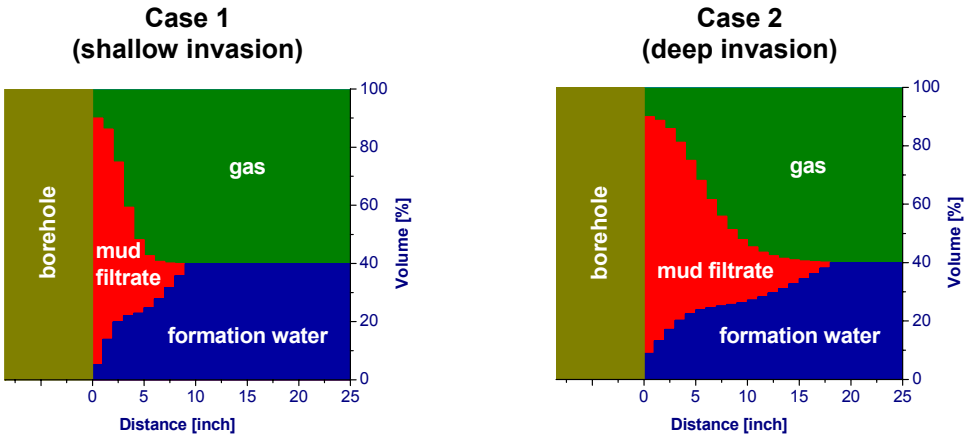

Figure 2. *Fluid distribution in the pore space as a function of the distance from the borehole wall.*

Calculations

Numerical calculations were performed using MCNP5 code ver. 1.30 with ENDF/B-VI.8 (ACTIA) continuous-energy neutron data library.

The cylindrical rock model of a diameter of 320 cm and a height of 300 cm was modeled. Parameters of the rock were taken according to the above assumptions. Borehole of a diameter of 216 mm was situated at the vertical axis of the rock model. The model was placed on a 1 m thick concrete layer and surrounded by water. The thickness of the water layer above the rock was 40 cm and around the rock – 120 cm. Such geometrical dimensions of the rock model and its surrounding guarantee the so called "infinity" of the system. It means, that only those neutrons, which are not able to reach the NNTE tool detectors, can leave the system.

The NNTE tool was modeled taking into account even small parts. It was placed in the borehole of the rock model, so it touched the borehole wall.
3 invaded zone examples were analyzed. Apart from “case 1” and “case 2” mentioned above, also “case 0” with no invasion was analyzed for comparison.
Fig. 3 presents the vertical and horizontal cross-section of the modeled systems.

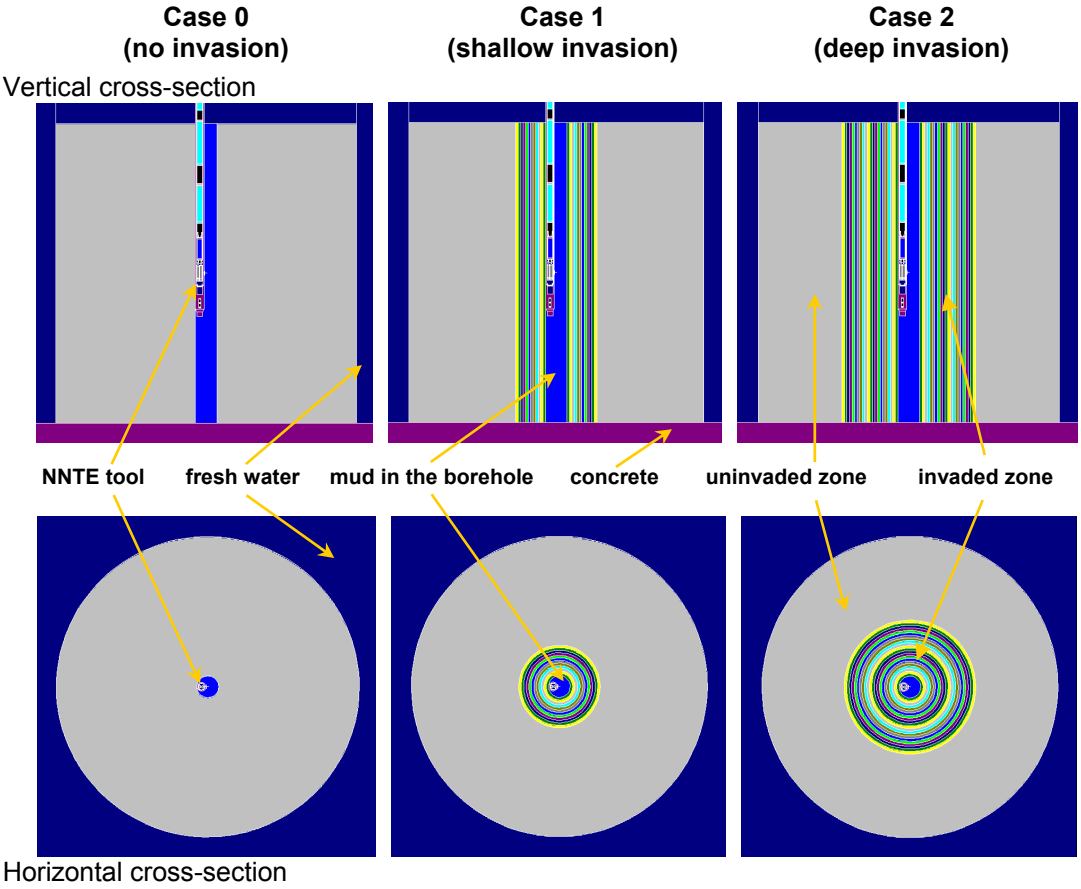

Figure 3. *Cross-sections of the modeled systems*

Results

The MCNP code gives results in the form of number of neutrons absorbed in the detector volume per 1 neutron leaving the source. To express the calculation results in the apparent neutron porosity units [%], it is necessary to recalculate the MCNP results using standard calibration curves. In Fig. 4., the standard calibration curves for the NNTE tool detectors are presented. The curves were created for the Miocene standard formation intersected by a 216 mm diameter borehole filled with fresh water. They were also created using the MCNP code.
Results of the calculations in the form of the apparent neutron porosity of the formation “seen” by each of the NNTE tool detectors are given in Table 1.

Table 1. *Apparent neutron porosity read by the NNTE detectors, results of the calculations.*

	Case 0			Case 1			Case 2		
Rock porosity	NEAR thermal, %	NEAR epi-thermal, %	FAR epi-thermal, %	NEAR thermal, %	NEAR epi-thermal, %	FAR epi-thermal, %	NEAR thermal, %	NEAR epi-thermal, %	FAR epi-thermal, %
10 p.u.	5.34	5.37	4.52	7.80	8.56	7.33	8.52	9.02	8.62
20 p.u.	9.70	10.24	9.12	16.72	16.14	14.37	18.21	16.64	15.61
25 p.u.	11.91	11.96	10.50	20.51	19.21	16.89	22.08	21.12	21.18
30 p.u.	13.92	13.86	12.51	24.23	24.39	21.31	26.90	25.44	24.16

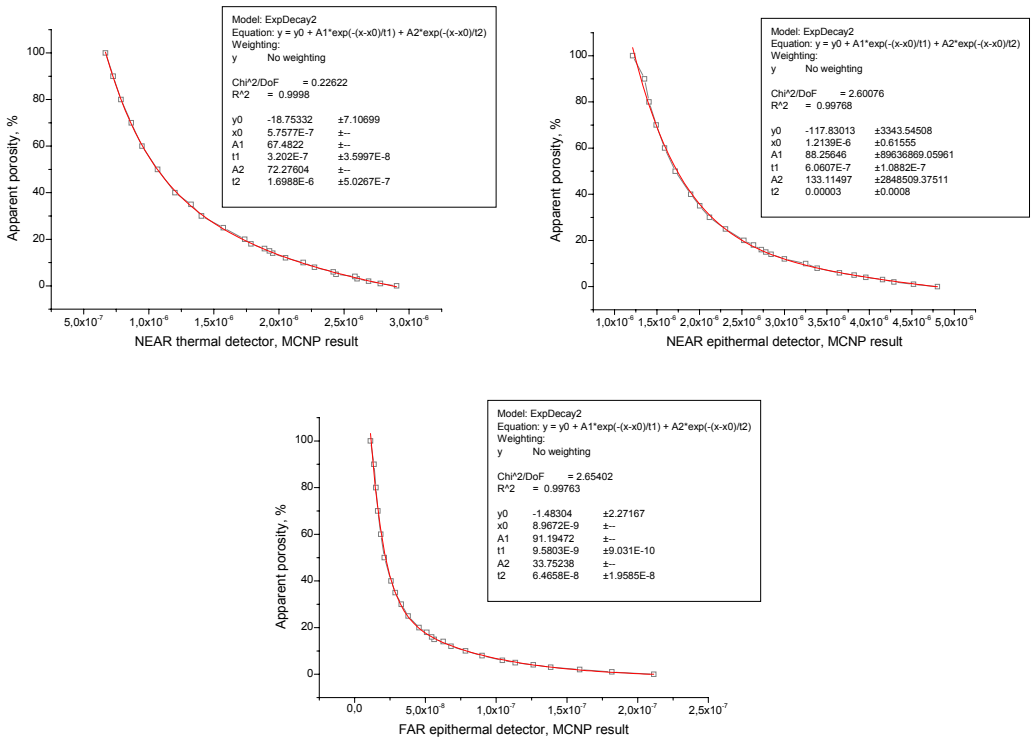

Figure 4. Standard calibration curves for the Miocene standard for the NNTE tool detectors.

Conclusion

Analyzing the results one must come to the conclusion, that the influence of the invaded zone on the neutron tool response is evident. It is well understood, when comparing the “case 1” (shallow invasion) and “case 2” (deep invasion) with the “case 0” (no invasion) results. On the other hand, the differences between shallow and deep invasion are not so significant.
To give more complex and thorough answer to the question of the influence of the invaded zone on the neutron logging tool response, it is necessary to analyze more examples of the invasion problem.

Acknowledgements

The work was partly sponsored by the Polish Ministry of Science and Higher Education under research project No 4 T12B 05629.
All calculations were performed on the PC RackSaver computer cluster at the Academic Computer Centre CYFRONET AGH Cracow, Poland.

References

[1] A. Mendoza, W. Preeg, C. Torres-Verdin, F. O. Alpak, “Monte Carlo Modeling of Nuclear Measurements in Vertical and Horizontal Wells in the Presence of Mud-Filtrate Invasion and Salt Mixing”, paper PP, SPWLA 2005, New Orleans, Louisiana, June.
[2] J. Galford, J. Truax, G. Moake, “Borehole and Formation Invasion Effects of Formate-Based Mud Systems on Nuclear Logs”, paper LL, SPWLA 2005, New Orleans, Louisiana, June.
[3] X-5 Monte Carlo Team MCNP, “A General Monte Carlo N-Particle Transport Code, Version 5 “, LA-UR-03-1987, Los Alamos National Lab, April 2003.
[4] T. Zorski, M. Stadtmuller, "Alternative Method of Shaliness Determination for Thin Bedded Miocene Gas Formation in SE Poland, Using the Thermal - Epithermal Neutron Logging Tool" - Internal report of research project No. 5.5.140.771, sponsored by the Polish Oil and Gas Company. AGH University of Science and Technology, Faculty of Geology, Geophysics and Environmental Protection, Kraków, September 2001 (in Polish).
[5] M. Bała, "Analysis of Water- and Gas Saturation Character and Resistivity Changes in Near-Wellbore and Virgin Zones Based on Data from Jasionka-4 Well”. Transactions of Oil and Gas Institute, No. 137, Conference Geopetrol Zakopane 2006, Recovery of Oil and Gas and Sustained Economical Development, Kraków 2006.

nELBE: A new facility to produce high brilliance pulses of fast neutrons for transmutation research by time of flight

A. R. Junghans[1)], R. Beyer[1)], J. Klug[1)], D. Légrády[1)], A. Wagner[1)], F. P. Weiss[1,2)] and E. Grosse[1,2)]

1) Forschungszentrum Dresden-Rossendorf, 01314 Dresden, Germany
2) Technische Universität Dresden, 01062 Dresden, Germany
a.junghans@fzd.de

Abstract: The Radiation Source ELBE at Forschungszentrum Dresden-Rossendorf (FZD), with electron energies up to 40 MeV, will be used to produce intense pulses of fast neutrons. The neutron radiator consists of a liquid lead circuit where bremsstrahlung photons generated from the electron beam at ELBE produce neutrons in (γ,n) reactions. Monte Carlo simulations with MCNP4C3/MCNP5 were performed to characterise neutron and photon intensities as well as time and energy distributions, and to optimise the neutron beam. The short beam pulses provide the basis for an excellent time resolution for neutron time-of-flight experiments, giving an energy resolution of about < 2 % with a flight path of ~ 5 m.

Introduction

In the EURATOM FP6 program partitioning of nuclear waste and transmutation of long-lived isotopes to nuclides with shorter lifetime are being investigated. Several transmutation schemes have been proposed and for an optimum solution detailed numerical simulations are under way or in preparation. Related to the development of new concepts to produce less waste via very high burn-up different designs involving critical reactors or sub-critical accelerator-driven systems (ADS) are being studied in view of their transmutation capabilities. The Generation IV International Forum (GIF) has selected six nuclear energy systems for which research and development are needed to confirm their viability and to demonstrate their expected performance that includes the objective of producing less waste. In the considerations for waste reduction the possible use of fast (i.e. un-moderated) neutrons as coming directly from the fission process is of great importance as most of the proposed systems are relying on no or only weak moderation. The strong processes induced by these fast neutrons are known in principle, but reliable predictions of the relevant physical processes and the optimization of the related facilities depend on the availability of high-quality nuclear data.

Photoproduction of neutrons at ELBE

As the fission neutron spectrum resembles very much the neutron distribution originating from the nuclear photo effect a high intensity electron beam allows suitable measurements in the fast neutron domain. The neutrons are generated by hitting high-Z material with the electrons and thus producing bremsstrahlung which in turn causes the very same material to emit neutrons. At the radiation source ELBE of the Forschungszentrum Dresden-Rossendorf 1 mA electrons are accelerated up to 40 MeV in cw-mode by superconducting rf-cavities of 1.3 GHz. As the set-up allows to inject electrons in every n^{th} micro-bunch only it can deliver high brilliance beams with variable time sequences for electrons, bremsstrahlung photons and finally neutrons.
The accurate knowledge of neutron induced nuclear reactions at the appropriate energies is of crucial importance for predicting the capabilities of new systems. This means that for detailed waste transmutation research and for design work on Gen-IV systems energy dispersive studies are needed. Among the ways to determine the neutron energy the one applicable for a wide range of energies is the time of flight method: starting with a broad spectrum the neutrons are tagged according to their energy by measuring their velocity. ELBE with its ultra-short electron bunches is especially well suited for this method and time of flight measurements with good resolution can be performed here even for fast neutrons.

The pulsing system

ELBE is the first superconducting electron linac combined with a neutron time of flight facility. A big advantage is the permanently present radiofrequency which allows the acceleration of nearly any

pulse repetition rate delivered by the electron gun. At ≈ 1 MeV a resolution ΔE/E of ≈ 2% will be reached with detectors of ≈ 1ns resolution. The time resolution of the e-beam is much better and due to the small radiator dimension of ≈1cm – as described in the following – the generated n-bunches are shorter than 1ns.
The shortness of the e-bunches is warranted by the accelerating radio frequency (RF), but for a useful time of flight facility a sufficiently large distance between subsequent pulses is absolutely necessary; a variation of this distance without intensity loss is an additional bonus. At ELBE the electron to be accelerated will be photo-produced by a high intensity laser with variable repetition rate in a superconducting RF gun with a bunch charge of up to 2 nC corresponding to a pulse separation of 2 µs at 1 mA average current of accelerated electrons.

The molten Pb neutron radiator

The neutron flux – which determines the statistical accuracy of a cross section measurement carried out in a given time – depends on the primary beam intensity and on the amount of converter target material put in the beam. At ELBE the limiting factor of flux is limited by the maximum beam power acceptable on the neutron producing target and not by the available beam current from the accelerator. On the basis of a molten lead circuit a technologically innovative solution for neutron converters suited for very high beam power deposition (≈ 5 kW/g) was designed in a collaborative effort of the FZD institutes for Radiation Physics and for Safety Research.
The most important feature of this source, advantageous for transmutation-related measurements, is the extremely high flux at still reasonable time resolution: The extremely high neutron density of more than 10^7 n/cm³ produced in the radiator by each micro-pulse (at ≈1 MHz) results in nearly 10^7 n/(s·cm²) at a flight path of roughly 5 m. Making use of the new superconducting RF-photo-gun of ELBE the repetition rate can be adjusted to the neutron energy range under study at the given flight path. Due to the unique high bunch charge of up to 2nC with this electron gun the full neutron flux is available for neutron energies above 20 keV.

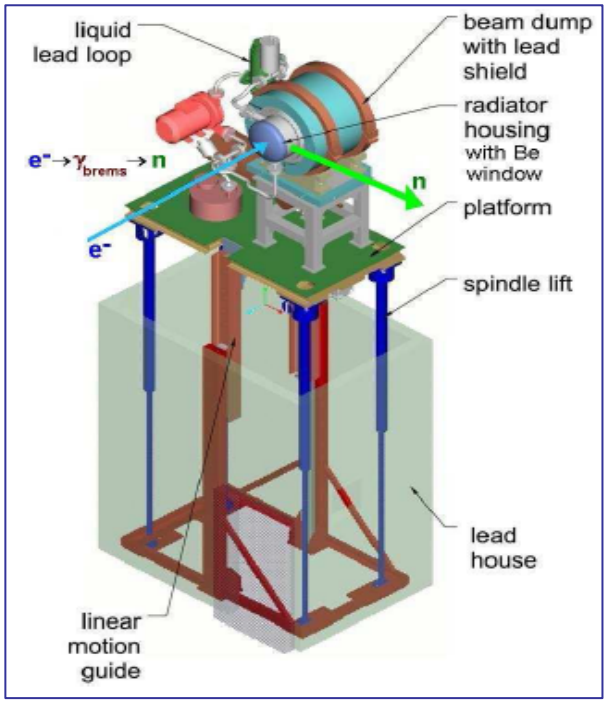

Figure 1. *Schematic view on the liqPb radiator*

Experimental set-up at nELBE

For the measurements at nELBE the neutrons are transferred through a massive concrete radiation shield (needed to warrant sufficient shielding between neutron radiator and experiment). The good emittance of ELBE in combination with an especially designed collimator results in a narrow neutron beam which allows the use of small targets and compact detector set-ups.

The measurements allow for photon detection following radiative neutron capture (4π-array of BaF_2 scintillators) and for the registration of neutrons scattered from the target (in specially equipped plastic scintillators). By using the photon and neutron detectors in coincidence inelastic neutron scattering can be identified. Both detector types reach time resolutions clearly below 1ns and are thus well suited for a proper time-of-flight tagging. The set-up will be devoted to measurements of transmutation-relevant data for actinides as well as for fission fragments.

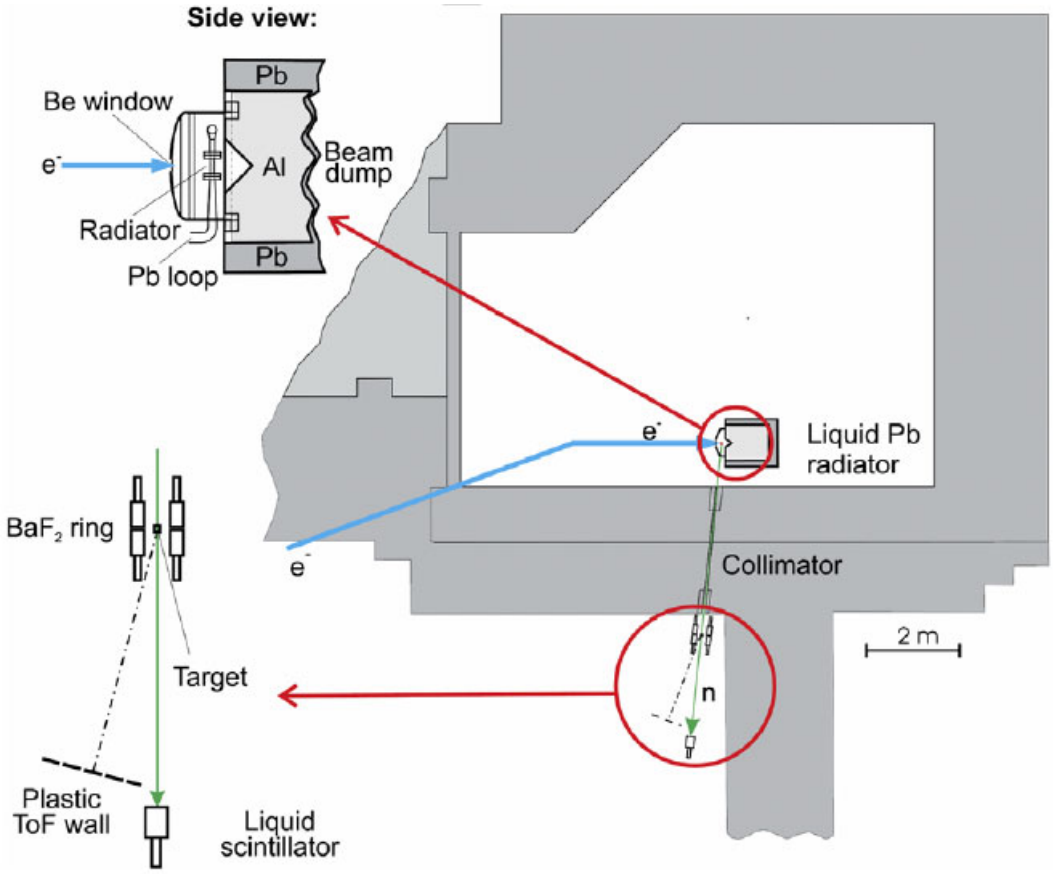

Figure 2. *Set-up for the measurements at nELBE.*

EFNUDAT, a EU-funded I3

The Rossendorf neutron time of flight facility nELBE is part of Integrated Infrastructure Initiative (I3) entitled: “European Facilities for Nuclear Data Measurements” (EFNUDAT) which has been created by a consortium of 10 experimental facilities in 7 european countries for nuclear data measurements. Joint Research Activities (JRA) within this I3 concern the fast digitizer data acquisition, quality assurance of nuclear data, and the development of neutron producing target technology. Transnational access to the EFNUDAT facilities is supported, for details see www.efnudat.eu.

Comparison to other time of flight facilities

The only two other neutron time of flight facilities within EFNUDAT have concentrated in the past on slower neutrons (including moderated, i.e. thermal ones). The installation at IRMM/Geel has considerably less primary beam power and thus less neutron flux. At the proposed short (20 m) flight path of CERN/n_ToF the flux will be larger as compared to nELBE in the energy range accessible here, but the energy resolution is predicted to be superior at Dresden-Rossendorf. The respective neutron beam properties are shown in Table 1, which also includes relevant US installations.

Table 1. *Beam properties of various neutron time of flight facilities.*

n-ToF-device	CERN n-ToF		LANL NSC	ORNL SNS	ORNL ORELA	IRMM GELINA	ELBE	ELBE with photo-gun
beam power / kW	10		60	1000	8	7	5	40
rep. rate / s-1	0.4		20	60	500	800	$8 \cdot 10^5$	$5 \cdot 10^5$
pulse charge / nC	$\approx 10^3$		$4 \cdot 10^3$	$3 \cdot 10^4$	≈ 100	≈ 100	0.07	2
flight path / m	183	≈ 20	60	84	40	20	5	5
n-pulse length / ns	> 7		125	100-700	> 4	> 1	< 1	< 1
Emin / eV	0.1	0.1	1	0.1	10	10	$5 \cdot 10^4$	$4 \cdot 10^4$
Emax / eV	$3 \cdot 10^8$		$\approx 10^8$	$\approx 10^8$	$5 \cdot 10^6$	$4 \cdot 10^6$	$7 \cdot 10^6$	$7 \cdot 10^6$
$\Delta E/E$ @ 1MeV	0.5%	5%	≈10 %	> 10 %	< 1 %	< 2 %	< 2 %	< 2 %
n-flux $(s \cdot cm^2 \cdot E\text{-decade})^{-1}$	10^5	$\approx 10^7$	$\approx 10^6$	10^6-10^7	10^4	$4 \cdot 10^4$	$2 \cdot 10^5$	$4 \cdot 10^6$

Acknowledgements
This project was supported by DFG and by EU. Thanks are due to many Dresden colleagues, especially from TU Dresden and FZD (Safety Research, Radiation Source ELBE, Research Technology and Radiation Physics).

References

[1] Altstadt, E., Beckert, C., Freiesleben, H., Galindo, V., Greschner, M., Grosse, E., Junghans, A. R., Naumann, B., Schneider, S., Seidel, K., Weiß, F.-P.; Scientific Technical Report, FZR-426, April 2005; Abschlussbericht DFG-Projekt Gr 1674/2.
[2] M. Salvatores; State of the art and perspectives in radioactive waste transmutation; CEA Cadarache 2005.
[3] Altstadt, E., Beckert, C., Grosse. E., Freiesleben, H., Klug, J., Junghans, A.R., Schlenk, R., Weiss, F.-P., et al.; Annals of Nuclear Energy 34 (2007) 36-50.
[4] Klug, J.; Altstadt, E.; Beckert, C.; Beyer, R.; Freiesleben, H.; Galindo, V.; Grosse, E.; Junghans, A. R.; Legrady, D.; Naumann, B.; Noack, K.; Rusev, G.; Schilling, K. D.; Schlenk, R.; Schneider, S.; Wagner, A.; Weiß, F.-P.; Nuclear Instruments and Methods in Physics Research A 577 (2007) 641.
[5] Beyer, R., Grosse, E., Heidel, K., Hutsch,J. Junghans, A.R., Klug,J., Legrady, D., Nolte, R., Röttger, S., Sobiella, M., Wagner, A.; Nuclear Instruments and Methods in Physics Research A 575 (2007) 449–455.

Evaluated data to study activation and transmutation of lead and bismuth irradiated with protons at energies up to 0.6 GeV

A.Yu. Konobeyev, U. Fischer

Institut für Reaktorsicherheit, Forschungszentrum Karlsruhe GmbH, 76021 Karlsruhe, Germany
konobeev@irs.fzk.de

Abstract: To satisfy growing needs in nuclear data at intermediate energies a new file with activation data for long-lived and stable lead and bismuth isotopes has been prepared. It contains excitation functions of nuclear reactions induced by protons with the incident energy up to 600 MeV.
The intranuclear cascade evaporation model combining the Monte Carlo method for the simulation of the non-equilibrium particle emission and the deterministic algorithm for the description of equilibrium emission was used to obtain cross-sections at proton energies above 150 MeV. The nuclear level density for equilibrium states was calculated using the generalized superfluid model. Inverse reaction cross-sections were calculated by the nuclear optical model. Calculated cross-sections are compared with predictions of other popular intranuclear cascade evaporation models.
Available experimental data were used for the correction of calculated excitation functions.

Introduction

The evaluation of nuclear reaction cross-sections at intermediate energies is important for the reliable prediction of changes in material compositions during the irradiation in various nuclear installations including accelerator driven systems and neutron generators.
Recently the Proton Activation Data File (PADF) containing excitation functions for proton induced reactions for 2355 targets and energies up to 150 MeV has been prepared [1]. In the present work data for lead and bismuth isotopes are extended up to 660 MeV.
The calculation of cross-sections has been performed using the CASCADE/ASF code [2] at the energies from 150 MeV to 660 MeV.
Available experimental data were applied for the final data evaluation.

Calculations using nuclear models

The non-equilibrium particle emission is described using the intranuclear cascade model implemented in the CASCADE code [3]. The model is combined with the deterministic equilibrium model, as described in Refs.[2,4].
The modelling of equilibrium emission is performed without the consideration of angular momentum. It is the simple consequence of the limited power of computers. The nuclear level density is calculated according to the generalized superfluid model [5]

$$\rho(U) = \rho_{qp}(U')K_{vib}(U')K_{rot}(U'),$$

where $\rho_{qp}(U')$ is the level density due to quasi-particle excitations [5], $K_{vib}(U')$ and $K_{rot}(U')$ are the vibrational and rotational enhancement factors at the effective energy of excitation U' calculated according to Refs.[5,6].
The nuclear level density parameters are calculated according to the following expression [5]

$$a(U) = \begin{cases} \tilde{a}\left(1+\delta W \varphi(U'-E_{cond})/(U'-E_{cond})\right), & U' > U_{cr} \\ a(U_{cr}), & U' \le U_{cr}, \end{cases}$$

where δW is the shell correction to the mass formula equal to the difference between experimental mass defect and one calculated from the liquid drop model, $\varphi(U)= 1-\exp(-\gamma U)$, $\gamma=0.4/A^{1/3}$ MeV^{-1}. The asymptotic value of nuclear level parameter is equal to $\tilde{a}$ =A(0.073 + 0.115A$^{-1/3}$).
The inverse reaction cross-section is calculated by the optical model. The parameters of the optical potentials for nucleons and light charged fragments are discussed in Refs.[7,8].

The probability of the photon emission is calculated according to Weisskopf-Ewing model with the photon absorption cross-section parameterized in Ref.[9]. The fission probability is obtained using the Bohr-Wheeler approach. The distribution of fission fragments is calculated according to Ref.[10].
Numerical calculations of equilibrium particle energy distributions were performed using the modified ALICE code [11].
Results of calculations were compared with experimental data available in EXFOR.
Following deviation factors [1] were used for the quantification of the difference between calculations and measured cross-sections

$$H = \left(N^{-1} \sum_{i=1}^{N} [(\sigma_i^{exp} - \sigma_i^{calc}) / \Delta\sigma_i^{exp}]^2 \right)^{1/2}, \qquad D = N^{-1} \sum_{i=1}^{N} \left| \sigma_i^{exp} - \sigma_i^{calc} \right| / \sigma_i^{exp},$$

$$R = N^{-1} \sum_{i=1}^{N} \sigma_i^{calc} / \sigma_i^{exp}, \qquad F = 10^{\left(N^{-1} \sum_{i=1}^{N} [\log(\sigma_i^{exp}) - \log(\sigma_i^{calc})]^2 \right)^{1/2}}$$

$$L = \left[\sum_{i=1}^{N} (\sigma_i^{calc} / \Delta\sigma_i^{exp})^2 \, [(\sigma_i^{calc} - \sigma_i^{exp}) / \sigma_i^{calc}]^2 \Big/ \sum_{i=1}^{N} (\sigma_i^{calc} / \Delta\sigma_i^{exp})^2 \right]^{1/2}, \qquad P_x = N_x/N,$$

where σ_i^{exp} and $\Delta\sigma_i^{exp}$ are the measured cross-section and its uncertainty, σ_i^{calc} is the calculated or evaluated cross-section, N is the number of experimental points, N_x is the number of points with the ratio

$$1/x < \sigma_i^{calc} / \sigma_i^{exp} < x.$$

Tables 1, 2 and Fig.1 show deviation factors obtained using reaction cross-sections measured for p+^{208}Pb interaction at the primary proton energy 0.5 GeV protons. Experimental yields for (p,xnyp) spallation reactions are taken from Ref.[12] and measured fission yields are from Ref.[13]. Deviation factors for CASCADE/ASF are compared with calculations with Bertini/MPM/Dresner, INCL4/ABLA and CEM03 models implemented in MCNPX [14].
The comparison of calculated cross-sections with all measured data available in EXFOR for Pb and Bi isotopes at energies from 150 to 600 MeV is presented in Table 3.
Results show that in most cases CASCADE/ASF provide the best agreement with experimental data.

Table 1. *Values of deviation factors obtained using (p,x) reaction cross-sections calculated by various nuclear models for ^{208}Pb irradiated with 0.5 GeV protons and experimental fission yields (Z < 60) [13]. Best results are underlined.*

Factors	Bertini/MPM/ Dresner	INCL4/ABLA	CEM03	CASCADE/ASF
H	5.49	4.07	4.74	<u>2.93</u>
D	0.677	0.567	0.588	<u>0.327</u>
R	0.430	0.454	0.560	<u>0.933</u>
F	4.09	2.68	3.32	<u>1.77</u>
L	1.35	1.23	0.902	<u>0.411</u>
$P_{1.3}$	0.0852	0.0330	0.140	<u>0.516</u>
$P_{2.0}$	0.261	0.299	0.418	<u>0.838</u>
$P_{10.0}$	0.962	0.992	0.948	<u>0.995</u>
Number of points	364	364	364	364

Table 2. *Values of deviation factors obtained using (p,x) reaction cross-sections calculated by various nuclear models for ^{208}Pb irradiated with 0.5 GeV protons and experimental spallation yields (Z > 60) [12]. Best results are underlined.*

Factors	Bertini/MPM/ Dresner	INCL4/ABLA	CEM03	CASCADE/ASF
H	15.30	5.74	6.72	<u>4.011</u>
D	1.21	0.487	0.644	<u>0.359</u>
R	1.85	1.25	1.33	<u>0.906</u>
F	3.30	<u>1.76</u>	2.15	2.21
L	0.748	0.473	0.559	<u>0.471</u>
$P_{1.3}$	0.337	<u>0.4802</u>	0.361	<u>0.4802</u>
$P_{2.0}$	0.525	<u>0.817</u>	0.708	0.777
$P_{10.0}$	0.951	<u>0.995</u>	0.990	0.975
Number of points	202	202	202	202

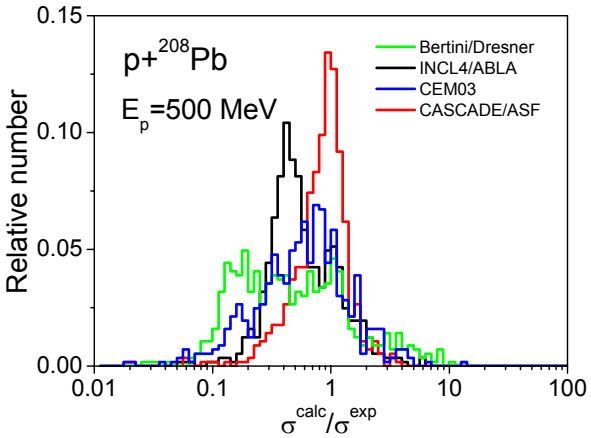

Figure 1. *The ratio of cross-sections calculated by various models to measured cross-sections [12,13]. Points are combined by histograms for the best view.*

Table 3. *Values of deviation factors obtained using (p,x) reaction cross-sections calculated using various models for Pb and Bi isotopes irradiated with protons with incident energies from 150 to 600 MeV. Experimental data from 1960 up to present time are applied.*

Factors	Bertini/MPM/ Dresner	INCL4/ABLA	CEM03	CASCADE/ASF
H	9.68	<u>4.64</u>	5.29	5.63
D	0.842	0.533	0.575	<u>0.405</u>
R	<u>0.995</u>	0.798	0.913	1.028
F	3.55	2.27	2.65	<u>1.92</u>
L	0.791	0.546	0.589	<u>0.509</u>
$P_{1.3}$	0.176	0.204	0.279	<u>0.482</u>
$P_{2.0}$	0.390	0.520	0.585	<u>0.785</u>
$P_{10.0}$	0.966	<u>0.993</u>	0.971	0.992
Number of points	716	716	716	716

Correction of the data using available experimental data

Experimental data available in EXFOR for proton induced reactions were used for the evaluation of nuclear reaction cross-sections including the fitting and correction of calculated excitation functions.
Following values of deviation factors correspond to evaluated cross-sections: H= 0.186, D= 0.008, R= 1.001, F= 1.044 , L= 0.023, $P_{1.3}$ = 0.991, and $P_{2.0}$ = 1.000. They are noticeably lower comparing with code calculations (Table 3).
Figures 2,3 show examples of evaluated fission cross-sections for ^{208}Pb and ^{209}Bi.

Content and format of the data set

Evaluated data were prepared for lead isotopes with the mass number from 202 to 210 and bismuth isotopes with the mass number from 205 to 210.
Data are written in the ENDF-6 format using MF=3/6, MT=5 representation. MAT numbers were assigned as for PADF files [1].

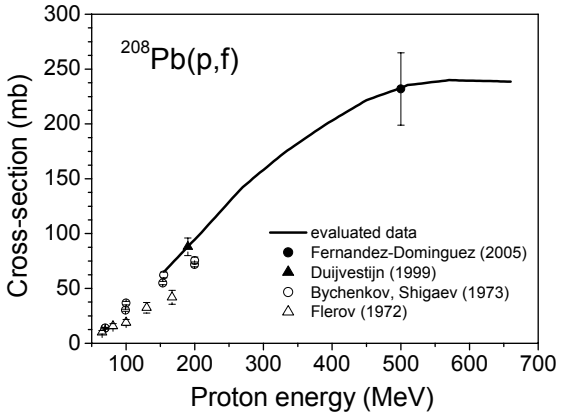

Figure 2. *Evaluated and experimental cross-section for the ^{208}Pb(p,f) reaction.*

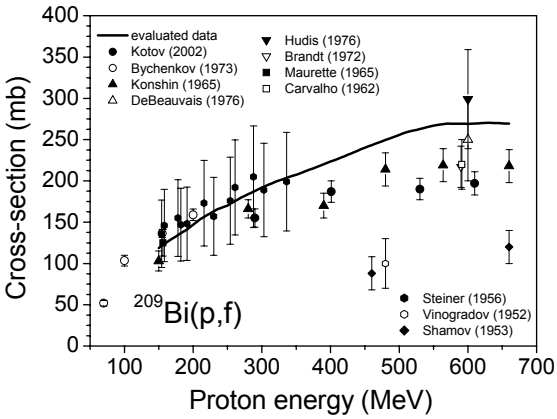

Figure 3. *Evaluated and experimental cross-section for the ^{209}Bi(p,f) reaction.*

References

[1] C.H.M. Broeders, U. Fischer, A.Yu. Konobeyev, L. Mercatali, S.P. Simakov, J., Nucl. Sci. Technol., 44, 933 (2007).
[2] C.H.M. Broeders, A.Yu. Konobeyev, Nucl. Instr. Meth. Phys. Res. A550, 241 (2005).
[3] V.S. Barashenkov, Comp. Phys. Comm. 126, 28 (2000).
[4] S. Yavshits, G. Boykov, V. Ippolitov, S. Pakhomov, A. Roschin, O. Grudzevich, INDC(CCP)-430, 83 (2001).
[5] A.V. Ignatyuk, “Level densities”, In: Handbook for Calculations of Nuclear Reaction Data, Report IAEA-TECDOC-1034 (1998) p.65; http://www-nds.iaea.or.at/ripl/ripl_handbook.htm
[6] G. Hansen, A. Jensen, Nucl. Phys. A406, 236 (1983).
[7] M. Blann, H.K. Vonach, Phys. Rev. C28, 1475 (1983).
[8] Yu.N. Shubin, V.P. Lunev, A.Yu. Konobeyev, A.I. Dityuk, INDC(CCP)-385 (1995).
[9] M. Blann, G. Reffo, F. Fabbri, Nucl. Instr. Meth. A265 490 (1988).
[10] A.Yu. Konobeyev, Yu.A. Korovin, M. Vecchi, Kerntechnik 64, 216 (1999).
[11] M. Blann, ALICE-91: Statistical Model Code System with Fission Competition, RSIC Code Package PSR-146.
[12] L. Audouin, L. Tassan-Got, P. Armbruster, et al., Nucl. Phys. A768, 1 (2006).
[13] B. Fernández Domínguez, P. Armbruster, L. Audouin, et al., Nucl. Phys. A747, 227 (2005).
[14] J.S. Hendricks, G.W. McKinney, J.W. Durkee, et al., LA-UR-06-7991 Dec.7 (2006).

p- and n-induced fission of ^{232}Th and ^{238}U up to 200 MeV

V.M. Maslov

Joint Institute for Nuclear & Energy Research, 220109, Minsk-Sosny, Belarus
maslov@bas-net.by

Abstract: The excitation energy and nucleon composition dependence of the transition from asymmetric to symmetric scission of fissioning Th(Pa) and U(Np) nuclei, investigated via ^{232}Th(n, F) & ^{232}Th(p, F) and ^{238}U(n, F) & ^{238}U(p, F) reactions, is shown to be different in case of n(p)+^{232}Th and n(p)+^{238}U interactions. Sharp increase of symmetric fission yield is reproduced for ^{232}Th(p, F) reaction and predicted for ^{232}Th(n, F) reaction at $E_{n(p)}$≥50 MeV. In case of p+^{232}Th interaction the fissilities of Pa nuclei are responsible for the higher value of the σ_{pF} than σ_{nF} cross section at 18≤ $E_{n(p)}$ ≤100 MeV. In case of ^{238}U target $\sigma_{pF} > \sigma_{nF}$ only at $E_{n(p)}$ ≥50 MeV, which is due to the isovector terms in real volume V_R^n and imaginary surface W_D^n potential terms. In case of ^{232}Th target the entrance channel (nucleon absorption cross section) plays a decisive role at $E_{n(p)}$ ≥100 MeV.

Introduction

The excitation energy and (Z,N)-dependence of the transition from asymmetric to symmetric scission of fissioning nuclei could be investigated for the ^{232}Th(n, F) & ^{232}Th(p, F) [1] and ^{238}U(n, F) & ^{238}U(p, F) [2] reactions. For ^{232}Th(n, F) reaction there are precise cross section data up to E_n = 200 MeV, while the data on the ^{232}Th(p, F) observed fission cross section are scattering quite a lot. A recent investigation of ^{232}Th(p, F) reaction [3] might very complementary. At the other hand, while there is virtually no data on the symmetric yield $r^{sym}(E_n)$ for ^{232}Th(n, F), scanty data on $r^{sym} = \sigma_{pF}^{SL} / \left(\sigma_{pF}^{SL} + \sigma_{pF}^{AS}\right)$ for ^{232}Th(p, F) [4-6] are available.

For ^{238}U(n, F) reaction detailed data on the symmetric fission yield [7] and observed σ_{nF} cross section allow infer the symmetric and asymmetric fission yields of U nuclides with A ≤239 [8]. The data on the ^{238}U(p, F) observed σ_{nF} are scattering a lot. In ^{238}U(p, F) and ^{237}Np(n, F) reactions excited Np nuclei undergo a binary fission in competition with successive emission of pre-fission (p, xnf) or (n, xnf) neutrons. Based on the ^{237}Np(n, F) data description an independent estimate of the ^{238}U(p, F) cross section was obtained in [2]. The U and Np nuclides near the beta-stability line and at low excitations demonstrate mostly asymmetric fission [9,10]. It is generally believed that with increase of the excitation energy the influence of the shell effects diminishes and fission observables should be dominated by the macroscopic nuclear properties. However, the pre-fission (pre-saddle) neutron emission decreases the excitation energy of the ensemble of fissioning nuclei. That peculiarity may quite influence the competition of the symmetric and asymmetric fission modes, decreasing the contribution of the symmetric one. In the emissive fission domain fission observables are composed of partial contributions of the ensemble of uranium fissioning nuclei, which emerge after emission of x pre-fission neutrons (up to x=20 at E_n = 200 MeV) [1,2,8,11].
The neutron-deficient Th or Pa nuclides, emerging in ^{232}Th(n, xnf) or ^{232}Th(p, xnf) reactions, might be more susceptible to symmetric fission even at relatively low excitations [12-14]. Interplay of this trend and the decrease of the intrinsic excitation energy due to pre-fission neutron emission, would define the Th fission observables at high excitations. Symmetric fission contribution r^{sym} in n(p)-induced fission of ^{232}Th target nuclides exhibits rather steep trends with excitation energy. Independent estimate of the ^{232}Th(p, F) reaction cross section might be obtained based on the consistent ^{232}Th(p, xn) and ^{231}Pa(n, F) data description.

^{232}Th and n+^{238}U interactions

Symmetric/asymmetric (n(p), xnf) contributions to observed fission cross sections are largely defined by the level density parameters a_f and a_n for fissioning and residual nuclides, damping of the rotational modes contributions to the level densities and saddle asymmetries [1,2,8,11].

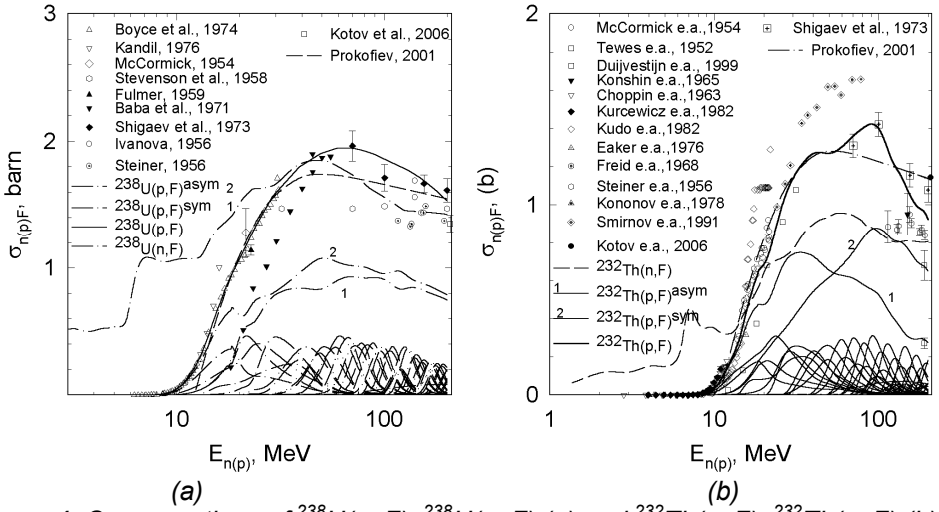

Figure 1. *Cross sections of ^{238}U(n, F), ^{238}U(p, F) (a) and ^{232}Th(n, F), ^{232}Th(p, F) (b).*

The deformed optical potential describes the n+^{232}Th(^{238}U) total cross section data up to E_n = 200 MeV [15,16]. For n+^{232}Th(^{238}U) interaction we adopted isovector terms, which depend on the symmetry parameter η =*(N-Z)/A*, only in a real volume V_R^n and imaginary surface W_D^n potential terms [17,18]. Values of V_R^p and W_D^p for incident protons are calculated as $V_R^p = V_R^p + 2\alpha\gamma$ and $W_R^p = W_R^p + 2\beta\gamma$, α=16 and β=8 [17,18]. For ^{232}Th $\sigma_R^p > \sigma_R^n$ estimate at $E_n \geq$ 50 MeV is compatible with the experimental data in the same way, as it was shown for the p+^{238}U interaction [15, 16].

The energy dependence of σ_{nF}^{SL} is defined by the symmetry of the outer saddle of a double humped fission barrier. For ^{238}U(n, f) it was found that rather thin but high axially asymmetric outer barrier E_{fBSL} corresponds to the mass symmetric fission, in contrary to the lower mass-asymmetric outer fission barrier E_{fBAS}. Actually, $(E_{fBSL} - E_{fBAS})$ = 3.5 MeV, was assumed for any U nuclide. In the emissive fission domain of ^{238}U(n, F) ratio of $r^{sym}(E_n)$ is described assuming that more fissions come from the neutron-deficient U nuclei via (n, xnf) fission chances with high number x of pre-fission neutrons [2,8]. For ^{238}U(p, F) estimate of the observed fission cross section [2], based on the ^{237}Np(n, F) data description, was obtained (see Fig.1a), which differs essentially from the phenomenological estimate [19].

The cross section of ^{232}Th(n, F) reaction is reproduced up to E_n = 200 MeV also under assumption that more fissions come from the neutron-deficient Th nuclei [1]. The data on ^{232}Th(p, F) and ^{232}Th(n, F) provide the complementary information on the evolution of the symmetric/asymmetric fission competition with increase of the projectile energy. The data on the ^{232}Th(p, F) (Fig. 1b) observed fission cross section (see [20] and EXFOR/CINDA compilation for references). are scattering much more, than in case of ^{238}U(p, F). The measured symmetric fission yields for E_p = 20-50 MeV [4] and E_p = 190 MeV [5, 6] provide an unambiguous evidence for the sharp increase of $r^{sym}(E_p)$ at $E_p \geq$ 30 MeV. There is a strong evidence [13], that fission of $^{233\text{-}x}$Pa and $^{233\text{-}x}$Th nuclei (x = 1-20) in case of ^{232}Th(p, F) or ^{232}Th(n, F) reactions, respectively, would provoke similar competition of symmetric and asymmetric fission events at $E_{n(p)}$ up to 200 MeV. An estimate of ^{232}Th(p, F) cross section might be obtained, based on the consistent description of the ^{232}Th(p, xn) and fission probabilities of $^{230\text{-}232}$Pa nuclides, fixed by the ^{231}Pa(n, F) data description.

Figure 2a shows the comparison of the ^{232}Th(p, n) and ^{238}U(p, n) reaction data descriptions (see EXFOR/CINDA compilation for references). The ^{232}Th(p, n) reaction cross

section is only ≈50% higher than ^{238}U(p, n) reaction cross section, as opposed to the measured data trend. Figure 2b shows comparison of the ^{232}Th(p, 3n) and ^{238}U(p, 3n)^{236s}Np

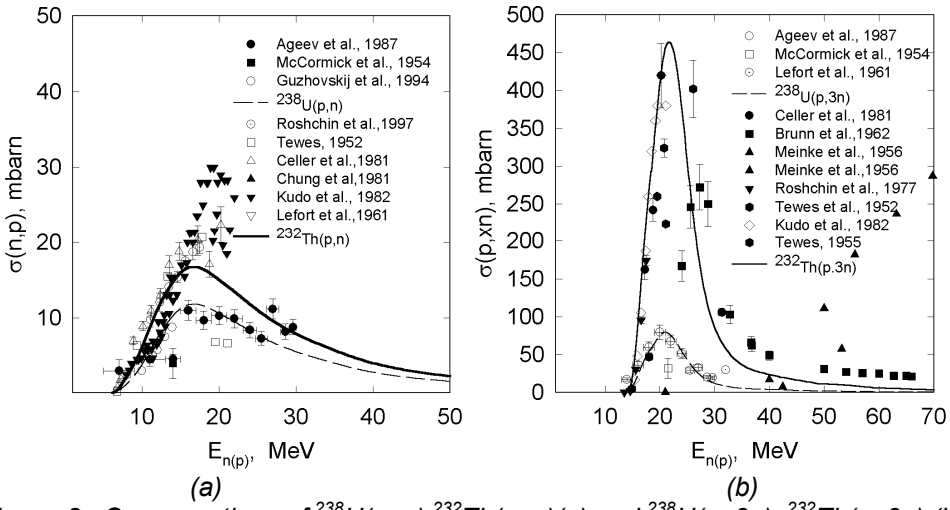

Figure 2. *Cross sections of ^{238}U(p, n),^{232}Th(p, n)(a) and ^{238}U(p, 3n), ^{232}Th(p, 3n) (b).*

data. A five-fold difference of the calculated cross section values in the peak region is supported by the precise data on ^{238}U(p, 3n)^{236s}Np. In case of ^{232}Th(p, 2n) there is a two-fold difference of the calculated and measured data in the peak region, while there is no data available in case of ^{238}U(p, 2n) reaction (see Fig. 3a).

The ^{232}Th(n, F) measured fission cross section data could be reproduced only for the fission chances distribution, corresponding to the preferential contribution of fission of neutron deficient Th nuclides [15]. Figure 1b shows the sharing of the ^{232}Th(n, F) fission cross section to SL- and AS-modes when $(E_{fBSL} - E_{fBAS)}$ = 1.5 MeV for Th nuclides with A≤226. That leads to the increase of symmetric fission yields in ^{232}Th(p, F) and ^{232}Th(n, F) reactions due to ^{232}Th(p,xnf) and ^{232}Th(n,xnf) fission reactions, respectively, at $E_{n(p)}$ ~ 50-200 MeV. nuclides. Sharing of the ^{232}Th(p, F) observed fission cross section to SL- and AS-modes is compatible with the measured estimates of σ_{pF}^{SL} and σ_{pF}^{AS} [5,6]. The estimate $(E_{fBSL} - E_{fBAS})$ =1 MeV is used for Pa nuclei with N ≤ 135 (^{232}Th(p, F) reaction). Most recent data by Smirnov et al. appear to overshoot the calculated ^{232}Th(p, F) cross section. Proton-induced fission cross section of ^{232}Th is higher than that of neutron-induced at $E_{n(p)}$ > 18 MeV, while in case of ^{238}U that happens only at $E_{n(p)}$ > 50 MeV [2]. That means in case of p+^{232}Th interaction the fissilities of Pa nuclei are relatively higher than those of respective Th nuclei for the n+^{232}Th interaction, which influences the observed fission cross section at $E_{n(p)}$ <100 MeV. In case of ^{238}U at $E_{n(p)}$ >50 MeV the decisive factor is the sign of the isovector terms in real volume V_R^n and imaginary surface W_D^n potential terms, while in case of ^{232}Th entrance channel plays a decisive role at $E_{n(p)}$ >100 MeV. Present estimate of ^{232}Th(p, F) cross section differs essentially from the phenomenological estimate [19].

Branching ratio of symmetric-to-observed fission events

Calculated symmetric fission yield $r^{SL}(E_p)$ for ^{232}Th(p, F) reaction predicts sharp increase at E_p = 57-200 MeV (see Fig. 3b). The $r^{SL}(E_{n)p)}$ is much dependent on the (n,xnf) or (p,xnf) fission chances distribution. Possible lowering of $r^{SL}(E_n)$ for ^{232}Th(n, F) reaction due to high emissive fission contribution is more than compensated, since for Th nuclei the relative heights of the symmetric and asymmetric outer fission barriers $(E_{fBSL} - E_{fBAS})$ changes in favor of symmetric fission. The excitation energies of the fissioning nuclides ^{229}Th and ^{226}Th [13], shown on Fig. 8 (~11 MeV), correspond to two-phonon excitation of GDR. The experimental estimate of the symmetric fission contribution to the observed fission fragment yield in ^{208}Pb(^{18}O,f) reaction [12] is shown for the E$_n$~20 MeV. The estimate of symmetric fission yield [5,6] for ^{232}Th(p, F) is quite compatible with the present estimate for ^{232}Th(n, F).

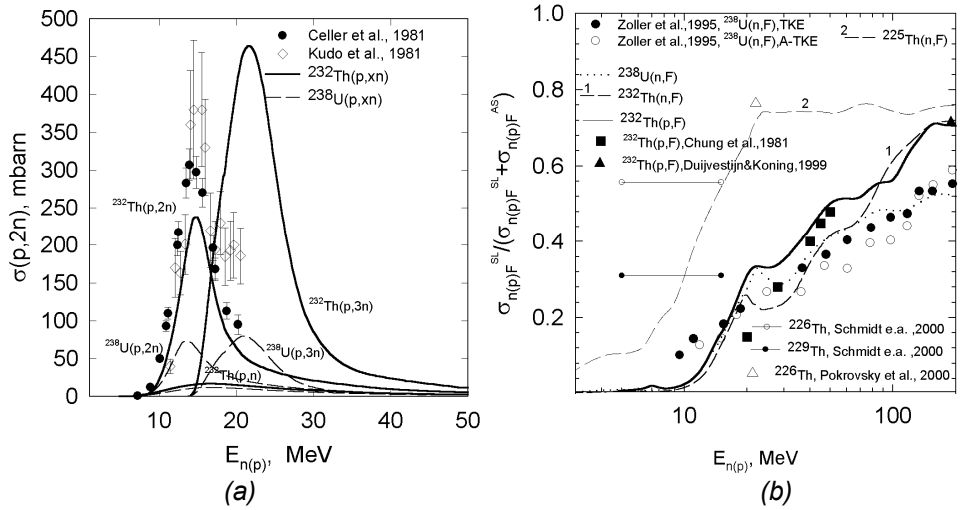

Figure 3. *Cross sections of ^{238}U(p, xn),^{232}Th(p, xn)(a); $r^{SL}(E_n)$ of ^{232}Th(p, F), ^{232}Th(n, F) (b).*

Conclusion

The influence of the interplay of fission barriers and entrance channel on the fission observables is different in case of n(p)+^{232}Th and n(p)+^{238}U interactions. In case of p+^{232}Th interaction the fissilities of Pa nuclei are responsible for $\sigma_{pF} > \sigma_{nF}$ at 18< $E_{n(p)}$ < 100 MeV. In case of ^{238}U target $\sigma_{pF} > \sigma_{nF}$ at $E_{n(p)}$ >50 MeV due to the isovector potential terms. In case of ^{232}Th the entrance channel plays a decisive role at $E_{n(p)}$ >100 MeV. Estimates of ^{232}Th(p, F) and ^{238}U(p, F) fission cross sections are obtained. The description of fission cross sections up to $E_{n(p)}$ = 200 MeV was achieved for preferential contribution of fission of neutron-deficient nuclides. The fission chances distribution was obtained by the consistent description of the observed fission cross section and symmetric fission yield for ^{238}U(n, F). The measured data on the symmetric fission yield for ^{232}Th(p, F) are reproduced, sharp increase of symmetric fission yield for ^{232}Th(n, F) reaction is predicted at E_n≥50 MeV.

References

[1] V.M. Maslov, Phys. Lett. B 649 (2007) 376.
[2] V.M. Maslov, Phys. Lett. B 581 (2004) 56.
[3] S. Isaev, R. Prieels, Th. Keutgen et al., Abstr. 2nd International Conference Frontiers in Nuclear Structure and Reactions, Aghios Nikolaos, Crete, Greece, 2007.
[4] C. Chung C. and J. Hogan, Phys. Rev. 24 (1981) 180.
[5] M.C. Duijvestijn, A.J. Koning, J.P. Beijers et al., Phys. Rev. C 59 (1999) 776.
[6] M.C. Duijvestijn, A.J. Koning and F.-J. Hambsch, Phys. Rev. C 64 (2001) 014607.
[7] C.M. Zoller et al., Fission fragment properties in the ^{238}U(n, F) reaction at incident neutron energies from 1 MeV to 500 MeV. IKDA 95/25, Institut fur Kernphysik, Darmstadt, 1995.
[8] V.M. Maslov, Nucl. Phys. A 717 (2003) 3.
[9] U. Brosa et al., Physics Reports, 197 (1990) 167.
[10] A. Turkevich and J.B. Niday, Phys. Rev., 84 (1951) 52.
[11] V.M. Maslov, EuroPhysics Journal. A 21 (2004) 281.
[12] M.G. Itkis, Yu. Ts. Oganesyan, G.G. Chubaryan et al., Proc. Of he Workshop on Nuclear Fission and Fission-Product Spectroscopy, Seissin, France, 1994, edited by H. Faust and G. Fioni (ILL, Grenoble, 1994). p. 77.
[13] K.-H. Schmidt et al., Nucl. Phys. A 665 (2000) 221.
[14] V. Pokrovsky M.G. Itkis, J.M. Itkis et al., Phys. Rev. C 62 (2000) 014615.
[15] V. M. Maslov, Nucl. Phys. A 757 (2005) 390.
[16] V.M. Maslov, Yu.V. Porodzinskij, N.A. Tetereva et al., Nucl.Phys. A, 736, (2004) 77.
[17] J.P. Delaroche, E. Bauge and P. Romain, In: Proc. International Conference on Nuclear Data for Science and Technology, Trieste, Italy, 1997, p. 206.
[18] P.G. Young , INDC(NDS)-335, p.109, 1994.
[19] A.V. Prokofiev, Nucl. Instrum. And Methods in Phys. Res. A 463 (2001) 557.
[20] A.A. Kotov, L.A. Vaishnene, V.G. Vovchenko et al., Phys. Rev. C74 (2006) 034605.

On modern computational techniques for improvement of nuclear model code performances

F.L. Roman

"Horia Hulubei" National Institute for Physics and Nuclear Engineering (IFIN-HH),
P.O. Box MG-6, 077125, Bucharest-Magurele, Romania
froman@tandem.nipne.ro

Abstract: In order to improve the performance of low-energy nuclear reaction computer codes modern computational techniques presently used worldwide have been also tested for nuclear data evaluation of activation cross sections.
Porting of the EMPIRE-II nuclear reaction code to computational Grids was done by integrating it on the GILDA Grid testbed and then integrated into the Genius Web Portal. The purpose was to reduce the time used to systematically evaluate in one run all reaction channels for all stable isotopes of a given element, and eventually neighbouring elements using local and/or regional parameters.
A modified local version of SCAT-2 nuclear code that searches for "best fit" nuclear optical model parameters has been ported to the parallel environment using OpenMPI and run on a local built cluster. Since the performance tests showed the code is highly scalable and thus perfect for the parallel and distributed computational environments, it was also ported in the framework of Enabling Grids for E-sciencE (EGEE) project using the Fusion Virtual Organization (VO) resources.
Based on the results obtained and as previously demonstrated within other application domains making use of the EGEE infrastructure, also the low-energy nuclear data activities would benefit from the Grid technology and eventual creation of a VO on the EGEE platform.

Introduction

There was always a stringent need for high accuracy nuclear data due to nuclear fusion and fission projects, and not only, that have intensified in the last years due to new foreseen facilities, e.g. ITER, IFMIF, SPIRAL-2 or FAIR [1]. On one side, experiments are becoming more complex, expensive and lack the power to measure all the required quantities and on the other side, the nuclear computer codes fall short in reproducing the measurements without a thorough local analysis [2]. Moreover, the evaluations are given without the estimates of uncertainties, only recent efforts beginning to address this through the generation of covariance files for nuclear model calculations [3].
The nuclear codes improvement is essential for the predicting power and reliability, obviously the most important aspects are the underlying physical models and parameters, yet another key part is the computational performance. Early studies on higher-precision data and associated techniques point to formidable computing challenges, e.g. the development of appropriate sensitivity and uncertainty propagation techniques. These in turn, point to major opportunities for development of novel high-performance computational techniques [4]. The merger of the two domains translates in reliable, safer and cost effective modern facilities and has a strong impact on many other industries as well.
In order to improve the performance of nuclear computer codes, modern computational techniques presently used worldwide, i.e. parallel and distributed computing, have been also tested for nuclear data evaluation of activation cross sections [5]. The proven success [6] of Grid technology due to the use of a distributed resource environment to achieve great performance in storage and computational power without the costs of a supercomputer and the improved support of the new user communities [7] for integrating applications in Grids made attractive to try this platform also for low-energy nuclear data evaluation.
The paper presents the requirements, porting process and the results obtained using two well-known nuclear computer codes used for low-energy nuclear data evaluation in the Grid infrastructure and also discusses using as eventual computational platform in the low-energy nuclear data evaluation research community the Grid computing infrastructure and the potential creation of a Virtual Organization (VO).

Computational techniques

The nuclear reaction computer codes presented in this section are one of the main nuclear computer codes used in low-energy nuclear data evaluation, and were chosen due to low dependencies, high computational time and good perspective for future development and integration within other frameworks. The computational approach used for porting both computer codes to the parallel and distributed environment was “single process multiple data” [8] schema, splitting the input parameters among the available computational resources.

Porting EMPIRE-II

EMPIRE-II [9] is a well-known state-of-the-art modular nuclear computer code used for nuclear data evaluations and was chosen as a first test of Grid platform since it is freely available [10], of general interest and at the same time involved in the author’s research activities. Its effectiveness as a tool for nuclear data evaluation has been widely proved including global analysis of nuclear reactions [11].
Porting the EMPIRE-II nuclear reaction code to computational Grids [12] required a Grid digital certificate issued by GILDA [13] Certification Authority and a user account in the User Interface (UI) configured to use the GILDA VO Grid resources [14]. The purpose was to reduce the time used to systematically evaluate in one run all reaction channels of all stable isotopes corresponding to a given element using local and/or regional parameters. The basic proposed workflow, *Figure 1,* splits the main computation for an element to one isotope per WorkerNode (WN) and after all the jobs are finished the results are retrieved in the UI or at a later stage in the Grid Web Portal.

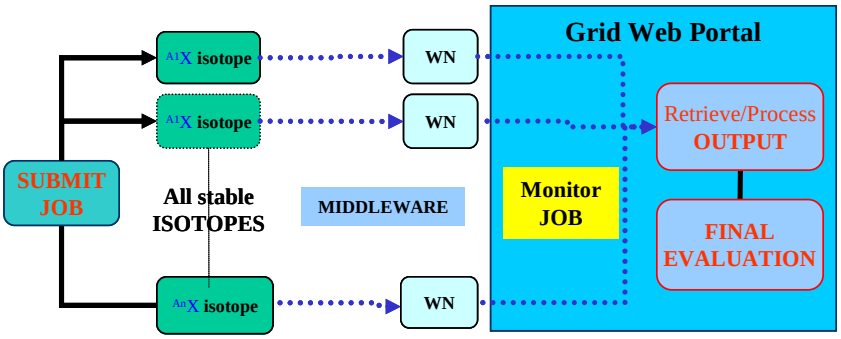

Figure 1. *Schematic of EMPIRE-II Grid Workflow and the role of the Grid Web Portal.*

EMPIRE-II was ported on the GILDA Grid testbed [14] by making a stripped version of the code source, removing the EXFOR experimental database, requirement imposed due to a 10 Mb file transfer limit within computing elements, and creating the specific files and scripts necessary to run the code instances on Grid, all the detail being presented elsewhere [12]. The code was added also as a service into Genius Web Portal [15], this allowing the job submission, monitoring, retrieving and processing the results directly in the Web Portal. The advantage of the Web Portal was firstly to hide the complexity of the Grid middleware but in future it could be used also as a framework for graphical representation of the results or as a collaborative environment.

Porting SCAT2MIN

The computer code SCAT-2 [16] is a spherical-nucleus optical model potential (OMP) code that provides calculated total cross sections, elastic scattering and non-elastic scattering cross sections as well as elastic-scattering angular distributions and it is also implemented as a subroutine in many other nuclear computer codes, e.g. EMPIRE-II.
A local modified version - SCAT2MIN - has been developed to search for “best fit” OMP parameters by minimizing a χ^2 function within analysis of experimental elastic scattering angular distributions. The usefulness of a preliminary version of this local version has been already proved in an OMP analysis of recent high-accuracy data of alpha-particle elastic scattering angular distributions [17].
The minimization procedure is very CPU intensive, a normal case, varying the OMP parameters within physically limits, will take roughly 3 months CPU time. This single computation is for only one experimental angular distribution, so for one element we have to

multiply this CPU time with the number of isotopes and the number of experimental angular distributions for each isotope, this justifying the parallel and distributed computational need.
Similar to the EMPIRE-II case the computational time was reduced by splitting the optical model parameter set among the available resources. The approach is embarrassingly parallelizable and SCAT2MIN was ported to the parallel environment using OpenMPI [18], the code being run at first on a "ad-hoc" local cluster. The key point was the MPI_REDUCE subroutine that after splitting the OMP parameters on the available WN, at the end of the run compares the χ^2–values obtained by all the nodes and does one last calculation on the master node with the optical model parameters corresponding to the minimum χ^2-value [19].
Due to the high demand of CPU power and since the code proved very scalable on the local cluster, the code was ported on the EC Integrated Project "Enabling Grids for E-SciencE" (EGEE) Project [20] using the Fusion VO [21] Grid resources.
The parallel version of the code failed to run due to the still weak MPI support in the EGEE infrastructure. Next, the serial code was tested by splitting the OMP parameters manually and this approach was only partially successful because of the unreliability of Grid resources, i.e. the actual increase of computing time compared with running the same instance on a local cluster due to various failures and resubmitting of jobs.
Figure 2 shows the timing of SCAT2MIN serial version using a testcase OMP parameter set split among 2, 4 and 10 WN in comparison with the same parameter set run on a single CPU, taken as a reference. This comparison shows that while the Grid can offer very good performance for independent jobs, e.g. Monte Carlo simulations, for dependent data there is a risk of having an overall computational time higher when using more resources than using less. This is the case of running on both 4 and 10 CPUs compared with the 2 CPU case, due to the failures and resubmitting of jobs.

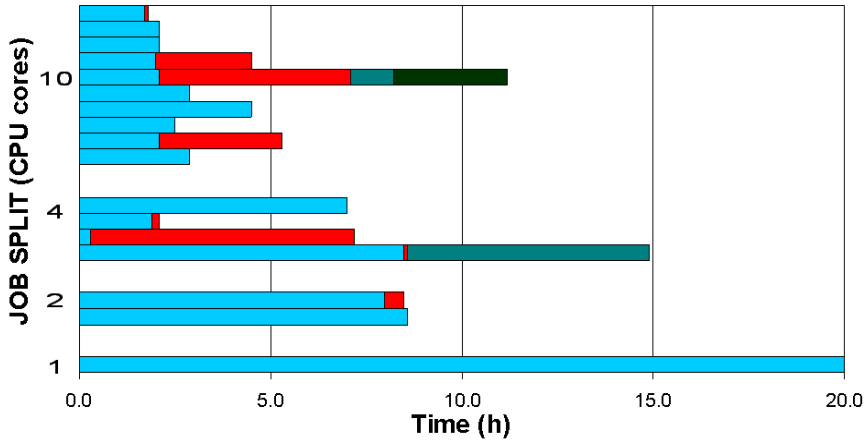

Figure 2. *Comparison of a SCAT2MIN test case using an OMP parameter set split on 2, 4 and 10 WN and the same parameter set run on one WN, taken as a reference.*

Conclusions

This work has showed that it is rather straightforward to integrate actual nuclear computer codes into modern computational environments. Following the achievement of this goal concurrently and performing large-scale computations with nuclear codes on Grids [5], the related outcome was firsthand the reduced computational time, and one of the first steps towards nuclear models uncertainties generation. Further work could address the reliability of Grid resources using dedicated tools, e.g. DIANE framework [22] or advanced workflow environments [23].
Most important and as previously demonstrated within other application domains [24], the low-energy nuclear data community would certainly benefit from the eventual creation of a Grid Virtual Organization on the EGEE platform. This would provide a collaborative environment specifically designed for low-energy nuclear physics research community that besides supporting nuclear intensive computer codes would also provide support for large databases, processing workflows, remote instrumentation and visualizations all integrated using a Service Oriented Architecture. A Grid Web Portal could be implemented as a service in the existing projects, eventually using the experience of the already established projects in the field, e.g. NEA HPRL [25].

Lastly, an early adoption of the Grid technology by the nuclear data evaluation community could greatly improve the overall nuclear research process, by fostering new ideas, provide training for young researchers, and create conditions for future inter-domain collaborations.

Acknowledgements
The author acknowledges Dr. Arjan Koning (NRG, Petten), Dr. M. Lamanna (LCG ARDA) and Dr. C. Loomis (EGEE NA4) for useful comments on Grid VO proposal. EC/JRC/IRMM-Geel for the NEMEA-4 attendance support, ICTP/INFN-Democritos Workshop on "Porting Scientific Applications on Computational GRIDs", in particular Giuseppe La Rocca for the Genius integration, and not least EGEE Gilda VO and Fusion VO for the Grid resources.

References

[1] European Roadmap for Research Infrastructures, http://cordis.europa.eu/esfri/.
[2] M. Avrigeanu, R. A. Forrest, A.J. Koning, F.L. Roman and V. Avrigeanu, On the role of activation and particle-emission data for reaction model, in Int. Conf. on Nuclear Data for Science and Technology (ND2007), 22 - 27 Apr., 2007, Nice, France.
[3] A.J. Koning, Generating Covariance Data with Nuclear Moldels, in Proc. Int. Workshop on Nuclear Data Needs for Generation IV Nuclear Energy Systems, 5-7 April 2005, Antwerpen, Belgium, World Scientific, Singapore, p. 153.
[4] Report of the Nuclear Physics and Related Computational Science R&D for Advanced Fuel Cycle Workshop, 10-12 August 2006, Bethesda, Maryland; www-fp.mcs.anl.gov/nprcsafc/Report_FINAL.pdf.
[5] F.L. Roman, M. Avrigeanu, On porting low-energy nuclear Reaction Codes on Grid, in Open Grid Forum 20) / 2nd EGEE User Forum, 7 - 11 May, 2007, Manchester, UK.
[6] EGEE-2 in numbers, http://egee-na2.web.cern.ch/egee%2Dna2/numbers.html.
[7] Registered EGEE VOs, http://cic.gridops.org/index.php?section=home&page=volist
[8] Algorithms and Theory of Computation Handbook, CRC Press LLC, 1999, http://www.nist.gov/dads/HTML/singleprogrm.html.
[9] M. Herman, P. Oblozinski, M. Sin, A. Trkov, A. Ventura, and V. Zerkin, Recent developments of the nuclear reaction code EMPIRE, in R.C. Haight, M.B. Chadwick, T. Kawano, and P. Talou, editors, Proc. of the Int. Conf. on Nuclear Data for Science and Technology, Sept 26 – Oct 1, 2004, Santa Fe, AIP, New York, p. 1184.
[10] Nuclear Reaction Model Code EMPIRE-II (ver. 2.19), www.nndc.bnl.gov/empire.
[11] V. Avrigeanu, M. Avrigeanu, F.L. Roman, R.A. Forrest, R. Eichin, H. Freiesleben, and K. Seidel, Sensitivity of activation cross sections of the hafnium, tantalum and tungsten stable isotopes to nuclear reaction mechanisms, in Proc. Int. Workshop on Nuclear Data Needs for Generation IV Nuclear Energy Systems, 5-7 April 2005, Antwerpen, Belgium, World Scientific, Singapore, p. 145.
[12] F. L. Roman, Porting Nuclear Reaction Codes for Nuclear Data Evaluations on GRIDs, ICTP/INFN-Democritos Workshop on Porting Scientific Applications on Computational GRIDs, 6-17 February 2006, ICTP, Trieste, Italy , http://cdsagenda5.ictp.trieste.it/full_display.php?smr=0&ida=a05191.
[13] INFN GILDA Project, https://gilda.ct.infn.it.
[14] INFN GILDA Grid Testbed, https://glite-tutor.ct.infn.it/.
[15] Genius Web Portal, https://genius.ct.infn.it.
[16] O.Bersillon, SCAT2:Un programme de modele optique spherique, Report CEA-N-2227 NEANDC(FR), INDC(E) 49 (1981); www.nea.fr/abs/html/nea-0829.html.
[17] M. Avrigeanu and V. Avrigeanu, Addendum to "Elastic α-scattering on 112Sn and 124Sn at astrophysically relevant energies, Phys.Rev. C 73, 038801 (2006).
[18] OpenMPI library, www.open-mpi.org.
[19] F.L. Roman, Porting Nuclear Reaction Codes for Nuclear Data Evaluations on GRIDs, in Proc. 2nd Int. Conf. on Distributed computing and Grid technologies in science and education", Dubna, Russia, 26-30 June, 2006.
[20] EC Integrated Project "Enabling Grids for E-SciencE" (EGEE-II), http://www.eu-egee.org/
[21] EGEE FUSION Virtual Organisation, http://grid.bifi.unizar.es/egee/fusion-vo/index.html
[22] DIANE framework, http://it-proj-diane.web.cern.ch/it-proj-diane/
[23] Grid Application Development and Computing Environment - ASKALON Project, http://www.dps.uibk.ac.at/projects/askalon/.
[24] EGEE-II NA2 Activity, http://egee-na2.web.cern.ch/egee%2Dna2/numbers.html.
[25] OECD/NEA High Priority Nuclear Data Request List, http://www.nea.fr/html/dbdata/hprl/.

Testing of cross section libraries for zirconium benchmarks

L. Snoj, A. Trkov, M. Ravnik

Jožef Stefan Institute, Jamova 39, SI-1000 Ljubljana, Slovenia
luka.snoj@ijs.si

Abstract: The purpose of this paper is to investigate the influence of ENDF/B-VI.8 and ENDF/B-VII cross section libraries on the multiplication factor of the TRIGA benchmark with fuel made of enriched uranium and zirconium hydride [1] and SB-n light-water reactor benchmarks with fuel made of fissile material in zirconium matrix [2]. The calculations are performed with the Monte Carlo computer code, MCNP [3], using ENDF/B-VI.8, and the newest ENDF/B-VII cross section libraries in Ace format [4]. Differences of ~ 600 pcm in k_{eff} are observed for the benchmark model of the TRIGA reactor. It is interesting that there are practically no differences in the k_{inf}. Therefore, an investigation was performed also for hypothetical systems with different leakage. The uncertainty analysis of the most important contributions to k_{eff} is presented. The main contributors to the difference in k_{eff} are Zr isotopes (especially ^{90}Zr and ^{91}Zr) and thermal scattering data for H and Zr in ZrH. As the differences in k_{eff} due to use of different cross section libraries are relatively large, there is certainly a need for a review of the evaluated cross section data of the zirconium isotopes.

Introduction

Triga Mark II research reactor

The research reactor at the Jožef Stefan Institute is a typical 250-kW TRIGA Mark II reactor, with fuel made of uranium mixed with zirconium hydride. The reactor core is immersed in light water, which also serves as coolant by natural convection [1].

The benchmark experiments were performed as part of the startup test after reconstruction and upgrading in 1991. All core components, with the exception of the graphite reflector around the core were replaced with new ones in the process [1].

The benchmark experiment was performed with standard commercial TRIGA fuel elements of 20 wt. % enrichment and 12 wt. % uranium concentration in U-$ZrH_{1.6}$. The benchmark was thoroughly validated and is included in the Handbook of Evaluated Criticality Safety Benchmark Experiments (ICSBEP) [1]. The experimental k_{eff} and the value of benchmark k_{eff} (which includes a bias due to model simplifications) and the corresponding uncertainties are presented in Table 1.

Table 1. *Experimental and benchmark model k_{eff} with the uncertainties* [1]

Case	experimental k_{eff}	Benchmark-model k_{eff}
Core 132	0.99865 ± 0.00015	1.0006 ± 0.0056
Core 133	1.00310 ± 0.00015	1.0046 ± 0.0056

SB-n light-water benchmarks

SB-n benchmarks are light water moderated thermal lattices with a thorium blanket and either ^{235}U or ^{233}U fissile component in zirconium matrix fuel. A brief description is given in Table 2.

Calculation method

The MCNP computer code [3] was used in the calculation of the effective multiplication factor, k_{eff}, and multiplication factor of an infinite medium, k_{inf}. MCNP is a general-purpose, continuous-energy, generalized-geometry Monte Carlo transport code. The calculations reported in this paper were performed with version 5.1.40 of the code and with two different cross-section libraries, i.e. ENDF/B-VI release 8 and ENDF/B-VII [4].

Calculations and results

TRIGA benchmark

The benchmark model of the TRIGA reactor was taken from the ICSBEP handbook [1]. The calculated values of k_{eff} using ENDF/B-VI.8 and ENDF/B-VII cross-section libraries are presented in Table . We can observe that k_{eff} calculated by using the ENDF/B-VII cross-

section library is approximately 600 pcm higher than k_{eff} calculated by using the ENDF/B-VI.8 cross-section library for both benchmark cores.

Table 2. *List of SB-n benchmarks and their brief description [2].*

ICSBEP Ident	Cases		Description
HEU-COMP-THERM-015	1	LWBR SB-1	93%$^{235}UO_2$+ZrO_2, ThO_2 blanket
	1	LWBR SB-5	93%$^{235}UO_2$+ZrO_2, ThO_2 blanket
U233-COMP-THERM-001	1	LWBR SB-2	97%$^{233}UO_2$+ZrO_2, ThO_2 blanket
	1	LWBR SB-2½	97%$^{233}UO_2$+ZrO_2, no blanket
	1	LWBR SB-3	97%$^{233}UO_2$+ZrO_2, UO_2+ThO_2 blanket
	1	LWBR SB-4	97%$^{233}UO_2$+ZrO_2, UO_2+ThO_2 blanket
	1	LWBR SB-6	97%$^{233}UO_2$+ZrO_2, ThO_2 blanket)
	1	LWBR SB-7	97%$^{233}UO_2$+ZrO_2, UO_2+ThO_2 blanket

Table 3. *Calculated values of k_{eff} using different cross-section libraries.*

Cross section set → Case ↓	ENDF/B-VI.8	ENDF/B-VII
Core 132	0.9999 ± 0.0001	1.0059 ± 0.0001
Core 133	1.0048 ± 0.0001	1.0107 ± 0.0001

In order to find the source of discrepancy between the calculated values of k_{eff}, we performed a thorough analysis of the contributions of individual isotopes to the difference in k_{eff} due to use of different cross section libraries. First we calculated the k_{eff} by using all cross section data from ENDF/B-VI.8. Afterwards cross sections data for individual isotopes were taken from the ENDF/B-VII cross section library. The differences between the k_{eff} calculated by taking individual isotopes from the ENDF/B-VII cross section library and the k_{eff} calculated by using all cross section data from ENDF/B-VI.8 are presented in Table .

Table 4. *Contributions of individual isotope cross section to the difference in k_{eff} due to use of different cross section libraries. The highest contributions are highlighted.*

Cross section data from ENDF/B-VII	Δ k_{eff}
^{235}U	15
^{238}U	63
^{90}Zr	-35
^{91}Zr	386
^{92}Zr	40
^{94}Zr	-13
^{96}Zr	38
all Zr isotopes	403
S(α,β) for H in ZrH and Zr in ZrH	210

We observe that the highest contribution to the difference in k_{eff} is due to the ^{91}Zr isotope (-400 pcm) and thermal scattering kernel for hydrogen in Zirconium lattice and Zr in Zirconium lattice (-200 pcm).

k_{inf} of U-ZrH

We also investigated the effect of cross section library on k_{inf} of U-ZrH. The multiplication factor of an infinite medium of U-ZrH was calculated by modelling a U-ZrH cube and applying reflecting boundary condition on the cube surfaces. The material composition was the same as in the standard TRIGA fuel element, i.e. 12 w/o of 20 % enriched U in U-ZrH.

Table 5. *Calculated values of k_{inf} using different cross-section libraries.*

Cross section set	k_{inf}
ENDF/B-VI.8	1.6250 ± 0.0001
ENDF/B-VII	1.6242 ± 0.0001

As the k_{inf} is much larger than unity (k_{inf} ~1.6250) it is more common to calculate the difference in reactivity and not in the multiplication factor. The differences between the reactivity (Δρ) calculated by taking individual isotopes from the ENDF/B-VII cross section

library (ρ_{VII}) and the reactivity calculated by using all cross section data from ENDF/B-VI.8 (ρ_{VI}) are presented in Table 6.

Table 6. *Contributions of individual isotope cross section to the difference in reactivity of infinite medium of U-ZrH due to use of different cross section libraries. The highest contributions are highlighted. $\Delta\rho = \rho_{VII} - \rho_{VI}$.*

data from ENDF/B-VII	Δρ
^{235}U	8
^{238}U	25
^{90}Zr	-229
^{91}Zr	264
^{92}Zr	-57
^{94}Zr	-14
^{96}Zr	24
S(α,β) for H in ZrH and Zr in ZrH	-19

The results show that there are practically no differences in k_{inf} when different cross section libraries are used. However, contributions of individual isotopes, such as ^{90}Zr and ^{91}Zr can be significant, i.e. more than 200 pcm. As there are significant difference in the k_{eff} and almost no difference in k_{inf}, we can conclude that the effect of cross section library on k_{eff} depends on the size of the system.

U-ZrH spheres

In order to find the relation between the size of the fissile system made of U-ZrH and the difference in k_{eff} or reactivity due to different cross section libraries, we modelled several U-ZrH spheres with different radii. The sphere radius was varied from 15 cm to 80 cm. First the k_{eff} of each sphere was calculated by using ENDF/B-VI.8 cross section library. Afterwards cross section data for individual Zr isotopes were replaced by the cross sections from ENDF/B-VII cross section library and for each case the k_{eff} was calculated. The differences between the reactivity (Δρ) calculated by taking individual Zr isotopes from the ENDF/B-VII cross section library (ρ_{VII}) and the reactivity calculated by using all cross section data from ENDF/B-VI.8 (ρ_{VI}) are presented in Figure 1 for all sphere sizes.

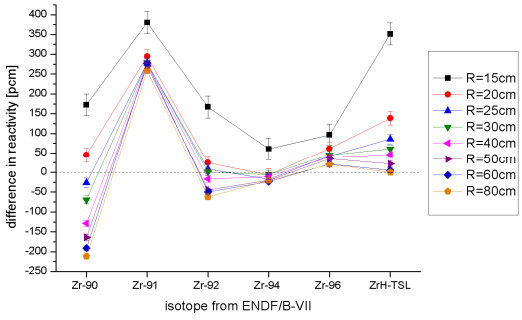

Figure 1. *Contributions of individual Zr isotopes from ENDF/B-VII cross section library to the reactivity calculated by using all isotopes from ENDF/B-VI.8 cross section library for various U-ZrH sphere sizes. ZrH-TSL denotes thermal scattering law for H in ZrH and Zr in ZrH.*

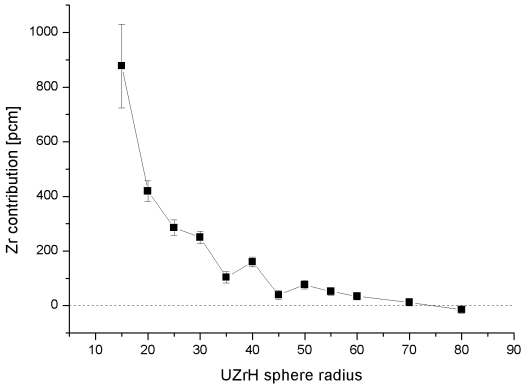

Figure 2. *Contributions of all Zr isotopes from ENDF/B-VII cross section library to the reactivity calculated by using all isotopes from ENDF/B-VI.8 cross section library in dependence of U-ZrH sphere radius.*

We observe in Figure 1 that the contribution of individual Zr isotopes from ENDF/B-VII cross section library to the reactivity calculated by using all isotopes from ENDF/B-VI.8 cross section strongly depends on the size of the fissile system. Contributions of ^{92}Zr, ^{94}Zr and ^{96}Zr to the difference in reactivity are relatively small and almost independent on the size of the system. On the other hand the contributions of ^{90}Zr, ^{91}Zr and thermal scattering law for H and Zr in ZrH are relatively large, i.e. more than 100 pcm, and strongly dependent on the size of the system. The ^{90}Zr contribution is positive for smaller systems (up to 22 cm) and negative

for larger systems (more than 23 cm). The contribution of ^{91}Zr isotope from ENDF/B-VII cross section library is always positive and almost constant for systems larger than 20 cm.
The total contribution of all Zr isotopes taken from ENDF/B-VII cross section library is always positive. However it strongly depends on the size of the system and it decreases as the system becomes larger. This can be clearly seen in Figure .

SB-n benchmarks
The results for the SB-n benchmarks obtained with the ENDF/B-VII library differ considerably from the results with ENDF/B-VI.8. However, most of the differences are due to the improvements in the data of the fuel materials. Therefore, the results with a pre-released version ENDF/B-VII-beta3 are also presented for comparison. This library does not contain some of the last-minute adjustments to the data, which were done on the Zr cross sections.
The results with the pre-released library ENDF/B-VII beta 3 were all within the experimental uncertainty. The adjustments to zirconium data in the final version of the library resulted in some positive bias, which caused a slight overprediction of reactivity in some of these benchmarks. This overprediction is significant in the lattices containing ^{233}U. The data of ^{232}Th are less likely to be responsible, since the same trend is observed in the SB-2½ lattice, which contains no thorium.

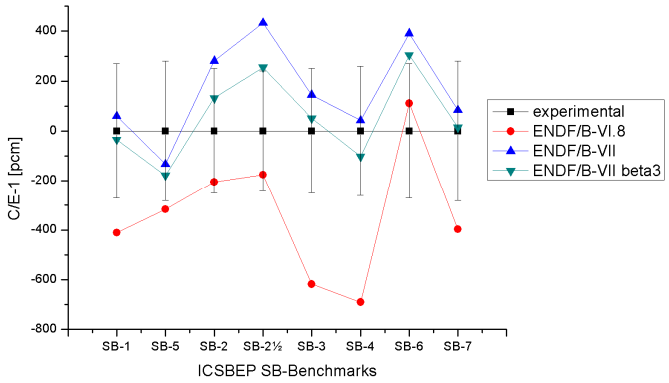

Figure 3. *Comparison of the results for the SB-n benchmarks using different data.*

Conclusion

The analysed benchmarks suggest that the reactivity of lattices containing significant amounts of zirconium is overpredicted with the ENDF/B-VII data. Although this overprediction in the SB-n lattices could originate from other data, the comparison with the results of the pre-released ENDF/B-VII.beta3 for these benchmarks indicates that the last-minute changes to the zirconium data have a significant effect. The overprediction of reactivity in the case of the TRIGA benchmark is even stronger. Additional artificial test cases with spheres of different radii show that k_{inf} is affected to a lesser extent, leading to the conclusion that the slowing-down properties of zirconium are mainly responsible for the change in k_{eff}. High-leakage lattices are affected more strongly.
As the differences in k_{eff} due to the use of different cross section libraries are relatively large, there is certainly a need for a review of the evaluated cross section data of the zirconium isotopes.

References
[1] R. Jeraj and M. Ravnik, "TRIGA Mark II benchmark Critical Experiments-Fresh Fuel, IEU_COMP-THERM-003", International Handbook of Evaluated Critical Safety Benchmark Experiments, Organization for Economic Cooperation and Development - Nuclear Energy Agency Data Bank, 1999.
[2] V.L. Putman (Evaluator), LWBR SB Core Experiments, U233-COMP-THERM-001, International Handbook of Evaluated Critical Safety Benchmark Experiments, Organization for Economic Cooperation and Development - Nuclear Energy Agency Data Bank, NEA/NSC/DOC(95)03, September 2006.
[3] J.J. Briesmeister, "MCNP5- A General Monte Carlo N-Particle Transport Code, Version 5 Los Alamos National Laboratory", March, 2005.
[4] Available from National Nuclear Data Center, Brookhaven, http://www.nndc.bnl.gov/exfor2/endf00.htm.

Bonner Sphere Spectrometer as an efficient system for neutron detection of a wide energy range for radiation protection purposes

U. Wiącek

The Henryk Niewodniczański Institute of Nuclear Physics Polish Academy of Sciences; ul. Radzikowskiego 152 ; 31-342 Kraków, Poland
Urszula.Wiacek@ifj.edu.pl

Abstract: The Bonner sphere spectrometer (BSS) with 4 x 4 mm ^{6}LiI(Eu) crystal scintillator is considered using the MCNP5 Monte Carlo code. Spheres, made of polyethylene of changeable radius, have been exposed to the ISO standard neutron sources, ^{241}Am-Be or ^{252}Cf. The response has been determined in the energy range from subthermal to 20 MeV.

Introduction

The Bonner Sphere Spectrometer (BSS) is the only system which covers a wide energy range for neutron spectrometry. For detection of thermalized neutrons the BSS with the ^{3}He counter in the centre of the spheres can be used. This type system becomes attractive of its considerably higher sensitivity and a better discrimination ability against photon radiation compared with the traditional LiI crystal system [1].
The spectrometer is constituted by a number of polyethylene spheres, usually from 6 to 10, with known diameter and density, with an active or passive thermal neutron sensor located at their centre. Since each sphere moderates the neutrons in a given energy range, the set of the measurements obtained from different spheres provides information on the energy distribution of the incident neutrons. In this problem, a typical BSS is considered. The sphere diameters are: 0” (bare detector), 2”, 3”, 5”, 8”, 10” and 12”. The density of polyethylene is 0.950 g cm^{-3}. Such configuration allows getting spectral information from subthermal to 20 MeV neutrons. In order to extend the energy range up to hundreds of MeV, an additional lead loaded 12” sphere has been added. This new configuration takes advantage of the (*n*, *xn*) reactions induced by high energy neutrons in the lead shell. The structure of the new sphere includes a 8 cm diameter polyethylene sphere around the central detector, surrounded by a 1 cm lead layer (two half shells), then polyethylene up to an external diameter of 12”. This sphere constitutes an interesting example of how the BSSs have been adapted to high energy fields. In this problem a cylindrical 4 mm (diameter) x 4 mm (height) 6LiI(Eu) (96% of ^{6}Li) active scintillator is used as the central detector. Thermal neutrons are detected through the ^{6}Li(n,α)^{3}H reaction (Q = 4.78 MeV). The electronic pulses from the photomultiplier are counted by a scaler. The photon sensitivity of the detector is assumed to be negligible.

Description of numerical calculation

A number of sets of the calculated responses of the BSS (mainly using the multigroup transport code, ANISN) are available in the literature [1]. Large differences were observed as well between different calculation results as in respect to experimental data. Modeling of the BSS was one of tasks in the frame of the European Union Coordinated Network for Radiation Dosimetry (CONRAD). The main aim was to perform calculations using modern Monte Carlo codes and obtain as good as possible agreement with experimental results. The work presented here is a part of the CONRAD and has been performed using the MCNP5 code version 5 [2].
Geometry in the MCNP calculations has been very realistic and delimited only to the important region. The whole assembly has a cylindrical geometry and is made of aluminum. A cross sectional view of the central detector is shown in *Figure 1.* The active part of the central detector is a cylindrical 4 x 4 mm ^{6}Li(Eu) crystal scintillator and its center is located at 0.9 cm from the right external surface of the Aluminium assembly. Spheres are made of polyethylene of changeable radius: 2”, 3”, 5”, 8”, 10” and 12”. Spheres have been exposed to

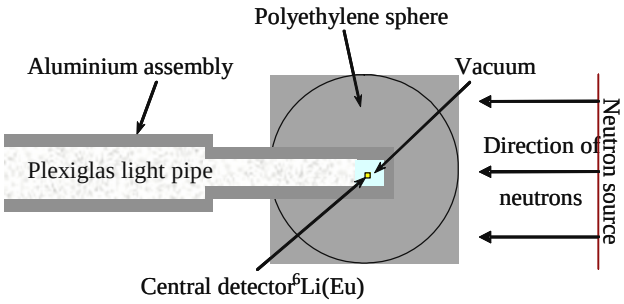

Figure 1. *Scheme of the example of geometry used in MCNP simulation.*

the ISO standard neutron sources ^{241}Am-Be or ^{252}Cf. The response has been determined in the energy range from thermal to 20 MeV. The light pipe connecting the scintillator to the photomultiplier is made of Plexiglas. Densities, material compositions and MCNP libraries for particular components used in the simulations are presented in *Table.1*.

Table 1*. Material composition data*

Material	Density [g/cm^3]	Elemental composition	MCNP library
Lithium Iodide	3.494	3.36 % ^{6}Li	*3006.66c*
		0.18 % ^{7}Li	*3007.62c*
		95.46 % I	*53127.92c*
PMMA ($C_5H_8O_2$)	1.19	8 % H	*poly.60t*
		60 % C	*6000.66c*
		32 % O	*8016.62c*
Aluminium	2.7	100 %	*13027.92c*
Polyethylene $(C2H_4)_n$	0.95	85.7 % C	*6000.66c*
		14.3 % H	*poly.60t*
Lead	11.35	24.5 % ^{206}Pb	*82206.66c*
		22.4 % ^{207}Pb	*82207.66c*
		53.1 % ^{208}Pb	*82208.66c*

Neutrons have been emitted in one direction from the surface of a disk source centered on and perpendicular to the axis of the central detector. The source has been homogenous. The radius of source's disk has been equal to the radius of used sphere. The response has been defined as the number of ^{6}Li(n,α) reactions per incident neutron fluency based on the track length estimate of the flux in the detector. The neutron spectral fluency has been folded with the macroscopic cross section of ^{6}Li (using the FM card). To get a consistency, each of responses has been multiplied by the appropriate source area. The number of ^{6}Li(n,α)^{3}H reactions in the scintillator has been assumed to be proportional to the number of pulses registered by the scaler.

Results

The ISO standard neutron source

For the ^{252}Cf and ^{241}Am-Be neutron sources, the responses of appropriate spheres exposed to a parallel neutron beam of the same cross sectional area of the spheres have been determined. The results have been normalized to the 8" sphere response and are presented in Table 2 and shown in Figure 2.

Table 2. *Response of the set of spheres exposed to ^{241}Am-Be and ^{252}Cf neutron sources.*

Sphere diameter [inch]	^{241}Am-Be			^{252}Cf		
	Response [cm^2]	Relative error	Response normalized to the 8”	Response [cm^2]	Relative error	Response normalized to the 8”
0	1.72E-04	3.00E-03	9.13E-04	-	-	-
2	4.96E-03	6.00E-03	2.63E-02	8.35E-03	4.60E-03	3.95E-02
3	2.96E-02	3.80E-03	1.57E-01	4.79E-02	2.90E-03	2.27E-01
5	1.20E-01	2.90E-03	6.37E-01	-	-	-
8	1.89E-01	3.60E-03	1.00E+00	2.11E-01	3.30E-03	1.00E+00
10	1.78E-01	4.50E-03	9.43E-01	1.67E-01	4.60E-03	7.92E-01
12	1.48E-01	5.90E-03	7.85E-01	-	-	-

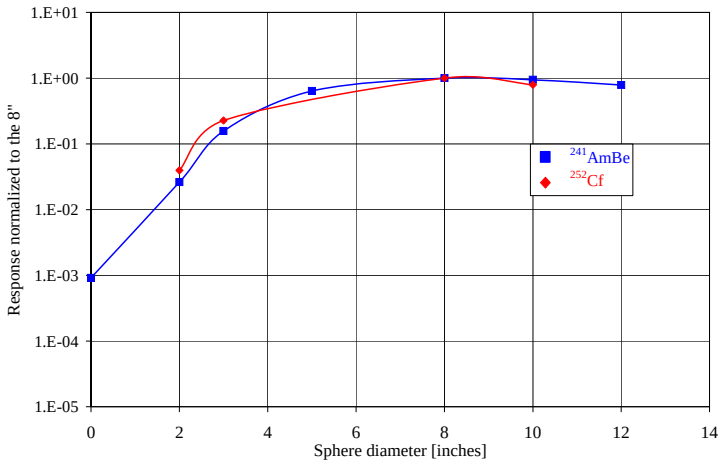

Figure 2. *Response of the set of spheres exposed to ^{241}Am-Be and ^{252}Cf neutron sources.*

The monoenergetic neutrons.

Next problem has been to check the responses of the 8” sphere exposed to a parallel monoenergetical neutron beam of the same cross sectional area of the spheres have. The sphere has been exposed to one of eleven selected neutron energies every time and the results are presented in *Table 3.* and shown in *Figure 3.*

Table 3. *Responses of the 8” sphere exposed to monoenergetical neutron beams.*

Energy [MeV]	Response of the 8” sphere [cm^2]	Relative error	Response normalized to the maximum value
2.53E-08	1.00E-02	0.0124	4.12E-02
1.00E-06	3.21E-02	0.0071	1.32E-01
1.47E-03	6.76E-02	0.0052	2.77E-01
1.12E-02	7.76E-02	0.005	3.18E-01
1.12E-01	1.10E-01	0.0044	4.53E-01
5.62E-01	1.96E-01	0.0034	8.03E-01
8.91E-01	2.23E-01	0.0032	9.16E-01
1.41E+00	2.44E-01	0.0031	1.00E+00
2.24E+00	2.40E-01	0.0032	9.84E-01
4.47E+00	1.97E-01	0.0035	8.07E-01
1.78E+01	7.53E-02	0.0056	3.09E-01

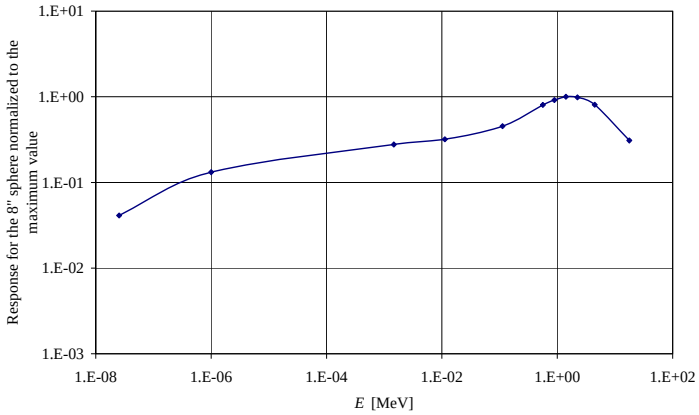

Figure 3. *Responses of the 8" sphere exposed to a monoenergetical neutron beams normalized to the maximum value.*

The neutron spectrum in the lenticular layer located inside the 8" sphere

For the 8" sphere exposed to ^{241}Am-Be and ^{252}Cf, the neutron spectrum within the inner thin lenticular layer (0.1 mm thick) inside the Bonner sphere towards the source and perpendicular to the beam axis, has been determined. The results are presented as histogram of fluency/lethargy ($\phi/\Delta U$) in given energy intervals. The lethargy has been calculated in the following way: $\Delta U = \ln(E_{n+1}/E_n)$. The energy is in logarithmic scale. The results are presented in *Figure 4.*

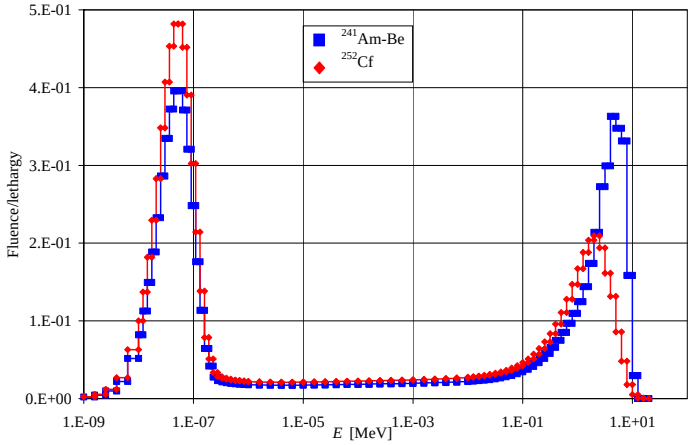

Figure 4. *The neutron spectrum within the inner thin lenticular layer (0.1 mm thick) inside the 8" sphere exposed to the ISO standard neutron sources.*

Summary

The response of the BSS system with 4 x 4 mm ^{6}LiI(Eu) scintillator has been obtained on the basis of the MCNP calculation. For a set of spheres exposed to the ISO standard neutron sources the responses have been determined. For the 8" sphere, exposed to monoenergetical neutrons beams, the responses have been obtained. For the thin lenticular layer located inside the 8" sphere, exposed to the ISO standard sources, the responses have been determined. These results, as a benchmark calculation, will be used in the CONRAD program.

Acknowledgements

This task is a part of the European Union Coordinated Network for Radiation Dosimetry (CONRAD) WP4 2005 - 2007.

References

[1] V. Mares, H. Schraube, Nucl. Instr. And Meth. A *337*(1994) *461 - 473*.

[2] X–5 Monte Carlo Team, MCNP – A general Monte Carlo N-Particle Transport Code Version 5, LA–CP–03–0284. Los Alamos National Laboratory, 2003.

Author index

European Commission

EUR 23235 EN – Joint Research Centre – Institute for Reference Materials and Measurements
Title: NEMEA-4, Neutron Measurements Evaluations and Applications, Nuclear data needs for Generation-IV and accelerator driven systems, proceedings of the CANDIDE workshop, 16-18 October 2007, Prague, Czech Republic
Editor: Arjan Plompen
Luxembourg: Office for Official Publications of the European Communities
2008 – 202 pp. – 21.0 x 29.7 cm
EUR – Scientific and Technical Research series – ISSN 1018-5593
ISBN 978-92-79-08274-0
DOI 10.2787/13092

Abstract
The CANDIDE workshop NEMEA-4, Neutron Measurements, Evaluations and Applications, Nuclear data needs for Generation-IV and accelerator driven systems was held from 16-18 October 2007 in Prague, Czech Republic. These proceedings collect the full papers summarising the contributions to this workshop.

The mission of the JRC is to provide customer-driven scientific and technical support for the conception, development, implementation and monitoring of EU policies. As a service of the European Commission, the JRC functions as a reference centre of science and technology for the Union. Close to the policy-making process, it serves the common interest of the Member States, while being independent of special interests, whether private or national.

JRC
EUROPEAN COMMISSION

LA- NA- 23235- EN- C

ISBN 978-92-79-08274-0

Publications Office
Publications.eu.int